IMPROVEMENTS IN THE EFFICIENCY AND THERMAL AGEING OF SINGLE AND PARALLEL MACHINE DRIVES

Thesis submitted in accordance with the requirements of the University of Liverpool for the degree of

Doctor in Philosophy

by

Philip Henry Mellor

December, 1983

To my Father

ACKNOWLEDGEMENT

The author is grateful to Professor J.H. Leck for providing the facilities of the Electrical Engineering Department for this research.

The author is beholden to his research supervisor, Mr D.R. Turner, for his invaluable advice, guidance and encouragement during the research and in the writing of the thesis.

Special thanks are due to Dr A. Borthwick for reading the manuscript and all those who helped in its completion.

The author appreciates the assistance rendered by Mr A. Gibson of Bass Brewery p.l.c., Runcorn and Brook Crompton Parkinson Motors p.l.c., Huddersfield.

The author would like to thank the SERC for supporting the research.

ABSTRACT

Energy can be conserved in machine drives by a careful matching of the rating of the machine to the expected load and through adjustments to the control used in parallel drive systems. This thesis investigates the full extent of the energy savings through a comprehensive theory on the drive performances.

Stochastic techniques are used to model the machine loads and to optimise the energy consumption with respect to the machine ratings and parallel control. The findings are illustrated through examples with particular reference to induction motor and pump drives. A case study was performed on an industrial pumping plant and positive energy savings were achieved.

The additional ageing caused by a fuller utilisation of electrical drives is considered. A direct method of estimating the ageing of single and parallel drives is obtained from the stochastic analysis and a linear thermal model of the machines. This formulation is tested against a deterministic analysis, which included the non linear effects of motor starting and the differences in thermal behaviour of stationary and rotating machines. The rotational method of ageing equilisation in parallel drives is discussed and an alternative improved ageing algorithm is presented.

The accuracy of using a linear model to describe the dynamic thermal performance of an electrical machine

is assessed by the development of such a model for a 5.5kW induction motor. The model is formulated out of purely dimensional information and constant thermal coefficients, and is applicable to any similar machine. Good agreement was obtained between the model and directly measured machine temperatures.

A microprocessor based thermal prediction device is described, which performs the model temperature calculations in real time. It could accurately estimate the motor's winding temperatures from only external inputs of the motor phase current and ambient temperature. The prediction device has applications in ageing control and as a stand alone motor protection device.

CONTENTS

LIST OF SYMBOLS

Capitals

A	ageing constant
	area
[A]	characteristic matrix
B	ageing constant
[B]	input matrix
C, [C]	thermal capacitance
[D]	diagonal matrix
[F]	vector function
[G]	Hessian matrix
H	head
[I]	unit matrix
L	length
	loss
M	mass
N	dimensionless number
Q	fluid flow

R	relative ageing
	electrical resistance
	thermal resistance
T	load period
[U]	upper triangular matrix
V,[V]	variance
W	electrical loading
	mechanical loading
	power
X	reactance
[X]	eigenvector
Y,[Y]	thermal admittance
Z	impedance

Small letters

a	loss constant
b	loss constant
c	induction motor equivalent circuit constant
	loss constant
	specific heat
d	head constant
e	head constnat
f	function
	head constant
[g]	gradient matrix
g'''	specific heat generation
h	convective film coefficient
i	current
k	constant
	load sharing factor
	thermal conductivity
l	length
n	rotor cooling hole number
	slot number
p	probability
	probability distribution function

r	radius
s	stacking factor
t	time
u, [u]	heat generation
v	velocity
	voltage
w	weighting factor
x	variable
[z]	vector variable

Greek letters

α	sizing factor
β	coefficient of volumetric expansion similarity index
Γ	ageing
γ	loss function
Δ	finite difference
δ	delta function
ε	error constant expectation operand
ζ	statistical event
η	efficiency
$\theta, [\theta]$	temperature
$[\Lambda]$	positional control matrix
λ	positional control element eigenvalue
$\mu, [\mu]$	mean viscosity
$[\xi]$	search vector
ρ	density
τ	time difference

$[\Phi]$	autocorrelation
ϕ	angle
ω	angular speed

Subscripts

a	aluminium
	axial
c	convective
	copper
e	endwinding
g	gap
I	current
i	input
ℓ	switching limit
m	magnetisation
	motor
max	maximum
n	sample n
p	constant pressure
	pump
pr	Prandl
Q	flow
R	relative ageing
ref	reference

s	slot
	mechanically stationary
	statistically stationary
	steel
	system
s/c	short circuit value
T	total distribution
ta	Taylor
u	generation
	Nusselt
v	voltage
θ	temperature
θT	total temperature distribution
λ	positional

Superscripts

I	integer operation
i	matrix element
k	step number
T	transpose
-1	inverse

CHAPTER 1

INTRODUCTION

The cost of energy has risen appreciably over the last decade and it has become increasingly desirable to save electrical energy whenever possible. This thesis investigates the possibilities of saving energy in machine drives on the basic criterion of matching the machine size to the expected load and through adjustments to the control used in parallel machine systems.

A survey[1] in America has disclosed that 64 per cent of industrial electricity in 1976 was used in electric motor drives. A further study[2] suggested that 83 per cent of the motor drive energy was consumed by a.c. motors that were rated within the range of 0.75 to 100 kilowatts. In the United Kingdom and the Federal Republic of Germany a lower figure of 50 per cent of the total industrial energy is expended in motor drives, because of a proportionally higher energy usage in arc furnaces. An estimated[3] 70 per cent of the wattage of electric motors produced in these countries is used in a.c. cage induction machines.

The world's entire electricity power output has to pass through several stages of distribution transformers before it reaches the consumer. Hence any schemes that increase the efficiency of distribution transformers or induction motors will have the potential of saving vast amounts of energy. In 1981, 226 TWh [4] of electricity was produced in the United Kingdom of which 84.5 TWh was

supplied to industry. An improvement of 0.25 per cent in transmission efficiency and 2 per cent in induction motor performances would reduce the required output by 1160 GWh, i.e. several power stations.

A variety of methods are available in which the electrical construction of transformers and induction motors can be altered to improve machine efficiency. One development in distribution transformers is the replacement of the conventional iron core with one wound from an amorphous magnetic material. This material has a third of the core losses of silicon iron[5], which can amount to gains of around 0.3% on the efficiency of a large transformer.

The performance of induction motors can be improved[3] by designing the machines with larger volumes of magnetic material and thicker conductors that operate at lower temperatures. A typical 11kW motor can have its efficiency increased by some 4 per cent[6] by this technique. However, these designs appear to be in conflict with the demands from industry to produce compact motors, with high power to weight ratios. An improved electrical construction will only be available at a greater capital cost and, of course, will require additional energy in the manufacture of the extra material.

Without making alterations in the design, potential energy savings can be found in a better utilisation of the machines [7,8,9]. Often induction motors are selected for duties[8] where they are required to run at partial loads

for long periods of time. This is particularly the case in machine tool, pump and compressor applications, where the ratio of maximum to minimum load is frequently high. At low loads the efficiencies and power factors of the machines are poor and result in unneccessarily high losses, both internally and externally in the supply cables.

The efficiency of induction motors can be boosted at part loads by adjusting the supply voltage, either with an electronic voltage controller[10] or by simple star/delta switching. Voltage controllers will introduce extra loss through their own efficiencies and the harmonics they may induce in the motor currents.

Alternatively,a more careful selection of the machine size on the original commissioning of the plant can reduce the overall losses. This selection should be based upon the economic criteria [9] of the original capital cost, the potential energy savings and the expected life and maintenance costs of the machines.

These considerations are apart from the various forms of system control, such as variable frequency drives, that improve the external load characteristics. Nor do they preclude the use of high efficiency machines or voltage controllers, as the potential gains from the increased utilisation of the combined machine and controller still exist.

Where a load has a wide range of duties, machines are often paralleled together to enhance the drive performance.

Here only the number of machines that are necessary to share the load will be running at any given time, whilst the others remain idle and do not waste power. Parallel systems are popular in sub-stations of distribution transformers and in process industries with pump and compressor plant. The individual machine duties are functions of both the external load and the internal control of the choice of the machines that are selected to meet the demand. Therefore, a greater scope exists for a control of the utilisation of the machinery, than in a single machine system.

This thesis is concerned with investigations into the latter methods of energy saving. It provides analytical methods by which the sizing of single, and both the sizing and control of parallel machine drives can be fitted to the load duty. The term 'machine drives' refers to induction motors, centrifugal pumps and transformers within the thesis. However, the theory is equally applicable to any form of electrical or mechanical machinery, where a simple efficiency curve can be used to describe its operation and where the losses are uniquely related over a range of machine sizes.

The load duties are modelled as stochastic distributions[11] as apposed to deterministic load time curves. This provides a greater flexibility in the analysis, since the only knowledge required of the load is its range and distribution of values. This may be further simplified to just a specification of the load's mean and variance, by taking a mathematical function to describe the distribution.

The machine sizing and parallel control are optimised with respect to cost functions equal to the energy consumed or losses in the drive, which were obtained from the efficiency characteristics of the machines. In principle, however, the cost function could be extended to include external effects, such as copper loss in the cabling to the machine drive. In this instance, it may be beneficial to use a function based upon an efficiency-power factor product, rather than pure efficiency.

The utilisation of machinery on an efficiency basis can imply that a drive rated at less than the maximum load should be used[7], which will be subject to short periods of overload. These overloads could well reduce the working life of the drive, with an associated cost penalty which must be weighed against the potential energy savings of the scheme. As a result, the third chapter of the thesis is devoted to an ageing analysis of induction motors or transformers, based upon the simple stochastic load model.

The ageing of electrical machines can be confined to the thermal deterioration of the insulation in their windings[12]. Electrical machines have a complex thermal structure and several different materials and cooling methods are incorporated in their design. In general a single RC thermal model[9] will not be sufficient to determine the necessary insulation temperatures to produce an accurate ageing analysis. Because of this, the work utilises a

multi-nodal thermal model of the machines in the ageing analysis. A detailed study of this type of model is provided in the latter part of the thesis, where it is applied to a 5.5kW TEFC cage induction motor.

The loss and ageing analysis for single and parallel machine drives are individually illustrated by results obtained from hypothetical systems. A complete cost optimisation is not presented, because it was not possible, within the time scale of the project, to expand the thermal model and ageing work to an analysis that holds for a range of machine sizes which complements the loss formulae.

An industrial case study of a multi-machine system was performed on a pumping station at Bass brewery, Runcorn. The switching control theory was applied to four parallel induction motor driven pumps and an assessment was made on the available energy savings. This case study is presented in Chapter 4.

Chapter 5 covers the details of the thermal model of the induction motor. Its accuracy is tested against experimental measurements taken from load tests on the motor in the following chapter.

Finally an offshoot of the work, which is also described in Chapter 6, was the development of a micro-processor based, thermal prediction device for the induction motor. The thermal model of the machine had a simple and compact mathematical form and could estimate the motor's temperatures from monitoring only the phase voltage and

current conditions. This implied that it should be possible to install the model into a simple microprocessor based device that could perform the thermal calculations in real time. Such a thermal prediction device could provide information to the type of control and ageing algorithms presented in the main body of the thesis.

A further application of the thermal prediction device is in motor protection. This useage is timely since a number of electronic protection devices [13,14] are now appearing on the market. These units use either analogue or microprocessor based circuits to monitor the terminal conditions of the induction motors and detect fault conditions of excessive currents or phase imbalance. They also provide overload protection by using simple RC or I^2t formulation of motor's thermal performance. The device proposed in this thesis is likely to give a more accurate assessment of the thermal performance of the machine and its software can be simply extended to include basic supply protection algorithms.

These devices have a number of advantages over the conventional technique of mounting thermistors in the machine windings, two of which are that they can be mounted anywhere on the machine supply lines without requiring additional cooling and can be fitted on a retrofit basis. A microprocessor based unit that contains a full thermal model can also estimate the temperatures at inaccessable areas in the machine. The 'intelligence' of the microprocessor can be exploited by a program that is able to predict future temperatures in the motor. This would be

accomplished by performing the thermal calculations at a faster rate than real time, given that the future load remains at a certain value. This facility would be useful in complex machine control, or in the relability assessment of motors mounted in remote or inaccessible locations.

CHAPTER 2

LOAD MODEL AND LOSS MINIMISATION

2.1 INTRODUCTION

This chapter develops the necessary mathematics to obtain machine sizing and system control parameters that will minimise the energy consumed by a number of prime movers that provide a known stochastic system load.

Initially methods are introduced by which the system load and the losses in the machinery are modelled. The simple case of a single machine providing the load is then analysed, and a result is obtained from which the optimum sizing of the machine can be determined from the load parameters. The final section deals with the analysis of a multi-machine system[15], where a number of prime movers are operated mechanically in parallel to provide the demanded load. The energy consumption is minimised by variation in the control of the power intervals, at which individual machines are switched, and the sizing of the machines. A direct solution is given for the optimum control switching limits and a numerical method is determined by which the machine sizing can be optimised.

2.2 STOCHASTIC SYSTEM LOADS

A system load may be defined exactly as a set of data or a graph, which may give the power output of a motor measured at short intervals over a period of time. Often, such detailed information of the load is not available and the case considered in this work is where there is only a statistical knowledge of the load. Here, at a given time the output power of the motor is not known, but the chances of it being a particular value are known.

The system load can be defined as a variable $W_s(t,\zeta)$ over a time period T and is bounded in value between zero and some maximum load W_{smax}.

$$\text{System Load} \doteq W_s(t,\zeta) \quad 0 \leqslant t \leqslant T \qquad (2.1)$$

$$0 \leqslant W_s \leqslant W_{smax}$$

In this definition $W_s(t,\zeta)$ represents an ensemble of all time records, a particular record ζ (itself a random variable) referring to a single time record. For example, if the system load is the power being consumed by an average household, then the record ζ may be the fact that a film is on the television, and the time t may be the start of an advertisement break.

A load W_s can only be defined for all times t, if the sequence of events ζ describing a particular load-time distribution is known. Different events will lead to different load-time distributions.

The loading of a system is defined as a stochastic process if the load $W_s(t,\zeta)$ is a random variable for every time t in the period T, over which the load is present. A system probability density function $p(W,t)$ is used to define the probability of any load W occurring at time t, for all events ζ, and is expressed as:

$$p(W,t) = P\ (W_s(t,\zeta) = W/all\zeta) \qquad (2.2)$$

The probability density function can be used to calculate the expected value of an arbitary function $f(W)$ of the load at a given time t, which in standard notation is written as:

$$\varepsilon\{f(W_s(t))\} = \int_0^{W_{smax}} f(W)p(W,t)dW \qquad (2.3)$$

Equation (2.3) can be used, for instance, to give the expected losses in a system at a time t, where $f(W)$ would be the function that defines the losses in terms of the load. Alternatively the equation can be applied to give simply the load's mean and variance.

The stochastic mean $\mu_w(t)$ of the system load is defined as the expected value of the load W_s at time t, whereas the variance $V_w(t)$ is the expected value of the square of the deviation of the load from the mean. These are written as:

$$\mu_w(t) = \varepsilon\{W_s(t)\} = \int_0^{W_{smax}} Wp(W,t)\,dW \qquad (2.4)$$

$$V_w(t) = \varepsilon\{(W_s(t) - \mu_w(t))^2\}$$

$$= \varepsilon\{W_s(t)^2\} - 2\mu_w(t)\varepsilon\{W_s(t)\} + \mu_w(t)^2$$

$$= \int_0^{W_{smax}} W^2 p(W,t)\,dW - \mu_w(t)^2 \qquad (2.5)$$

Here the event symbol ζ has been dropped, this is because these equations, as with the system probability density functions, are defined over all events.

When considering the energy requirements of the stochastic load system, a time average over the period T of the mean system load will be required. The time average will, itself, be a random variable with its own particular probability density function $p_T(W)$, where:

$$p_T(W) = \frac{1}{T}\int_0^T p(W,t)\,dt \qquad (2.6)$$

The expected value of the time average of a function $f(W)$ of the load can be found directly from this probability distribution, since:

$$\varepsilon\{\frac{1}{T}\int_0^T f(W_s(t))dt\} = \int_0^{W_{smax}} \frac{1}{T}\int_0^T f(W)p(W,t)\,dt\,dW$$

$$= \int_0^{W_{smax}} f(W)p_T(W)\,dW \qquad (2.7)$$

In the case where f(W) gives the system losses, then Equation (2.7) will yield the average loss during the period T and the total energy loss will be T times this average.

Equation (2.7) can be applied because the energy consumed by the system is not influenced by the actual time a particular load occurs, but depends only upon the frequency of occurrence of that load. Thus a knowledge of the time average probability function $p_T(W)$ is all that is required for an analysis of the load control with the aim of optimising the system energy consumption.

In the next chapter however, the thermal ageing of the system machinery is considered. For this analysis, the machine ageing not only depends upon the load, but also the load history, and it becomes necessary to introduce assumptions of stationarity to simplify the analysis.

A stochastic load system is stationary if the load probability density function p(W,t) is independent of the time t, which suggests that a given value of load has an equal probability of occurring at any time within the load period, thus:

$$p(W,t) = p_s(W) \tag{2.8}$$

where $p_s(W)$ is the stationary density function, and also from Equation (2.6):

$$p_T(W) = p_s(W) \tag{2.9}$$

Hence in a stationary system, the load can be represented entirely by a single probability density function.

The probability density functions $p_T(W)$ and $p_s(W)$ are modelled by βeta [16] functions:

$$p_T(W) = \frac{1}{B(p,q)} W^{p-1} (W_{smax}-W)^{q-1} \qquad (2.10)$$

where

$$B(p,q) = \int_o^{W_{smax}} W^{p-1}(W_{smax}-W)^{q-1} dW$$

These bounded functions gave a good match with load distribution found in practice and were easy to use since their higher moments could be found directly from tables. The means and variances of the distributions are determined by the indices p and q, such that:

$$\text{Mean} \quad \mu_T = \frac{p}{p+q} W_{smax} \qquad (2.11)$$

$$\text{Variance} \quad V_T = \frac{pq}{(p+q)^2(p+q+1)} W_{smax}^2$$

2.3 LOSS FUNCTION

The losses in a particular electrical or mechanical machine, which is providing a load W, can be determined by using a dimensionless loss function $\gamma_r(W)$. The loss function, in a similar manner to that of an efficiency characteristic, defines the losses in the machine as a proportion of the output power, such that:

$$\text{Losses} = W\gamma_r(W) \tag{2.12}$$

Often a relationship will exist between the loss function of a set of geometrically similar machines, which can be expressed in terms of a sizing factor α. The sizing factor α relates the size of any machine within the series to that of a reference machine, such that the rated power output of the machine will be α times the rating of the reference. The loss functions of the series then can be written as:

$$\gamma(\alpha,W) = \alpha^{-\beta}\gamma_r(W/\alpha) \tag{2.13}$$

where

$\gamma(\alpha,W)$ = loss function for machine size α in terms of its output power W

$\gamma_r(W/\alpha)$ = loss function of reference machine with argument referred to W

β = similarity index

The similarity index β determines the rate at which the percentage losses reduce, or the efficiencies increase, as the machines become larger.

The geometrical conditions required for Equation (2.13) to apply and the value of the sizing index β will vary depending upon the type of machine considered. For electrical machinery, such as induction motors and transformers, the equation will apply to a series of machines

that are of indentical electrical design and that have a geometrically proportional magnetic circuits. Whereas for a series of centrifugal pumps, the conditions are that the pumps have a set of similarly designed impellers.

For simplicity, the reference loss function $\gamma_r(W)$ is assumed to be of the quadratic form:

$$\gamma_r(W) = \frac{a}{W} + b + \frac{W}{c} \qquad (2.14)$$

This approximation holds particularly well with electrical machinery.

In Equation (2.14) the parameters a, c have dimensions of power, whereas parameter b is dimensionless. When the equation is applied to a transformer, for example, the a term will give the majority of the machine's core losses; the proportional b term will be zero; and the quadratic c term will give it's copper, iron and remaining core losses. The evaluation of these parameters and the similarity index β for a series of TEFC cage induction motors and a series of centrifugal pumps are given in Appendices A1. and A2.

2.4 SINGLE MACHINE

The size of a single machine providing a known load can be optimised such that the energy losses in the machine are minimised. By introducing a stochastic load, as defined in Section 2.2, this optimisation can be achieved solely from the load's time average density distribution

$p_T(W)$. The assumption of a quadratic machine loss function can be shown to imply that only a knowledge of the mean and variance of this distribution is required.

Using the notation of the previous sections, the mean energy loss in a machine sized α can be given by:

$$\text{Energy loss } L = \tilde{T} \int_0^{W_{smax}} W\gamma(\alpha,W)\, p_T(W)\, dW \qquad (2.15)$$

The loss function $\gamma(\alpha,W)$ is a well behaved convex function, hence the losses can be minimised by setting the partial deviative of L with respect to the machine size α to zero.

$$\frac{\partial}{\partial\alpha} T \int_0^{W_{smax}} W\gamma(\alpha,W)\, p_T(W)\, dW = 0 \qquad (2.16)$$

Substituting the quadratic loss function of Equations (2.13) and (2.14) into the above gives:

$$\frac{\partial}{\partial\alpha} T \int_0^{W_{smax}} W\alpha^{-\beta}\left[\frac{a\alpha}{W} + b + \frac{W}{c\alpha}\right] p_T(W)\, dW = 0 \qquad (2.17)$$

Hence:

$$\frac{\partial}{\partial\alpha} T \int_0^{W_{smax}} \left[a\alpha^{1-\beta} + b\alpha^{-\beta} W + \frac{W^2}{c}\alpha^{-(\beta+1)}\right] p_T(W)\, dW = 0 \qquad (2.18)$$

Evaluating the partial derivative yields:

$$\int_0^{W_{smax}} \left[a(1-\beta)\alpha^{-\beta} - b\beta\alpha^{-(\beta+1)} - (\beta+1)\alpha^{-(\beta+2)}\frac{W^2}{c}\right] p_T(W)\, dW = 0 \qquad (2.19)$$

Multiplying through by $\alpha^{(\beta+2)}$ and re-arranging gives:

$$a(1-\beta)\alpha^2 \int_o^{W_{smax}} p_T(W)dW - b\beta\alpha \int_o^{W_{smax}} W p_T(W)dW - \frac{(\beta+1)}{c} \int_o^{W_{smax}} W^2 p_T(W)dW = 0 \quad (2.20)$$

Probability theory identifies the integral of $p_T(W)$, $Wp_T(W)$ and $W^2 p_T(W)$ as being equal to unity, the mean time average load μ_T and the expected average of the square of the load respectively. Equation (2.20) evaluates the latter in terms of the mean μ_T and variance V_T of the time average load density function, such that:

$$\varepsilon\{\frac{1}{T}\int_o^T W_s(t)^2 dt\} = \int_o^{W_{smax}} W^2 p_T(W)dW = V_T + \mu_T^2 \quad (2.21)$$

Equation (2.20) thus becomes:

$$a(1-\beta)\alpha^2 - b\beta\alpha\mu_T - \frac{(\beta+1)}{c}(V_T + \mu_T^2) = 0 \quad (2.22)$$

This equation can be solved directly for the positive root α, by using the standard quadratic solution.

$$\alpha = \frac{1}{2a(1-\beta)}\sqrt{b^2\beta^2\mu_T^2 + \frac{4a}{c}(1-\beta^2)(V_T + \mu_T^2)} - \frac{b\beta\mu_T}{2a(1-\beta)} \quad (2.23)$$

Equation (2.23) can be used to select the most efficient size of machine for a known stochastic load, To illustrate this sizing optimisation a series of TEFC cage induction motors were considered.

The motors were all 4 pole, 3 phase, IP44 machines with a range of powers from 5.5 to 22kW. An 11kW motor was used as a reference motor and had the loss function (see Appendix A1):

$$\gamma(\alpha,W) = \alpha^{-0.25}\left(\frac{0.757}{W} + \frac{W}{118.3}\right) \qquad (2.24)$$

where W is the machines output power in kilowatts. The losses of the other machines in the series calculated from Equation (2.24) are compared with the manufacturers data at $\frac{1}{2}$, $\frac{3}{4}$ and full load are given in Table 2.1. It can be seen that the results developed from the loss function agree within approximately 10 per cent of manufacturers data. However this agreement was difficult to quantify exactly, as the manufacturers data, which was derived from efficiency figures given to the nearest percent, were only accurate in the losses to around 8 per cent.

Three load distributions were considered, each with Beta distributions and a maximum load of 18kW, with means of 6, 9 and 12kW. The load distributions and their parameters are given in Figure 2.1. The results of applying the size optimisation Equation (2.23) to these loads are given in Table 2.2, Also in the table, the losses calculated from Equation (2.15) of the optimum motors are compared with those of machines selected from the motor series.

For a maximum load of 18kW, a conservative method of machine selection would at least choose an 18.5kW, and possibly a 22kW motor. However, as the results show, the

loads with a low mean can result in up to a 16% saving in the losses with respect to using the 18.5kW machine. This saving would be equivalent to a 3% reduction in the total system energy consumption, which in this example amounts only to a few watts, but when applied to transmission transformers may amount to several Megawatts over the country.

To achieve these savings it is necessary to overload the motors for short periods of time and clearly the effects of these overloads on the machine's life must be taken into account and included in the overall cost equation [9]. In the example, the use of a 11kW motor to provide the 6kW mean load would require the machine to be overloaded up to 1.6 times its rating, an overload which may well be impractical. The assessment of such overloads on a machine's life is the purpose of the work in Chapter 3.

2.5 MULTI-MACHINE SYSTEM

In this section the efficiency optimisation of the multi-machine system, where geometrically similar machines are operated with their outputs connected mechanically or electrically in parallel, is considered. In the system, the machines are controlled purely by switching them on or off, such that at any time the number of machines that are running will depend upon the system load. Thus, for example where there is a small load only one machine will be running and as the load increases additional machines will be

switched on to meet the rising demand. Multi-machine systems of this type can be found in many applications including electrical transmission where distribution transformers are operated in parallel and process industries where pumps are often paralleled.

A system is defined where n machines are used in parallel to provide a load over a time period T. A machine's position i refers to the location of the machine within the order of switching and remains constant throughout the load period. The machine in position 1 will always be running when there is a system load present and the next machine to be switched on with an increase in load will be in position 2. The switching limit $W_{\ell i}$ is defined as the load at which the machine in position i+1 is switched, such that when the system load is equal to $W_{\ell i}$, the machines in position 1 to i will be running and as the load increases past $W_{\ell i}$ the additional machine will be switched on. Conversely, as the system load decreases through $W_{\ell i}$ the machine in position i+1 will be switched off.

In this multi-machine system the overall system losses will depend upon the two sets of independent variables, the machine sizes α_i and the control switching limits $W_{\ell i}$. The method of analysis used is similar to that of the single machine problem, using stochastic load modelling. Assuming that the load is shared in proportion to the machines' individual sizes or ratings, the overall system energy loss L can be written as:

$$L = T \sum_{i=1}^{n} \int_{W_{\ell i-1}}^{W_{\ell i}} p_T(W) \sum_{j=1}^{i} \gamma(\alpha_j, k_{ji}W) k_{ji} W \, dW \qquad (2.25)$$

where k_{ji} is the load sharing factor

$$k_{ji} = \alpha_j / \sum_{m=1}^{i} \alpha_m \qquad (2.26)$$

The loss function $\gamma(\alpha,W)$ is the function defined in the previous section and the switching limits $W_{\ell n}$, $W_{\ell 0}$ are the upper and lower limits of the system load, equal to W_{smax} and zero respectively.

The energy losses L can be minimised with respect to the machine sizes α_i and switching limit $W_{\ell i}$, by setting the partial derivative of L to each of these independent variables to zero. It can be shown that direct solutions to the optimum switching limits are available, but numerical methods are required to obtain the best machine sizes.

Denoting the required switching limit as $W_{\ell r}$, for r between 1 and n-1, then

$$\frac{\partial L}{\partial W_{\ell r}} = \frac{\partial}{\partial W_{\ell r}} T \sum_{i=1}^{n} \int_{W_{\ell i-1}}^{W_{\ell i}} p_T(W) \sum_{j=1}^{i} \gamma(\alpha_j, k_{ji}W) k_{ji} W \, dW \qquad (2.27)$$

The R.H.S of Equation (2.27) can be expanded into two integrals between 0 and $W_{\ell i}$, and 0 and $W_{\ell i-1}$. The terms in the summations that do not contain $W_{\ell r}$ can then

be discarded, as their partial derivatives will be zero. This yields:

$$\frac{\partial L}{\partial W_{\ell r}} = \frac{\partial}{\partial W_{\ell r}} T \int_{o}^{W_{\ell r}} p_T(W) \sum_{j=1}^{r} \gamma(\alpha_j, k_{jr} W) k_{jr} W dW \qquad (2.28)$$

$$- \frac{\partial}{\partial W_{\ell r}} T \int_{o}^{W_{\ell r}} p_T(W) \sum_{j=1}^{r+1} \gamma(\alpha_j, k_{jr+1} W) k_{jr+1} W \, dW$$

The partial differentiation can now be performed, to give:

$$\frac{\partial L}{\partial W_{\ell r}} = T p_T(W_{\ell r}) \sum_{j=1}^{r} \gamma(\alpha_j, k_{jr} W_{\ell r}) k_{jr} W_{\ell r} \qquad (2.29)$$

$$- T p_T(W_{\ell r}) \sum_{j=1}^{r+1} \gamma(\alpha_j, k_{jr+1} W_{\ell r}) k_{jr+1} W_{\ell r}$$

The setting of the partial derivative to zero, will yield the switching limit $W_{\ell r}$, that minimises the losses, in the equation:

$$\sum_{j=1}^{r} \gamma(\alpha_j, k_{jr} W_{\ell r}) k_{jr} = \sum_{j=1}^{r+1} \gamma(\alpha_j, k_{jr+1} W_{\ell r}) k_{jr+1} \qquad (2.30)$$

The solution of Equation (2.30) will give the optimum switching limits $W_{\ell r}$, for r=1 to n-1, in terms of the machine sizes α_i. The particular case where all n machines are of equal size α is covered in Reference (15) where Equation (2.30) reduces to:

$$\gamma(\alpha, \frac{W_{\ell r}}{r}) = \gamma(\alpha, \frac{W_{\ell r}}{r+1}) \qquad (2.31)$$

This has the simple solution, for the quadratic form of loss function in Equation (2.14) of:

$$W_{\ell r} = r\sqrt{\frac{r+1}{r} ac} \qquad (2.32)$$

The solutions of Equations (2.30) and (2.31) are intuitively the results that would be expected. The r th optimum switching limit is at a power level where the losses of r machines became equal to those of r+1. However, they demonstrate that the optimum switching limits are independent of the system load. Thus given any multi-machine system a set of switching limits can be obtained that will minimise the system losses whatever the system load. Providing these limits do not require excessive overloads on the machinery, this theory can be applied directly to any existing system without further analysis, simply by resetting the switching controller. Chapter 4 examines an industrial multi-machine system and shows that changes in the switching limits can result in energy savings of several percent.

Unfortunately, the optimum switching limits are no longer independent of the load when the losses are minimised by variation of both the machine sizing and the switching limits. For this problem a direct analytical solution cannot be obtained, and a 'Newton-type descent' numerical method [17] has to be employed.

The system losses can be expressed as a function of the machine size only, by repeatedly applying Equation (2.30). Denoting the set of machine sizes α_i as the vector $[\alpha^{(k)}]$, during the kth interation of the numerical method, and the system losses as $L([\alpha^{(k)}])$; then the basis of the loss minimisation is to find successive values of $[\alpha^{(k)}]$ such that:

$$L([\alpha^{(k+1)}]) < L([\alpha^{(k)}]) \qquad (2.33)$$

until the machine sizes converge to the optimum values within a specified accuracy.

On each iteration, a descent method calculates a direction of search vector $[\xi^{(k)}]$ and a positive step length $\delta^{(k)}$, which are used to obtain the next sizing vector $[\alpha^{(k)}]$ from:

$$[\alpha^{(k+1)}] = [\alpha^{(k)}] + \delta^{(k)}[\xi^{(k)}] \qquad (2.34)$$

The search vector $[\xi^{(k)}]$ is determined from derivative information of L computed in the immediate neighbourhood of $[\alpha^{(k)}]$. The step lengths $\delta^{(k)}$ must be chosen to obtain a new loss $L([\alpha^{(k+1)}])$ which is sufficiently lower than the previous loss to guarantee a good convergence of the method. The Taylor expansion at $L([\alpha^{(k)}] + [\xi^{(k)}])$ about the vector $[\alpha^{(k)}]$ yields:

$$L([\alpha^{(k)}] + [\xi^{(k)}]) = L([\alpha^{(k)}]) + [g^{(k)}][\xi^{(k)}] + \tfrac{1}{2}[\xi^{(k)}]^T[G^{(k)}][\xi^{(k)}] + O||[\xi^{(k)}]||^3 \qquad (2.35)$$

where $[g^{(k)}]$ and $[G^{(k)}]$ are the gradient and Hessian matrices of L, evaluated at the point $[\alpha^{(k)}]$. Neglecting terms of $|||[\xi^{(k)}]|||^3$ and above, Equation (2.35) becomes a quadratic approximation to $L([\alpha^{(k)}] + [\xi^{(k)}])$. For the loss minimisation process, the Hessian matrix $[G^{(k)}]$ is positive definite. and the quadratic approximation will have a minimum when :

$$[G^{(k)}][\xi^{(k)}] = -[g^{(k)}] \qquad (2.36)$$

Equation (2.36) can be solved for the search vector $[\xi^{(k)}]$ by using a Cholesky decomposition on the Hessian matrix. In this method the matrix is expressed as a product of a lower and upper triangular matrices. Because the Hessian matrix is symmetrical, the lower triangular matrix will be the transpose of the upper, hence:

$$[G^{(k)}] = [U^{(k)}]^T[U^{(k)}] \qquad (2.37)$$

and:

$$[U^{(k)}]^T[U^{(k)}][\xi^{(k)}] = -[g^{(k)}] \qquad (2.38)$$

The above can be reduced to the two linear equations:

$$[U^{(k)}]^T[z] = -[g^{(k)}] \qquad (2.39)$$

$$[U^{(k)}][\xi^{(k)}] = [z] \qquad (2.40)$$

which can be solved for $[\xi^{(k)}]$ by direct forward and then backward substitutions.

In summary, the numerical method involved the calculation of a search direction vector $[\xi^{(k)}]$ at each step of the iteration. This vector was obtained from the gradient and Hessian matrices of the loss Equation (2.25), by using a Cholesky decomposition as outlined in Equations (2.37) to (2.40). The gradient and Hessian matrices were developed from the loss equation by using the optimum switching limits Equation (2.30) and the partial derivatives:

$$[g] = \frac{\partial L}{\partial [\alpha]} + \frac{d[W_\ell]}{d[\alpha]} \frac{\partial L}{\partial [W_\ell]} \tag{2.41}$$

$$[G] = \frac{\partial^2 L}{\partial [\alpha]^2} + \frac{d[W_\ell]}{d[\alpha]} \frac{\partial^2 L}{\partial [W_\ell]\, \partial [\alpha]} \tag{2.42}$$

$$+ \frac{\partial^2 L^T}{\partial [W_\ell]\, \partial [\alpha]} \frac{d[W_\ell]^T}{d[\alpha]} + \frac{d[W_\ell]}{d[\alpha]} \frac{\partial^2 L}{\partial [W_\ell]^2} \frac{d[W_\ell]^T}{d[\alpha]}$$

Equation (2.41) was reduced further, since the requirement of optimum switching limits are that $\partial L/\partial [W_\ell]$ should be zero, thus:

$$[g] = \frac{\partial L}{\partial [\alpha]} \tag{2.43}$$

Appendix A3 gives a detailed evaluation of these matrices using the quadratic loss function of Equations (2.13) and (2.14).

After obtaining the search vector, the next set of machine sizes were found from equation (2.34), with a value of step length $\delta^{(k)}$ chosen for the required working accuracy.

A computer program was used to optimise the machine sizes and switching limits for a number of loads. In this program the loss equation and the gradient and Hessian matrices were normalised by evaluating the machine sizes and switching limits as per unit values to the base of the maximum system load W_{smax}. The base machine of the loss function was also taken as a theoretical machine rated at W_{smax}. The load frequency distribution was assumed to be the Beta distribution of Equation (2.9) and the integrals of the load between the switching limits were calculated at each stage using Simpsons rule.

The step length $\delta^{(k)}$ was chosen in this program such that the maximum change in any of the machines sizes would be less than some constant ε, then:

$$\delta^{(k)} = \frac{\varepsilon}{\xi_{max}(k)} \qquad (2.44)$$

where $\xi_{max}{}^{(k)}$ was the maximum element of the search vector $[\xi^{(k)}]$. With a value of ε selected such that the machine sizes would be calculated to 3 significant figures, the program was found to converge to the minimum loss within 50 interations.

An imaginary system that uses parallel induction motor to provide a mechanical load is considered here to illustrate the energy savings that are available from a loss optimisation of electrical machines. In the next section a total optimisation is applied to an industrial based

pumping station,where both centrifugal pumps and their driving induction motors are fitted to the load.

The set of induction motors used in the analysis of Section 2 were fitted to load with a maximum value of 22kW, and a mean and deviation of 7.9kW and 4.6kW respectively. The results of the analysis are presented in Table 2.3. Here the optimised machine sizing and switching requires two machines and is compared with the use of four, three and single machines at both rated and optimum switching limits.

From the table it can be seen that the available savings in energy are only in the order of one percent in the efficiency, which is equivalent to an 9% reduction in the losses. The application of the optimum switching limits has little effect and the main improvements are achieved from the selection of the machine sizing. For this particular load the second of the optimum pair of machines will be running for only 10% of time and thus there is little improvement over a correctly selected single machine. However the single machine will have to sustain overloads of up to 58%, whereas the first machine of the optimum pair will be overloaded by 23%.

2.6 TOTAL PUMP SYSTEM LOSS OPTIMISATION

In Chapter 4 the application of the switching limit optimisation to an industrial multi-machine system is discussed in detail. These results are briefly extended here to illustrate a total machine size and switching limit optimisation.

Four centrifugal pumps were operated in parallel to provide a varying flow of fluid. The system demand on the pumps was a specific flow of fluid, because of this the analysis referred the pump loss function $\gamma(\alpha,Q)$ and switching limits $Q_{\ell i}$ to this flow Q rather than the pump output powers. The pumping station performance was modelled and optimised on the computer and the results were presented in per unit qualities to the bases of the maximum flow 928 m^3/hr and output power 100kW, of the station.

The system flow demand was modelled with a βeta distribution which had a mean of 0.36 p.u. and a deviation of 0.21 p.u. This was equivalent to the load present during the first week of measurements in Chapter 4. The pump loss functions, Appendix A2, were derived from a reference machine with a rating of 1.0 p.u. and are given by:

$$\gamma(\alpha,Q) = \alpha^{-0.1}\left(\frac{0.84\alpha}{Q} - 1.31 + \frac{Q}{1.31\alpha}\right) \qquad (2.45)$$

such that $Q\gamma(\alpha,Q)$ gives the pump's losses in per unit to the base of 100kW.

Three sets of pumps and switching limits were analysed. The first had four pumps that were equally sized and switched at their ratings of 0.25 p.u., the second had the same pumps switched at the optimum limits and the final set had machines that were optimised both in size and switching. In each case the pump losses were evaluated

by performing the integration in Equation (2.25). The pump output powers were obtained from a similar integration with the loss function replaced by a head function $H(\alpha,Q)$, which described the pump output head in terms of its flow. A quadratic approximation to the head function was used, where:

$$H(\alpha,Q) = \left(-\frac{0.26\alpha}{Q} + 2.02 - \frac{Q}{1.31\alpha}\right) \qquad (2.46)$$

and $QH(\alpha,Q)$ gives the pump output power in per unit at flow Q.

The head function does not include a sizing index, as the pumps were assumed to have geometrically similar impellers and hence have proportionately identical head characteristics. A more detailed discussion on the approximation of a quadratic head function is contained in Chapter 4.

The results for the three sets of pumps are shown in Table 2.4. Here, the loss figures are given in per unit to the 100kW power base and are equivalent to the average energy loss over the entire period of the load. The output power of the pumping station decreases with the optimisation, since the minimum available head reduces as the machines are loaded more heavily.

The switching limit optimisation can be seen to give a 17 per cent reduction in the losses, whereas the inclusion of the sizing optimisation extends the loss savings to 23 per cent. These savings are reflected in proportionally smaller increases in the system efficiency, due to

the fall off in the output power mentioned above.

The input power distribution $p_j(W)$ taken by the pump at position j could be obtained from the Beta load distribution p(Q), from the equations:

$$p_j(W) = \sum_{i=j}^{4} \frac{1}{k_{ji}} p_i^* \left(\frac{Q}{k_{ji}}\right) / \frac{dW}{dQ} \qquad (2.47)$$

$$W = Q(\gamma(\alpha_j, Q) + H(\alpha_j, Q)) \qquad (2.48)$$

the load sharing factor:

$$k_{ji} = \frac{\alpha_j}{\sum_{m=1}^{i} \alpha_m}$$

and the positional load distributions:

$$p_i^*(Q) = p(Q), \; Q_{\ell i-1} \leqslant Q < Q_{\ell i} \qquad (2.49)$$

$$= 0, \; Q < Q_{\ell i-1}, \; Q \geqslant Q_{\ell i}$$

Individually sized induction motors were fitted to the third set of pump input distributions, again on the criterion of maximum efficiency. In Table 2.5, the positional distribution means and deviations are listed together with the appropriate sizing of induction motor, selected in the manner described earlier in this chapter. The estimated percentage running time of each pump is also given in the table. The final result of this optimisation

is compared in Table 2.6 against the rated motor-pump sets described in Chapter 4.

The analysis demonstrates that a power saving of 5.4kW in the losses can be achieved in the pumping station, equivalent to an 8 per cent reduction in the original plant power consumption (a further 8 per cent drop in the input occurs from the loss of system head).

The above has outlined briefly the steps involved in applying the mathematics of this chapter to an actual machine system and illustrates the possible energy savings. Before any plant is commisioned for a known load other practical considerations will need to be taken into account. Care must be taken to ensure that the overloading of the pumps, implied in the optimum switching limits, would not damage the machines or that the resultant drop in head is not detrimental to the performance of the plant load. The pump and induction motor sizes can only be selected from those available in the manufacturer's product range and several sizings may have to be modelled to obtain a best fit to the optimum. A more rigorous consideration of these details is available in Chapter 4.

Table 2·1 Comparison of Losses in a Series of 4 Pole TEFC Cage Induction Motors

Frame Size	Rating kW	1/2 Load † %	1/2 Load * %	3/4 Load † %	3/4 Load * %	Full Load † %	Full Load * %
D132S	5·5	20	21	19	19	20	19
D132M	7·5	22	20	19	18	19	18
D160M	11	18	18	16	16	16	16
D160L	15	16	17	14	15	14	15
D180M	18·5	15	16	14	14	14	14
D180L	22	14	15	12	14	12	14

† = Manufactures data.
(Brook Crompton Parkinson Motors)

* = Losses calculated from loss function based on the 11kW machine.

Table 2·2 Single Motor Losses for Example Load Distributions

		Load Distribution ①	②	③
Load Mean kW		6·0	9·0	12·0
Optimum Size kW		9·7	14·2	18·6
Motor Losses kW	Optimum	1·10	1·47	1·80
	11 kW	1·11	1·52	2·05
	15 kW	1·20	1·47	1·84
	18·5 kW	1·31	1·52	1·80
	22 kW	1·42	1·59	1·82

Table 2·3 Induction Motor Parallel Drive Optimisation

Number of Machines		Four Rated	Four Optimum	Three Rated	Three Optimum	Two Optimum	One
	α_1	5·5	5·5	7·3	7·3	11·8	13·9
Machine	α_2	5·5	5·5	7·3	7·3	13·6	
Size kW	α_3	5·5	5·5	7·3	7·3		
	α_4	5·5	5·5				
Switching	W_{l1}	5·5	6·7	7·3	8·9	14·6	
Limits	W_{l2}	11·0	11·6	14·5	15·4		
kW	W_{l3}	16·5	16·4				
Losses kW		1·56	1·55	1·49	1·48	1·42	1·43
Efficiency %		83·5	83·6	84·1	84·2	84·8	84·7

Load Mean :- 7·9 kW
Deviation:- 4·6 kW

Table 2·4 Pump Parallel Drive Optimisation

Case		①	②	③
Pump Size p.u.	α_1	0·25	0·25	0·103
	α_2	0·25	0·25	0·154
	α_3	0·25	0·25	0·182
	α_4	0·25	0·25	0·215
Switching Limits p.u.	Q_{l1}	0·25	0·398	0·182
	Q_{l2}	0·5	0·689	0·376
	Q_{l3}	0·75	0·974	0·598
Losses p.u.		0·204	0·170	0·156
Output Power p.u.		0·386	0·337	0·333
Input Power p.u.		0·590	0·507	0·489
Efficiency %		65·4	66·5	68·1

Case ① Rated pumps and limits.
② Rated pumps and optimum limits.
③ Optimum pumps and limits.

p.u. base:- power 100 kW
flow 928 m^3/hr

Table 2·5 Optimum Pump Input Distributions and Driving Motor Ratings

Position	Mean Power kW (when running)	Deviation kW	Running Time %	Optimum Motor Rating kW
1	15·2	2·0	100	23
2	22·6	1·9	76	34
3	26·6	1·8	44	40
4	31·3	1·1	15	47

Table 2·6 Total Power Consumption of Pumping Station

	Rated System	Optimised System
Losses p.u.	0·272	0·218
Output Power p.u.	0·377	0·333
Input Power p.u.	0·649	0·551
Efficiency %	58·2	60·4

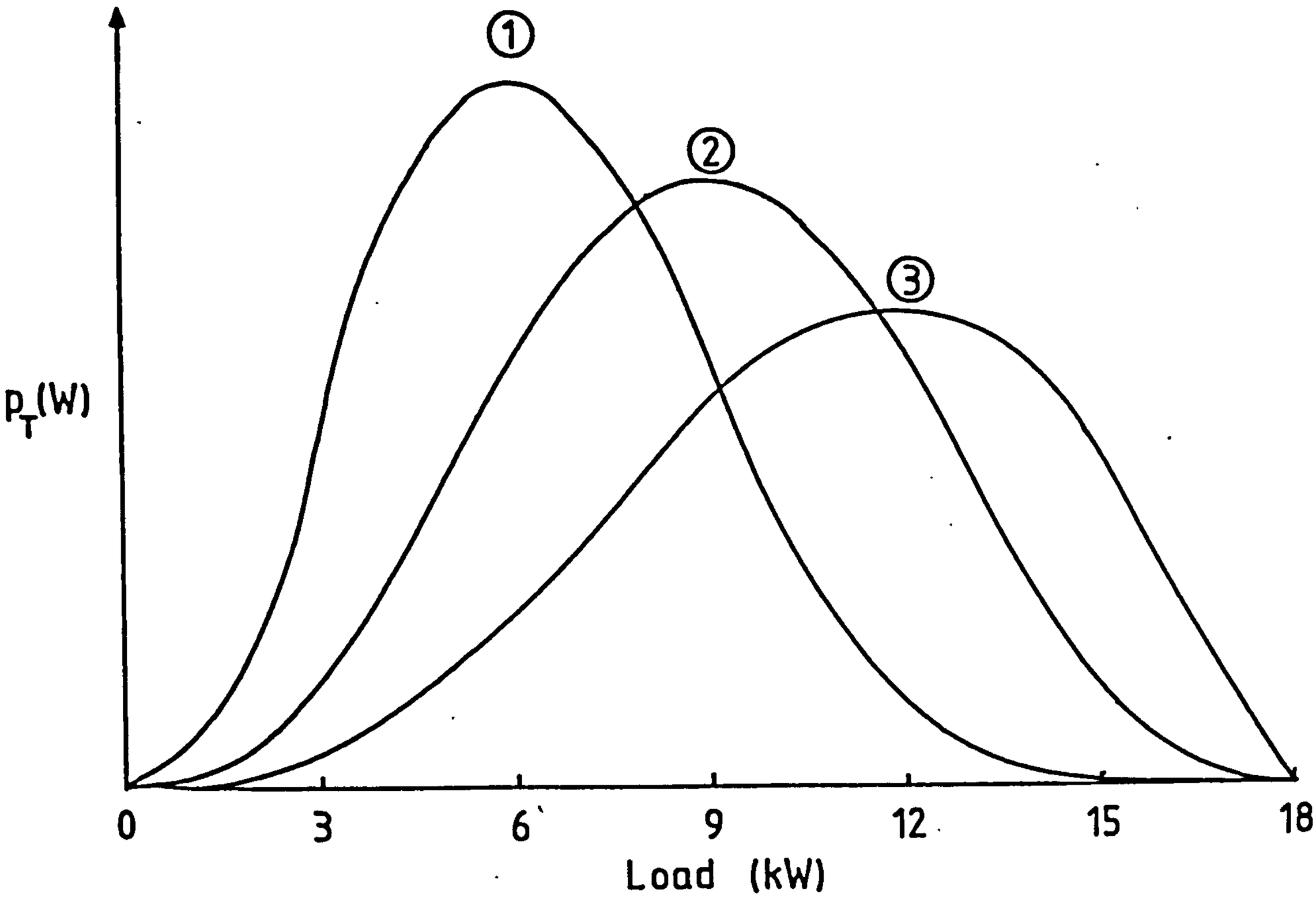

Distribution	①	②	③
Mean kW	6·0	9·0	12·0
Variance kW^2	5·8	9·0	9·6
Beta p	3·0	3·0	3·0
Parameters q	6·0	3·0	1·5

Figure 2·1 Example Load Distributions

CHAPTER 3

STOCHASTIC AGEING ANALYSIS

3.1 INTRODUCTION

The work of the previous chapter gives a method by which the energy consumption of a single and a multi-machine system can be minimised by the selection of suitably size machinery to drive the system, and in the case of the multi-machine system, by the switching limit control. Inherent in this work is that prime movers are used to a maximum extent, which could well involve running the machines above their ratings. Whenever a machine is overloaded, especially in the case of electrical machinery, an assessment must be made of the effect that the overload has upon the ageing or life expectancy of the machine. Given such information it is then possible to make an overall costing of the energy optimisation techniques, where the gains in efficiency are weighed against the possible reduction in the life of the machinery.

In this chapter a probabilistic ageing analysis is presented for the single and multi-machine stochastic load systems of the previous chapter. Throughout the work assumptions are made about the nature of the system load which enable direct solutions to the equations to be obtained.

A particular multi-machine system is considered where all the prime movers are equally rated, where it is

possible to institute a control upon each machine's ageing by changing the positional order in which they share the load. For this system, the rotational control requirements that will give minimum ageing in each machine and a control algorithm that attempts to meet them are presented. However, this algorithm does not meet the assumptions made in the original theory and it becomes necessary to use a computational deterministic method to evaluate the performance of the control. The deterministic approach also provides a method by which the validity of the assumptions made in the stochastic theory can be assessed.

Finally, results are presented for a hypothetical machine system and these are used to illustrate the theory.

3.2 AGEING OF ELECTRICAL MACHINES

The life of an electrical machine depends upon the rate of its mechanical and electrical deterioration. If maintained properly the mechanical components, such as the bearings, will generally last for the entire service life of the machine. The electrical life of the machine is influenced by the deterioration of the winding insulation due to thermal and voltage stresses.[18] Failures in the insulation are most likely to occur in the regions of the windings where there is a high electrical stress and maximum temperatures, known as 'hot spots'. For example, in an induction motor insulation failures often occur in the endwindings at positionswhere different phase coils touch or enter slots.

Since the voltage applied to the machines remain constant thoughout their lives, the life of electrical machines can be estimated from the thermal deterioration of the insulation of these high stress areas. The accepted equation for the thermal ageing of insulation is that from the work of Dakin[19,20]

$$\Gamma = (B/\Theta - A) \qquad (3.1)$$

where

Γ = expected life of insulation at temperature Θ

Θ = absolute winding temperature, K

A,B = insulation constants

The experimental confirmation of this rule has been confined to constant temperature accelerated life tests. However it is generally accepted by workers in the field[18-20,25,26] that, in the absence of evidence to the contrary, the ageing is cumulative with varying temperatures. Under these circumstances it is more convenient to use the concept of relative ageing R. Here the insulation life is expressed as a proportion of its expected life Γ_{ref} at a constant temperature Θ_{ref} such that:

$$R = \Gamma_{ref}/\Gamma \qquad (3.2)$$

and

$$\Gamma_{ref} = \exp (B/\Theta_{ref} - A) \qquad (3.3)$$

A value of unity for the relative ageing R will suggest that the winding insulation has deteriorated the same amount as if it had remained at the reference temperature throughout its life. Combining Equations (3.1) to (3.3) yields the expression for R:

$$R = \exp(B(1/\theta_{ref} - 1/\theta)) \qquad (3.4)$$

If the temperatures of the winding 'hot spots' are identified, the above equation can be used to obtain the effects of different loadings upon the life expectancy of the machine.

The overall ageing effects of a repetitive load cycle is found by integrating Equation (3.4) over the time duration T of the load cycle:

$$R = \frac{1}{T} \int_0^T \exp(B(1/\theta_{ref} - 1/\theta))dt \qquad (3.5)$$

3.3 THERMAL REPRESENTATION OF AN ELECTRICAL MACHINE

The expected life or ageing of an electrical machine can be determined from a knowledge of the thermal history of the positions of high insulation stress on the machine's windings. In order to obtain such information, it is necessary to isolate these particular points and determine their temperatures from the load history of the machine. This can be achieved by developing a thermal model of the machine.

A bulk component thermal model [21,22] is particularly suitable for such an analysis, because of its simple mathematical construction and the ease with which the areas of interest can be isolated within the model. Here the machine is considered as a complex network of thermal components. Each component is a model of a particular part of the construction of the machine, with a thermal capacitance and a heat source associated with it. A component is assumed to act as lumped body[23], which is a thermal body with a uniform temperature and a constant thermal capacitance. The heat flow between adjacent components is then taken to be uniform and depends upon their temperatures and constant values of thermal resistance. Thus, for instance, the endwinding of a machine may be considered as a seperate body, with a heat generation derived from the copper losses within the winding and connecting thermal paths to the surrounding cooling air and the slot windings.

Using the above assumptions, a linear thermal model can be constructed for any electrical machine. The number of components in the model will be determined from the complexity of the construction of the machine and must be sufficient to allow for the calculation of the temperatures at the regions of interest,to a reasonable accuracy. Such a thermal model has been applied to a three phase cage TEFC induction motor and is described in detail in Chapter 5.

The transient performance [22] of a bulk component thermal model is described by the following matrix equation:

$$[C]\ \frac{d[\theta(t)]}{dt} = [Y][\theta(t)] + [u(t)] \qquad (3.6)$$

where

[C] = diagonal matrix of the thermal capacities of each component.

[Y] = matrix of thermal admittances between adjoining components.

$[\theta(t)]$ = component temperature matrix at time t.

[u(t)] = heat generation in each component.

The component heat generations [u(t)] will be distributed out of the total loss within the machine and can be expressed as some function of the loading on the machine.

3.4 STOCHASTIC THERMAL ANALYSIS FOR A SINGLE MACHINE

Initially the case of a single machine providing a load is considered in a manner similar to the loss analysis of Chapter 2.

Equation (3.6) can be rewritten in the form:

$$\frac{d[\theta(t)]}{dt} = [A][\theta(t)] + [G][u(t)] \qquad (3.7)$$

where

$$[A] = [C]^{-1}\ [Y]$$

$$[G] = [C]^{-1}$$

The nature of the thermal model of Equation (3.7) is such that [Y] will be a negative symmetric matrix, [G] a real diagonal matrix and [u(t)] a column matrix. The generation is directly related to the loading W(t), on the machine, and can be expressed as some vector function [F(W(t))] of the load:

$$[u(t)] = [F(W(t))] \tag{3.8}$$

The function [F(W(t))] , as does the loss function of the previous chapter, will encompass the entire motor control and the load characteristic. It will need to relate the copper, iron and stray losses to the machine's current and voltage, which in turn will be related to the torque speed characteristic of the load and any voltage or frequency control applied to the machine. This function is assumed to be independant of time, which implies that the machine and load characteristics remain constant throughout the load period.

Clearly, with a known deterministic load variation W(t) the machine temperatures can be solved from the linear differential Equation (3.7) and the generation function. The 'hot spot' temperatures can then be identified, and the machine ageing estimated from Equation (3.5).

However, the work of this thesis is concerned with the more general case where the loading on the machine is a random variable $W(t,\zeta)$ with a known probability distribution. Equation (3.7) now becomes a stochastic model where the heat

generation and temperatures in the machine are also random variables $[u(t,\zeta)]$ and $[\theta(t,\zeta)]$. The model equations are now written as:

$$\frac{d[\theta(t,\zeta)]}{dt} = [A][\theta(t,\zeta)] + [G][u(t,\zeta)] \qquad (3.9)$$

$$[u(t,\zeta)] = [F\ (W(t,\zeta))] \qquad (3.10)$$

The generation vector will have a mean $[\mu_u(t)]$ and an autocorrelation $[\Phi_{uu}(t_1,t_2)]$ [24] which can be obtained from Equation (3.10) and are defined from probability theory as:

$$[\mu_u(t)] = \varepsilon\{[F(W(t,\zeta))]\} \qquad (3.11)$$

$$[\Phi_{uu}(t_1,t_2)] = \varepsilon\{[F(W(t_1,\zeta))]\,[F(W(t_2,\zeta))]^T\} \qquad (3.12)$$

In the above, $[\mu_u(t)]$ will be a column matrix with elements that contain the means of each generation term. The autocorrelation $[\Phi_{uu}(t_1,t_2)]$ will be a square matrix with the diagonal elements equal to the correlation in time of each of the generation terms, and the remaining elements equal to the cross correlation between all the generation terms. This matrix relates the generation within the machine at some time t_1 with the expected generation in some past or future time t_2. The variance of the generation $[V_u(t)]$ is obtained from the auto-correlation at time $t_1 = t_2 = t$ since:

$$[\Phi_{uu}(t,t)] = [V_u(t)] + [\mu_u(t)]\,[\mu_u(t)]^T \qquad (3.13)$$

A differential equation for the temperature mean $[\mu_\theta(t)]$ can be obtained by taking the expected value of both sides of Equation (3.9) over all events ζ. Hence:

$$\frac{d[\mu_\theta(t)]}{dt} = [A][\mu_\theta(t)] + [G][\mu_u(t)] \qquad (3.14)$$

The autocorrelation $[\Phi_{\theta\theta}(t_1,t_2)]$ of the temperature can be found from a similar pair of differential equations, as shown below:

$$\frac{\partial}{\partial t_1}[\Phi_{\Theta u}(t_1,t_2)] = [A][\Phi_{\Theta u}(t_1,t_2)] + [G][\Phi_{uu}(t_1,t_2)] \qquad (3.15)$$

and

$$\frac{\partial}{\partial t_2}[\Phi_{\theta\theta}(t_1,t_2)] = [\Phi_{\theta\theta}(t_1,t_2)][A]^T + [\Phi_{\Theta u}(t_1,t_2)][G]^T \qquad (3.16)$$

The intermediate term $[\Phi_{\Theta u}(t_1,t_2)]$ is the cross-correlation between the generation in the machine at time t_2 and the temperature at time t_1.

The above set of equations can be solved for the temperature statistics from a knowledge of the time variation of the load's mean and autocorrelation.

A specific solution is available on the assumption that the load random variable $W(t,\zeta)$ is stationary, that is, its probability distribution is independant of time. In this case, the load mean and variance and hence the

generation means and variances will also be independant of time. The autocorrelation at two unequal times now becomes purely a function of the difference between the two times, and can be shown [24] to be even:

$$[\Phi_{uu}(t_1,t_2)] = [\Phi_{uu}(\tau)] = [\Phi_{uu}(-\tau)] \qquad (3.17)$$

where $\tau = t_1 - t_2$

The temperature mean $[\mu_\theta(t)]$ is solved directly from Equation (3.14), the initial condition $[\mu_\theta(0)]$ and stationary generation mean $[\mu_u]$, to give:

$$[\mu_\theta(t)] = [e^{At}][\mu_\theta(0)] + [A]^{-1}([e^{At}] - [I])[G][\mu_u] \qquad (3.18)$$

An expression for the temperature autocorrelation can only be obtained if the load or generation autocorrelation is specified. In any load system the generation auto-correlation will lie between the two extremes of a constant valued function over all time lags τ and a 'white' uncorrelated function. The former implies that the load is single valued throughout the entire load period and thus gives a trivial solution for the temperature.

A white system load requires that there is no correlation between the load at a given time t, and the load at any other time not equal to t. This suggests that the

load can change instantaneously from a maximum to a minimum, an event which is very unlikely to occur in practice. However, this assumption can give a reasonable approximation for stochastic loads with narrow correlation functions.

The generation autocorrelation function can be written for a white load as:

$$[\Phi_{uu}(\tau)] = [\mu_u][\mu_u]^T + [V_u]\delta(\tau) \qquad (3.19)$$

where $[V_u]$ is the stationary generation variance and $\delta(\tau)$ is the delta function, which has the formal mathematical definition of:

$$\int_{-\infty}^{\infty} f(\tau)\delta(\tau)d\tau = f(0) \qquad (3.20)$$

for an arbitary function $f(\tau)$.

The cross-correlation $[\Phi_{\Theta u}(t_1,t_2)]$ is computed from the above and Equation (3.15) to yield:

$$[\Phi_{\Theta u}(t_1,t_2)] = [e^{At_2}][\Phi_{\Theta u}(0,t_2)] \qquad (3.21)$$

$$+ [A]^{-1}([e^{At_1}]-[I])[G][\mu_u][\mu_u]^T$$

$$+ [e^{A(t_1-t_2)}]\, U(t_1-t_2)[G][V_u]$$

where $U(t_1-t_2)$ is the unit step function.

Examination of Equation (3.21) reveals that the final term in the expression is dimensionally incorrect. This is caused by the application of the delta function in Equation (3.20) and must be corrected for by dividing the term by the 'impedance' [A] of the thermal system.

The temperature autocorrelation satisfies Equation (3.15) with the input of Equation (3.21) and can be shown to be equal to:

$$[\Phi_{\theta\theta}(t_1,t_2)] = [e^{At_1}][\Phi_{\theta\theta}(0,0)][e^{At_2}]^T \qquad (3.22)$$

$$+ [A]^{-1}([e^{At_1}]-[I])[G][\mu_u][\mu_u]^T[G]^T([e^{At_2}]^T - [I])[A]^{-1T}$$

$$- [e^{A|t_2-t_1|}][A]^{-1}[G][V_u][G]^T[A]^{-1T}\tfrac{1}{2}([e^{2At_2}]-[I])$$

with the initial condition $[\Phi_{\theta\theta}(0,0)]$.

From Equations (3.18) and (3.22) it can be seen that as the time t becomes large compared with the time constants of the machine, the mean and auto-correlation will tend towards the values:

$$\mu_\theta(t) = -[A]^{-1}[G][\mu_u] \qquad (3.23)$$

$$[\Phi_{\theta\theta}(t_1,t_2)] = [A]^{-1}[G][\mu_u][\mu_u]^T[G]^T[A]^{-1T}$$

$$+ \tfrac{1}{2}[e^{A|t_2-t_1|}][A]^{-1}[G][V_u][G]^T[A]^{-1T} \qquad (3.24)$$

Hence, the temperature distribution, itself, becomes stationary. Over a large load period T the total distribution will also approximate to this limiting distribution and it's mean $[\mu_{\theta T}]$ will be given by Equation (3.23). The total distribution variance $[V_{\theta T}]$ can be taken from Equation (3.24) by setting t_1 equal to t_2 and recognising that the first term in the equation is equal to square of the temperature mean. The total temperature mean and variance can be further simplified from the initial definition of the thermal model , Equation (3.7), to yield:

$$[\mu_{\theta T}] \simeq -[Y]^{-1} [\mu_u] \qquad (3.25)$$

$$[V_{\theta T}] \simeq \tfrac{1}{2}[Y]^{-1}[V_u][Y]^{-1T} \qquad (3.26)$$

In comparison to this white system load, a system with a constant autocorrelation function can be shown to have the same total temperature mean and a variance which is twice that of Equation (3.26).

The total temperatures in a machine which is connected to a generalised stationary load will have the mean of Equation (3.25) and a variance that lies between these extremes and can be expressed as:

$$[V_{\theta T}] \simeq (1- \frac{k_w}{2})[Y]^{-1}[V_u][Y]^{-1T}, \qquad (3.27)$$

$$1 \leqslant k_w \leqslant 0$$

The constant k_w in Equation (3.27) is a measure of the 'whiteness' or autocorrelation of the load and has a maximum value of unity for a white stationary load. For example, the stochastic load given in Figure 3.1 which consists of a series of steps each with an expected duration of ΔT has an auto-correlation function of:

$$[\Phi_{uu}(\tau)] = [\mu_u][\mu_u]^T + [V_{uu}]\ (1 - \frac{|\tau|}{\Delta T}) \qquad (3.28)$$

In this case, the constant k_w is a matrix and satisfies:

$$[k_w] = \frac{([e^{A\Delta T}] - [I])[A]^{-1}}{\Delta T} \qquad (3.29)$$

and will have the limits of zero and unity as ΔT becomes large or tends to zero.

The relative ageing of a particular area of the machine's windings is calculated from the mean of the area's time average ageing distribution. This can only be precisely obtained from a knowledge of the entire total temperature probability distribution $p_{\theta T}(\theta)$ of that area over the load period. Mathematically this is expressed through the use of Equations (2.7) and (3.5) as:

$$\mu_R = \mathcal{E}\{\frac{1}{T}\int_0^T \exp(B(\frac{1}{\theta_{ref}} - \frac{1}{\theta}))dt\} \qquad (3.30)$$

$$= \int_{all\theta} \exp(B(\frac{1}{\theta_{ref}} - \frac{1}{\theta}))p_{\theta T}(\theta)d\theta$$

Here, θ must be calculated in degrees Kelvin. The mean μ_R of a winding 'hot spot' will be the value used to determine the minimum life expectancy of the machine in any subsequent analysis.

In a stationary system the ageing time average probability distribution will tend towards a single valued function equal to μ_R, over large load periods T.

The analysis has been confined to deriving expressions for the mean and variance of the total temperature probability distribution $p_{\theta T}(\theta)$. This is because an approximation to the ageing mean can be obtained which uses only the values of the 'hot spot' average total mean $\mu_{\theta T}{}^{i}$ and variance $V_{\theta T}{}^{ii}$ selected from Equations (3.19) and (3.20). Here the superscript i refers to the elements of the mean and variance matrices which are equal to the 'hot spot' mean and self-variance respectively. The development of this approximation is given in the Appendix A4 and yields the following expression for μ_R:

$$\mu_R \simeq \left(1 + \frac{V_{\theta T}^{ii} B^2}{2(\mu_{\theta T}^{i})^4}\right)\exp\left(B\left(\frac{1}{\theta_{ref}} - \frac{1}{\mu_{\theta T}^{i}} - \frac{V_{\theta T}^{ii}}{(\mu_{\theta T}^{i})^3}\right)\right) \quad (3.31)$$

where $\mu_{\theta T}^{i}$ is in degrees Kelvin.

In summary, the equations in this section yield a method by which it is possible to obtain an approximation of the ageing effects of a stochastic load upon an electrical machine. It is inherent in the analysis that the load must have a distribution that is time independant or stationary.

The above ageing analysis can be used to estimate the probability that a machine will need to be replaced over the lifetime of the system in which it is operating. This information, in conjunction with the energy consumption analysis of Chapter 2, will enable a cost evaluation to be made on the initial choice of the size of machine weighed against its cost of replacement and the potential energy savings.

3.5 STOCHASTIC AGEING OF A MULTI-MACHINE SYSTEM

The theory of the previous section can be directly applied to a multi-machine system of the form described in Section 2.4 by simply treating each machine seperately. The individual machine load distributions $p_{Tr}(W)$ are obtained from the total load distribution $P_T(W)$ and the switching limits $W_{\ell i}$ through the use of the following equations:

$$p_{Tr}(W) = \sum_{j=r}^{n} p_j^*\left(\sum_{m=1}^{i} \frac{\alpha_m}{\alpha_r} W\right), \quad W > 0 \qquad r=1,\ldots,n \tag{3.32}$$

$$p_{Tr}(0) = \int_0^{W_{\ell r-1}} p_T(W)\, dW \tag{3.33}$$

where

$$p_j^*(W) = 0 \qquad W < W_{\ell j-1}$$

$$p_j^*(W) = p_T(W) \qquad W_{\ell j-1} \leqslant W < W_{\ell j}$$

$$p_j^*(W) = 0 \qquad W \geqslant W_{\ell j}$$

and

n = the number of machines

r = the machine being considered

$p_j^*(W)$ = the jth position probability distribution.

In the above, Equation (3.33) gives the probability of no load on a machine and $p_j^*(W)$ gives the probabilities of the load lying between the various switching limits.

In a multi-machine system which has been fully optimised for efficiency the machine sizes α_r will not be equal. A thermal model will be needed for each of the n machines for an ageing analysis and an economic appraisal of the system. In the optimised system there will be unequal ageing between the individual machines, since the pole machine will always be loaded whilst the machines in other positions will only be loaded as the system load crosses the appropriate switching limits.

However, in a system where the machines have identical ratings, the unequal ageing effects can be reduced by rotating the machines with respect to their positions. In this way,

a particular machine will spend only part of its service life, for example in the pole position. Here, the energy consumption can still be minimised relative to the system switching limits.

The ageing analysis in the remainder of this section is confined to such an equal machine system and the ageing effects of the switching limits and the control method, by which the machines are rotated, are considered.

Given the multi-machine system where n identical machines, each with a loss function of $\gamma(W)$, provide a stochastic system load with the stationary load distribution $p_T(W)$; then the optimised switching limits $W_{\ell r}$ can be found through Equation (2.31) and are the solution of:

$$\gamma(W_{\ell r}) = \gamma\left(\frac{r}{r+1} W_{\ell r}\right) \quad r=1,\ldots,n-1 \tag{3.34}$$

The load distributions $p_{Tr}(W)$ of a machine in position r is obtained from the simplified version of Equations (3.32) and (3.33) below:

$$P_{Tr}(W) = \sum_{j=r}^{n} p_j^*(jW) \qquad \begin{matrix} W>0 \\ r=1,\ldots,n \end{matrix} \tag{3.35}$$

$$P_{Tr}(0) = \int_0^{W\ell_{r-1}} p_T(W)\,dW \tag{3.36}$$

and

$$P_j^*(W) = 0 \qquad W < W_{\ell j-1}$$

$$P_j^*(W) = P_T(W) \qquad W_{\ell j-1} \leq W < W_{\ell j}$$

$$P_j^*(W) = 0 \qquad W \geq W_{\ell j}$$

In the deterministic sense, at a time t of a load event ζ each of the n machines of the system will be allocated a particular position. This can be expressed mathematically in terms of a control vector $[\Lambda(t,\zeta)]_r$, which is a column matrix of order n with elements $\lambda_{ri}, i=1,\ldots,n$, either equal to zero or unity. If an element λ_{ri} is equal to unity, then for that particular time and event, the machine r will be in position i. A more formal definition of the control matrix is given below:

$$[\Lambda(t,\zeta)]_r^T = [\lambda_{r1},\lambda_{r2},\ldots\ldots,\lambda_{rn}]^T \quad r=1,\ldots,n \tag{3.37}$$

For $\lambda_{ri} = 1,0 \qquad i = 1,\ldots,n$

$$\sum_{i=1}^{n} \lambda_{ri} = 1$$

and $$\sum_{r=1}^{n} \lambda_{ri} = 1$$

In the above, the two summations imply that a given machine can only occupy one position and that no two machines can share the same position. If the deterministic load is represented by a load vector $[W(t,\zeta)]$ of order n.

with elements that are equal to the load demand at each of the n positions, then the load $W_r(t,\zeta)$ on the rth machine is given by:

$$W_r(t,\zeta) = [\Lambda(t,\xi)]_r^T [W(t,\zeta)] \quad r=1,\ldots,n \qquad (3.38)$$

When considering the stochastic equivalent of Equation (3.40), the binary nature of the control matrix suggests that as the system is evaluated over all the random events ζ, the elements of the control matrices become equal to the probability of a machine being in a particular position at a given time. The control vector in Equation (3.38) can thus be replaced by a control probability vector $[p_\Lambda(t)]_r$. If the rotation of the machine system is independent of the load value, then the load probability $p_r'(W,t)$ of each machine can be obtained from the stationary positional load probabilities $p_{Tr}(W)$ and the control probability vector $[p_\Lambda(t)]_r$, as shown below:

$$p_r'(W,t) = [p_\Lambda(t)]_r^T [p(W)] \quad r=1,\ldots,n \qquad (3.39)$$

Here $[p(W)]$ is the vector of the positional load probabilities $p_{Tr}(W)$ taken from Equations (3.35) and (3.36).

The loading on the machines are no longer stationary distributions because of the time dependance of their position. However, the assumption that the rotational control is independant of the system load still permits a reasonable simplification of the thermal equations.

The mean $[\mu_u(t)]_r$ of the heat generation in the rth machine is derived from the definition of Equation (3.11) and the machine's probability distribution in Equation (3.39), since :

$$[\mu_u(t)]_r = \varepsilon\{[F(W_r(t,\zeta))]\}$$

$$= \int_W [F(W)]\, p_r'(W,t)\, dW$$

$$= \int_W [F(W)]\, [p_\Lambda(t)]_r^T\, [p(W)]\, dW \qquad (3.40)$$

In the above the elements $p_{\Lambda ri}(t)$, i=1,...,n, of the control probability matrix can be taken outside the integration as they are independant of the load W, to yield:

$$[\mu_u(t)]_r = \sum_{i=1}^{n} p_{\Lambda ri}(t) \int_W [F(W)]\, p_{Ti}(W)\, dW \qquad (3.41)$$

The integral is equal to the positional generation mean, denoted as $[\mu_{uT}]_i$ obtained from the positional probability distribution $p_{Ti}(W)$. Equation (3.41) can thus be rewritten as:

$$[\mu_u(t)]_r = \sum_{i=1}^{n} p_{\Lambda ri}(t)[\mu_{uT}]_i \qquad (3.42)$$

In a similar, but slightly more complex manner, the variance $[V_u(t)]_r$ of the generation in the rth machine is derived from the following:

$$[V_u(t)]_r = \varepsilon\{[F(w_r(t,\zeta))][F(w_r(t,\zeta))]^T\}$$

$$-[\mu_u(t)]_r[\mu_u(t)]_r^T$$

$$= \sum_{i=1}^{n} p_{\Lambda ri}(t) \int_W [F(W)][F(W)]^T p_{Ti}(W)\,dW$$

$$-[\mu_u(t)]_r[\mu_u(t)]_r^T$$

$$= \sum_{i=1}^{n} p_{\Lambda ri}(t)([V_{uT}]_i + [\mu_{uT}]_i[\mu_{uT}]_i^T)$$

$$-[\mu_u(t)]_r[\mu_u(t)]_r^T \qquad (3.43)$$

Where $[V_{uT}]_i$ is the generation variance of the machine in position i. Substituting Equation (3.42) into the above gives:

$$[V_u(t)]_r = \sum_{i=1}^{n} p_{\Lambda ri}(t)\{[V_{uT}]_i + [\mu_{uT}]_i([\mu_{uT}]_i - \sum_{j=1}^{n} p_{\Lambda rj}(t)\,[\mu_{uT}]_j^T)\} \qquad (3.44)$$

The temperature distribution mean and variance for each of the n machines can now be solved from the generation parameters and the differential Equations (3.14) to (3.16).

With the background of the preceeding equations, it is now possible to consider two particular rotational control algorithms and the effects they have upon the machines ageing. The first control considered is the common practice of equally sharing the loading between the machines by rotating their positions at constant time intervals. For example, the machines may be rotated monthly, so that after several months each machine would have been in every position. Throughout a rotational interval a machine will remain in the same position, and that position's probability will always be unity. If, say, initially machine 1 is in position 1, machine 2 is in position 2 and so on, then the machines' temperatures mean and autocorrelation can be solved during the first rotational time interval from the general solutions of Equations (3.18) and (3.22).

As the length of the rotational time interval is generally long compared with the time constants of the machines, the approximations of Equations (3.25) and (3.27) can be applied to obtain the total temperature distribution parameters, $[\mu_{\theta T}]_r$ and $[V_{\theta T}]_r$, for the first time interval, to give:

$$[\mu_{\theta T}]_r = -[Y]^{-1}[\mu_{uT}]_r \tag{3.45}$$

$$[V_{\theta T}]_r = (1-\frac{k_w}{2})[Y]^{-1}[V_{uT}]_r[Y]^{-1T} \tag{3.46}$$

If at the next rotational interval, the machines are rotated such that machine 1 goes to position 2 and so on, then a similar expression to the above can be obtained for the total distributions over that interval. After n such rotations, where now every machine has been in each position, the final total distribution can be found by stochastically summing the distributions of each interval, to yield values to the total mean and variance of:

$$[\mu_{\theta T}]_r = -\frac{1}{n}[Y]^{-1}\sum_{i=1}^{n}[\mu_u]_i \tag{3.47}$$

$$[V_{\theta T}]_r = \frac{1}{n}[Y]^{-1}\sum_{i=1}^{n}\{(1-\frac{k_w}{2})[V_{uT}]_i + [\mu_{uT}]_i([\mu_{uT}]_i^T - \frac{1}{n}\sum_{j=1}^{n}[\mu_{uT}]_j^T)\}[Y]^{-1T} \tag{3.48}$$

$$r = 1, \ldots, n$$

As would be expected, these total means and variances are identical for each machine.

The second rotational ageing control considered is that which, intuitively, will yield the optimum, that is, minimum ageing for all the machines in the system compared with any other form of rotational control. This optimum occurs if at all times the probability of a machine being in one position is equal to the probability of it being in any other position. For n machines, this is expressed mathematically in the notation of Equation (3.43) onwards as:

$$p_{ri}(t) = \frac{1}{n} \qquad (3.49)$$

$$r=1,\ldots,n \quad \text{and} \quad i=1,\ldots,n$$

This form of control may be considered as an extreme of the first rotational control, where the time intervals of rotation are no longer large, but tend towards zero. Clearly, its implementation is practically impossible, as a continuous rotation of the machines will totally disrupt the power output of the system and the starting surges could well result in a machine failure.

However, as will be shown in a later section, this optimum can be approximated to by a practically feasable control algorithm that will yield a machines positional probability of $\frac{1}{n}$, but is such that this probability is no longer independant of the load or temperature. It is still important to consider the optimum control, as it will give a yardstick by which other control algorithms can be judged. As before, values of the average total temperature means and

variances can be obtained for a large time period of load and by the application of Equations (3.44) and (3.46) they can be shown to be equal to:

$$[\mu_{\theta T}]_r = -\frac{1}{n}[Y^{-1}] \sum_{i=1}^{n} [\mu_{uT}]_i \qquad (3.50)$$

$$[V_{\theta T}]_r = (1-\frac{k_w}{2})\frac{1}{n}[Y]^{-1} \sum_{i=1}^{n} \{ [V_{uT}]_i + [\mu_{uT}]_i([\mu_{uT}]_i^T - \frac{1}{n}\sum_{j=1}^{n}[\mu_{uT}]_j^T)\}[Y]^{-1T} \qquad (3.51)$$

Examination of these equations and their equivalent for the first rotational case will show that the temperature mean is identical in both cases, but the variance in the optimum case for a non zero k_w is smaller than that of the normal rotational control. Because of the exponential nature of the ageing function, the total mean ageing will increase with an increase in temperature variance. This effect can be seen mathematically in Equation (3.31), which demonstrates that the optimum control does produce a lower ageing in the machines than a normal rotational control.

3.6 AGEING CONTROL ALGORITHM

In an equally sized multi-machine system, it has been suggested that the electrical ageing of the machines can be minimised by using a form of rotational control that will result in there being an equal probability of a given machine being in any load position at any time. However, it is important that any control should not unduely increase

the starting stresses on the machines by demanding a large number of stops and starts over any period of the load. The algorithm discussed below meets this requirement as it does not switch the machinery any more times than it is necessary to provide for the fluctuations in the load.

The basis of this control algorithm is that the machines are positioned from a knowledge of the temperatures at the areas in their windings where the insulation is at maximum stress, i.e. the 'hot spots'. The positioning only occurs when the load change is such that a switching limit boundary is crossed. If the load increases across a switching limit an additional machine will have to be switched on, and it is choosen as the machine with the lowest 'hot spot' of all the machines that are not running. Conversely if the load drops across a switching limit, then the hottest machine out of those that are running is switched off.

The control attempts to minimise the variance of the temperature in each machine and thus reduce the overall ageing. Unlike a rotational method, it does not require any additional stopping and starting of machines, but some form of temperature monitoring device will need to be added to each machine. The development of such a device is discussed in the latter part of this thesis.

With a stochastic system load the temperatures in the machines become random variables and hence under the above control the positions of the machines will also be

random. It can be shown that the effect of the control will approximate to the requirement of the positional probability being equal for all positions for each machine. However, the machine positions will no longer be independant of the load history. The mathematics of the previous section can no longer be applied and it is necessary to use a deterministic computational method to analyse the performance.

3.7 DETERMINISTIC ANALYSIS OF A MULTI-MACHINE SYSTEM

The theory in the previous sections uses a number of approximations in order that simple solutions can be obtained to the stochastic equations. To test the validity of these assumptions in a real machine system and also to investigate the response of systems that cannot readily be simplified by such methods, a deterministic approach is needed.

In a deterministic method, a computer program is used to calculate the system temperature and ageing response to a number of load-time characteristics or events ζ. A series of load events are chosen such that, after a large number of samples the load at all times acts as a random variable with the required input system load distribution. The stochastic response of the system can then be determined statistically directly from the information evaluated over each event. Using the same notation as before, the temperature in each machine r, during the load event ζ, can

be obtained from the equations:

$$\frac{d[\theta(t,\zeta)]_r}{dt} = [A][\theta(t,\zeta)]_r + [G][u(t,\zeta)]_r \qquad (3.52)$$

where

$$[u(t,\zeta)]_r = [F([\Lambda(t,\zeta)]_r^T [W(t,\zeta)])] \qquad (3.53)$$

The computer solution to these thermal equations was performed by taking a discrete approximation of the system load. Here, the load is assumed to remain constant over small intervals of time ΔT. The accuracy of the method will hold provided the intervals ΔT are sufficiently small compared with the total load period T. Denoting the load during the kth time interval as $[W(k,\zeta)]$, a step by step solution to the differential Equation (3.52) can be obtained and is given in the following equations:

$$[\theta(k+1,\zeta)]_r = [A'][\theta(k,\zeta)]_r + [G'][u(k,\zeta)]_r \qquad (3.54)$$

$$[u(k,\zeta)]_r = [F([\Lambda(k,\zeta)]_r^T [W(k,\zeta)])] \qquad (3.55)$$

where

$$[A'] = [e^{A\Delta T}]$$

$$[G'] = [A]^{-1}([e^{A\Delta T}] - [I])[G]$$

The modified [A'] matrix is obtained from the original by using the eigenvalue techniques described in

Chapter 6. The above equations enable the machines' temperatures to be calculated from a known starting temperature $[\theta(0,\zeta)]_r$ at every time step. The positional load vector $[W(k,\zeta)]$ is obtained from the total system load $W_s(k,\zeta)$ and the switching limits. Its elements $W_i(k,\zeta)$ are given by:

$$W_i(k,\zeta) = W_s(k,\zeta)/n_r \qquad i \leqslant n_r \tag{3.56}$$

$$W_i(k,\zeta) = 0 \qquad i > n_r$$

where n_r is the number of machines running and is obtained from the switching limits such that:

$$W_{\ell n_{r-1}} \leqslant W_s(k,\zeta) < W_{\ell n_r} \tag{3.57}$$

When the system load is modelled to act as a random variable with a white stationary distribution, the load $W_s(k,\zeta)$ can be obtained at every time interval and load event from a single random load generating function $R(j)$. This would generate load values, from every jth call of the function, that have a distribution equal to the stationary system model. Hence:

$$W_s(k,\zeta) = R(k\zeta) \tag{3.58}$$

The relative ageing $R(k,\zeta)$ of each machine's insulation can be calculated at every step from the hot spot temperature $\theta_r^i(k,\zeta)$ in degrees Kelvin, and Equation (3.4) to give:

$$R(k,\zeta) = \exp B\left(\frac{1}{\theta_{ref}} - \frac{1}{\theta_r^1(k,\zeta)}\right) \tag{3.59}$$

The major result required from this deterministic analysis is the time average mean ageing of the machine over the load period T which is by definition the mean over every time step k and load event ζ. If k_{max} steps are required to cover the load period T and ζ_{max} load events need to be taken to make the load significant with the given stationary load distribution, then the total mean ageing is given by:

$$\mu_R = \sum_{\zeta=1}^{\zeta_{max}} \sum_{k=1}^{k_{max}} R(k,\zeta) \tag{3.60}$$

Obviously this is not the only information that can be obtained using a deterministic approach. Other results of interest are the total temperature mean and variance, which are calculated using:

$$[\mu_{\theta T}] = \sum_{\zeta=1}^{\zeta_{max}} \sum_{k=1}^{k_{max}} \frac{[\theta(k,\zeta)]}{\zeta_{max} k_{max}} \tag{3.61}$$

$$[V_{\theta T}] = \sum_{\zeta=1}^{\zeta_{max}} \sum_{k=1}^{k_{max}} \frac{[\theta(k,\zeta)][\theta(k,\zeta)]^T}{\zeta_{max} k_{max}} - [\mu_{\theta T}][\mu_{\theta T}]^T \tag{3.62}$$

In addition, the entire ageing and temperature distributions at each time step can be found, or alternatively the variation of the rotational control positional probability with time quantified.

The deterministic method allows additional non linearities to be included in the temperature analysis, such as motor starting or thermal matrices that are load dependant. For example, the thermal effects of the large surge currents that occur in induction motors, when they are started directly on line, can be included in the temperature equations.

If the starting is considered to occur at the beginning of an iterative time step kT over a period ΔT_{start} that is short compared with ΔT, then it can be included as an initial temperature rise $[\theta_{start}]_r$ in the iterative Equation (3.52) by:

$$[\theta(k+1,\zeta)]_r = [A']([\theta(k,\zeta)]_r + [\theta_{start}]_r) + [G'][u(k,\zeta)]_r \quad (3.63)$$

The temperature rise is obtained from the additional heat generation of the start $[u_{start}]_r$ from the equation:

$$[\theta_{start}]_r = [A]^{-1}([e^{A\Delta T_{start}}] - [I])[G][u_{start}]_r \quad (3.64)$$

Often electrical machines are cooled by internal or external fans on their mainshaft. These fans will only be effective when the machine is running and a seperate thermal model will need to be used to describe the machine when it is stationary. This can be included in Equation (3.54) by the use of two thermal matrices $[A'_H]$ and $[A'_C]$ for the running and stationary models respectively. Here

the generation matrix [G'] will be evaluated from the running model, such that:

$$[\theta(k+1,\zeta)]_r = [A'_H][\theta(k,\zeta)]_r + [G'][u(k,\zeta)]_r \qquad (3.65)$$

$$\text{for} \quad [u(k,\zeta)]_r > 0$$

and

$$[\theta(k+1,\zeta)]_r = [A'_C][\theta(k,\zeta)]_r \qquad (3.66)$$

$$\text{for} \quad [u(k,\zeta)]_r = 0$$

3.8 RESULTS

3.8.1 System Description

This section tests the ageing theory, by considering a hypothetical parallel machine system. A deterministic analysis was performed on the system, which included the non-linearities mentioned in the previous section. The deterministic results are discussed in detail and compared against the simpler theory. The example demonstrates how the method of analysis should be applied to a real machine system and indicates the expected form of the results.

The system consisted of four identical 5.5kW TEFC cage induction motors connected mechanically in parallel to provide a stochastic system load. The machines were assumed to be operated through perfect clutches, which would be disengaged when the machines were not contributing to the load. At no load the machines would be both mechanically

and electrically isolated from the system and stationary. This isolation would be observed mechanically in a pumping station, or electrically with parallel distribution transformers.

The load distribution was described by a stationary Beta function with a maximum value of 22kW or 1.0 per unit, a mean of 0.7 per unit and a standard deviation of 0.115 per unit. This distribution is shown in Figure 3.2 and has the parameters p,q of Equations (2.10) and (2.11) of 10.5 and 4.5 respectively.

The optimum switching limits that would minimise the system energy consumption were calculated directly from the motors' loss function parameters. In the following discussion, the ageing effects of the optimum limits are compared with those when the switching limits are at the machines' ratings. The loss function parameters, switching limits and system energy consumption are summarized in Table 3.1. The application of the optimum limits can be seen to give a saving of around 3% in the machine losses and 1% in the total energy consumption.

Thermal models have been developed for the stationary and rotational performance of the induction motors and are the subject of the second part of this thesis. The model used in this analysis is the original thermal model that was later to be programmed into the microprocessor based prediction device (Chapter 6). The thermal behaviour of each motor was successfully modelled by a linear differential equation of order eight. The 'hot spot'

temperature was identified as being in the centre of the endwindings and was included as an element of the model. By assuming a constant supply voltage, the heat generation in the nodes of the model could be calculated directly as functions of motor load current squared. This generation could be transformed to a simple function of the motor output power since there exists a linear relationship between the squaresof an induction motors current and output power, which is expressed in Appendix A7, in terms of the induction motor's equivalent circuit parameters, as:

$$i^2 = \frac{(Z_m + 2X_{s/c})}{9v^2 Z_m} W^2 + \frac{v^2}{c^2 Z_m^2} \qquad (3.67)$$

where W is total motor output power and v and i are the phase voltage and current.

The induction motors were wound with enamelled wire with a Class B thermal rating. This insulated classification has a recommended maximum temperature of $130^{o}C$. As no further specific information was available on the type of insulation used, arbitary values[25] of 16,000 for the ageing constant B and $120^{o}C$ for the reference temperature were choosen for the ageing Equation (3.5). The value of B lies within measurements[26] taken for various types of insulation, which suggested a range of 13 to 21 thousand for B and an insulation life of approximately 10,000 hours at the $120^{o}C$ reference temperature.

An iterative step length of 5 minutes was used for the deterministic analysis. This was considered to be sufficiently small to give an accurate assessment of variations in the machines' temperatures with changes in load. The choice of the length of the load cycle was purely arbitary and a short period of 24 hours was choosen solely to restrict computational requirements.

The deterministic load was generated at each 5 minute interval with the Beta function distribution, by the use of a numerical library routine[27]. The load approximated to a 'white' stationary system, because of the short time intervals between successive load generations. Motor starting was included by an additional heat generation equivalent to a starting current of 7 per unit for 0.5 seconds.

3.8.2 Deterministic Results

The deterministic analysis was performed for rotational ageing control with an increasing number of machine rotations within the 24 hour load cycle. Ideal control was approximated by rotating the machines every 5 minute iterative time step and thermal control was instituted using the algorithm laid out in Section 3.6. For each ageing control, results were obtained with and without the inclusion of starting effects and for the system operated at rated and optimum switching limits. In all cases two thermal models were used to describe the induction

motors' rotating and stationary performances.

A constant ambient temperature of 20°C was assumed and all the machines were started from cold, i.e. ambient, at the beginning of the 24 hour period.

Figures 3.3 through to 3.6 give the variation in the mean ageing of each motor with the number of position rotations, which were derived from the estimated maximum and winding temperatures. The ageings converge towards a constant as the number of rotations increase. The initial divergence is due to the machines different starting positions and is emphasised because they start from cold.

When the effect of starting is neglected, the ageing continually decreases as the number of rotations increase, towards the point of ideal sharing of ageing. With the inclusion of starting, the ageing fall tails off as the gains in the load sharing are overtaken by the additional ageing of the starts.

The application of the optimum switching limits produces a constant increase in ageing for all controls. This increase is relatively small compared to the total extent of the ageing variation. This is because the load distribution is such that the lower values of load, where the machines are most likely to be overloaded under optimum control, have a very low probability.

For simplicity, the discussion concentrates on the results for only one of the four motors, but similar data was available for the other three machines. Figure 3.7

compares the parameters of the motor total temperature distribution with the rotational control and the system conditions. Table 3.2 gives details of some points on this graph, and also includes results obtained under thermal control. In confirmation with the original theory, the temperature means remain effectively constant over the control variations and the ageing decreases as a direct result of the reduction in the variance (the square of the deviation) of the total temperature.

The inclusion of starts causes mainly an increase in the temperature mean, with little effect upon the deviation except at higher rotations. The two sets of switching limits appear as slight changes in both the temperature means and deviations.

Included in Table 3.2 are values for the ageing mean taken from the approximation given in Equation (3.31). These calculations are a consistent 11 to 13% higher than the deterministic results. This suggests that the form of the relationship is correct, but more accuracy could be induced by the inclusion of a second order exponential term, which is likely to be a function of the total temperature mean rather than variation.

Table 3.3 summarises the three basic types of control; rotational, thermal and ideal. The thermal control can be seen to give a significant reduction in machine ageing as compared with a 6 hourly rotation. Ignoring the effects of starting, the thermal control produces an ageing equivalent to approximately half-hourly rotational control.

Once starting is introduced the thermal control becomes preferable to any rotational methods.

The additional ageing induced by starting is small in both the thermal and 6 hourly rotation control. Again this can be attributed to the nature of the system load, because there is a low probability of the load transgressing the switching limits and the number of starts caused by load fluctuations are few. Figures 3.8 to 3.10 show the total temperature and time average ageing distributions for the three controls of Table 3.3, with no starting and optimum switching limits. The time average ageing distributions approximate to unity value functions. The small variation that is present is a result of the numerical limitations of a deterministic method using a finite number of time steps and sample events.

The total temperature distributions can be seen to have an erratic form, the overall shape being influenced by the system load distribution and the switching limits. The larger area of the distributions is created when the load is in the lower three switching bands, where there is a high probability of the machines being loaded. The lower region, which is a third of the area of the higher, accounts for the machines in the final switching position. Here there is a low probability of the machines running and an associated lower spread of winding temperatures.

The positional probabilities of the machine under thermal control is given in Figure 3.11. From the initial

starting points, the motor settles down to a positional probability of 0.25 in every position within 2 hours. This is the effect required by the thermal algorithm for it to be able to approximate to an ideal control.

3.8.3 Theoretical Results

The theoretical analysis presented earlier in the chapter was only applicable to the two extremes of the X4 rotational and ideal controls. In the former case, the 6 hour rotational intervals were long compared with the time constants of the machine and the approximations of the theory could be applied.

The steady state endwinding temperatures were expressed as direct functions of the load squared, by substituting Equation (3.67) into the model generation terms in Chapter 5, Equation (5.20), and multiplying them by the appropriate row of the inverse impedance matrix. The steady state endwinding temperatures θ_e of a rotating machine were given by the following formulae:

$$\theta_e = [Y]^{-1} [F(W(t,\zeta))]\Big|_{endwinding} + \theta_{amb}$$

$$= 63.7\ W(t,\zeta)^2 + 21.5 + \theta_{amb} \qquad (3.68)$$

where $W(t,\zeta)$ = per unit induction motor load (base 5.5kW)

θ_{amb} = ambient temperature .

From the above equation, the endwinding temperature mean and variance were calculated from the theory of Section 3 and the mean and variance of the load squared. The positional load data for both rated and optimum switching limits are given in Table 3.4. The nature of a Beta distribution with parameters p,q is such that its nth moment can be read from the distribution table of a Beta function with parameters p+n, q. This allowed an easy determination of the load data directly from tables of the Beta function[16].

The theoretical endwinding temperature mean and deviation and the relative ageing, computed from the approximate expression, are compared against the deterministic results in Table 3.5. The deterministic values for the rotational control are averaged over the four machines and differ slightly from those given for Motor 1 earlier in Table 3.2.

The ideal thermal control results would be expected to be in good agreement as both the deterministic and theoretical analysis model exactly the same system. This was true for the means, but the theoretical variances were a little high. The error is attributed to computational errors in both the deterministic computer program and in the development of the theoretical load parameters.

The deterministic rotational control temperature mean was lower than the theory, whereas the variance was higher. The finite rotational interval of 6 hours used in

the deterministic analysis would be expected to reduce the mean. The use of a second, higher impedance, thermal model for a stationary motor would increase the mean and variance, especially when the machine was operating in the final switching position where it would be stationary for the majority of the time. The differences between the direct theory and the deterministic results would be caused by a combination of these two processes.

Higher theoretical ageings were obtained throughout, with errors ranging from 23 to 17%. A major contributor to the error is the 11-13% involved in applying the ageing approximation. The proportional differences in ageing for changes in both the switching limits and ageing control are maintained in the theoretical results.

In conclusion, the ageing theory gives a simple method of estimating the ageing effects of energy optimisation on parallel and single machine systems. The theory produces a conservative, but not too inaccurate, method of analysing rotational and ideal thermal control in parallel machine drives. The deterministic analysis demonstrated that a thermal control algorithm can produce good improvements in the ageing compared with a conventional rotational control. The ageing studies are based upon an assumption of a stationary load system. This assumption, although not restrictive, would need to be verified for each particular case study considered.

Table 3·1 Example System Parameters

Loss Function Parameters

a	0·0288
b	0·0
c	32·4

Switching Limits

Position	Rated	Optimum
1	0·25	0·30
2	0·5	0·53
3	0·75	0·74
4	1·0	1·0

System Energy Consumption

Output	0·70
Losses: Rated	0·152
Optimum	0·147

p.u. base:- 22kW

Table 3·2 Motor 1 Deterministic Results
No Starting

Rated Switching Limits:

Ageing Control	Temperature °C Mean	Deviation	Ageing Mean	Approx. Formulae	% Error
Rotational X4	78·5	17·2	0·0227	0·0255	+12
X12	78·9	16·1	0·0220	0·0248	13
X24	79·1	15·1	0·0210	0·0236	12
X48	79·2	14·3	0·0199	0·0224	13
X96	79·1	13·9	0·0191	0·0215	13
Ideal	79·3	12·5	0·0175	0·0197	13
Thermal	79·2	14·2	0·0198	0·0223	12

Optimum Switching Limits:

Ageing Control	Temperature °C Mean	Deviation	Ageing Mean	Approx. Formulae	% Error
Rotational X4	78·6	17·2	0·0233	0·0258	+11
X12	79·0	16·2	0·0225	0·0252	12
X24	79·2	15·2	0·0215	0·0240	11
X48	79·3	14·4	0·0204	0·0228	12
X96	79·2	14·1	0·0196	0·0220	13
Ideal	79·3	12·5	0·0180	0·0199	11
Thermal	79·3	14·8	0·0205	0·0232	13

Table 3·3 Motor 1 Ageing under Rotational, Thermal and Ideal Control

	Switching Limits	Control Rotational X4	Thermal	Ideal
No Starting	Rated	0·0227	0·0198	0·0175
	Optimum	0·0233	0·0205	0·0180
Starting	Rated	0·0229	0·0203	—
	Optimum	0·0236	0·0209	—

Table 3·4 Positional Load Squared Distribution Parameters

Position	Rated Limits Mean	Rated Limits Variance	Optimum Limits Mean	Optimum Limits Variance
1	0·726	0·0222	0·735	0·0227
2	0·726	0·0222	0·734	0·0228
3	0·684	0·0464	0·665	0·0556
4	0·241	0·1059	0·250	0·1065

p.u. bases:- mean $(5{\cdot}5\,kW)^2$
variance $(5{\cdot}5\,kW)^4$

Table 3·5 Comparison of Theoretical with Deterministic Results

	Ageing Control	Endwinding Temperature °C Mean *	Mean †	Deviation *	Deviation †	Ageing Mean *	Ageing Mean †
Rated Limits No Starting	Rotational	78·7	79·4	17·2	16·4	0·0224	0·0267
	Ideal	79·2	79·4	12·5	13·6	0·0175	0·0215
Optimum Limits No Starting	Rotational	78·8	79·5	17·2	16·4	0·0232	0·0272
	Ideal	79·3	79·5	12·5	13·7	0·0180	0·0221

* Deterministic results
† Theoretical results

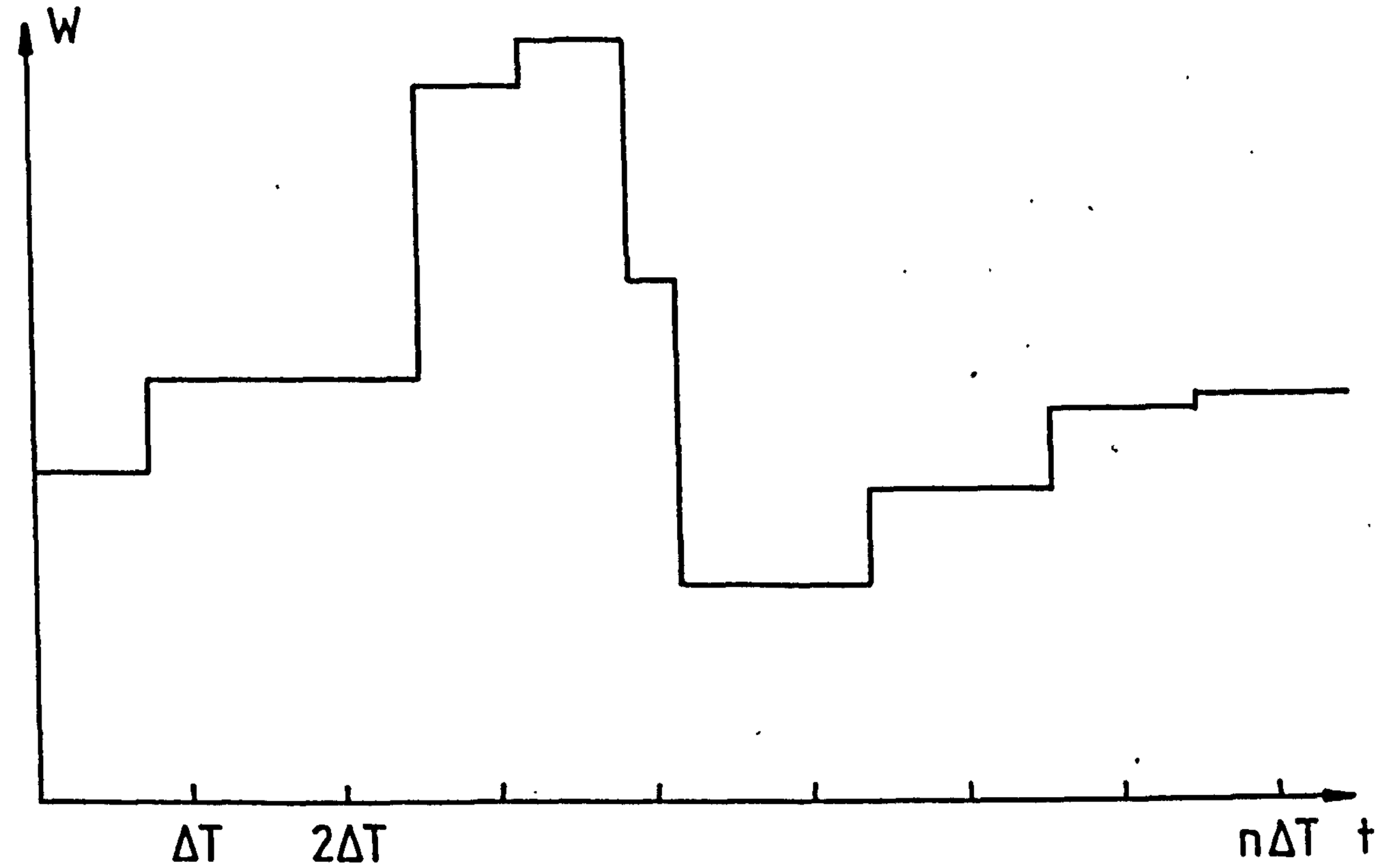

Random Step Load

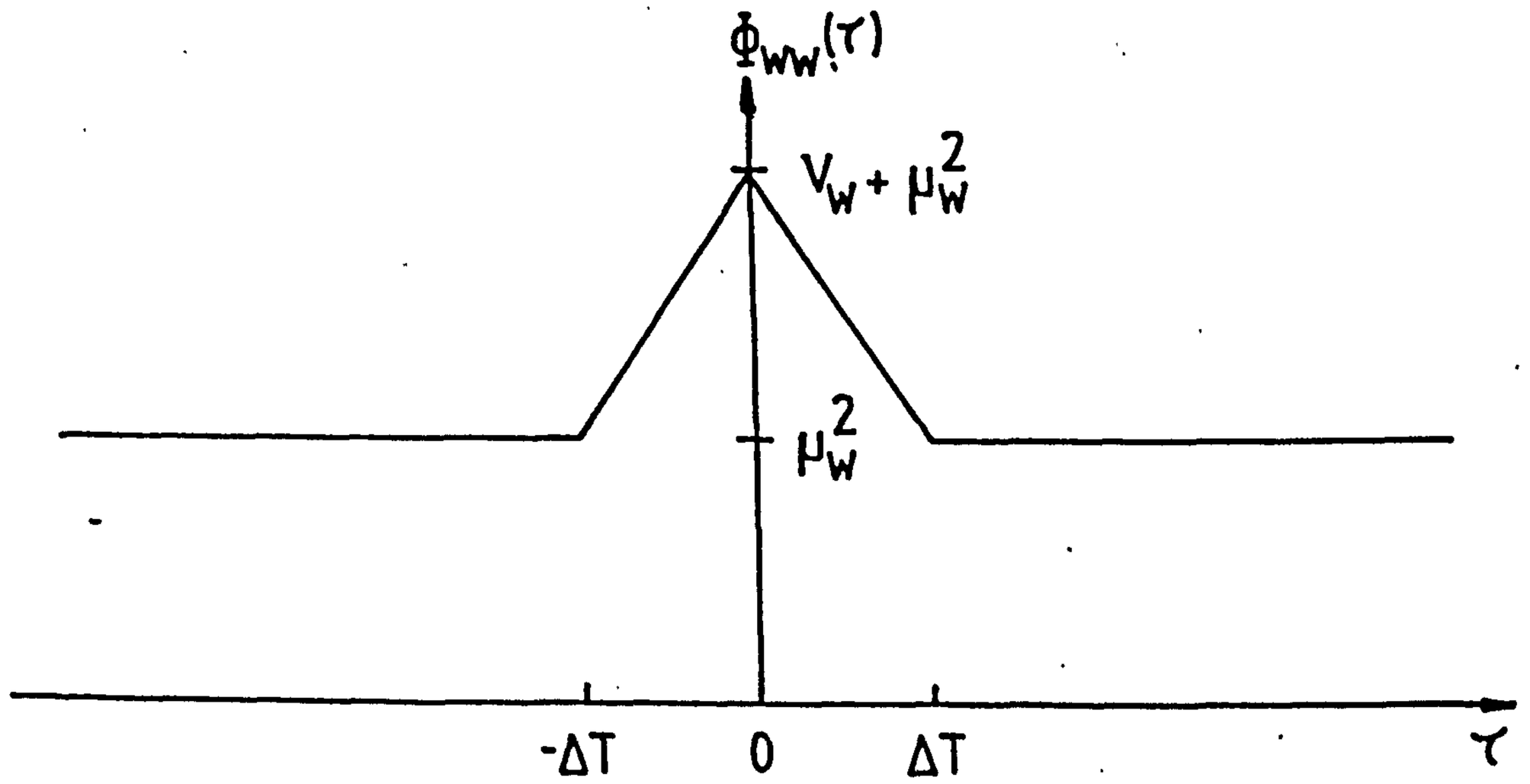

Load Autocorrelation Function

Figure 3·1 Example Autocorrelation Function

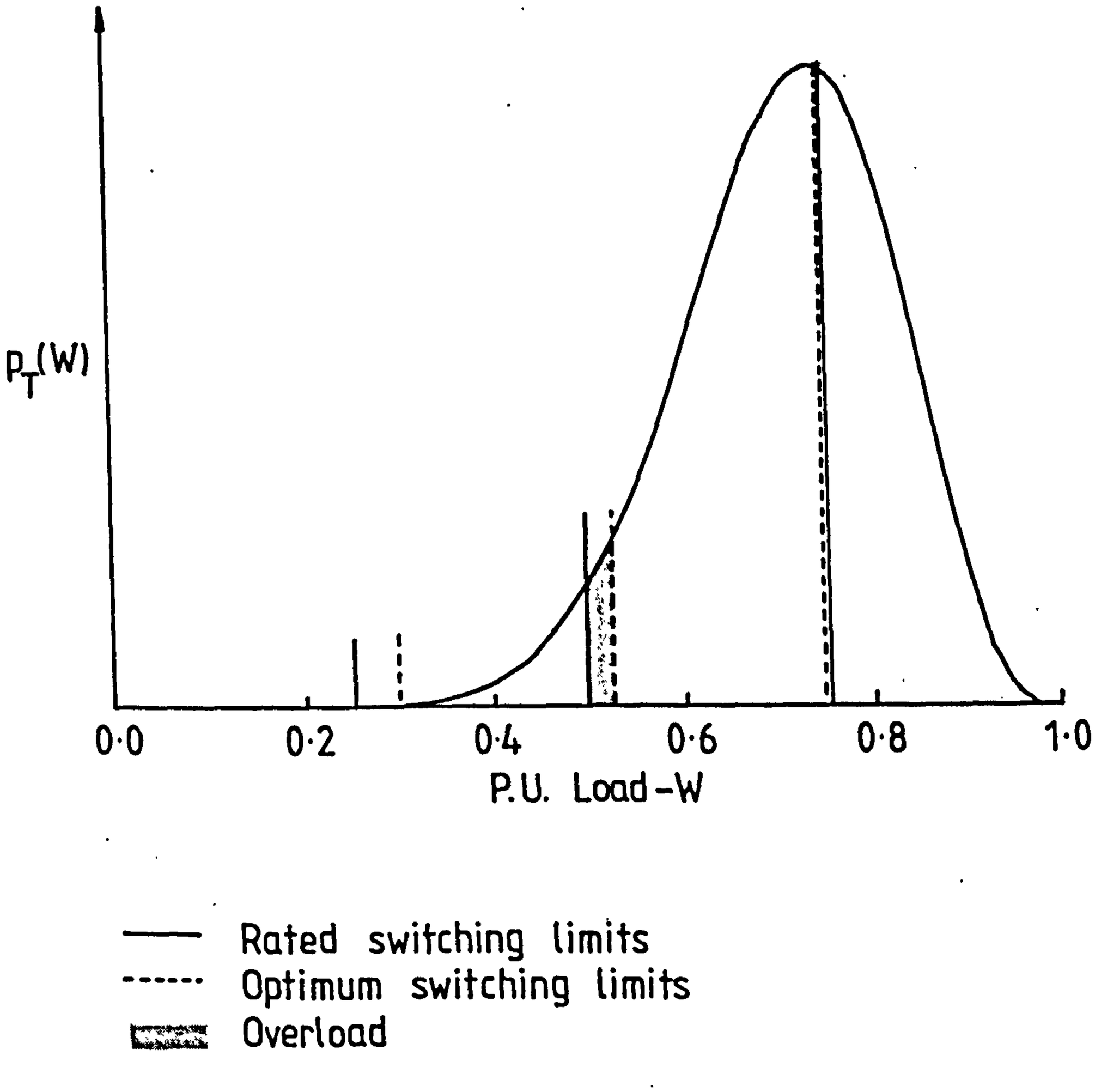

Figure 3·2 Parallel System Load Distribution

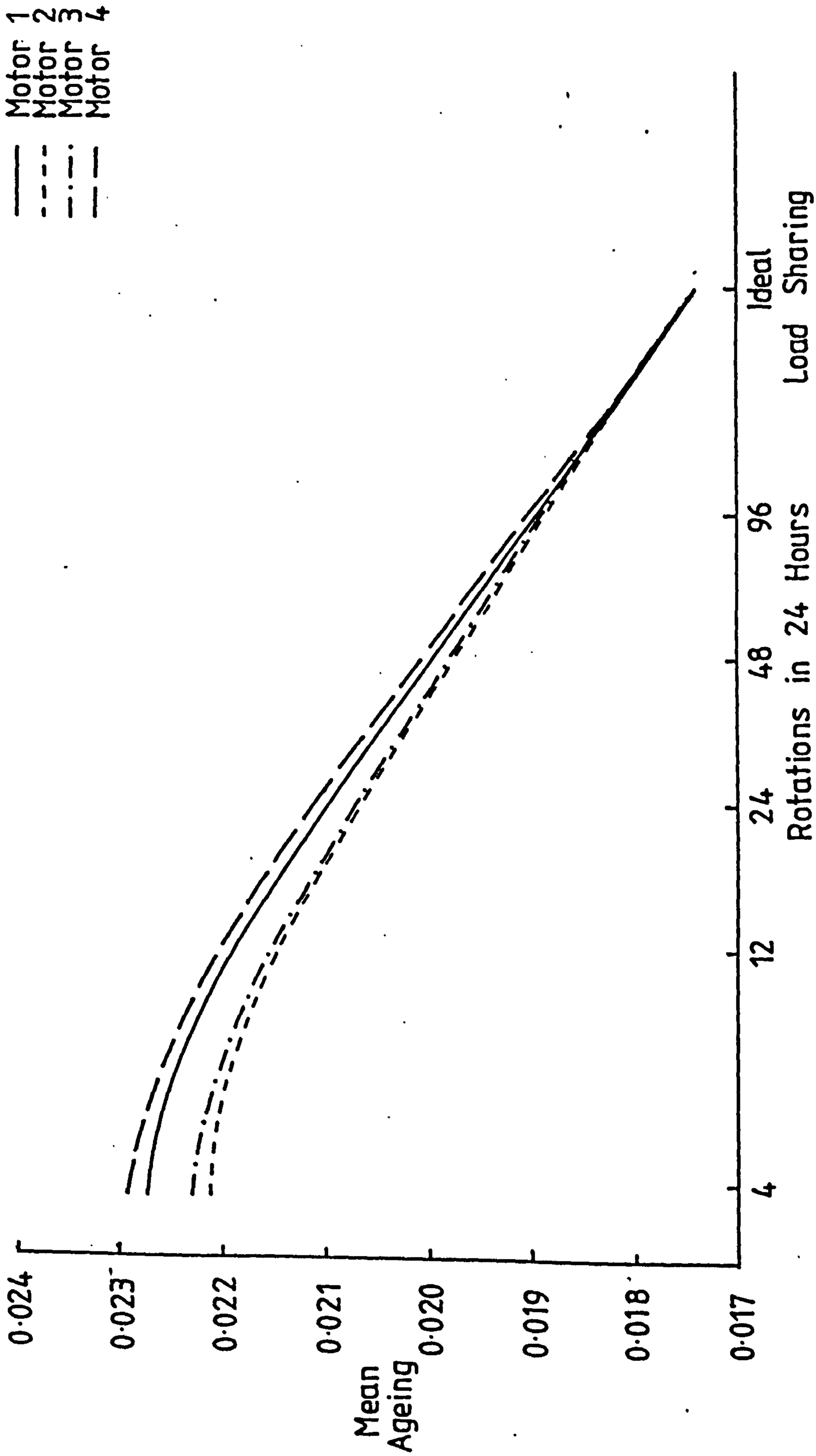

Figure 3·3 Motor Time Average Mean Ageing: No Starting and Rated Switching

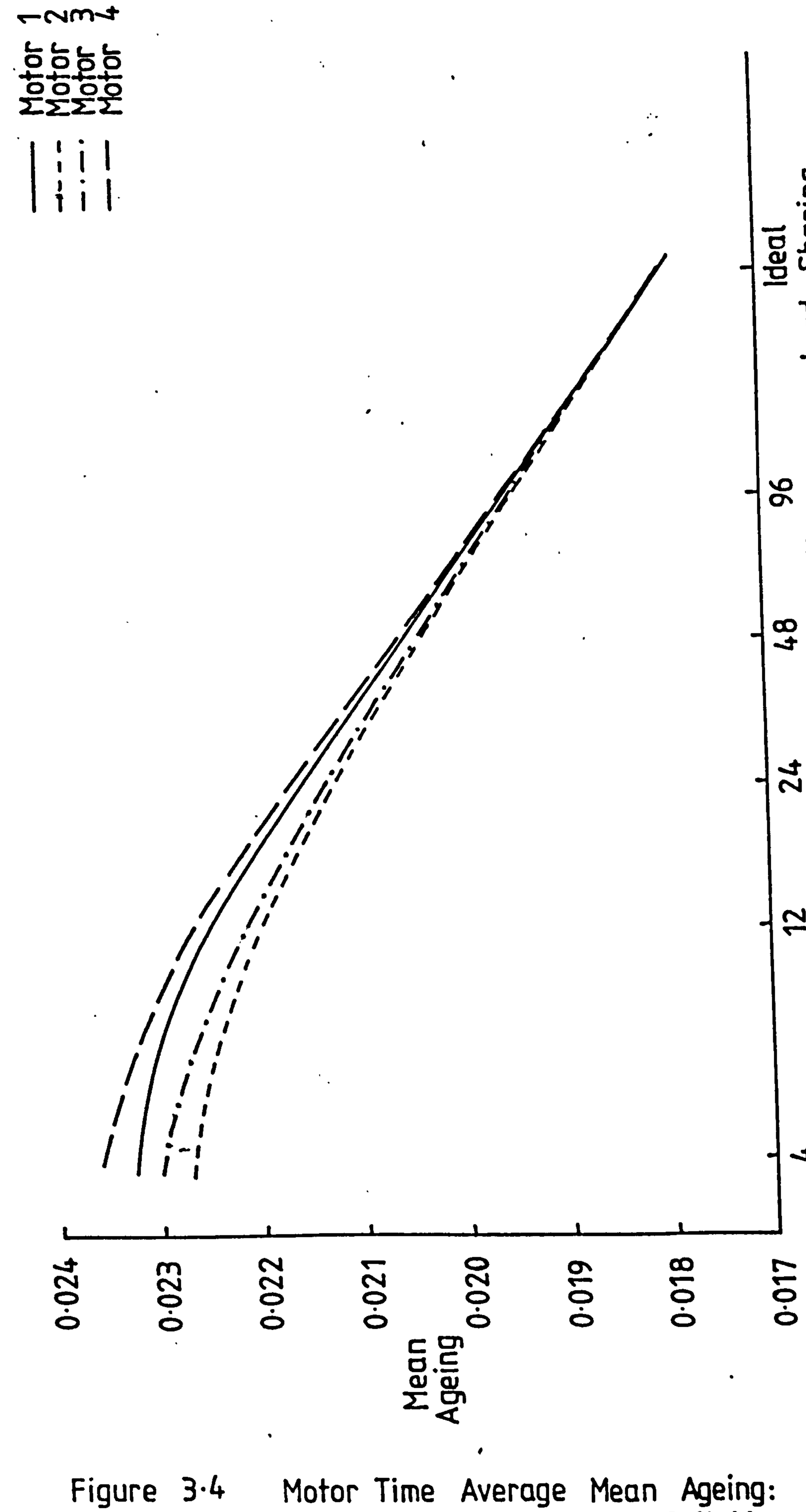

Figure 3·4 Motor Time Average Mean Ageing: No Starting and Optimum Switching

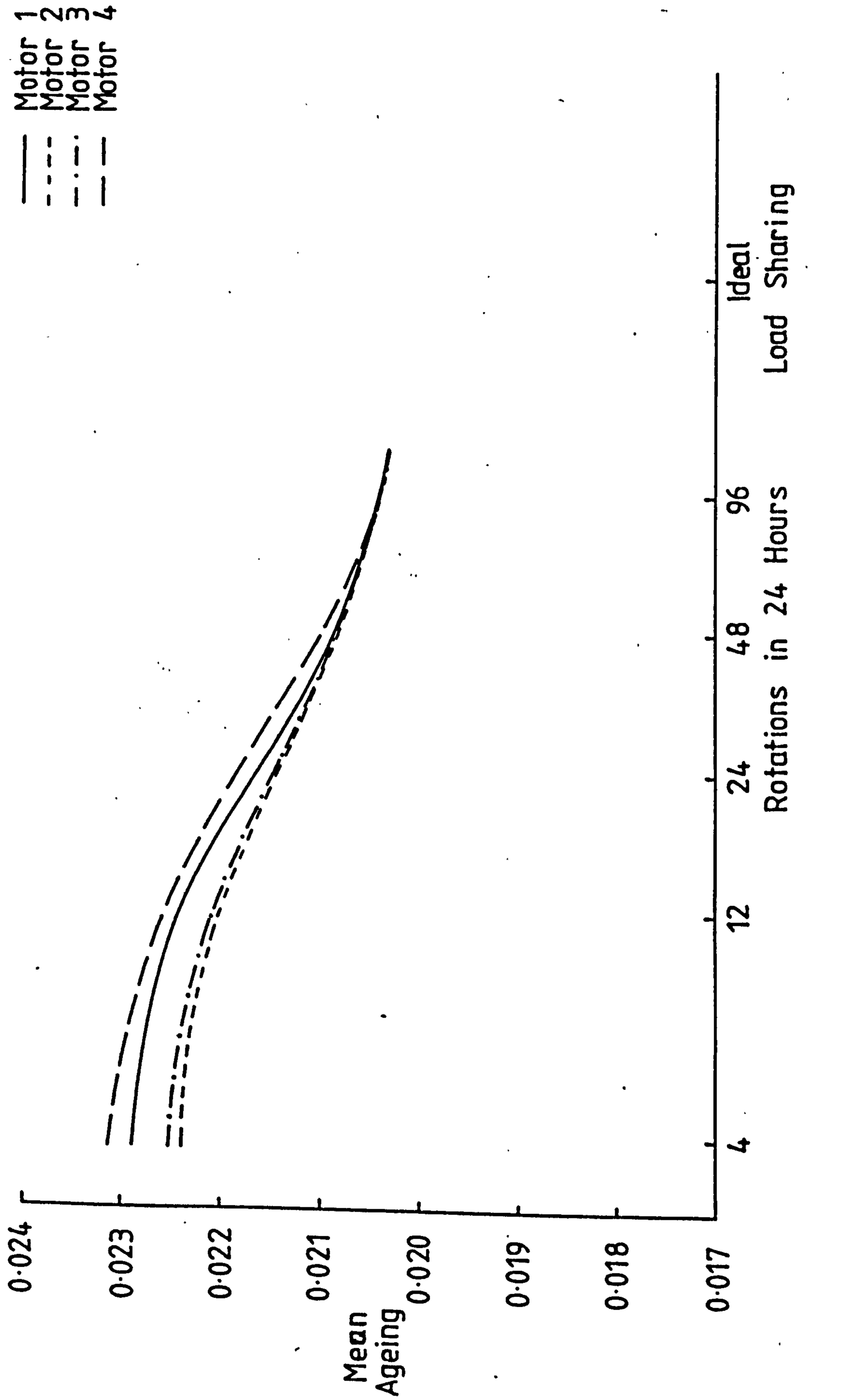

Figure 3·5 Motor Time Average Mean Ageing: Starting and Rated Switching

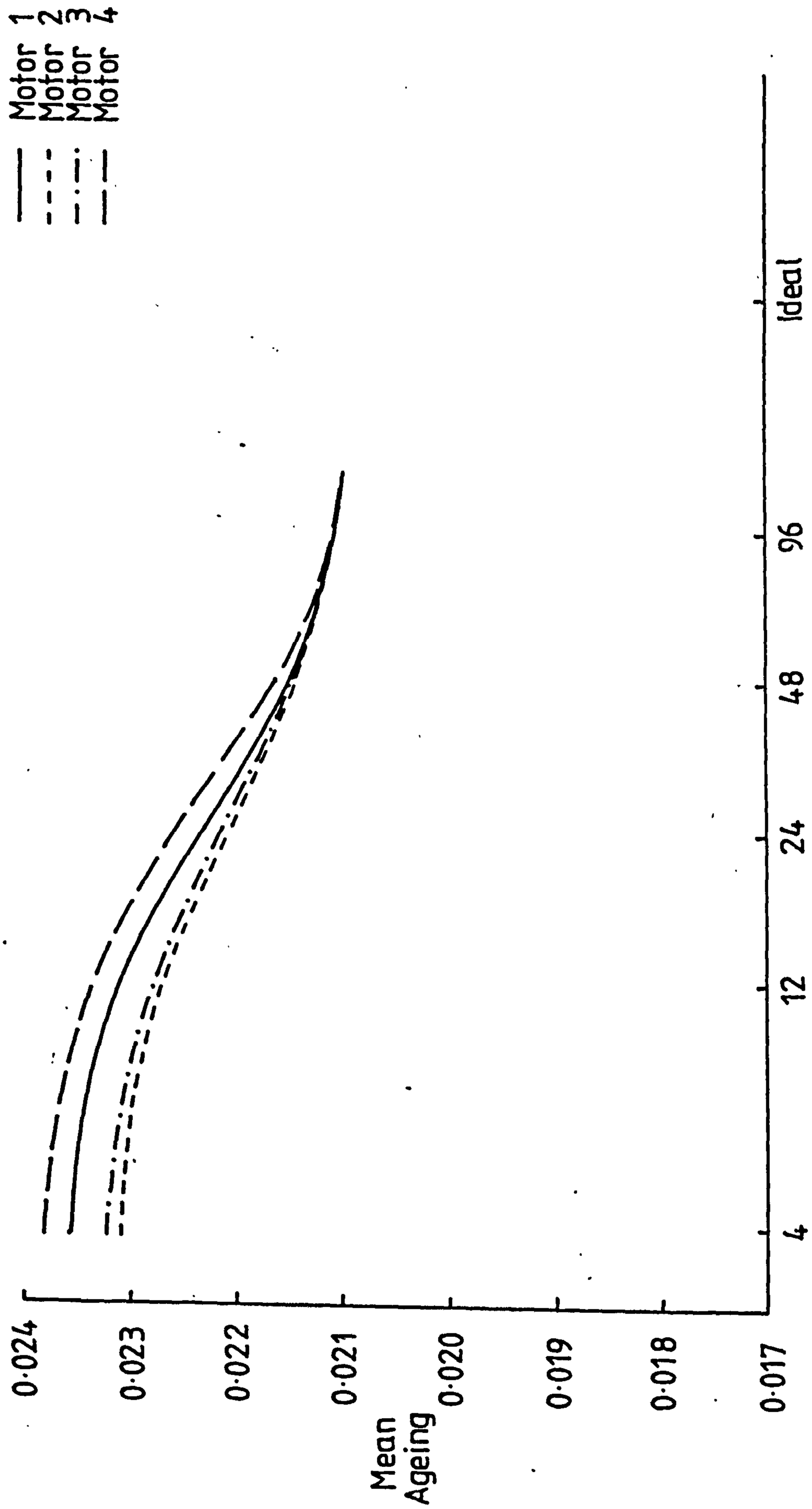

Figure 3·6 Motor Time Average Mean Ageing: Starting and Optimum Switching

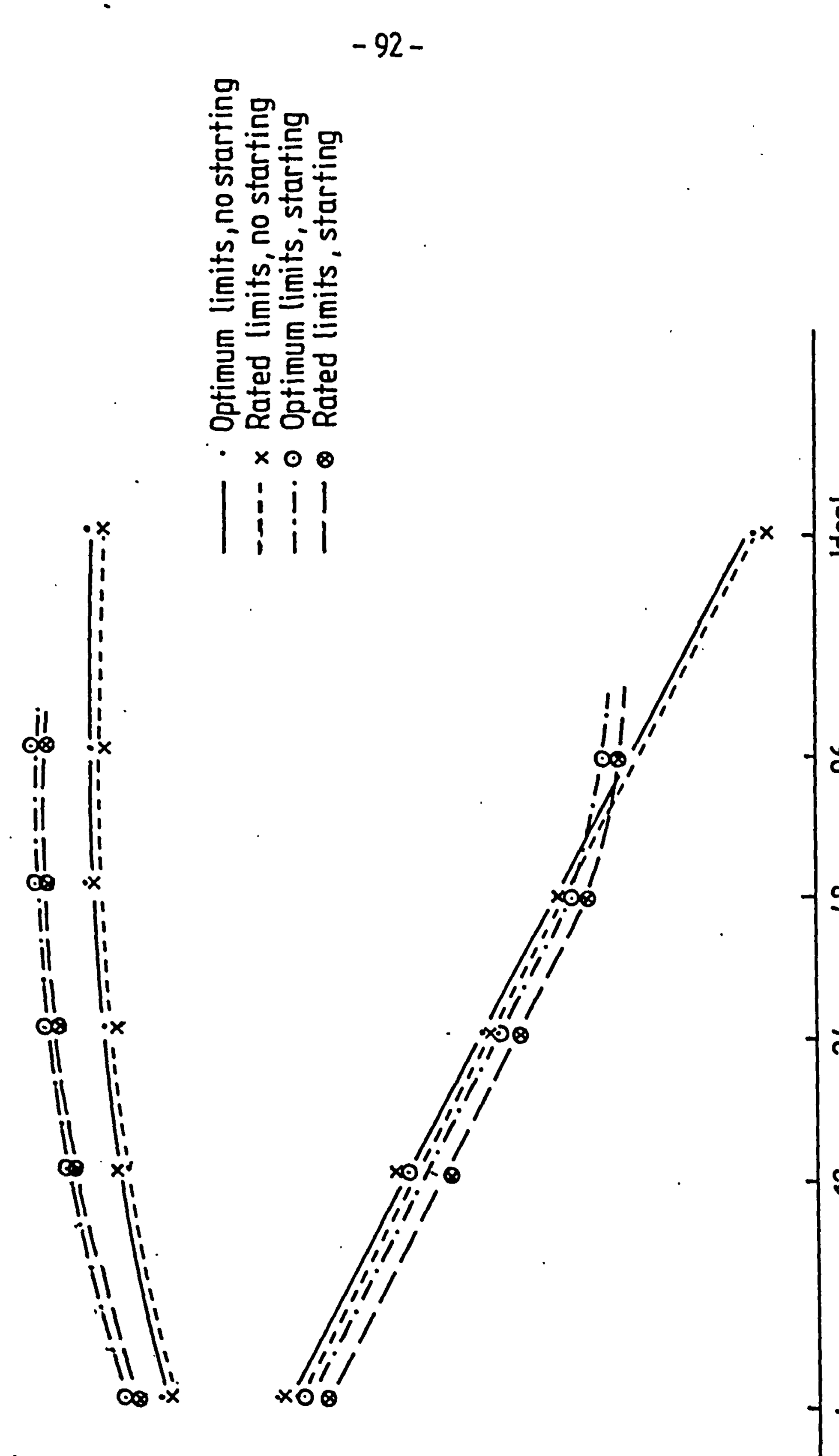

Figure 3·7 Endwinding Total Temperature Mean and Deviation: Motor 1

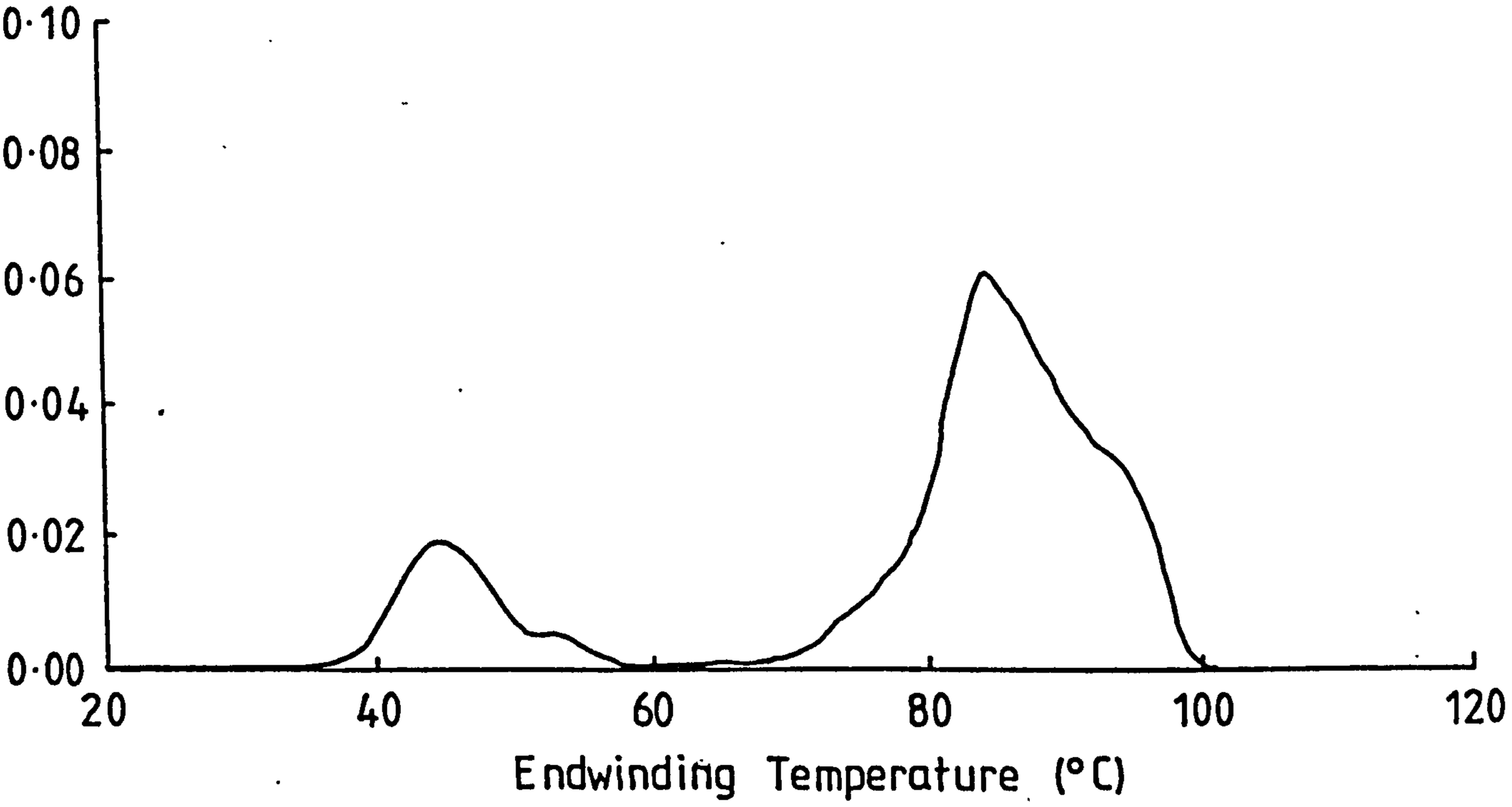

Figure 3·8a Endwinding Total Temperature Distribution: Motor 1, No Starting and Optimum Switching, x4 Rotational Control

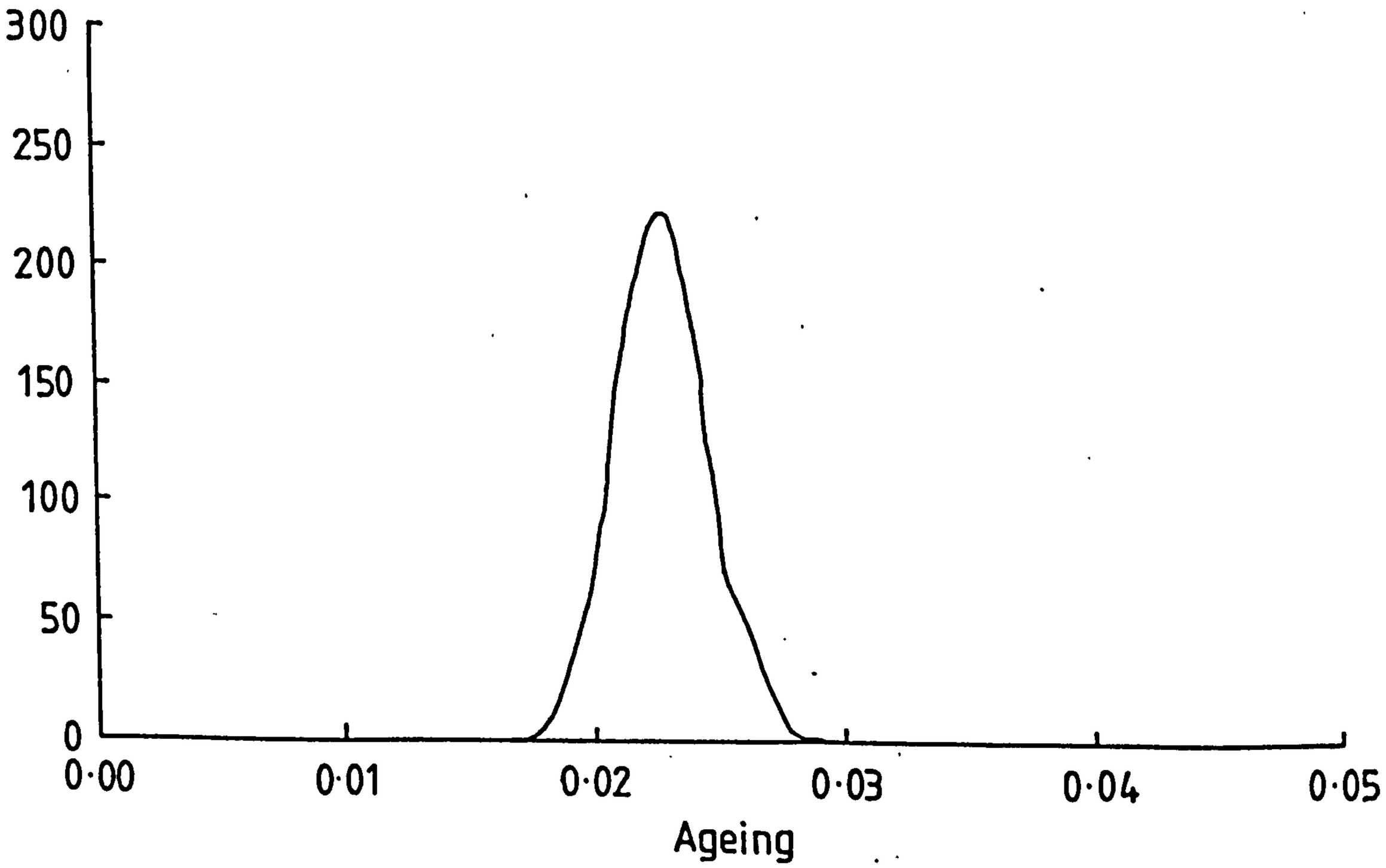

Figure 3·8b Time Average Ageing Distribution: Motor 1, No Starting and Optimum Switching, x4 Rotational Control

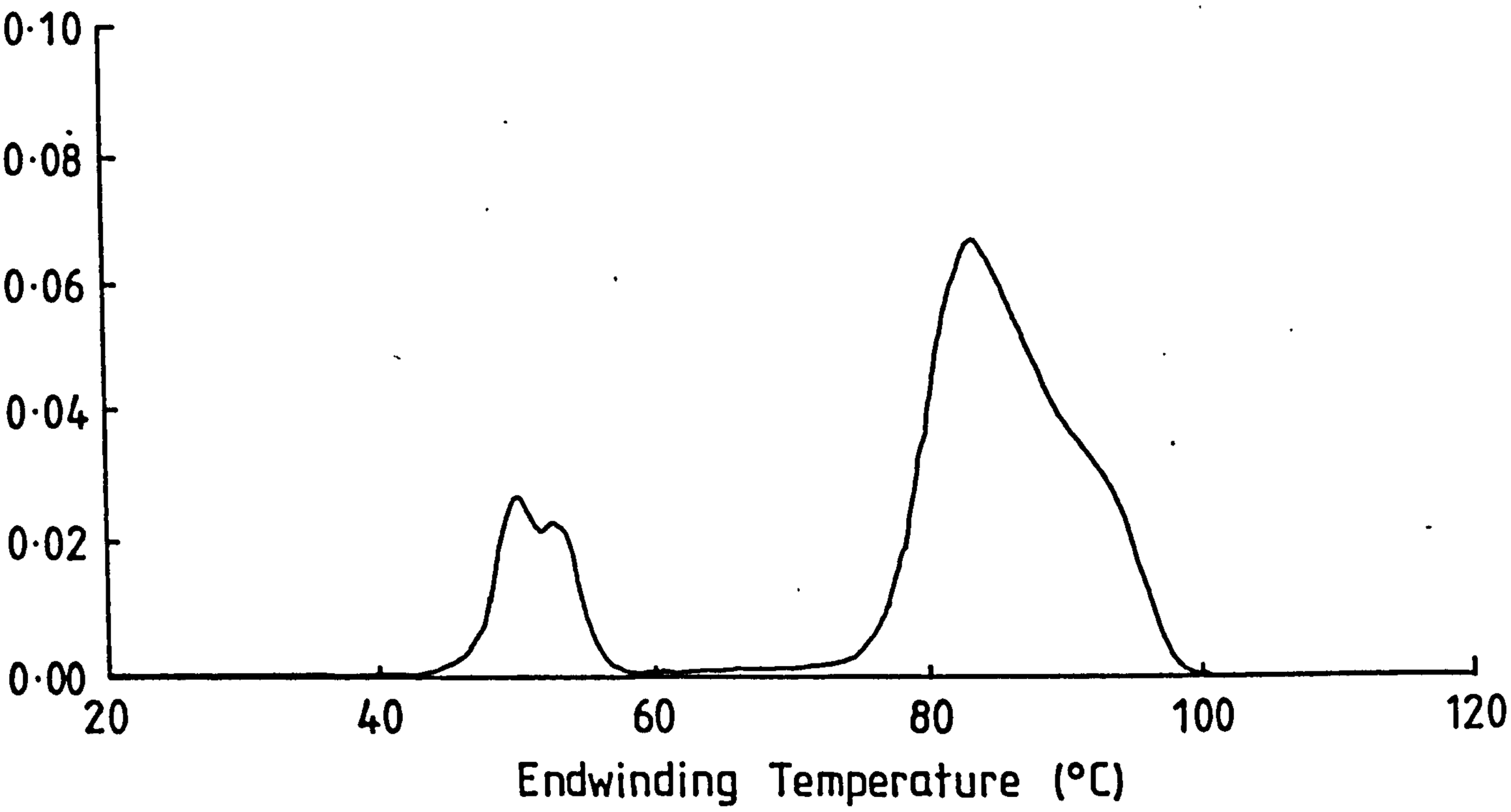

Figure 3·9a Endwinding Total Temperature Distribution: Motor 1, No Starting and Optimum Switching, Thermal Ageing Control

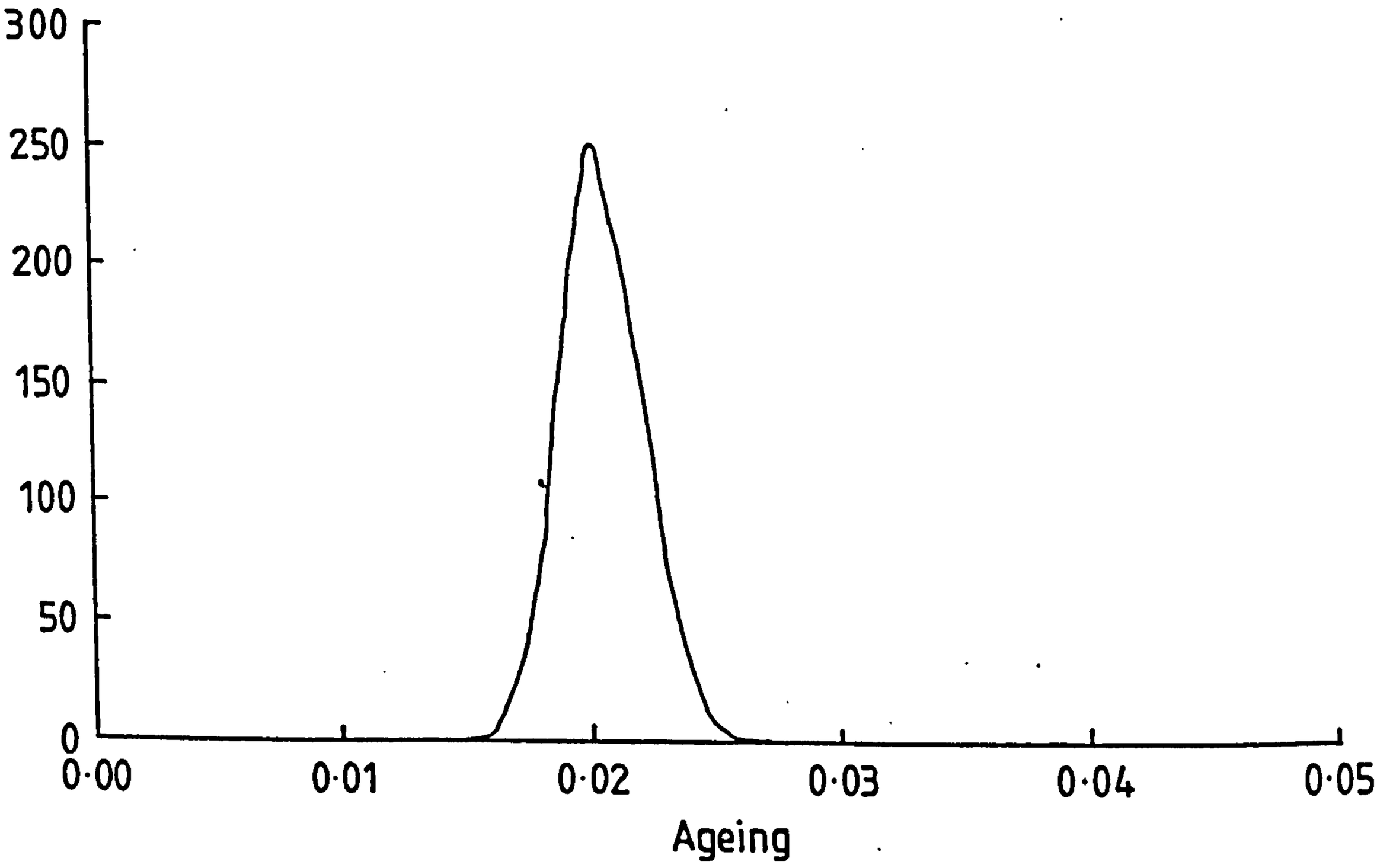

Figure 3·9b Time Average Ageing Distribution: Motor 1, No Starting and Optimum Switching, Thermal Ageing Control

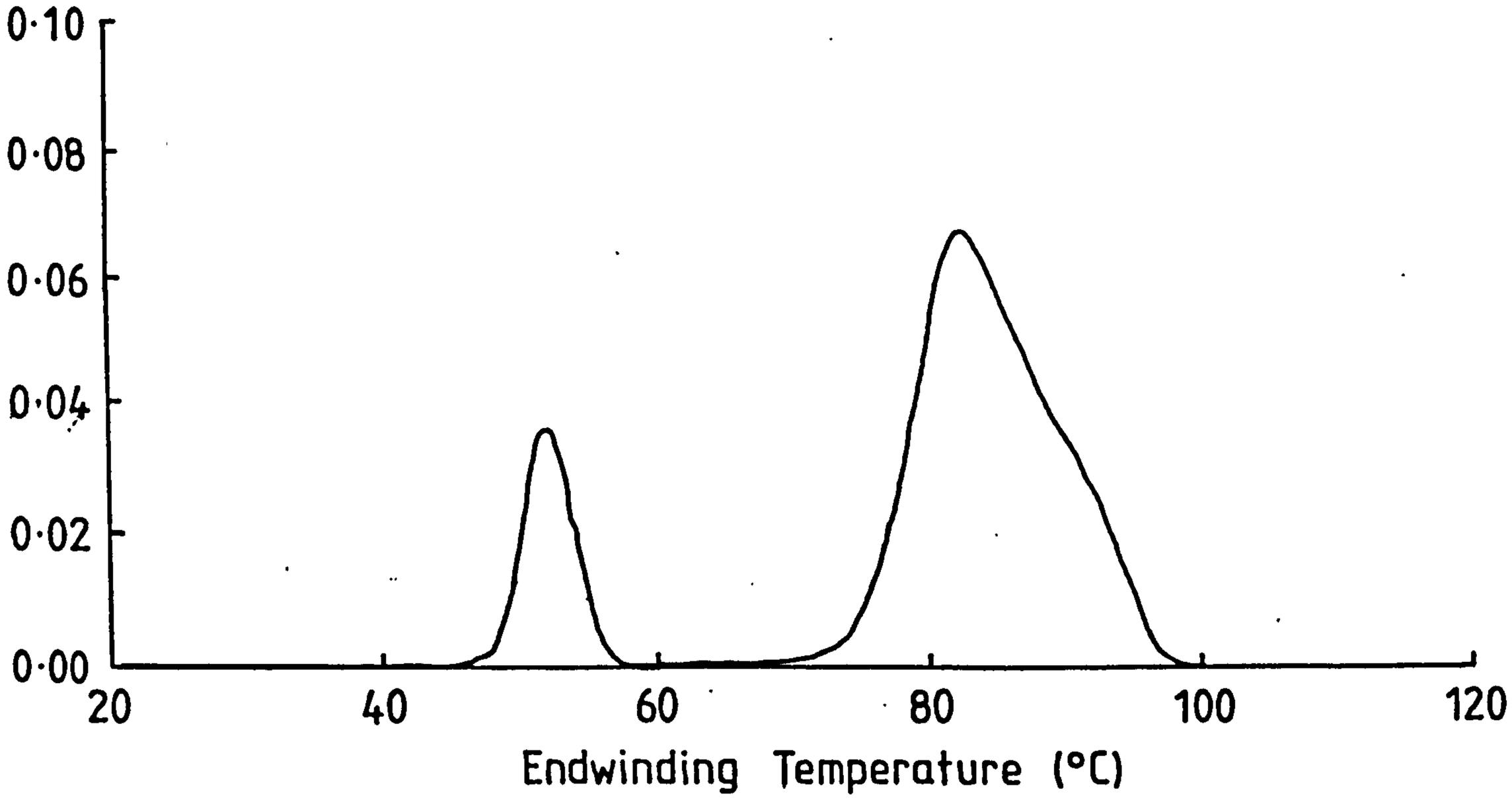

Figure 3·10a Endwinding Total Temperature Distribution: Motor 1, No Starting and Optimum Switching, Ideal Load Sharing

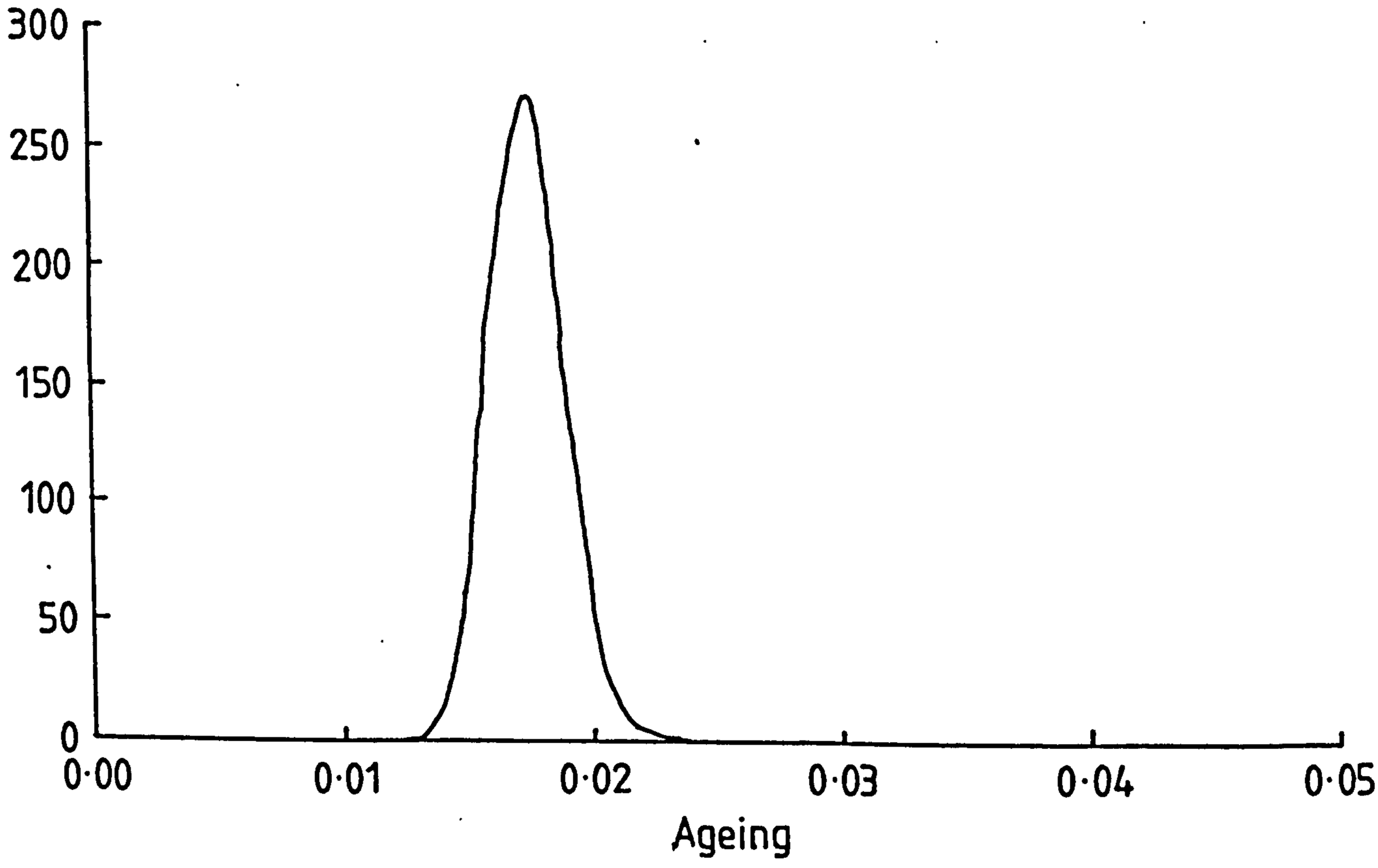

Figure 3·10b Time Average Ageing Distribution: Motor 1, No Starting and Optimum Switching, Ideal Load Sharing

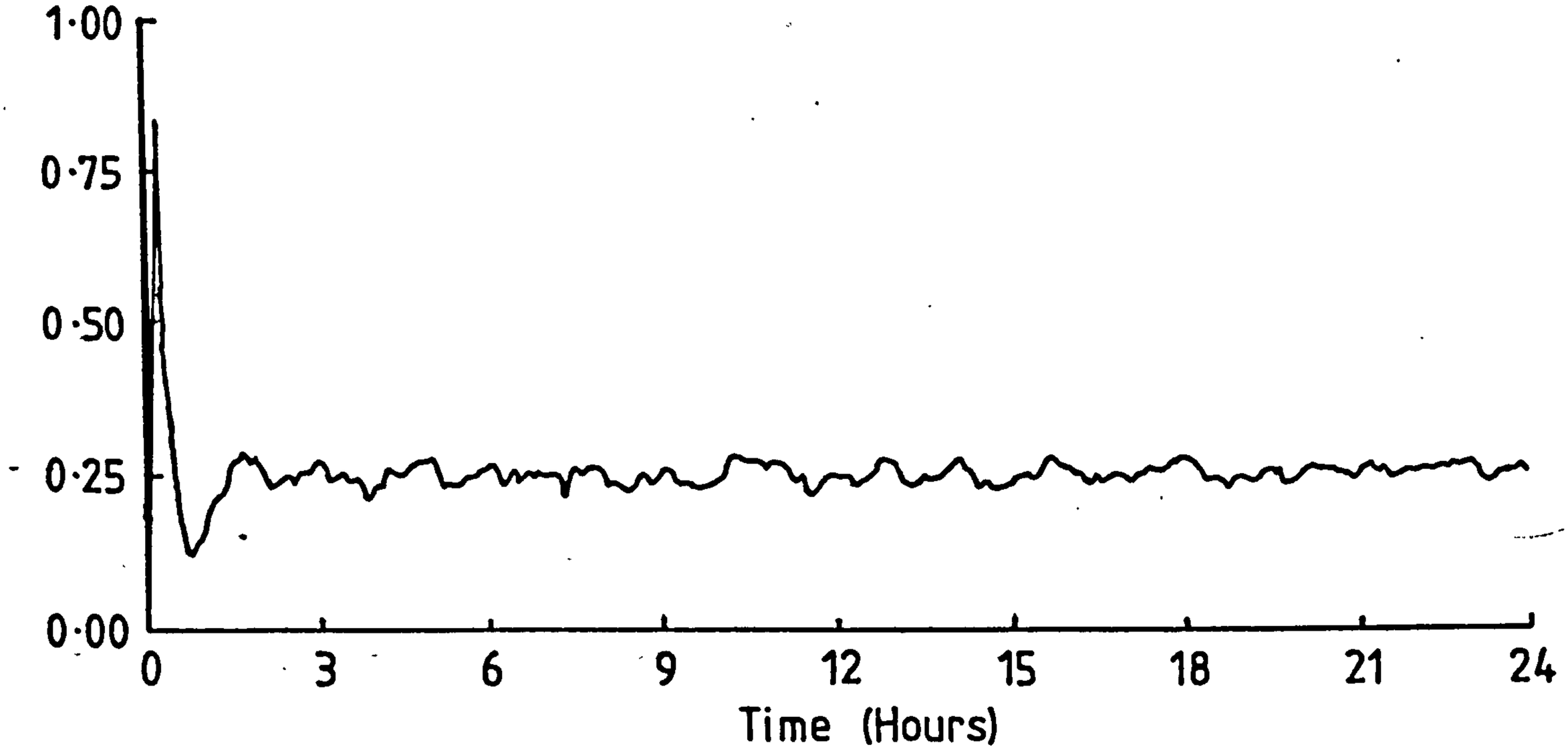

Figure 3·11a Probability of Motor 1 being in Position 1

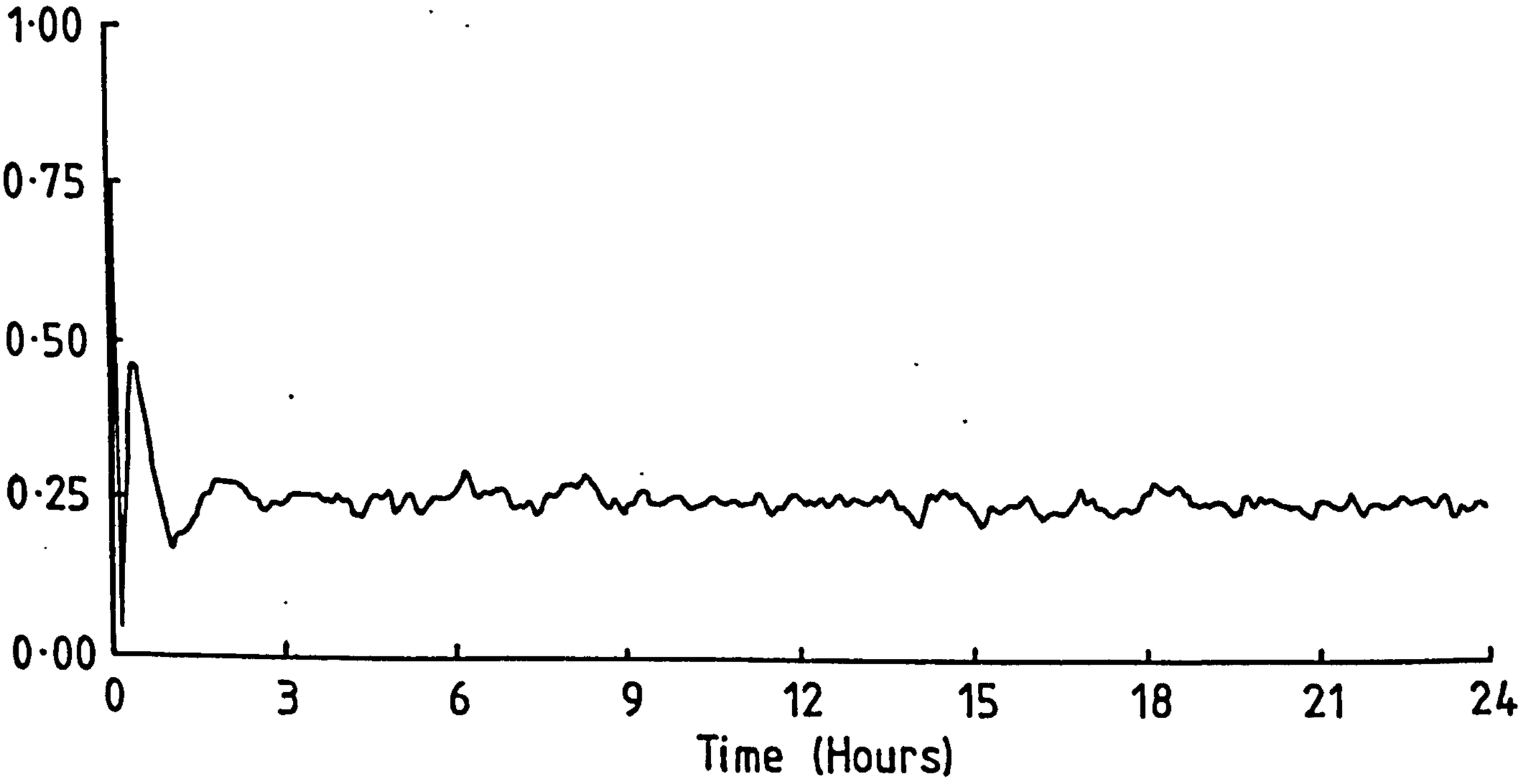

Figure 3·11b Probability of Motor 1 being in Position 2

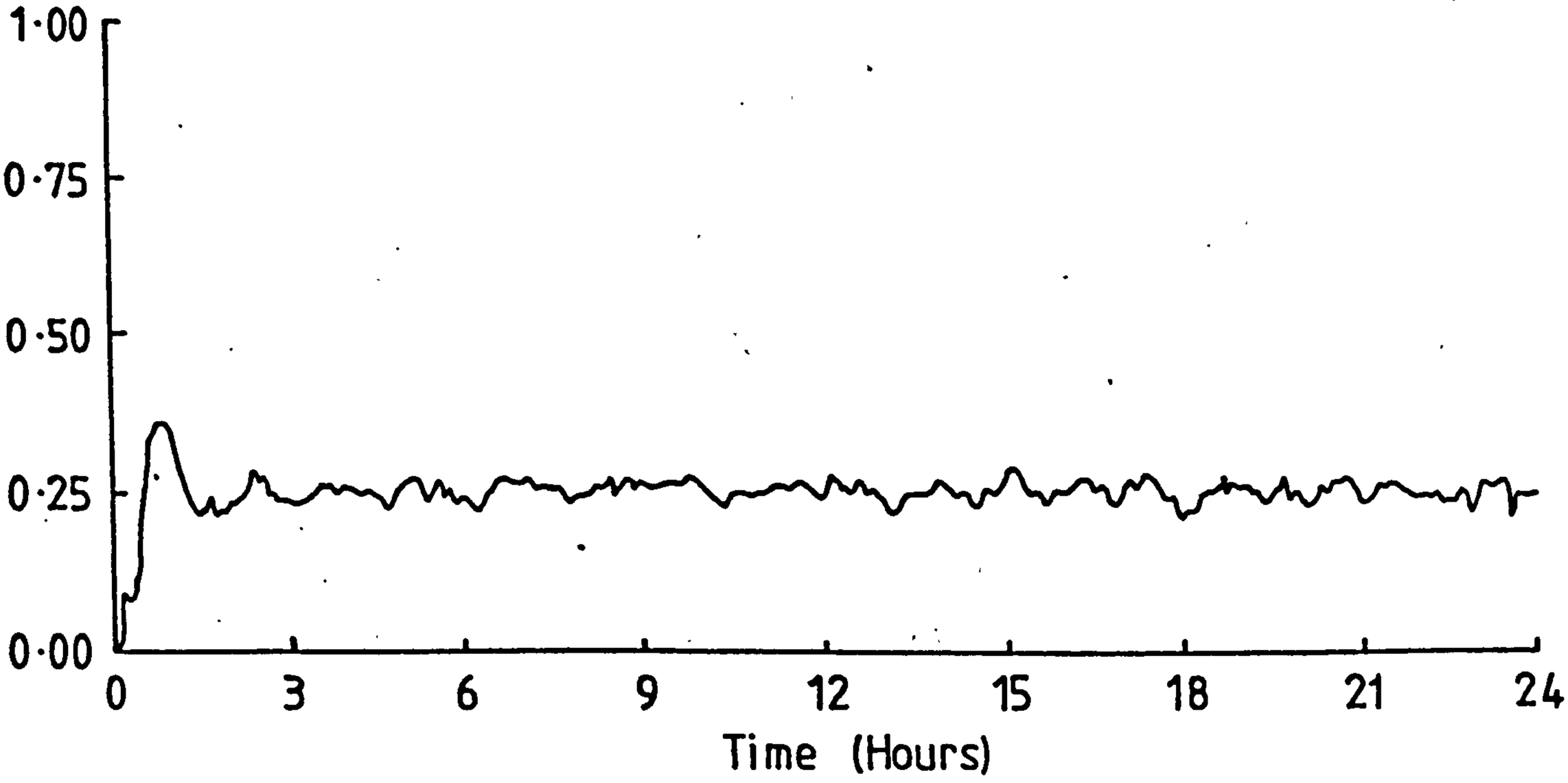

Figure 3·11c Probability of Motor 1 being in Position 3

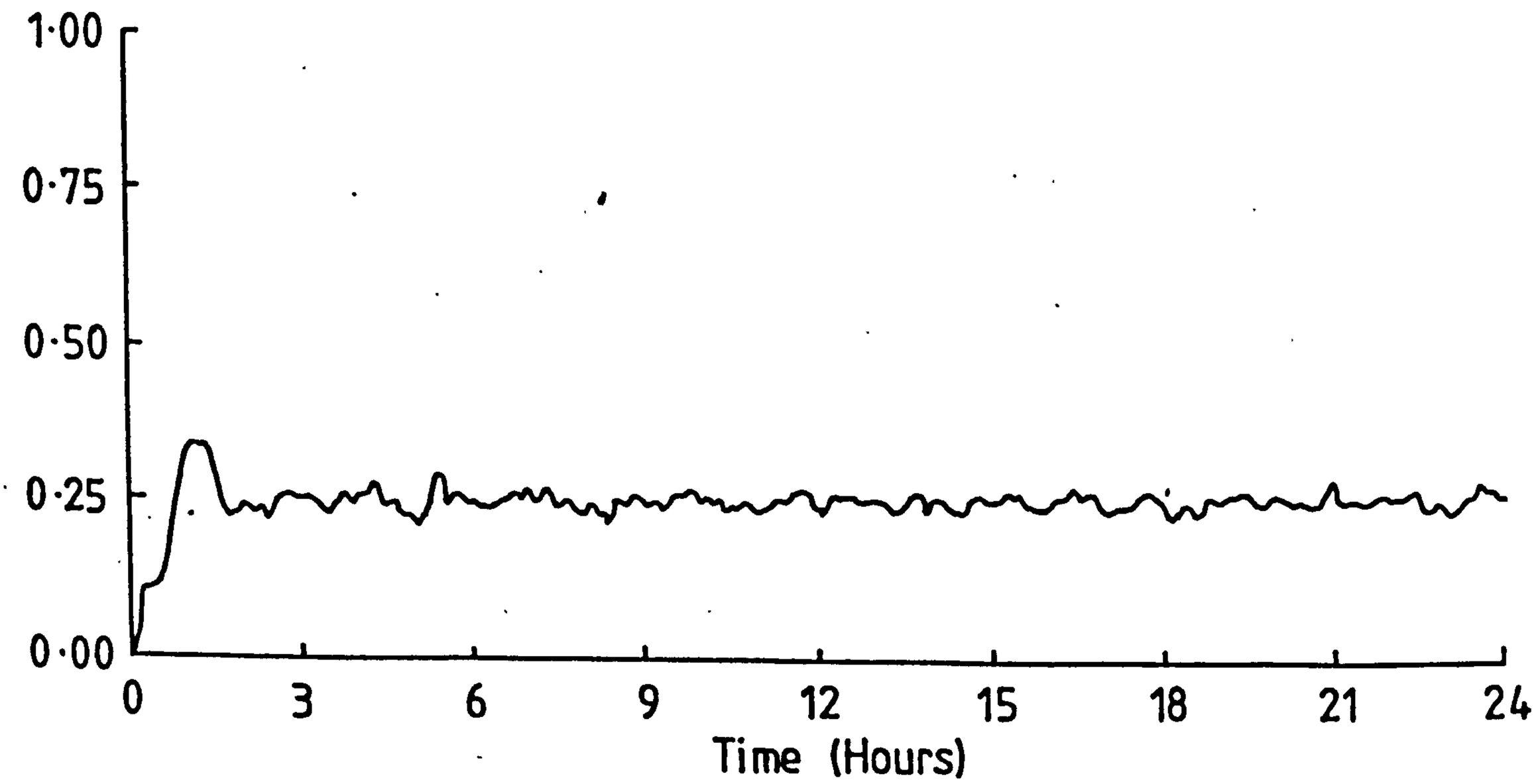

Figure 3·11d Probability of Motor 1 being in Position 4

CHAPTER 4

PROCESS INDUSTRY CASE STUDY

4.1 INTRODUCTION

In many industries, machines are operated in parallel under control schemes similar to those laid out in the multi-machine analysis of Chapter 2. In particular, process and water industries often use pumps in parallel to circulate varying flows of fluids. An example of this was found in a local brewery, owned by Bass p.l.c., where centrifugal pumps were used in parallel to provide a flow of refrigerant to the brewing process.

The theoretical analysis[15] has suggested that significant energy savings could be achieved in a multi-machine system by a careful selection of the control parameters. With the aim of confirming these findings experimentally, the management of the brewery were approached and they agreed to allow measurements to be taken on one of their pumping stations.

The performance of the station was monitored over a full week and a theoretical model was set up from the results. Through this model, the effects of changing the control parameters were investigated, and the level of possible energy savings quantified. The findings were reported to Bass and recommendations were made on the changing of the control. A copy of this report is given as reference in

the Appendix. Again the management were co-operative and agreed to adjust the pumping station controller. A second week of data was then taken and used to confirm that savings in energy had taken place.

This chapter describes the method by which the data was recorded at the plant, the subsequent analysis of the data and how it was used to set up a model of the pumping station. The validity of the model is then confirmed with the original data and the estimated improvement in the system performance presented. Finally, the second week of data is analysed and is also compared against the model.

4.2 PLANT DESCRIPTION

The modern brewery has transformed the fermentation of beer into a fully automated process industry. Today's beer can be brewed from the original malt and hops to the barrel in a few days, as opposed to the several weeks required by traditional methods. A necessary part of the modern process is the fast cooling of the beer to kill the yeast after fermentation, before it goes on to be clarified and carbonated. In order to achieve this a large amount of refrigeration is required.

At Bass Brewery in Runcorn two refrigeration plants are used for the process, one producing chilled water at $2^{o}C$ and the other glycol at $-5^{o}C$. These plants are sited remotely from the brewing process, to which the coolants are provided through two low pressure mains. The flow of coolant is maintained by a pumping station at the start of

each main, consisting of a number of induction motor driven centrifugal pumps operating in parallel.

This particular study was focused on the glycol coolant pumping station. Four 50 HP TEFC cage induction motors were used to drive centrifugal pumps rated at a maximum flow output of $232m^3/h$ and at a head of 39.2 mWG, as shown in Figure 4.1. The pumps were connected in parallel, which gave a total system capacity of $928m^3/h$ of glycol with all four pumps running. As the plant demand of coolant varied the motor-pump sets would be switched on or off to maintain the required head. The switching of a pump set was purely a function of glycol flow and its position in the switching sequence.

An outline of the pumping station control circuit is also given in Figure 4.1. The total glycol flow was measured using an electronic pressure transducer connected to a Dahl tube on the coolant main. The output of this transducer was in the form of a d.c current signal with a magnitude that was directly proportional to the flow. This signal was applied to four electronic relays, whose contacts could be programmed to close as the current exceeded a preset value. The outputs of the relays were then connected through a selection switch to the supply contactors of the four motor-pump sets. Additional timing relays were used to ensure that once a machine was switched on or off it would remain in that state for a preset time and thus protect the induction motors against excessive numbers of starts.

The selection switch could be used to change the position of a particular motor-pump set in the switching sequence and so alter its duty cycle. This enabled the plant operators to perform a crude manual form of load sharing, and attempt to minimise the overall plant ageing.

4.3 EXPERIMENTAL MEASUREMENT

The experimental measurements on the pumping station were performed for two purposes. Firstly, the system needed to be quantified for the stochastic optimisation theory. This required a knowledge of both the total system load probability and the pump motor loss functions. The former could be obtained from a continuous record of the glycol flow over a set period, and the latter was estimated initially from manufacturer's data and subsequently determined from measurements.

Secondly, a set of results needed to be obtained from which the findings of the stochastic theory could be qualified. A suitable test of the theory would be an experimental comparison with each of the input load distributions of the motor-pump sets. This would require a recording of the power input to each of the induction motors in addition to the flow measurements. Finally, information should be available with which the assumed pump-motor loss functions and control switching limits could be confirmed.

The data was measured on site by using a 'PET' microcomputer and a dedicated data logging peripheral. The

data logger was designed as a versatile system, suitable for many applications including the above. A brief description of this device is given in the Appendix A5.

The inputs to the data logger were in the form of five scaled d.c voltage signals, of which one was proportional to the level of glycol flow and the remaining four were proportional to the motor-pump input powers. The glycol flow input was achieved by inserting a calibrated resistor in series with the output of the installed flow transducer. The power inputs were obtained from commercial wattmetric transducers, each connected via a single current transformer and a phase neutral voltage tap to the motor supplies.

This method of power measurement was chosen to minimise the number of current transformers, although it was necessary to assume that the motors were always operating under balanced conditons.

The data logger performed three functions, it acted as a real time clock, it averaged the inputs over successive intervals of 15mins and stored them in an internal memory, and it could also provide instantaneous readings of the inputs. A suite of commands were used by the controlling 'PET' micro computer to access the data logger via an IEEE 488 bus. A short BASIC program on the 'PET' was used to periodically dump the averaged values, after appropriate scaling and formatting, onto a digital cassette tape. In addition, the program continually monitored the instantaneous data recordings to detect the occurrence of any motor

switching. When a switching took place, the samples immediately prior to and after the switching were registered and stored, together with the time of the event, onto a second digital cassette.

The information on the first cassette could then be used to give the glycol flow and motor-pump power means and a measure of their distributions. Data on the second tape would give the time, power and flow values at which switching occurred, from which the switching limits and the motor-pump power to flow characteristics could be extracted.

Denoting the nth averaged flow sample as Q_n and the input power sample, for the ith motor-pump set, as W_{in}; then the total flow and power means μ_q and μ_{wi} are given by:

$$\mu_q = \frac{1}{n_s} \sum_{n=1}^{n_s} Q_n \qquad (4.1)$$

$$\mu_{wi} = \frac{1}{n_s} \sum_{n=1}^{n_s} W_{in} \quad , i = 1, \ldots, 4 \qquad (4.2)$$

where n_s = total number of samples.

Although these samples were formed from data continuously averaged over short periods, they can be used to give a representation of the data frequency distributions. This is because the lengths of the averaging periods were small compared with the total time over which the data was

recorded. In effect, the averaging of the data was equivalent to passing it through a low pass filter.

The probability of the flow Q lying between the values Q_1 and Q_2 can be obtained from:

$$p(Q_2 > Q \geqslant Q_1) = \frac{1}{n_s} \sum_{n=1}^{s} m_n \qquad (4.3)$$

where $m_n = 0$ $\quad Q_n \leqslant Q_1$

$m_n = 1$ $\quad Q_2 > Q_n \geqslant Q_1$

$m_n = 0$ $\quad Q_n > Q_2$

However, when analysing the power input distributions, the averaged data W_{in} needed to be adjusted to allow for the switching of the machines. If, for example, a motor-pump set was running at the start of a particular 15 minute sampling period and then was switched off during that period; then the recorded data would not be equal to the true average power input to the machine whilst it was running. Here the data would be corrected by increasing it in proportion to the time that the machine was not running.

Let t_{in} be equal to the dimensionless proportion of the nth sampling period that the ith machine was running, then the frequency of the input power W_i of that machine is given by:

$$p(W_2 > W_i \geqslant W_1) = \frac{1}{n_s} \sum_{n=1}^{n_s} m_n \qquad (4.4)$$

where $m_n = 0$ $\quad \frac{W_{in}}{t_{in}} > W_2$

$m_n = t_{in}$ $\quad W_2 > \frac{W_{in}}{t_{in}} \geqslant W_1$

$m_n = 0$ $\quad \frac{W_{in}}{t_{in}} \leqslant W_1$

On installation, the total system was calibrated by programming the 'PET' microcomputer to repeatedly display the scaled instantaneous data samples. It was not possible to check the flow readings over the full range, because during the calibration period there was little fluctuation in the glycol flow. However, the readings taken did agree well with the industrial flow meter. The power readings were calibrated by connecting moving coil watt-meters in series with the wattmetric transducers and then using the manual pump selection switch to load each of the four machines. All the readings taken lay on the same curve, Figure 4.2, and it was found that the recordings were well within the expected accuracy of 2% of the total data logging system.

Also during calibration, it was confirmed that the load was shared equally between the machines that were running. The load sharing was seen to be good, apart from one particular motor-pump set which took only a small proportion of the total load, to the extent that the remaining machines were overloading in trying to meet the demand. It was subsequently discovered that the pump had

an undersized impeller and had been running in this condition for a considerable length of time.

It should be noted that, during the weeks of measurements on the pumping station, this faulty pump was switched to the last position in the load sharing sequence and the glycol flow was never large enough to require its use.

4.4 MOTOR-PUMP LOSS FUNCTION

The glycol pumping system is similar, in many respects, to the theoretical multi-machine system described in the earlier chapters. However, certain alterations are required to the earlier analysis in order that it may be applied directly to this particular case.

The system demand on the pumping station is a specific flow of the glycol coolant and the switching control of the motor-pump sets is based upon this flow. Thus, an analysis of the system should be based upon the glycol flow rather than the absolute output power.

The power losses in the motor-pump sets were modelled in terms of the glycol flow by a quadratic loss function $\gamma(Q)$ such that the power loss in a particular set which was pumping glycol at the rate of Q m^3/hr would be given by:

$$\text{Set Power Loss} = Q\gamma(Q) \quad \text{kW} \tag{4.5}$$

$$\text{where} \quad \gamma(Q) = \frac{a}{Q} + b + \frac{Q}{c} \tag{4.6}$$

for constants a,b,c,

The actual power output of the set is the product of the flow Q and the system head, The system head is characterised by the pumps used and can be modelled in terms of the pump flow by a head function H(Q). As with the losses, the head function was approximated by a quadratic fit to the manufacturers data. The power output was thus equal to:

$$\text{Set Power Output} = QH(Q) \quad \text{kW} \qquad (4.7)$$

where $$H(Q) = \frac{d}{Q} + e + \frac{Q}{f} \qquad (4.8)$$

for constants d,e,f.

It follows that the total power input to one of the motor-pumps is the sum of the losses and the output power, such that:

$$\text{Set Power Input} = Q(\gamma(Q) + H(Q)) \text{ kW} \qquad (4.9)$$

The set loss function $\gamma(Q)$ was formed from a combination of the individual loss functions $\gamma_m(W)$ and $\gamma_p(Q)$ of the induction motor and pump respectively. The induction motor loss function (Appendix A1) was expressed, in terms of its output power W, as:

$$\gamma_m(W) = \frac{a_m}{W} + \frac{W}{c_m} \qquad (4.10)$$

Whereas for the pump loss function a quadratic form was taken in terms of the output flow Q, as shown by:

$$\gamma_p(Q) = \frac{a_p}{Q} + b_p + \frac{Q}{c_p} \qquad (4.11)$$

The input power to the pump, and hence the output power W of the induction motor, is given by Equation (4.9) as:

$$W = Q(\gamma_p(Q) + H(Q)) \tag{4.9}$$

$$= Q\left(\frac{(a_p+d)}{Q} + (b_p+e) + Q\left(\frac{1}{f} + \frac{1}{c_p}\right)\right) \tag{4.12}$$

The overall losses in the set are the sum of the motor and pump losses, which expressed in terms of W and Q are:

$$Q\gamma(Q) = W\gamma_m(W) + Q\gamma_p(Q) \tag{4.13}$$

Substituting Equations (4.11) and (4.12) yields

$$Q\gamma(Q) = a_m + \frac{1}{c_m}((a_p+d) + (b_p+e)\,Q + Q^2\left(\frac{1}{f} + \frac{1}{C_p}\right))^2 + a_p + Qb_p + \frac{Q^2}{c_p} \tag{4.14}$$

The input power of a centrifugal pump is approximately a linear function of the flow and in general the term $(1/f + 1/c_p)$ in Equation (4.14) can be neglected. Hence $\gamma(Q)$ can be reduced to the quadratic form:

$$\gamma(Q) = \frac{a}{Q} + b + \frac{Q}{c} \tag{4.6}$$

$$\text{where} \qquad a = a_m + a_p + \frac{(a_p+d)^2}{c_m} \qquad (4.15)$$

$$b = b_p + 2\left(\frac{(a_p+d)\ (b_p+e)}{c_m}\right)$$

$$c = \frac{1}{\left(\frac{1}{c_p} + \frac{(b_p+e)^2}{c_m}\right)}$$

The pump loss and head function parameters were calculated from a fit to the manufacturer's performance curves. Figure 4.3 gives the performance curves and shows that a good agreement was obtained.

Data was not directly available for the induction motor loss parameters and so they were extrapolated from the losses of a typical TEFC induction motor, using the scaling laws laid out in the Appendix A1. These parameters, together with those of the pump loss and head characteristics, are given in Table 4.1 . The values are in per unit to a flow base of 232 m^3/hr (the rating of the pumps) and a power base of 25kW.

The total motor-pump set loss function parameters, as calculated from Equation (4.15), are given in the upper part of Table 4.2 . The set input power, calculated from Equation (4.9), is plotted against output flow in Figure 4.4 . This curve is compared with points obtained from the instantaneous samples taken during the load measurements on site. The spread on the points was considered to be a

result of readings that were taken in transient conditions, when the machines were being switched or there were sudden changes in the system load. However, the majority of the samples fitted the slope of the theoretical curve well, but there appeared to be a constant difference of approximately 3kW between the points and the curve. This offset was attributed to additional friction losses in the sets. Such losses would be a result of wear in the pump and motor bearings and the common shaft coupling and extra fluid friction losses caused by wear on the surfaces of the pump impellers.

These additional losses were taken into account by increasing the 'a' term in the set loss function. The modified loss function is given in the lower half of Table 4.2 and is seen to give an improved fit to the experimental points in Figure 4.4 .

4.5 SYSTEM EQUATIONS

The stochastic theory of Chapter 2 was applied by assuming that the system load acted as a random variable with a known frequency distribution. In this particular case, the frequency distribution p(Q) was measured in terms of the glycol flow Q. Although a knowledge of this distribution was not needed in the optimisation of the switching limits, a model of the flow distribution was required if the effects of the optimisation were to be evaluated. Beta functions were used to model the flow distributions for the two weeks

of results and their parameters were chosen such that both the model and the data would have the same mean and variance.

A simplified version of Equation (2.25) was used to obtain the overall system losses, as clearly the machine sizes were fixed. Here, the load sharing factor was simply the reciprocal of the number of machines running, which gave the total losses as:

$$\text{Total losses} = \sum_{i=1}^{4} \int_{Q_{\ell i-1}}^{Q_{\ell i}} p(Q)\gamma(Q/i)QdQ \qquad (4.16)$$

for switching limits $Q_{\ell i}$, $i = 1, \ldots, 4$

Similarly the total output power was expressed as:

$$\text{Total Output Power} = \sum_{i=1}^{4} \int_{Q_{\ell i-1}}^{Q_{\ell i}} p(Q)H(Q/i)QdQ \qquad (4.17)$$

Expressions for the input power distributions for each of the pump-motor sets were also required, to examine the total model performance.

The input power distribution $p_i^*(W)$ of ith motor-pump set was determined in terms of its input power W, from the load distribution p(Q) by the following equations:

$$p_i^*(W) = \sum_{j=1}^{4} jp(jQ)/\left|\frac{dW}{dQ}\right| \qquad (4.18)$$

$$Q_{\ell j-1} \leq jQ < Q_{\ell j}$$

$$W = Q(\gamma(Q) + H(Q)) \qquad (4.19)$$

and Q = flow through jth pump

The form of Equation (4.18) is applicable where only a single value of output flow can be associated with a given input power. This condition can be seen to be valid from Figure 4.4 .

The switching limits that minimised the system losses were obtained from Equation (2.30). Again a simplified version of this equation could be used and is given below:

$$(Q_{\ell r}/r) = \gamma(Q_{\ell r}/(r+1)) \qquad (4.20)$$

for $r = 1, \ldots, 3$

With the quadratic loss function of Equation (4.6), the above could be solved directly for the switching limits, to yield:

$$Q_{\ell r} = \sqrt{r(r+1)ac} \qquad (4.21)$$

4.6 RESULTS

Two sets of data were measured at the Runcorn plant, each over a period of one week. From the first set, the original system performance was evaluated. Recommendations were then made for values of switching limits that would improve the overall system efficiency. The new values were programmed into the control system at Runcorn and the second set of data was taken to confirm that the system performance had been improved.

4.6.1 Week 1

The measured flow and input power distributions are given, in histogram form, in Figures 4.5 through to 4.7 and their means and deviations (square root of variance) in Table 4.3 . The flow and power are given in per-unit, to the bases of 928 m^3/hr and 39.2kW, which were equal to the maximum rated output of the pump station and the rated inputs of the motor pump sets respectively. Over the week, the flow demand was never large enough to require the use of the fourth pump.

The values of flow at which the pumps switched were observed from the second data cassette. The switchings appeared to occur over quite a large range of flows, as can be seen from Table 4.4 which gives the mean and range of the switching limits of the second and third stage. This effect could be attributed to two causes; sampling errors by the data logger and noise on the system flow.

Errors in the sampling were considered to be small. The pump station inputs were sampled approximately every 20 seconds and hence the time difference between the recorded data, prior to and after a switching was minimal. The limits were determined from the flow before the switching, because immediately after the switch the system head would change and cause a corresponding transient in the flow.

However, if the response of the system controller was slow, a feature which would be built in to make it immune to load noise, the sampling time of the data logger would

be several times smaller than the controller time constant. Thus, the recorder could register noise on the flow to which the controller would be unable to respond.

From Table 4.4 it was seen that the mean values of the switching limits were different to the set values expected; i.e. multiples of the pump ratings, which suggested that either the original settings were inaccurate or there was a calibration error in the controller. The plant operators were unable to provide further information on this point.

The theoretical model used a Beta function for the flow distribution, which had equal mean and variance to the measured flow. The mean values of above were used for the switching limits. The model of the flow distribution together with the calculated power input distributions are shown as continuous curves on the histograms of Figures 4.5 to 4.7 . A comparison of the means and deviations of these distributions is given in Table 4.3 .

The measured flow, Figure 4.5, did not have a very smooth distribution, but still the Beta function model was a reasonable fit. The flow distribution would have been improved if the measurements were performed over a greater period than a week, but unfortunately this was not possible due to time constraints.

The input load distributions were seen to be in good agreement, both in mean and variance values and in the fit of the theoretical curves to the histograms. There was a discrepancy in the lower powers where the actual machines appear to be running below the minimum switching limits.

This was a result of the variance in switching limits mentioned above.

The model was within an agreement of 3% error, on the total measured input energy. This could be attributed to a combination of errors introduced from the motor-pump loss model, the Beta distribution match to the measured flow and the variance of the switching limits. The latter appeared to be the major contributor to the errors. The input distribution of the third motor-pump set had the poorest agreement in the results, which was seen from Figure 4.7 to come from the spread in the measured distribution caused by the range of switching limits.

The magnitude of the input distribution error is in the order of the loss savings suggested in the following section, when small (10%) changes in the switching limits are applied. However, the error is half that of the loss reduction with optimum switching limits. The model was thus considered to be sufficiently valid to be used to evaluate the system performance with a variety of switching limits.

4.6.2 Variation in System Performance with Switching Limits

Five sets of switching limits were considered and are listed below.

1) The limits with which the system was operating during the measurement week.
2) The limits equal to the rated output of the pumps, which were the values that should be set on the system controller.

3) The limits equivalent to a 10% overload on each of the pumps.
4) The limits equivalent to a 15% overload on each of the pumps.
5) The optimum switching limits obtained from Equation (4.21).

These limits and the system performance are given in Table 4.5 . Here the loss and the input is given as a total energy consumption over the week.

The last three sets of switching limits all would exert overloads on the motor-pump sets. In particular the optimum switching limits required overloads of 63% on the first pump and 41% on the second pump and suggested that only three pumps would be needed to meet the maximum flow demand. Clearly the effects of these overloads had to be considered before a change in switching limits could be applied.

An overload on a centrifugal pump results in a reduction in the output head. There will be no significant reduction in the life expectancy of the pump on overload unless the head becomes sufficiently small for cavitation to occur [28]. Cavitation would result in a considerable increase in the wear on the pump's impeller. However, this is unlikely to occur in a closed system, such as the glycol refrigeration circuit, as long as the head remains above the pump's characteristic net positive suction head (NPSH).

An overload on an induction motor will result in

an increase in the machine's winding temperature, which will accelerate the ageing of the winding insulation. Whether, this causes any significant reduction in the expected lifespan of the motor is dependent upon the machine's load distribution and control, and is the subject of Chapter 3.

In Table 4.5 the overloading is summarised by giving values of the expected minimum system head and the percentages of the total time the induction motors would be overloaded. The induction motors are overloaded only when the maximum pump output is increased by above 15%, because of the generous difference between the pump and motor ratings. It is clear from the results that the application of the optimum switching limits would cause excessive overloads.

From the table it can be seen that as much as a 17% reduction in losses can be achieved by altering the switching limits. Resetting the controller to the correct rated switching limits would give a slight increase in performance. With an increase in the switching limits to 10% above the rated values, the losses are reduced by 8%, with a slight decrease in the minimum system head. A further 5% increase in the limits will give an extra 2% reduction in losses with a corresponding 4% decrease in the minimum head.

The system performance over a full range of switching limits from the measured running conditions to the optimum

values is shown graphically in Figure 4.8. Here the system losses, efficiency and minimum head are plotted against the limits, and are all expressed as p.u. values to a base of the conditions at rated switching limits. Also shown in the figure are the percentages of time the first and second induction motors would be expected to be overloaded. The system efficiency reaches a maximum at approximately a 30% increase in the switching limits. This occurs when the reduction in losses becomes comparable with fall of the total output power, caused by the lowering of the head. The final choice of switching limits would have to be a compromise between the savings in energy and the minimum allowable system head and maximum motor overloadings.

The results of this analysis were reported in Bass brewery[29]. It was recommended to reset the switching to values of 10% above the pump ratings. This small change would result in 8% and 4.7% savings in their losses and total energy respectively, compared with their present operation. The effect on the overall system head was seen to be small.

4.6.3 Week 2

A second week of data was logged whilst the system was operated with the increased switching limits. Unfortunately over this period the glycol demand was small and the results were not directly comparable with those of the first week.

The system was modelled using the techniques described before, and the results are presented in Figures 4.9 to 4.11 and Tables 4.6 and 4.7. The glycol flow

distribution was jagged and discontinuous, hence the Beta distribution model did not give a very good fit to the data. A poorer agreement was obtained with the power distributions than for the first week, with the modelled total energy consumption within 9% of the measured value. It was thus impossible to make any definite statement as to whether the change in the switching limits had resulted in any improvement.

Again there was a considerable variation in the switching limits, Table 4.7, and the mean values were measured as being equivalent to 6% and 4% above the rated values for the first and second limits respectively. The increase was lower than recommended due to a conservative setting of the controller by the operators. However, even those small increases in switching limits should result in energy savings, estimated as a 5% reduction in losses from Figure 4.8.

A comparison on the model between the previous week's and the uprated switching limits is given in Table 4.8. The change has resulted in a reduction of 3.4% in the losses and a corresponding increase of 1.2% in the efficiency. These savings are lower than those expected from the first week's results. This was because the loading on the system was such that for the majority of the time, only the first pump was running and consequently the operating time around the switching limits was small. A higher loading would have resulted in a proportionately greater saving in energy.

Table 4·1 Per Unit Loss and Head Function Parameters.

Pump Loss Function $\gamma_p(Q)$	a_p	0·84
	b_p	-1·31
	c_p	1·31

Motor Loss Function $\gamma_m(W)$	a_m	0·077
	c_m	21·6

Head Function H(Q)	d	-0·26
	e	2·02
	f	-1·31

Per Unit Bases: Flow 232 m^3/hr

Power 25 kW

Table 4·2 Per Unit Motor-Pump Set Loss Function Parameters

Set Loss Function $\gamma(Q)$	a	0·932
	b	-1·27
	c	1·27

Modified Loss Function $\gamma(Q)$	a	1·06
	b	-1·27
	c	1·27

Per Unit Bases: Flow 232 m^3/hr

Power 25 kW

Table 4·3 Week 1 Load Distributions

	Measured Mean	Measured Deviation	Model Mean	Model Deviation	Error Mean	Error Deviation
Flow p.u.	0·36	0·21	0·36	0·21	-	-
Motor 1 p.u.	0·82	0·08	0·85	0·11	+0·03	+0·03
Motor 2 p.u.	0·55	0·42	0·54	0·43	-0·01	+0·01
Motor 3 p.u.	0·38	0·48	0·30	0·43	-0·08	-0·05
Motor 4 p.u.	0·0	0·0	0·0	0·0	-	-
Total Energy p.u.	1·75		1·69		-0·06	

p.u. base:- flow 928 m^3/hr
power 39·2 kW
energy 6·58 MW-hr over 1 week

Table 4·4 Week 1 Switching Limits

	Min.	Max.	Mean
Q_{l1} p.u.	0·22	0·30	0·26
Q_{l2} p.u.	0·41	0·47	0·44

Table 4·5 Variation In System Performance With Switching Limits

Case		①	②	③	④	⑤
Switching Limits	Q_{l1} m^3/hr	245	232	255	267	381
	Q_{l2} m^3/hr	407	464	510	534	661
	Q_{l3} m^3/hr	696	696	766	800	928
	Q_{l4} m^3/hr	928	928	928	928	—
Total Loss	MW-hr	4·7	4·6	4·3	4·2	3·9
Total Input	MW-hr	11·1	10·9	10·6	10·4	9·4
Efficiency	%	57·6	58·2	59·0	59·3	58·5
Minimum System Head	mWg	38	39	37	35	20
Percentage of Time that Pumps are Running	1 %	100	100	100	100	100
	2 %	62	64	60	57	37
	3 %	33	25	19	16	6
	4 %	0	0	0	0	0
Percentage of Time that Motors are Overloaded	1 %	0	0	0	0·9	36·0
	2 %	0	0	0	0·5	11·2
	3 %	0	0	0	0	0
	4 %	0	0	0	0	0

Case
① As set
② Rated
③ 10% overload
④ 15% overload
⑤ Optimum

Table 4·6 Week 2 Load Distributions

	Measured Mean	Measured Deviation	Model Mean	Model Deviation	Error Mean	Error Deviation
Flow p.u.	0·20	0·17	0·20	0·17	-	-
Motor 1 p.u.	0·83	0·11	0·77	0·14	-0·06	-+0·03
Motor 2 p.u.	0·36	0·41	0·26	0·40	-0·10	-0·01
Motor 3 p.u.	0·04	0·19	0·05	0·21	+0·01	+0·02
Motor 4 p.u.	0·0	0·0	0·0	0·0	-	-
Total Energy p.u.	1·75		1·69		-0·06	

p.u. base:— flow 928 m^3/hr
power 39·2 kW
energy 6·58 MW-hr over 1 week

Table 4·7 Week 2 Switching Limits

	Min.	Max.	Mean
Q_{l1} p.u.	0·23	0·31	0·27
Q_{l2} p.u.	0·49	0·55	0·52

Table 4·8 Estimated Energy Improvement during Second Week

	Previous Limits	Uprated Limits	Change %
Total Loss MW-hr	3·8	3·6	3·4
Total Input MW-hr	7·3	7·1	2·4
Efficiency %	48·2	48·8	0·6

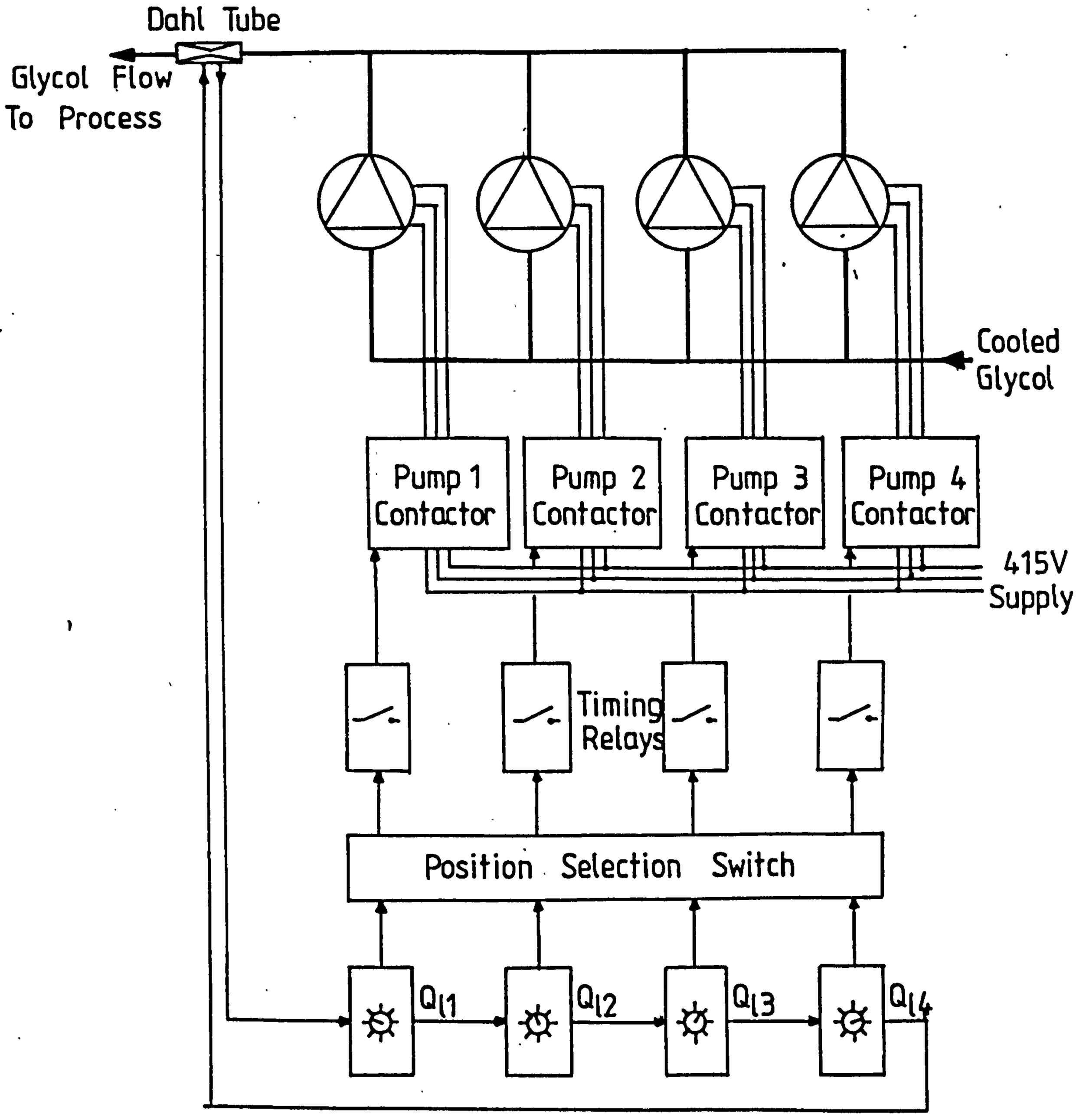

Machine Capacities:	Pumping Rate	232 m^3/hr
	Head	39·2 mWG
	Speed	2900 rpm
	Motor Capacity	50 HP (37·5 kW)
	Absorbed Power	42·7 HP (31·8 kW)

Figure 4·1. Pump Station Schematic.

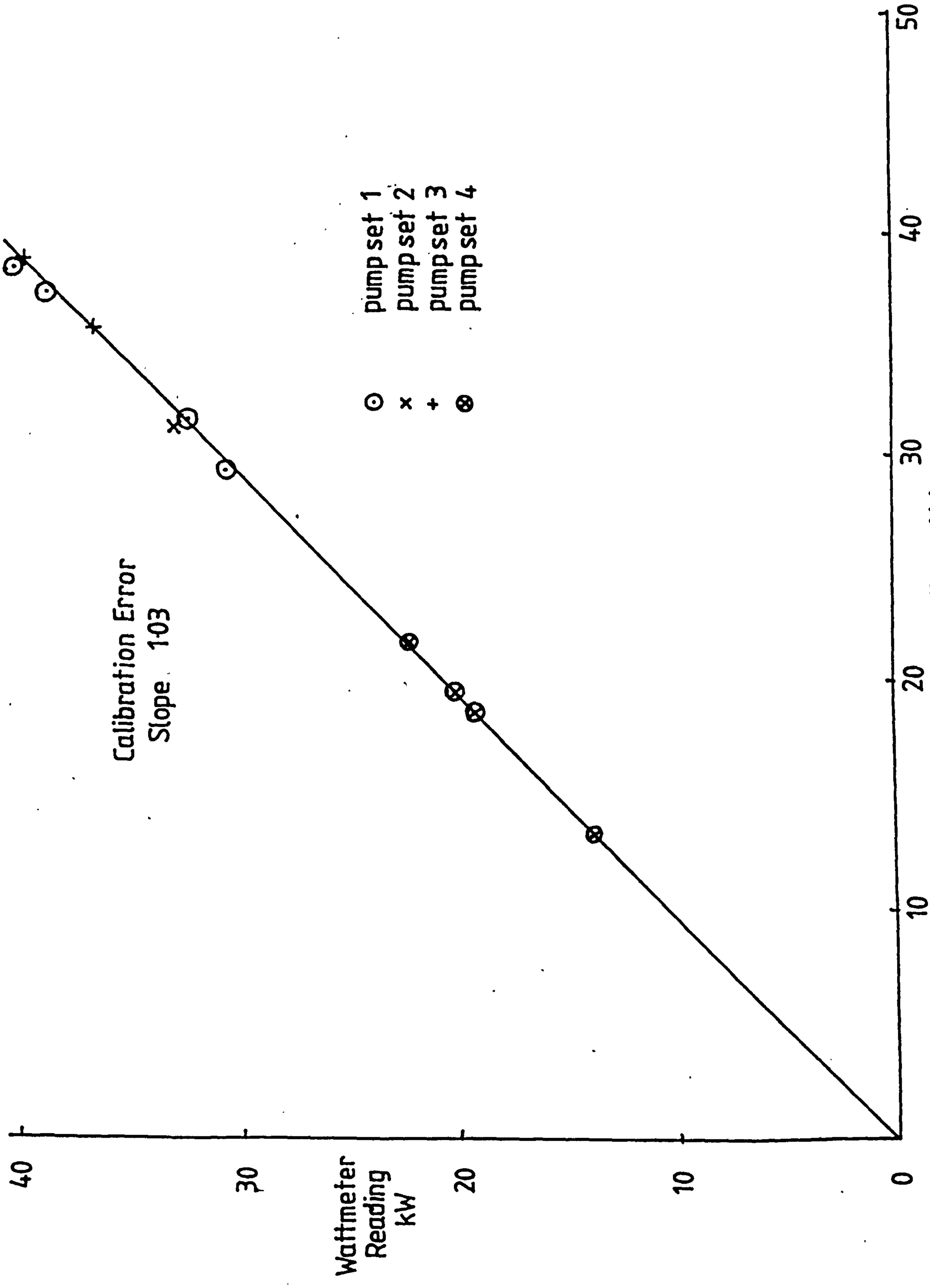

Figure 4.2. Recorded Power Calibration Curve

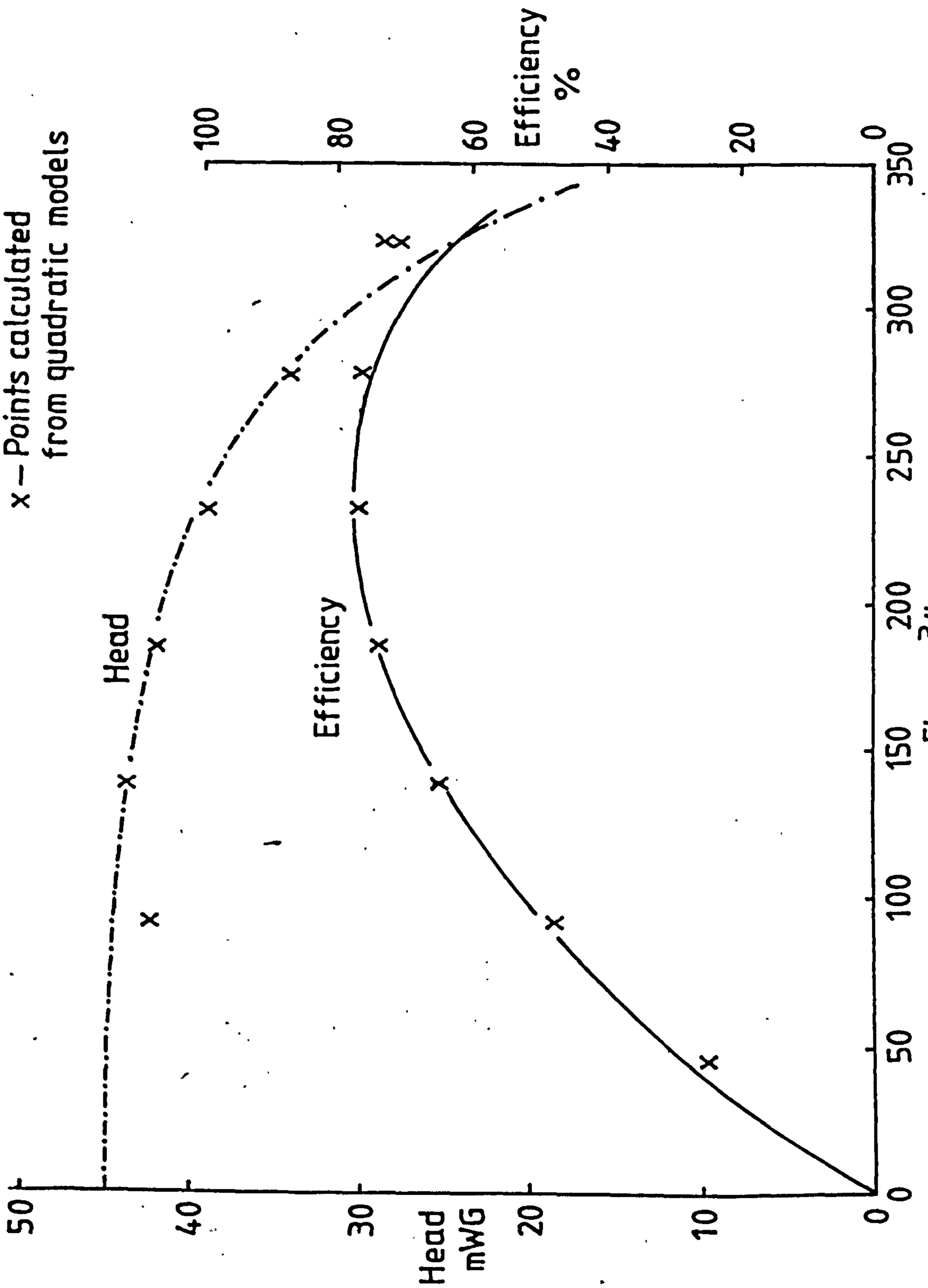

Figure 4.3. Comparison between Pump Performance Curves and values derived from Quadratic Loss and Head Functions

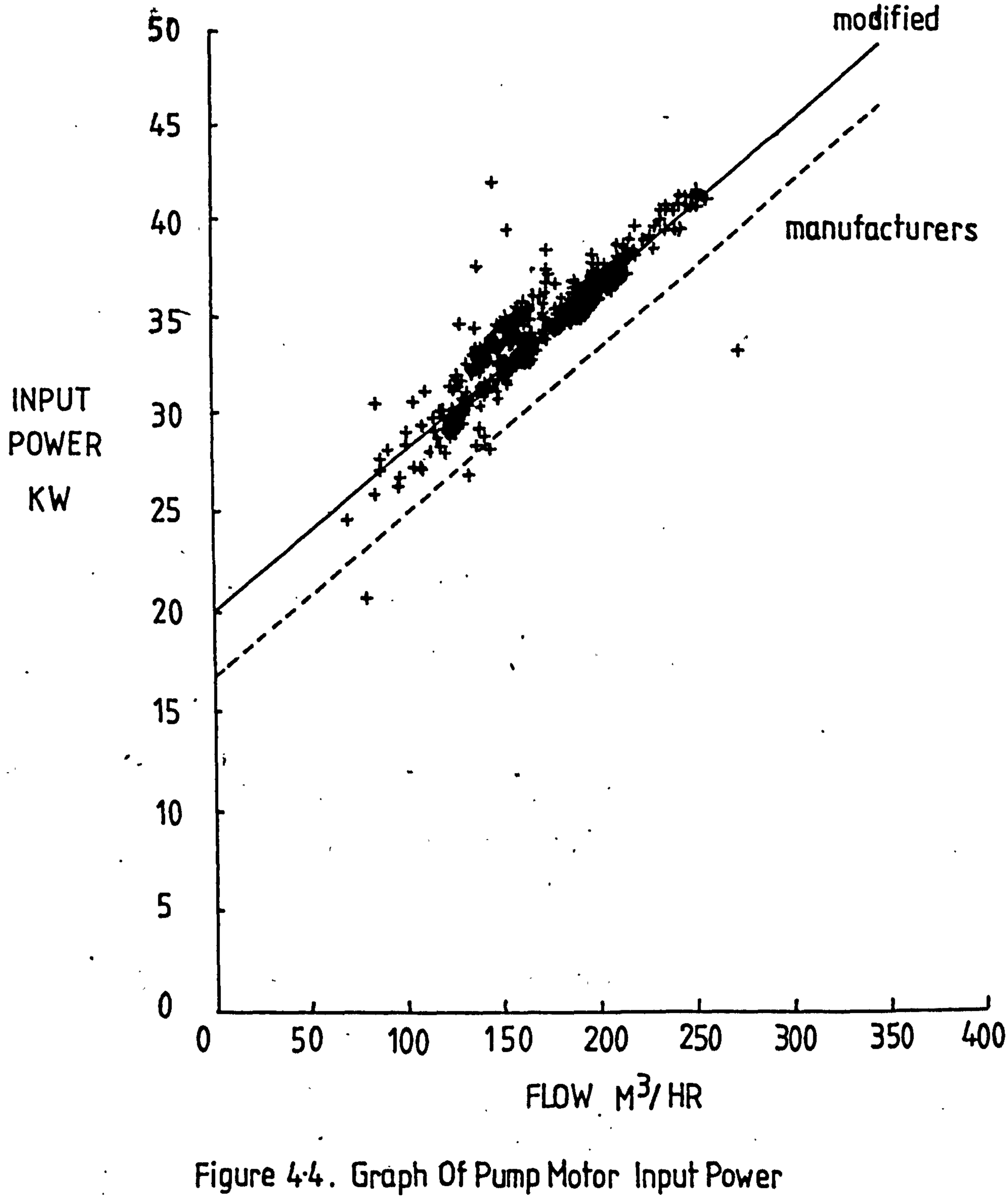

Figure 4.4. Graph Of Pump Motor Input Power Against Flow

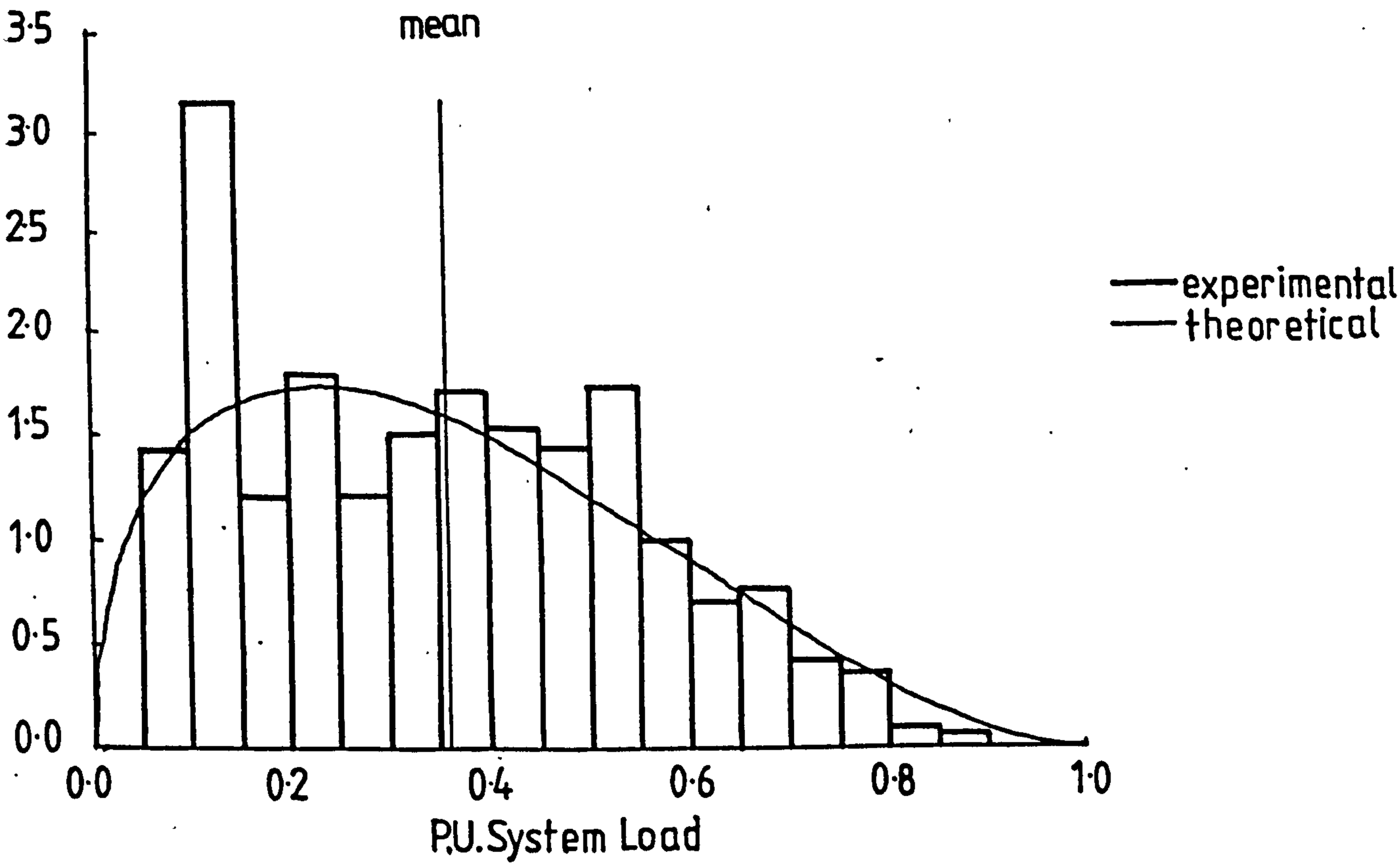

Figure 4.5. System Load Distribution—Week 1

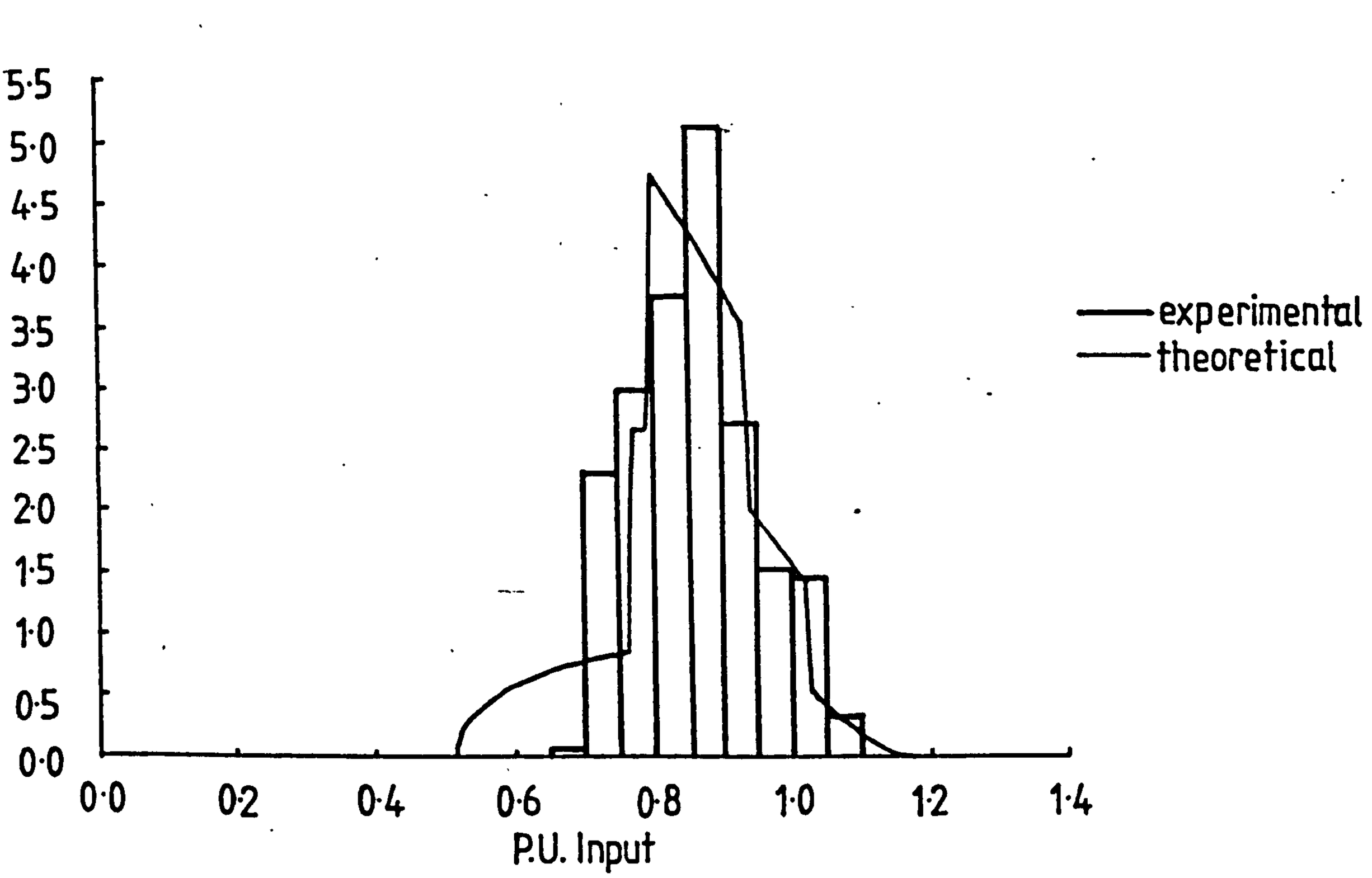

Figure 4·6a. Machine Number 1 Input Load Distribution —Week 1

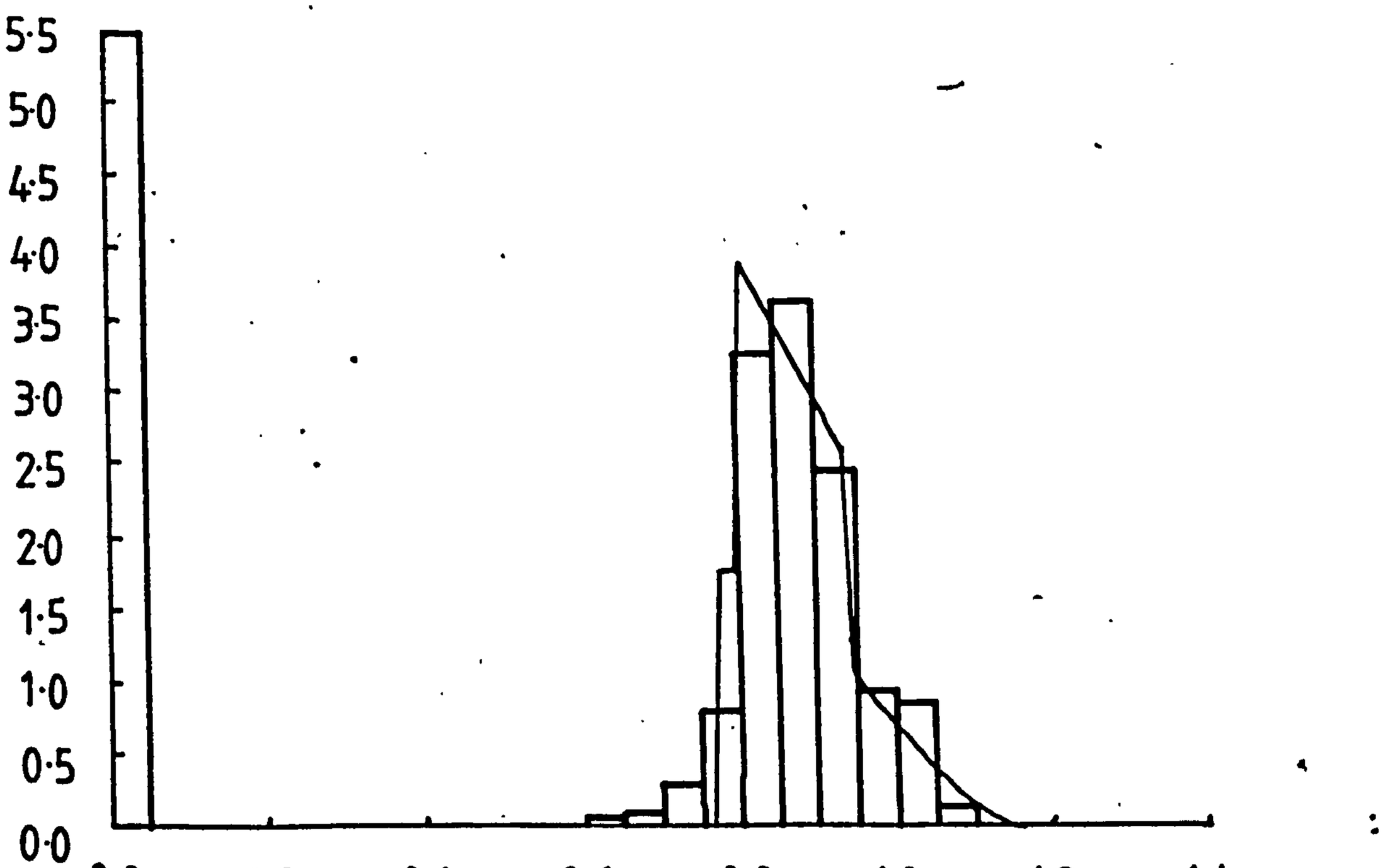

Figure 4·6b. Machine Number 2 Input Load Distribution— Week 1

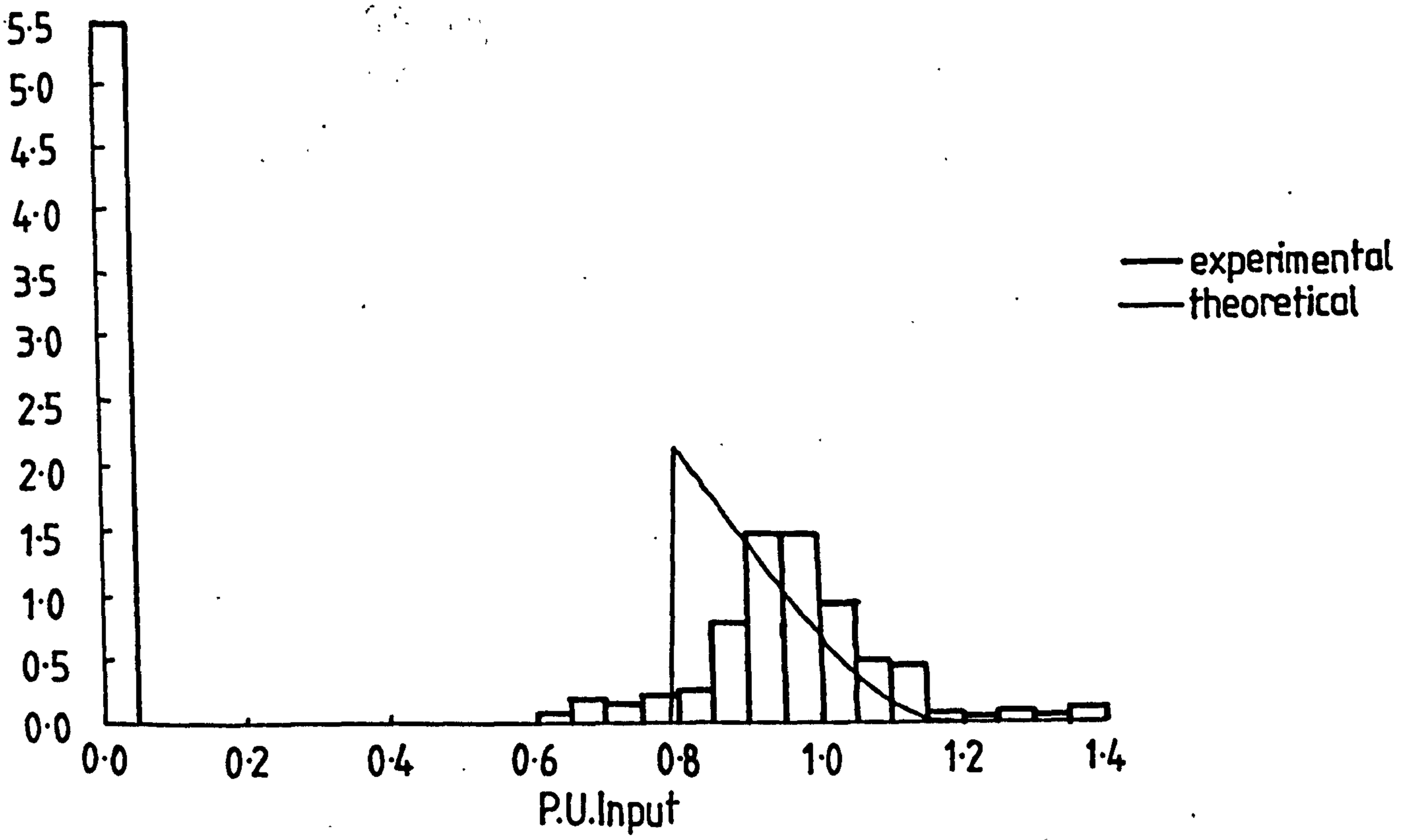

Figure 4·7a. Machine Number 3 Input Load Distribution—Week 1

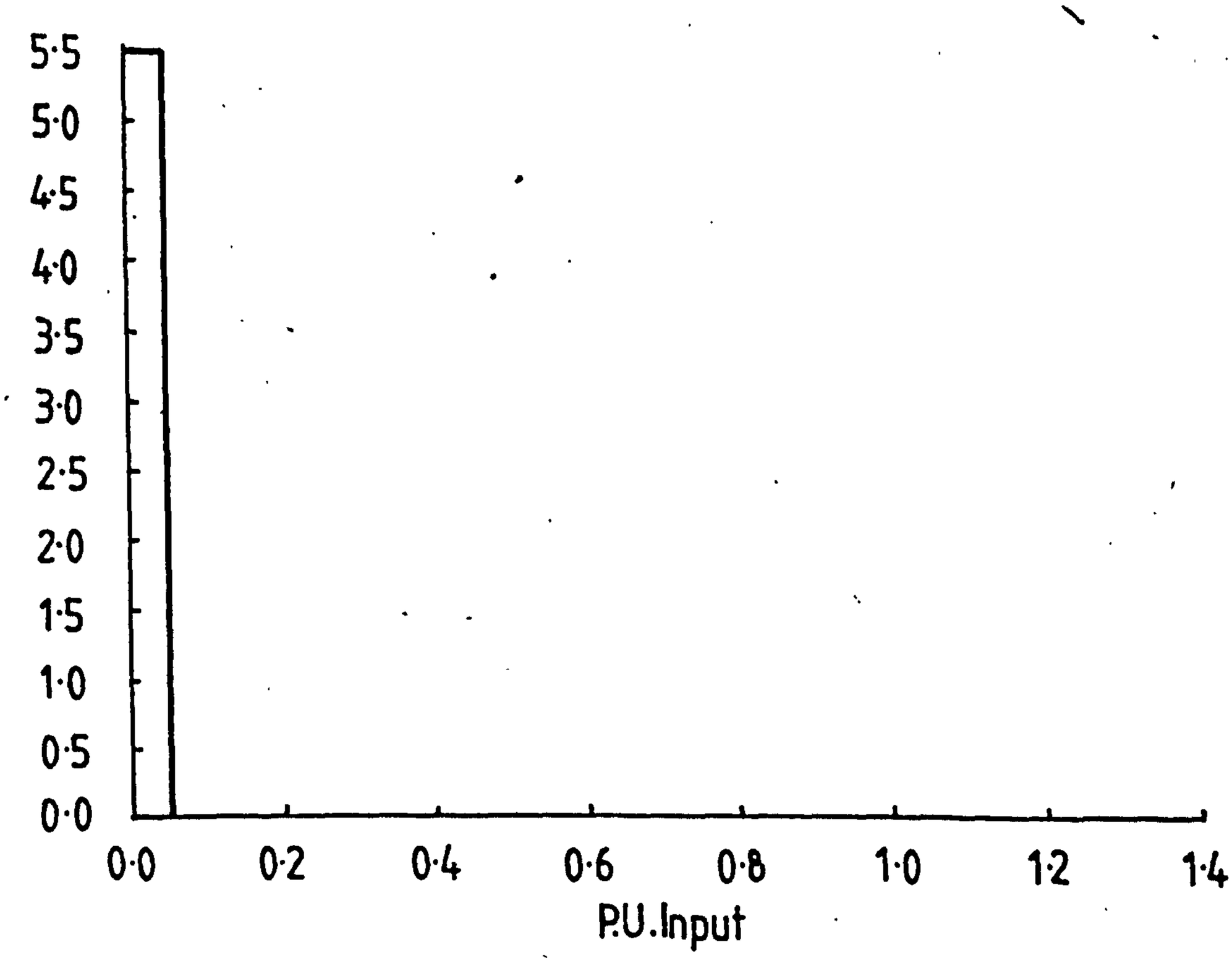

Figure 4·7b. Machine Number 4 Input Load Distribution—Week 1

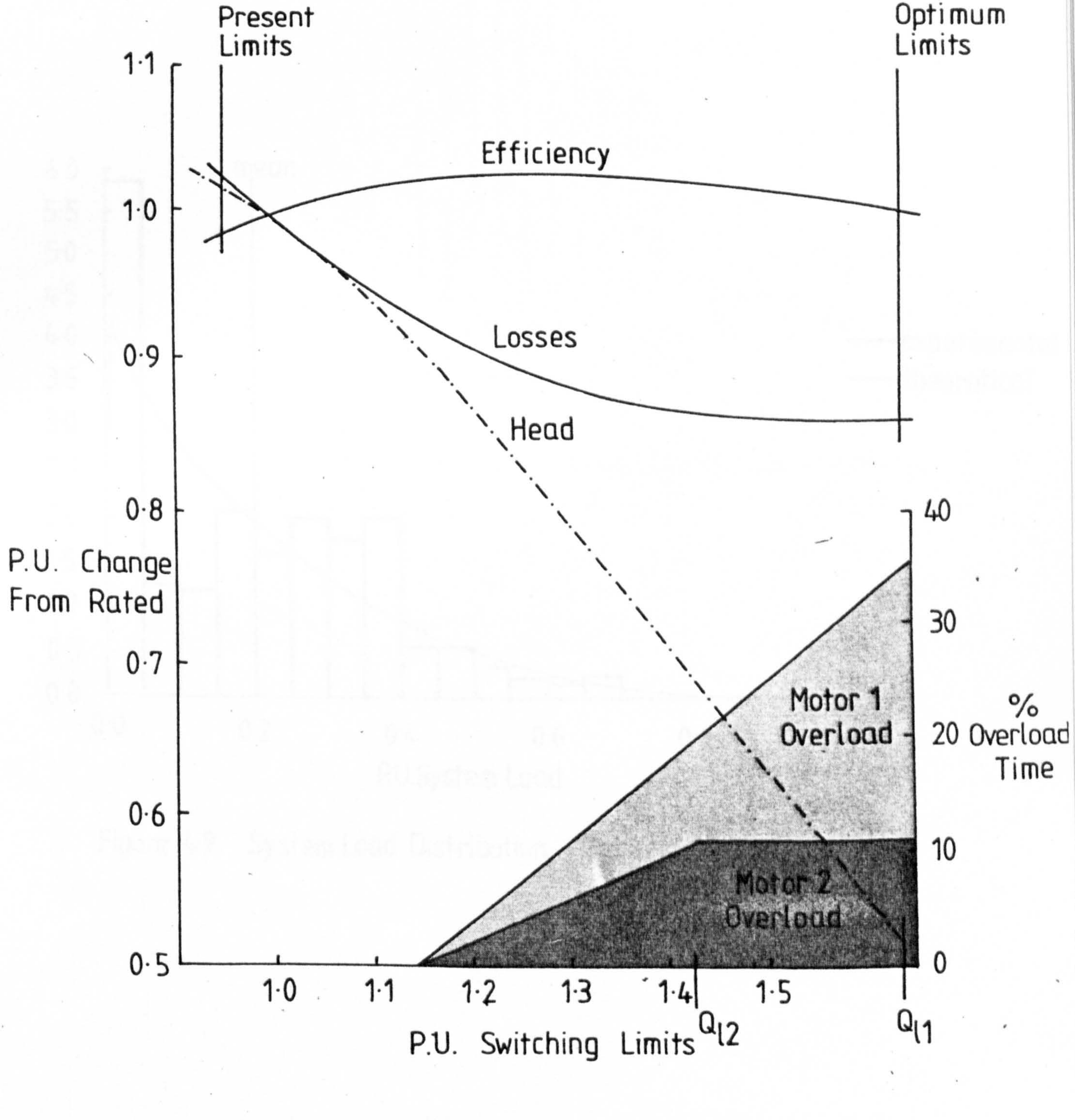

Figure 4·8 Modelled Pump Station Performance During Week 1

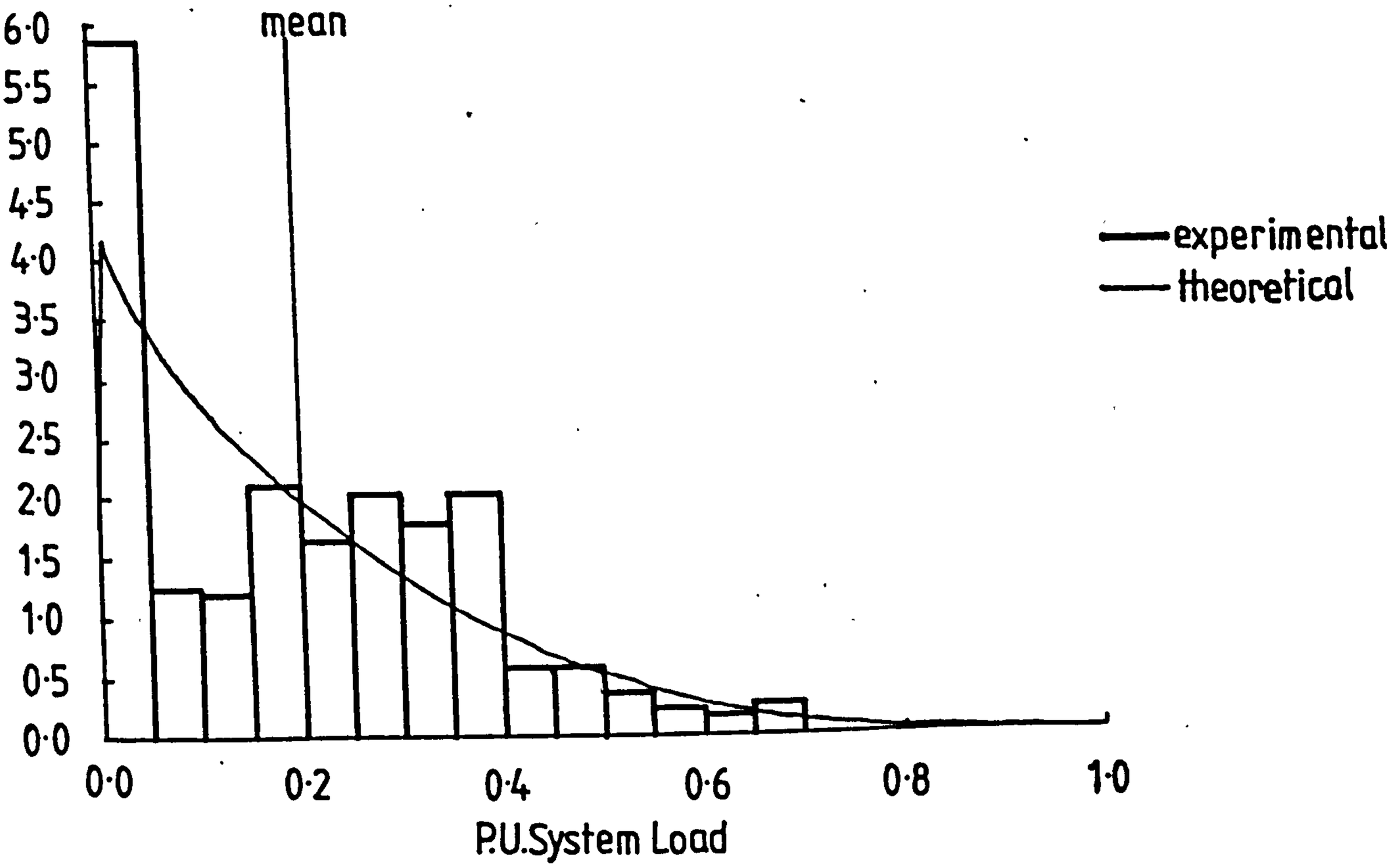

Figure 4·9. System Load Distribution — Week 2

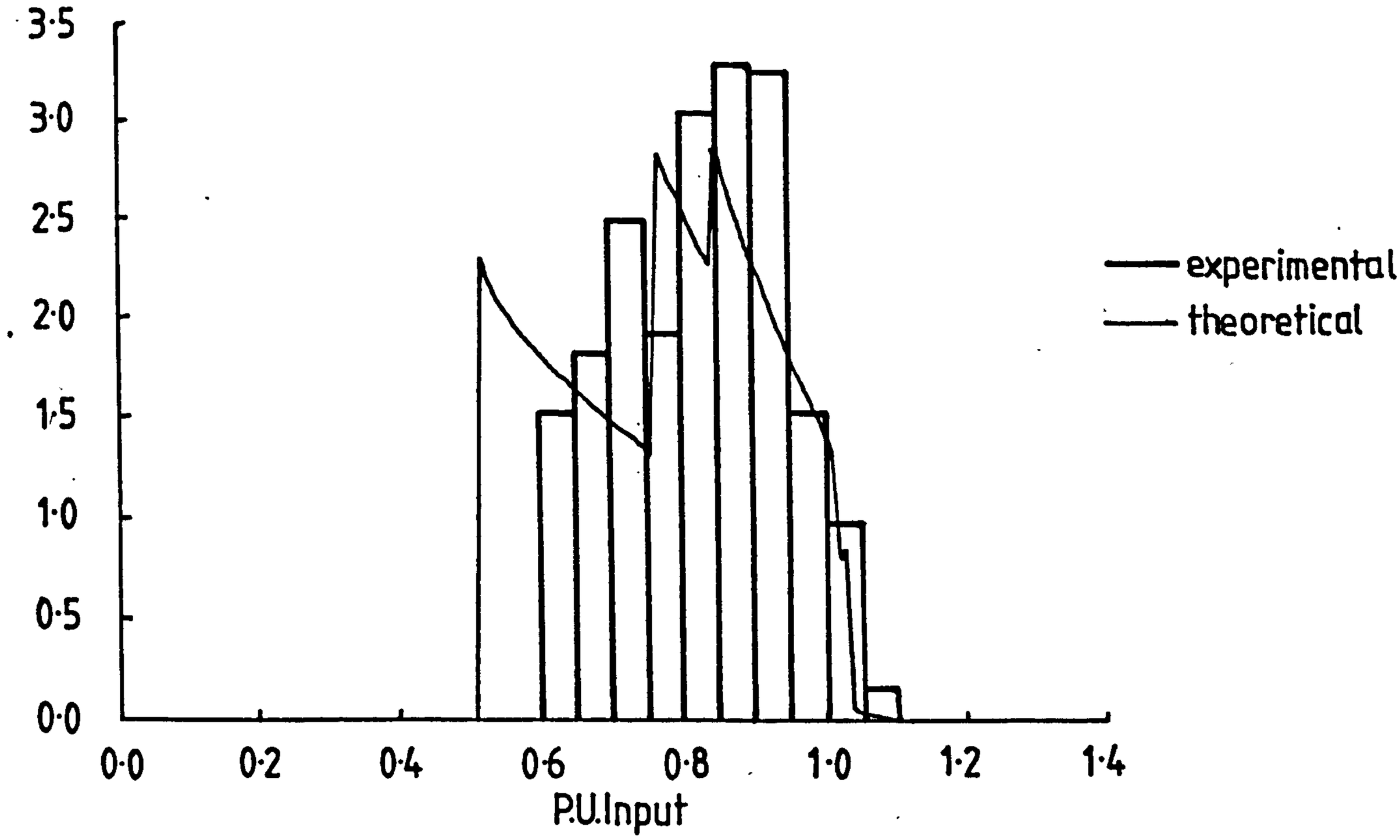

Figure 4·10a. Machine Number 1 Input Load Distribution — Week 2

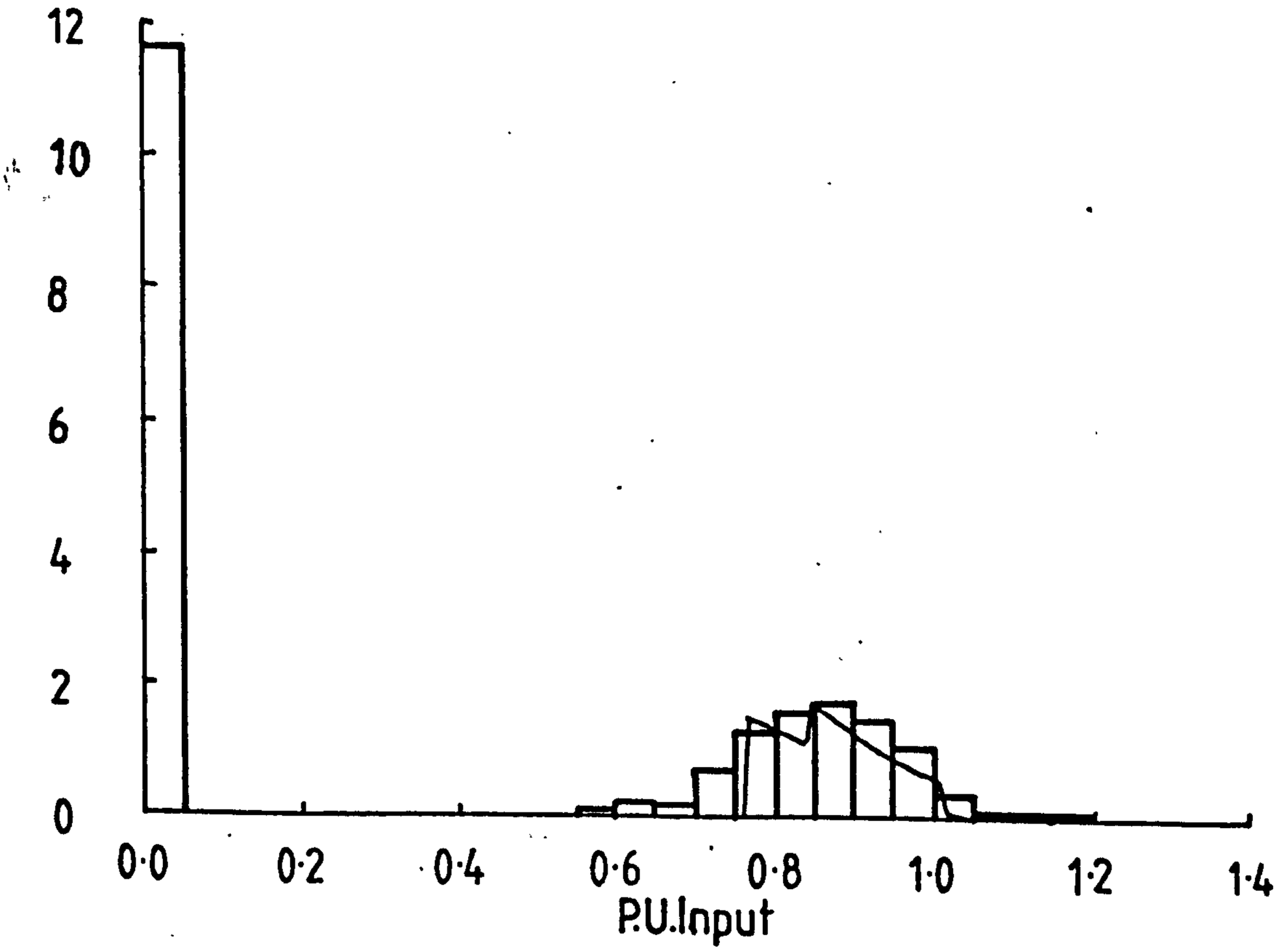

Figure 4·10b. Machine Number 2 Input Load Distribution — Week 2

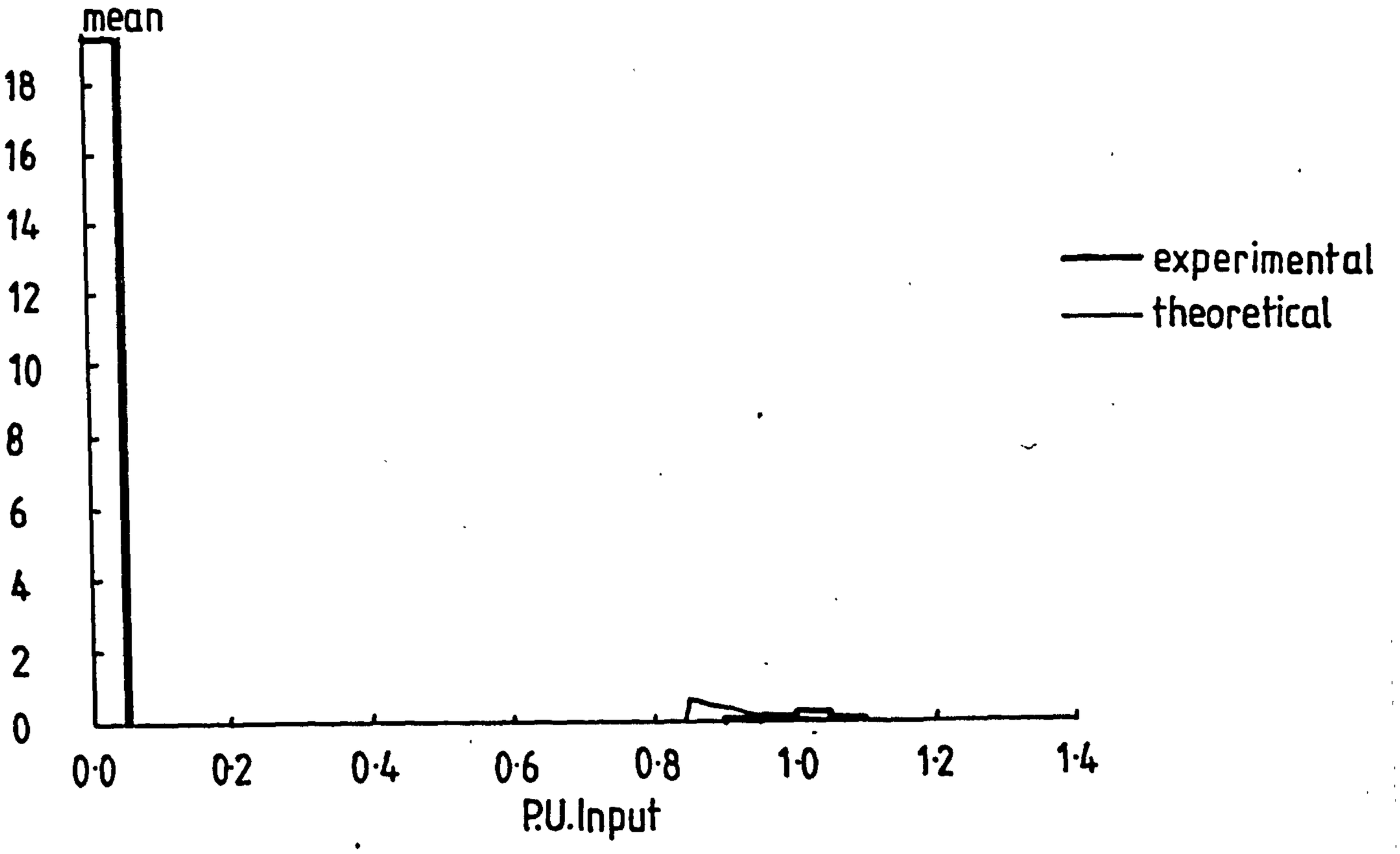

Figure 4·11a. Machine Number 3 Input Load Distribution—Week 2

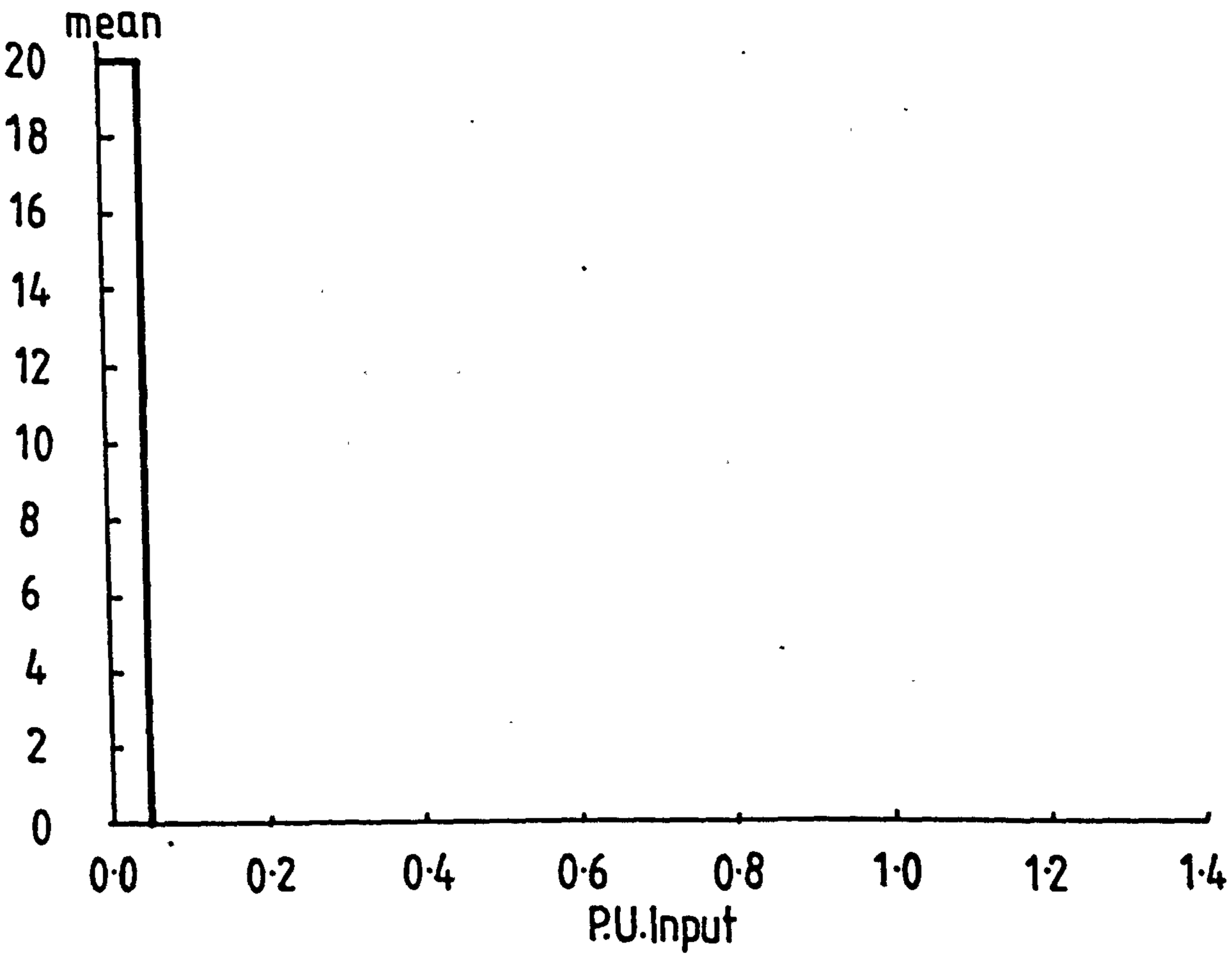

Figure 4·11b. Machine Number 4 Input Load Distribution—Week 2

CHAPTER 5

INDUCTION MOTOR THERMAL MODEL

5.1 INTRODUCTION

The major requirement in the ageing analysis of an electrical machine is that of a linear thermal model. The model should be sufficiently detailed, for it to be possible to determine the temperatures of the machine's winding insulation at the positions where insulation failure is most likely to occur.

In this chapter such a model is provided for a TEFC induction motor, which uses techniques that can be applied to all electrical machines. The work concentrates on a revision of an earlier model, which was developed for the results provided in Chapter 3 and reported elsewhere[30]. The original model was also used for thermal prediction device described in the next chapter. However there are no reasons, in principle, why the improved model could not have been applied to the ageing and microprocessor work, had time been available. The model performance is compared with the earlier version and actual temperatures measured in a machine in the latter part of Chapter 6.

The thermal models, reported in the literature, fall into two catogories; those that use finite difference or finite element techniques and those that use bulk parameters. In the first method [31],[32] the machines are divided into a large number of small elements or a fine mesh,

and the temperatures are evaluated at every node. This produces a complex thermal model, which requires a large amount of computation and involves the calculation of a lot of unneccessary detailed information.

The second technique[33-36] is to seperate the machine into a number of bulk components and then use a thermal 'equivalent circuit' to describe the heat transfer between each component. This method has the advantage in that a small number of equations can be used to describe the machine, and the 'hot spot' temperatures can be easily identified. However, care must be taken not to over-simplify the machine's geometry[33] or to introduce assumptions that give a poor picture of the thermodynamics processes in the bulk components[34].

The works of Soderberg[35] and Perez[21] et al., give methods by which the heat transfer coefficients, between the various bulk components, can be successfully determined in the steady-state. A number of authors[22,36] have applied such steady state models to the transient case, by associating a thermal capacitance with each bulk component, to a good effect.

It was thus decided to use a bulk component method to thermally model the induction motor, because of its small computational requirements.

5.2 GENERAL DESCRIPTION OF THERMAL MODEL

The bulk component thermal model separates the geometry of a machine into a number of individual sections. The thermal behaviour of each of these sections or components is modelled by a node of uniform temperature from which heat is transferred to the component surroundings through thermal resistances. Any heat generation or storage in the component is then assumed to occur at the node. Heat transfer between the bulk components will be caused by a combination of conduction, convection and radiation effects.

The geometry of the three phase, cage induction motor is given in Figure 5.1 and the model component structure in Figure 5.2. In this particular machine, the heat transfer by radiation is neglected, as it is usually small compared with the other two modes of heat transfer. Since both conduction and convection are linear effects, neglecting radiation allows the overall thermal performance of the motor to be described by a simple linear model.

From the heat conduction equation and the theorem of conservation of energy, the heat balance equation for any node i in the model can be written as:

$$C_i \frac{d\theta_i}{dt} = \sum_j \frac{1}{R_{ji}}(\theta_j - \theta_i) + u_i \qquad (5.1)$$

where C_i = node thermal capacitance

θ_i = node temperature

R_{ji} = thermal resistance between node i and any adjoining node j

u_i = heat generation at node i

The accuracy of the lumped parameter equivalent of each bulk component depends upon the selection of the nodal temperature and the evaluation of the thermal resistances. In this respect, the best choice of nodal temperatures would be those that approximate to the mean temperatures of the bulk components at all times. Thermal storage is then assumed to act only as an additional external heat source, related to the mean temperature and the component's total thermal capacity.

In order to obtain simple, but physically significant, expressions for the internodal thermal resistances, two further assumptions[21] are made about the bulk components. First, that the heat flow can be divided into three independant orthogonal vectors and second, that the mean temperatures along each vector direction are identical. This enables the thermal resistances to be calculated from simple one dimensional heat equations.

From these assumptions basic building blocks can be developed for use in the construction of the induction motor thermal model.

5.3 GENERAL TWO DIMENSIONAL CYLINDRICAL SECTION

A cylindrical section is shown in Figure 5.3. This could be part of the stator or the rotor iron in an induction motor. Symmetry is assumed about the component's axis and a radial plane through its centre. The latter implies that the temperatures θ_3 at each end of the section are equal and that should any axial temperature gradient exist, its effect would be small.

The mean surface temperatures of the component are given as θ_1 to θ_3. Uniform heat generation is assumed to occur within the section, and here this would be equal to the hysterisis and eddy current losses in the iron.

In the axial direction, the internal heat generated flows by conduction through the element to the end surfaces and then to the surroundings. The axial temperature distribution is taken to be parabolic[21]. The mean temperature will then be the sum of the surface temperature and two thirds of the difference between the maximum central element temperature and the surface. Hence, the thermal behaviour of the component in this direction can be represented by the network:

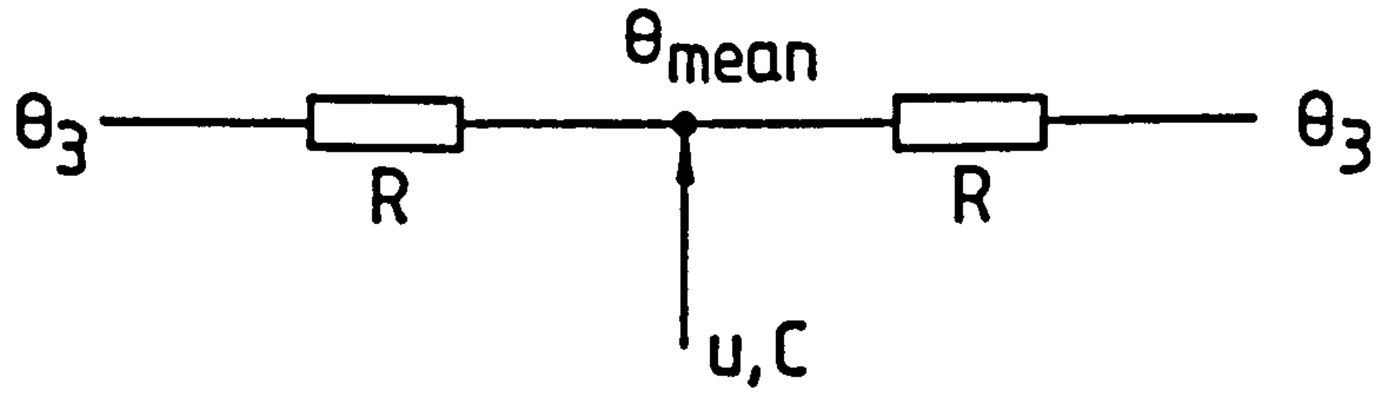

where $$R = \frac{L}{6\ (r_2^2 - r_1^2)\, k_a} \qquad (5.2)$$

and k_a is the thermal conductivity in the axial direction. In the above u,C represent the total heat generation and thermal capacity within the section.

In the radial direction, there will be an external heat flow through the element, which will result in a complex temperature distribution. However, the mean temperature can be obtained by the use of the T network[21]

of thermal resistances below:

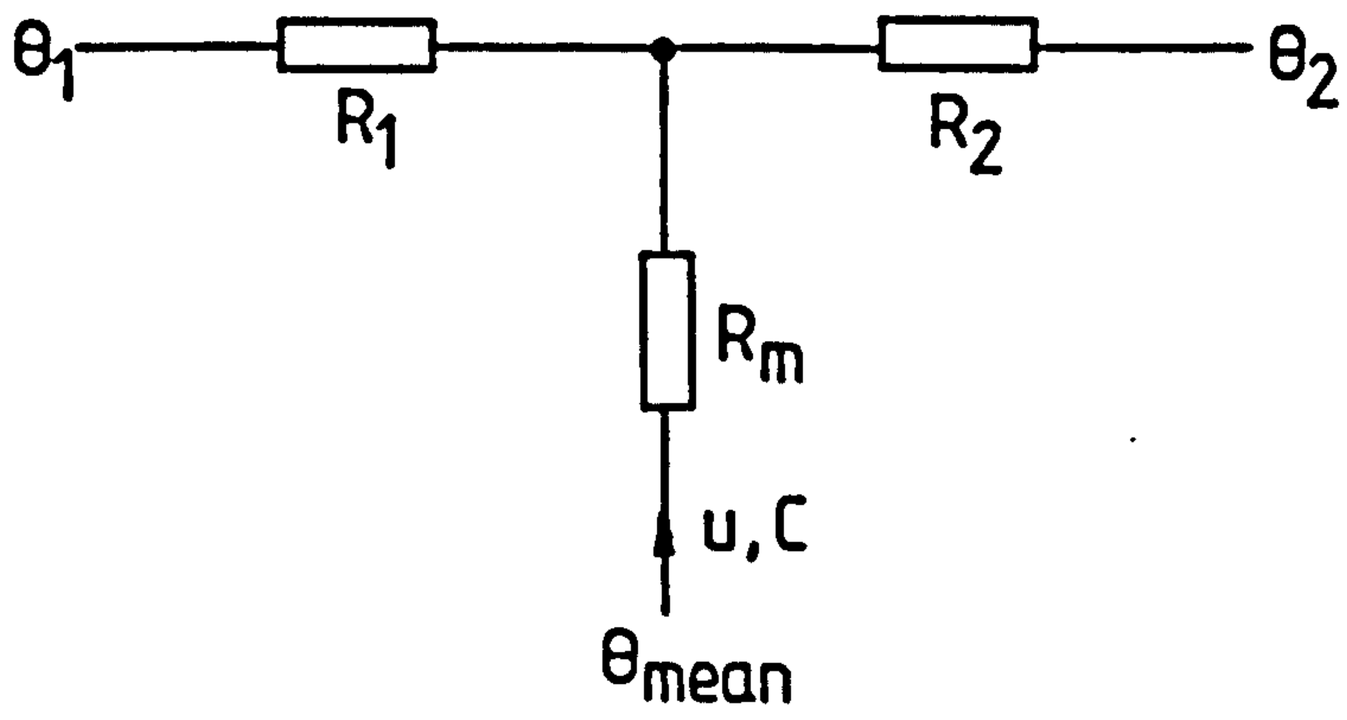

where $R_1 = \frac{1}{4\pi k_r L}\left(\frac{2r_2^2 \log_e r_2/r_1}{r_2^2 - r_1^2} - 1\right)$ (5.3)

$$R_2 = \frac{1}{4\pi k_r L}\left(1 - \frac{2r_1^2 \log_e r_2/r_1}{r_2^2 - r_1^2}\right)$$

$$R_m = \frac{-1}{8\pi k_r L(r_2^2 - r_1^2)}\left(r_1^2 + r_2^2 - \frac{4r_2^2 r_1^2 \log_e r_2/r_1}{r_2^2 - r_1^2}\right)$$

and k_r is the thermal conductivity in the radial direction.

The derivation of the thermal resistance values is given in Appendix A6. The central node of the T network represents the point of maximum radial temperature and thus R_m takes a negative value, since the mean temperature must be less than this maximum.

The two thermal networks can be combined under the assumption that the mean temperatures are equal in both the radial and axial directions. This yields the final equivalent network of the component as:

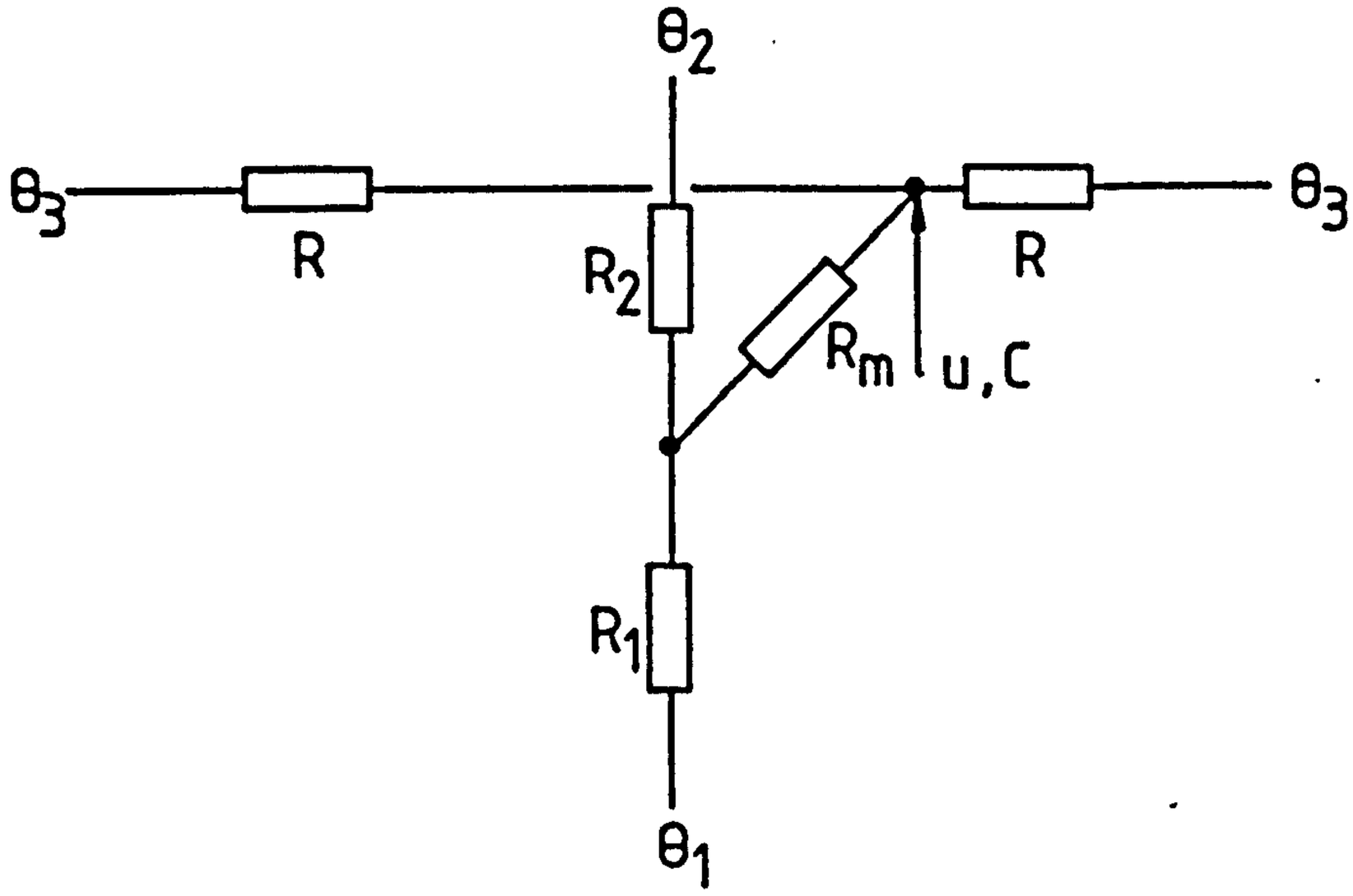

Although the network represents a single lumped component, it contains two nodes of Equation (5.1), one with zero thermal capacitance and heat generation.

This network can be used to model all sections of the induction motor's stator and rotor. It also can be used for cylindrical windings, by calculating the resistance values in the limit as the inner radius r_1 tends to zero and neglecting the R_1, θ_1 thermal branch.

5.4 CONVECTIVE HEAT TRANSFER

The heat transfer between the solid sections of the machine and the internal or external cooling air is by convection. It is modelled by the single thermal resistance:

where $R_c = \frac{1}{h_c A}$ (5.5)

and h_c = convective heat transfer coefficient

A = area of contact surface

The value of the convective heat transfer, or film, coefficient h_c is influenced by a number of factors. These include the nature of the cooled surface and the physical properties, velocity and temperature of the cooling fluid.

The film coefficients in the induction motor were determined from mathematical expressions or experimental results obtained by several authors [34-42], which related to the flow of air around similar geometries to those found in the machine. Four sets of coefficients were used in the model and are listed below.

(i) h_{1s}, h_{1r} - heat transfer between the frame and external air

(ii) h_{2s}, h_{2r} - heat transfer between the stator or rotor and air gap

(iii) h_{3s}, h_{3r} - heat transfer between the stator iron, rotor iron, endwindings or endcaps and the endcap air.

(iv) h_{4s}, h_{4r} - heat transfer between the rotor cooling holes and circulating endcap air.

At each heat transfer surface two values of film coefficient are required, one to be used when the machine is stationary, where the external and internal cooling fans are ineffective; and the other to be used when the machine is rotating. These two values are denoted by the suffixes s and r respectively.

The coefficients h_{1s} and h_{1r} were found directly from experimental tests on the machine. The central surface temperature of the motor was measured with a flat platinum resistance themometer. The motor was then run at constant load until thermal equilibrium was obtained, and the coefficient h_{1r} was determined by comparing the surface temperature with the total machine loss calculated from its equivalent circuit. Whereas, h_{1s} was found from a low voltage locked rotor test, where, under thermal equilibrium, the heat dissipated from the motor surface would be equal to the total electrical power input.

Over the air gap the rotor and stator act as two concentric cylinders rotating with respect to each other. A number of pieces of work[37,38] concerned with such geometries could be utilised to determine the airgap film

coefficients. In the induction motor considered, there was little or no axial flow along the air gap and hence the majority of the heat flowing into the air gap from the rotor will be transferred directly to the stator. This was represented in the thermal model by assuming an infinite resistance between the air gap and the endcap cooling air.

The rotational film coefficient h_{2r} can be expressed in terms of the air gap's dimensionless Nusselt number N_u. This is a function of the cooling fluid's Taylor and Prandtl numbers, denoted as N_{ta} and N_{pr} respectively. These numbers are defined for the air gap as:

$$N_u = \frac{h_{2r} \ell_g}{k} \qquad (5.6)$$

$$N_{ta} = \frac{\rho \omega r \ell_g}{\mu} \left(\frac{\ell_g}{r}\right)^{0.5} \qquad (5.7)$$

$$N_{pr} = \frac{c_p \mu}{k} \qquad (5.8)$$

where c_p = specific heat of air at constant pressure

k = thermal conductivity of air

ρ = density of air

μ = viscosity of air

ω = angular speed of rotor

r = air gap log mean radius

ℓ_g = air gap

Taylor[32] has shown that the convective heat transfer between two rotating smooth cylinders is dependant upon the number N_{ta}, such that:

$$N_u = 2.0 \qquad N_{ta} \leq 41 \qquad (5.9)$$

$$N_u = 0.212 N_{ta}^{0.63} N_{pr}^{0.27} \qquad 41 < N_{ta} < 100 \qquad (5.10)$$

The critical value of 41 for N_{ta} represents physically a change from laminar to disturbed air flow between the two cylinders. The former is defined in Equation (5.9) where the heat transfer across the air gap occurs only by conduction. The latter equation is valid for Taylor numbers up to 100, and will generally apply to small air gap rotating machines.

In a practical machine however, there will be a greater heat transfer across the air gap than described by the smooth cylinder equations, because of additional fluid disturbances caused by the winding slots in the rotor and stator. Experimental results obtained by Gazley[39] for a number of different rotor and stator configurations suggest that, within the above range of Taylor numbers, these slot effects will cause approximately a ten per cent increase in the film coefficient.

The film coefficient equations for a small air gap machine can thus be modified to:

$$N_u = 2.2 \qquad N_{ta} \leqslant 41 \qquad (5.11)$$

$$N_u = 0.23 N_{ta}^{0.63} N_{pa}^{0.27} \qquad 41 < N_{ta} < 100 \qquad (5.12)$$

The fluid constants within these two equations are temperature dependant. Care should be taken to ensure that the values used are valid for the expected temperature range in the air gap.

When the machine is stationary, the heat transfer across the air gap will be by conduction only. Equation (5.9) was thus applied to calculate h_{2s}.

In the endcap region a single set of film coefficients was used to determine the amount of heat that was transferred to and from the circulating endcap air. Clearly, this was simplification of the exact transfer mechanism that occured within the endcap. Seperate film coefficients would apply to each of the different surfaces in the path of the cooling air. However, the complex analysis that was required to evaluate a set of seperate film coefficients could not be justified, after a consideration of the poor accuracy to which they could be obtained.

The values of the film coefficients, h_{3s} and h_{3r}, were found from the experimental work of Luke[40], on the dissipation of heat from endwindings by forced ventilation. The velocity v of the cooling air, that was forced through the endwindings by the rotor fan, was estimated from the log mean radius of the fan r_m, its angular speed ω_s and efficiency η, by the expression:

$$r = r_m \omega_s \eta \qquad (5.13)$$

where $$r_m = \frac{r_2 - r_1}{\log_e (r_2/r_1)}$$

and r_2, r_1 are the outer and inner radii of the fan, respectively.

The results of Luke can be approximately linearised for small cooling air velocities v, as:

$$h_{3r} = 15.5\ (0.39v + 1) \quad Wm^{-2}\ {}^{o}C^{-1} \qquad (5.14)$$

$$v < 7.5\ ms^{-1}$$

The constant term in Equation (5.14) represents the heat transfer from the endwindings by natural convection, and is the film coefficient value h_{3s} that should be applied in the stationary model. In the calculation of the rotational film coefficient h_{3r} for the induction motor, a fan efficiency of 50% was assumed. The resultant magnitude of h_{3r}, Table 5.1, was similar to the endwinding heat transfer coefficient of 38.7 $Wm^{-2}\ {}^{o}C^{-1}$ suggested by Roberts[41] from experimental measurement.

The final film coefficients of interest are those for the rotor cooling holes. The stationary value h_{4s} was taken to be equal to the natural convection component of Equation (5.14). There was difficulty in finding any experimental work from which the rotational film coefficient h_{4r} could be obtained. A theoretical analysis, however, has been presented by Mori and Nakayama[42]. This was

concerned with the heat transfer in a pipe rotating around a parallel axis.

In the paper, the Nusselt number for the pipe heat transfer was expressed as the product of the Reynolds number R_e and the Rayleigh number R_a, of the centrifugal field of air within the pipe. The results of this analysis are given as:

$$N_u = \frac{48}{11} \; 0.19(R_e R_a)^{1/5} \qquad (5.15)$$

where the dimensionless numbers N_u, R_e and R_a are equal to:

$$N_u = \frac{2ah_{4r}}{k} \qquad (5.16)$$

$$R_e = \frac{2av\rho}{\mu} \qquad (5.17)$$

$$R_a = N_{pr} \cdot \frac{R\omega^2 \Delta\theta \beta \rho^2 a^4}{\mu^4} \qquad (5.18)$$

with a = pipe radius

R = radius of rotation of pipe axis

ω = angular speed of rotation of pipe

$\Delta\theta$ = temperature gradient along pipe wall

v = velocity of air flow along pipe

β = coefficient of volumetric expansion of air

and the other air constants as defined for Equations (5.6) to (5.8).

In the estimation of h_{4r} for the induction motor, low values were taken for the temperature gradient and the velocity of flow of air along the 'pipe', i.e. a rotor cooling hole. This was because of the symmetrical nature of the machine, which suggested that only small temperature and pressure differences would exist between the two sides of the rotor.

The film coefficients used in the induction motor model are summarised in Table 5.1. They were derived from estimates of several formulae and parameters. Their accuracy can only be justified against the experimental findings of some of the authors mentioned above and the final performance of the thermal model.

5.5 NODAL HEAT GENERATION

The internal heat generation within the electrical machine was divided into two parts, voltage dependant iron losses and current dependant copper losses. Stray load losses, which are in the main made up of high frequency core losses in the stator and rotor teeth and harmonic copper loss in the rotor, were included in the two catogories.

With the induction motor operating under balanced conditions, the heat generation u in the windings or the core are given by simple expressions of the form:

$$u = u_v v^2 + u_I i^2 \qquad (5.19)$$

where u = nodal heat generation

v = supply voltage (phase)

i = motor load current (phase)

The constants u_v, u_I relate to the section of the machine at which the generation occurs and the machines electrical performance. Appendix A7 develops them from the parametors of the induction motor equivalent circuit used by Say[43], Figure 5.4. Here the generation constants for the total iron loss, stator copper loss and rotor copper loss, with respective suffixes of 1, 2 and 3, are shown to be given, in the equivalent circuit notation of Say, by:

$$u_{v1} = \frac{R_m}{cZ_m^2} - \frac{R_1}{cZ_m(Z_m + 2X_{s/c})} \qquad (5.20)$$

$$u_{I1} = \frac{cR_1Z_m}{(Z_m + 2X_{s/c})} - R_1$$

$$u_{v2} = 0$$

$$u_{I2} = R_1$$

$$u_{v3} = \frac{-R_2}{Z_m(Z_m + 2X_{s/c})}$$

$$u_{I3} = \frac{c^2Z_mR_2}{(Z_m + 2X_{s/c})}$$

The equivalent circuit parameters were measured by a load test on the machine and the resultant values of the generation constants are given in Table 5.2. A

description of the load test is also given in Appendix A7 and a comparison is made between it and the conventional locked rotor and no-load induction motor tests.

So far in the analysis, the heat generation is assumed to occur only from electrical losses. Other sources of heat would be the mechanical losses in the machine's bearings and the fluid loss in the cooling medium. These effects were considered to be small because of the basic mechanical structure of the induction motor, and were neglected for simplicity.

5.6 DETAILED DESCRIPTION OF MODEL COMPONENTS

The induction motor model was divided into the ten components shown in Figures 5.1 and 5.2. The machine was taken to be symmetrical about the axis of its shaft and a central radial plane. The entire surface of the motor was assumed to be at a uniform temperature, which implied that any temperature gradient across the surface, caused by the external fan, was negligable.

Figures 5.5.1 through to 5.5.10 show the geometrical construction of each component and the formulae used for the thermal resistances. Corresponding Tables 5.3.0 through to 5.3.10 give the values of the parameters used.

In the following sub-sections, the assumptions applied and the details of the parameter evaluations are given, where the sub-numbers refer to both the parts of Figure 5.5 and Table 5.3, and the component locations in Figure 5.2.

5.6.1 Frame

The motor had a cast aluminium alloy frame to which iron endcaps were bolted, to carry the shaft bearings. The heat transfer from the frame to the ambient was a function of the total surface area, the efficiency[23] of the cooling fins and the convective film coefficient of the forced cooling air. This heat transfer was measured experimentally and the film coefficient determined from the estimated effective surface area.

A uniform heat distribution was assumed across the frames narrow cross section. During the manufacture of the motor, the aluminium frame was shrunk fit over the stator core and secured with a small dowel. A significant thermal resistance existed across this join, because of the poor contact surface of the stator laminations. The magnitude of the contact resistance was obtained from an experimental curve[44], which expressed the thermal resistance across an aluminium shim, sandwiched between two laminated steel blocks, as a function of the contact pressure. A higher value of contact resistance was used than would be expected in a production machine, because the stator of the induction motor that was modelled, had been previously removed from the frame to enable the insertion of temperature detectors in the windings. On its subsequent replacement, only a small contact pressure existed between the stator and the frame.

5.6.2 Stator Iron

The stator iron was modelled with the standard building block of Section 5.4. The coefficient of thermal conductivity across the core laminations was obtained from data published in reference (37).

In the radial direction a 'stacking factor' was introduced to accommodate for the proportion of the core length that was taken up by the insulation of the laminations.

The iron and stray core losses were confined in equal proportions to the stator and the rotor teeth. In these areas the greatest changes of magnetic flux would occur and the contribution to the iron loss by the stator iron portion of the model was taken to be negligable.

5.6.3 Stator Teeth

The effects of the core laminations in the stator teeth were included in the manner described in the previous section.

In the radial direction, the stator teeth were modelled by an equivalent arc sector, with an area equal to that of the actual tooth cross-section.

5.6.4 Stator Winding

The array of conductors and insulation which formed the stator winding was modelled as a cylindrical bar. The heat transfer, axially along the bar, was assumed to occur only in the conductors.

However, in the radial direction, the winding was modelled as a homogeneous material with thermal properties equivalent to the mixture of copper and insulation in its cross-section. The thermal conductivity of this material was considered to be a factor F greater than the insulation conductivity. The value of this factor was obtained from Reference (37).

A thin strip of insulation seperated the winding from the sides of the stator slot and was represented by an additional term in the model.

5.6.5 Air Gap

The thermal capacitance of the air gap was assumed to be negligable. The thermal resistances between the air gap and the rotor and stator components were calculated from the film coefficient of Section 5.4 and the areas exposed to the air gap.

5.6.6 Endwinding

The endwinding was modelled as a homogeneous toroid with 'legs', that is short cylindrical extensions of the stator windings. The material constants were calculated by the methods used in the stator winding.

Heat was transferred from the toriod surface by either convection to the encap air or conduction through the proportion of the surface area connected to the legs.

The thermal equations were weighted to give a nodal temperature equal to the central and maximum temperature of the toroid. This was performed by assuming that the difference between the maximum temperature of the component and the toroidal surface temperature was a factor w higher than the mean rise above the surface. The maximum temperature could then be obtained from the thermal model by increasing the component thermal resistances and reducing the thermal capacitance to maintain energy balance. The 'leg' thermal resistances were not weighted as they would provide a direct thermal path to the centre of the toroid. A parabolic temperature distribution was assumed across the toroid and hence a value of 1.5 was taken for the factor w.

This proceedure was seen to give a temperature approximating to that of the endwinding 'hot spot', and thus enabled a more accurate determination of the ageing of the winding insulation.

5.6.7 Endcap Air

The thermal branches of the endcap air component were obtained in a similar manner to those of the air gap and, as with the air gap, the thermal capacitance was neglected.

5.6.8 Rotor Winding

The rotor winding was modelled as a continuous aluminium cylinder surrounding the rotor iron core. This method was used for simplicity and because a good thermal contact existed between the extruded aluminium bars and rotor laminations. The thickness of the cylinder was chosen so that its volume would be equal to the total volume of aluminium used in the conductors of the cage winding.

The cage bars were connected to endiscs, which also formed the rotor cooling fans. This was modelled by making the heat transfer area between the ends of the equivalent rotor cylinder and the endcap air equal to the endisc surface area. The winding thermal capacitance also included the endiscs.

The heat generation in this component was taken as the sum of the rotor copper losses and half the core iron loss.

5.6.9 Rotor Iron

The rotor iron model used the basic building block of the stator core. The thermal resistances in both the radial and axial directions were increased in proportion to the reduction in the rotor cross-sectional area, caused by the insertion of the cooling ducts.

The internal surfaces of the cooling ducts were assumed to be at the rotor iron mean temperature. A convective thermal branch could then be introduced between the rotor iron and endcap air component nodes.

5.6.10 Shaft

The shaft acted as a thermal link between the mean temperature of the shaft-rotor interface and the frame via the bearings. A good thermal contact was assumed to exist between the shaft and the bearings. The external ends of the shaft would then be at the frame temperature and any heat loss through the coupling between the shaft and the load could be included in the model of the frame component.

The area of contact between the shaft and the endcap air was sufficiently small to be neglected.

5.7 COMPLETE MODEL EQUATIONS

The complete induction motor thermal model was obtained by combining all the components outlined in the previous section and is given in Figure 5.6.

The structure has fifteen nodes and ten thermal components. Four of the components have two nodal models associated with them and there is an additional junction node between the stator teeth, winding and iron. The values of some of the branch thermal resistances and the presence of any heat generation are dependant upon whether the machine is stationary or running.

The temperatures at each of the model nodes are determined from their individual heat balance, in the form of Equation (5.1). These equations can be collected together to give two sets of matrix equations, one for a stationary and the other for a rotating machine, as shown below:

$$[C'] \frac{d[\theta]}{dt} = [Y']_s[\theta] \tag{5.21}$$

$$[C'] \frac{d[\theta]}{dt} = [Y']_r[\theta]+([u'_I]i^2+ [u'_v]v^2) \tag{5.22}$$

where $[C']$ = matrix of nodal thermal capacitance

$[\theta]$ = nodal temperatures

$[Y']_s$ = stationary inter-nodal thermal conductances

$[Y']_r$ = rotational inter-nodal thermal conductances

$[u'_r]$ = current dependant generation matrix

$[u'_v]$ = voltage dependant generation matrix

i = motor phase current

v = motor phase voltage

The solution of the equations will give the temperature rise of the motor above the ambient. The ambient must therefore be added as an offset to these values to obtain the absolute temperatures.

Seven of the matrix row equations have no thermal capacitance or heat generation associated with them. These are the secondary nodes mentioned above and the nodes of the air gap and endcap air components. The elements of these rows can be removed from the coefficient matrices by Guassian elimination[45], to produce a set of matrix equations of order eight. These equations can be expressed in the form:

$$[C]\ \frac{d[\theta]}{dt} = [Y][\theta] + [u] \qquad (3.6)$$

where: $[Y] = [Y]_s$

$[u] = 0$

when the motor is stationary

and : $[Y] = [Y]_r$

$[u] = [u_I]i^2 + [u_v]v^2$

when the motor is running

The matrix elements of Equation (3. 6), for the model described in this chapter, are given in Table 5.4. The corresponding values for the original thermal model are listed in Table 5.5.

The earlier model was different to the later one in three ways. A simple, single node, building block was used in the development of the stator and rotor iron components; the same values of internal film coefficients were applied in both the stationary and rotational models and finally the endwinding temperatures were not weighted to give the maximum values. This model had initially only a ten node structure that was similarly reduced to an eight order equivalent.

Equation (3. 6) is in a suitable form for the stochastic ageing analysis of Chapter 3. Only eight equations need to be evaluated at any time to describe the total thermal performance of the induction motor. Hence, their application to the deterministic analysis in the latter part of Chapter3will not require excessive computation. Such a

compact model is also suitable for programming into a microprocessor based thermal monitoring device and this idea is developed in the next chapter.

Table 5·1 Induction Motor Convective Film Coefficients

Stationary		Rotating	
h_{1s}	9·1	h_{1r}	47·4
h_{2s}	61·8	h_{2r}	67·9
h_{3s}	15·5	h_{3r}	38·9
h_{4s}	15·5	h_{4r}	18·8

All values in $W/m^2°C$
Internal coefficients calculated for air at 80 °C.

Table 5·2 Induction Motor Generation Constants

u_{v1}	0·84 mS
u_{I1}	-0·15 Ω
u_{v2}	0
u_{I2}	1·68 Ω
u_{v3}	-0·43 mS
u_{I3}	1·17 Ω

Table 5·3·0 Thermal Constants

Lamination axial conductivity	k_{al}	1·97	W/m°C
Lamination radial conductivity	k_{rl}	45·2	W/m°C
Aluminium conductivity	k_a	204	W/m°C
Copper conductivity	k_c	385	W/m°C
Insulation conductivity	k_i	0·26	W/m°C
Steel conductivity	k_s	41·3	W/m°C
Aluminium specific heat	c_a	896	J/kg°C
Copper specific heat	c_c	383	J/kg°C
Steel specific heat	c_s	502	J/kg°C
Aluminium density	ϱ_a	2707	kg/m^3
Copper density	ϱ_c	8954	kg/m^3
Steel density	ϱ_s	7850	kg/m^3

Table 5·3·1 Frame

Stator length	L	120·7	mm
Stator outer radius	r	101·6	mm
Frame surface area	A_f	0·285	m^2
Steel endcap mass	M_e	3·9	kg
Aluminium frame mass	M_f	4·2	kg
Stator-frame contact coefficient	h_c	387·5	$W/m^2°C$

Table 5·3·2 Stator Iron

Stator length	L	120·7 mm
Stator inner radius	r_1	82·8 mm
Stator outer radius	r_2	101·6 mm
Stacking factor	s	0·97

Table 5·3·3 Stator Teeth

Stator length	L	120·7 mm
Stator inner radius	r_1	63·5 mm
Tooth outer radius	r_2	82·8 mm
Stator tooth pitch	ϕ_p	10·0°
Equivalent tooth arc	ϕ_e	5·6°
Stacking factor	s	0·97
Number of teeth	n	36

Table 5·3·4 Stator Winding

Stator length	L	120·7 mm
Insulation width	h	0·5 mm
Equivalent stator winding radius	r	5·0 mm
Equivalent area of copper in winding	A	42·4 mm^2
Radial conductivity factor	F	2·5
Slot to endwinding length ratio	α	0·389
Number of slots	n	36

Table 5·3·5 Air Gap

Stator length	L	120·7 mm
Stator inner radius	r_1	63·5 mm
Rotor radius	r_2	62·5 mm
Stator tooth pitch	ϕ_p	10·0 °
Equivalent tooth arc	ϕ_e	5·6 °
Air gap	l_g	1·0 mm

Table 5·3·6 Endwinding

Stator length	L	120·7 mm
Slot winding overhang	l	34·0 mm
Endwinding cross section radius	r_1	12·0 mm
Equivalent slot winding radius	r_2	5·0 mm
Endwinding toriod radius	r_3	79·0 mm
Equivalent area of copper in winding	A_c	42·4 mm^2
Radial conductivity factor	F	2·5
Slot to endwinding length ratio	α	0·389
Maximum temperature weighting factor	w	1·5
Number of slots	n	36

Table 5·3·7 Endcap Air

Surface area of endcap	A_1	0·067 m^2
Surface area of stator iron	A_2	0·0109 m^2
Surface area of stator teeth	A_3	0·0049 m^2
Surface area of endwinding	A_4	0·0759 m^2
Surface area of rotor endisc	A_5	0·0216 m^2
Surface area of rotor iron	A_6	0·0044 m^2
Surface area of rotor cooling holes	A_7	0·012 m^2

Table 5·3·8 Rotor Winding

Rotor length	L	120·7 mm
Endisc width	l_e	9·5 mm
Equivalent rotor winding radius	r_1	57·6 mm
Rotor radius	r_2	62·5 mm
Endisc inner radius	r_3	38·1 mm
Volume of endisc and fan	V_e	84·0 cm^3

Table 5·3·9 Rotor Iron

Rotor length	L	120·7	mm
Rotor inner radius	r_1	22·2	mm
Rotor outer radius	r_2	57·6	mm
Cooling hole radius	r_3	6·4	mm
Stacking factor	s	0·97	
Number of holes	n	5	

Table 5·3·10 Shaft

Rotor length	L	120·7	mm
Bearing length	l_b	25·4	mm
Distance between bearing centre and rotor mean	l_m	93·1	mm
Shaft radius	r	22·2	mm

Table 5·4 Revised Thermal Model Matrices

$$[C] = \begin{bmatrix} 3674 \\ 2512 \\ 1146 \\ 314 \\ 331 \\ 474 \\ 1901 \\ 768 \end{bmatrix}$$

$$[Y_S] = \begin{bmatrix} -18\cdot750 & 16\cdot513 & -2\cdot161 & -0\cdot078 & 0\cdot367 & 0\cdot125 & 0\cdot092 & 1\cdot293 \\ & -98\cdot610 & 79\cdot337 & 2\cdot845 & 0\cdot045 & -0\cdot142 & 0\cdot013 & 0\cdot0 \\ & & -88\cdot437 & 10\cdot656 & 0\cdot020 & 0\cdot584 & 0\cdot001 & 0\cdot0 \\ & & & -21\cdot642 & 7\cdot918 & 0\cdot304 & -0\cdot002 & 0\cdot0 \\ & & & & -8\cdot551 & 0\cdot114 & 0\cdot086 & 0\cdot0 \\ & & \text{Transpose of} & & & -79\cdot203 & 79\cdot142 & -0\cdot931 \\ & & \text{upper triangle} & & & & -81\cdot574 & 2\cdot237 \\ & & & & & & & -2\cdot599 \end{bmatrix}$$

1	2	3	4	6	8	9	10

$$[Y_r] = \begin{bmatrix} -30\cdot385 & 16\cdot576 & -2\cdot133 & -0\cdot078 & 0\cdot919 & 0\cdot147 & 0\cdot162 & 1\cdot293 \\ & -98\cdot722 & 79\cdot369 & 2\cdot838 & 0\cdot083 & -0\cdot159 & 0\cdot016 & 0\cdot0 \\ & & -88\cdot595 & 10\cdot680 & 0\cdot038 & 0\cdot640 & 0\cdot002 & 0\cdot0 \\ & & & -21\cdot690 & 7\cdot918 & 0\cdot335 & -0\cdot003 & 0\cdot0 \\ & & & & -9\cdot187 & 0\cdot271 & 0\cdot122 & 0\cdot0 \\ & & \text{Transpose of} & & & -79\cdot717 & 79\cdot169 & -0\cdot931 \\ & & \text{upper triangle} & & & & -81\cdot676 & 2\cdot237 \\ & & & & & & & -2\cdot599 \end{bmatrix}$$

Table 5·5 Original Thermal Model Matrices

$$[C] = \begin{bmatrix} 3674 \\ 2512 \\ 1146 \\ 314 \\ 498 \\ 474 \\ 1901 \\ 768 \end{bmatrix}$$

$$[Y_s] = \begin{bmatrix} -23\cdot134 & 19\cdot583 & 0\cdot074 & 0\cdot0 & 0\cdot848 & 0\cdot236 & 0\cdot343 & 0\cdot800 \\ & -60\cdot847 & 38\cdot034 & 3\cdot006 & 0\cdot133 & 0\cdot037 & 0\cdot054 & 0\cdot0 \\ & & -45\cdot168 & 6\cdot476 & 0\cdot060 & 0\cdot499 & 0\cdot024 & 0\cdot0 \\ & & & -14\cdot414 & 4\cdot361 & 0\cdot571 & 0\cdot0 & 0\cdot0 \\ & & & & -5\cdot868 & 0\cdot190 & 0\cdot276 & 0\cdot0 \\ & & \text{Transpose of} & & & -43\cdot805 & 42\cdot271 & 0\cdot0 \\ & & \text{upper triangle} & & & & -65\cdot490 & 22\cdot523 \\ & & & & & & & -23\cdot323 \end{bmatrix}$$

$$\begin{matrix} 1 & 2 & 3 & 4 & 6 & 8 & 9 & 10 \end{matrix}$$

$$[Y_r] = \begin{bmatrix} -34\cdot884 & 19\cdot583 & 0\cdot074 & 0\cdot0 & 0\cdot848 & 0\cdot236 & 0\cdot343 & 0\cdot800 \\ & -60\cdot847 & 38\cdot034 & 3\cdot006 & 0\cdot133 & 0\cdot037 & 0\cdot054 & 0\cdot0 \\ & & -45\cdot168 & 6\cdot476 & 0\cdot060 & 0\cdot499 & 0\cdot024 & 0\cdot0 \\ & & & -14\cdot414 & 4\cdot361 & 0\cdot571 & 0\cdot0 & 0\cdot0 \\ & & & & -5\cdot868 & 0\cdot190 & 0\cdot276 & 0\cdot0 \\ & & \text{Transpose of} & & & -43\cdot805 & 42\cdot271 & 0\cdot0 \\ & & \text{upper triangle} & & & & -65\cdot490 & 22\cdot523 \\ & & & & & & & -23\cdot323 \end{bmatrix}$$

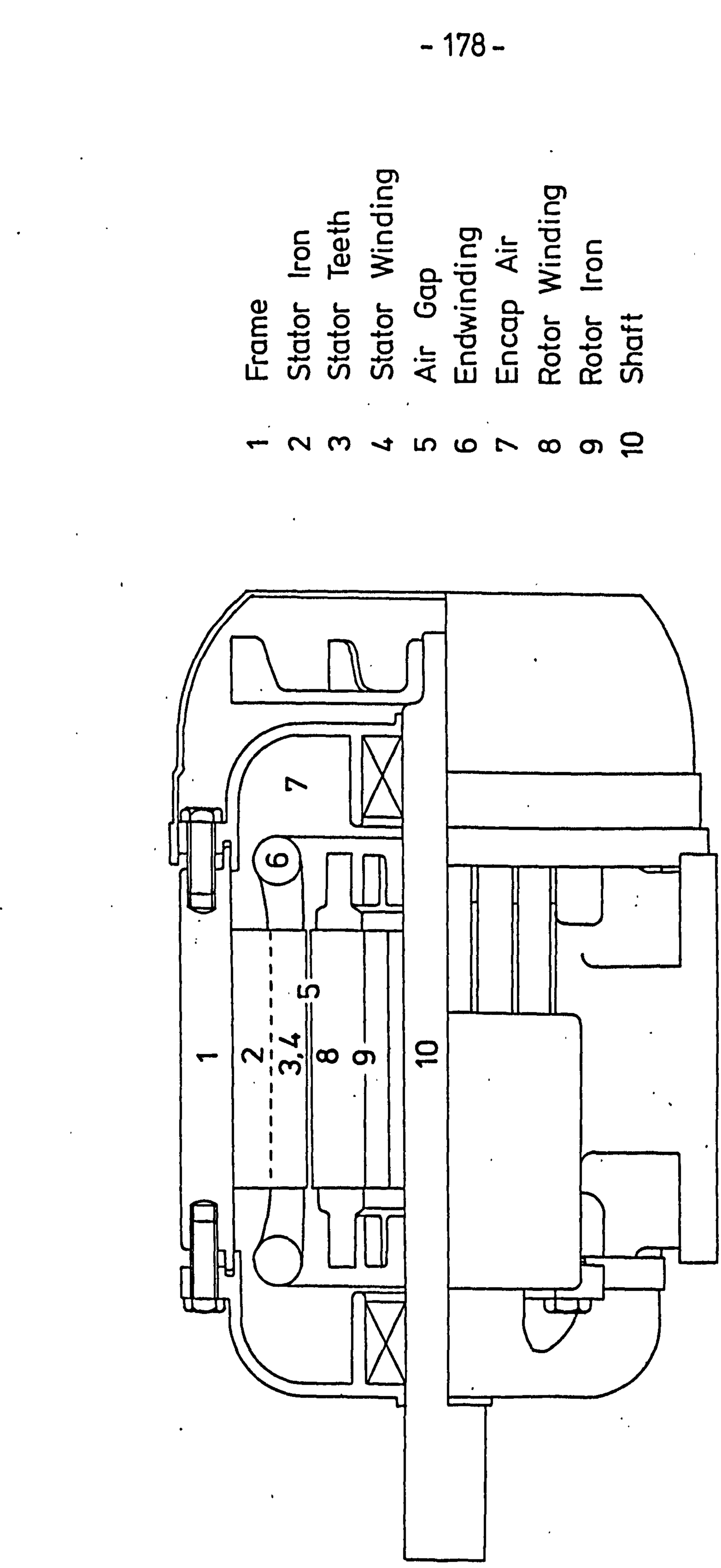

Figure 5·1 Induction Motor Construction

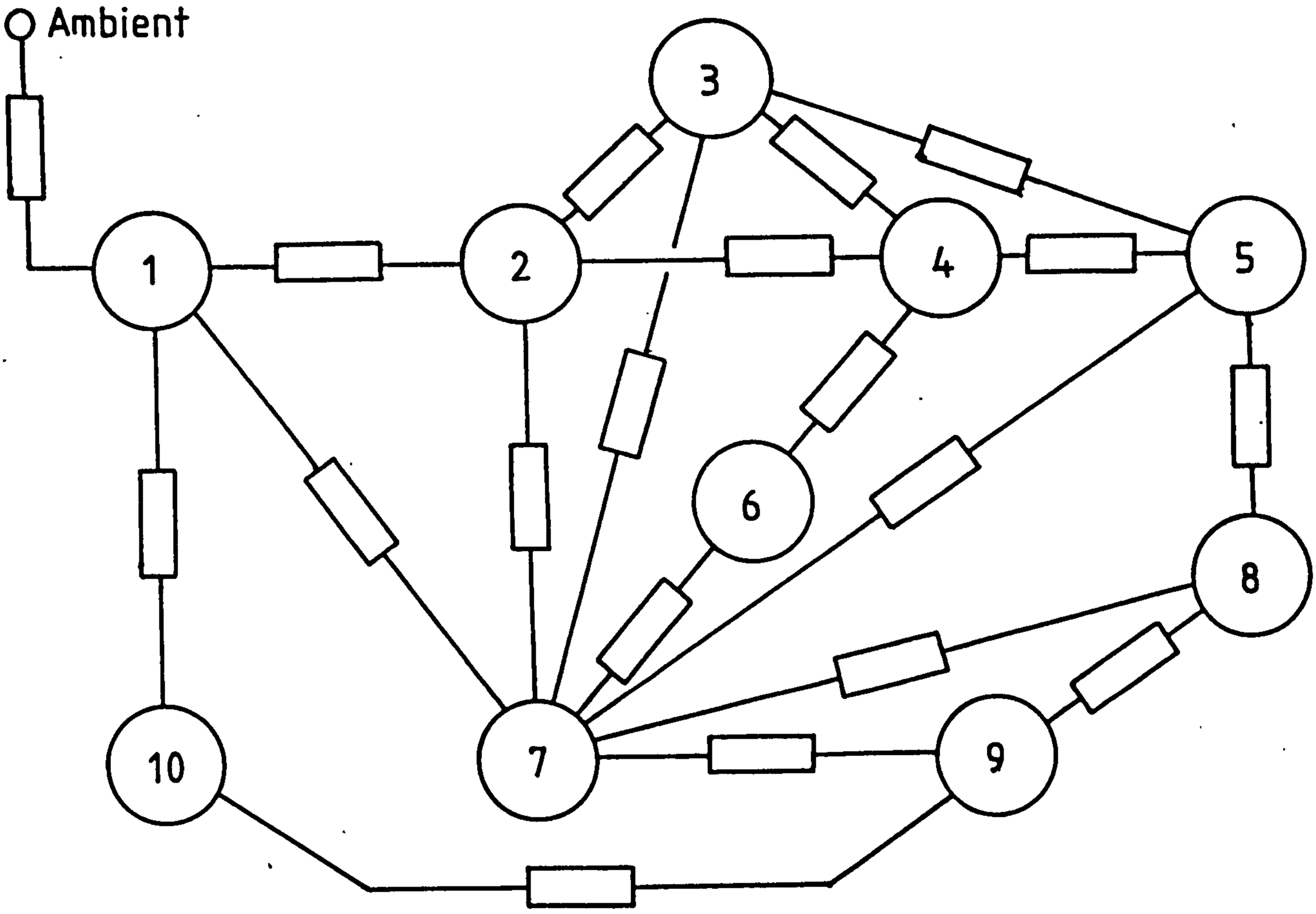

1 Frame
2 Stator Iron
3 Stator Teeth
4 Stator Winding
5 Air Gap
6 Endwinding
7 Endcap Air
8 Rotor Winding
9 Rotor Iron
10 Shaft

Figure 5·2 Thermal Model Structure

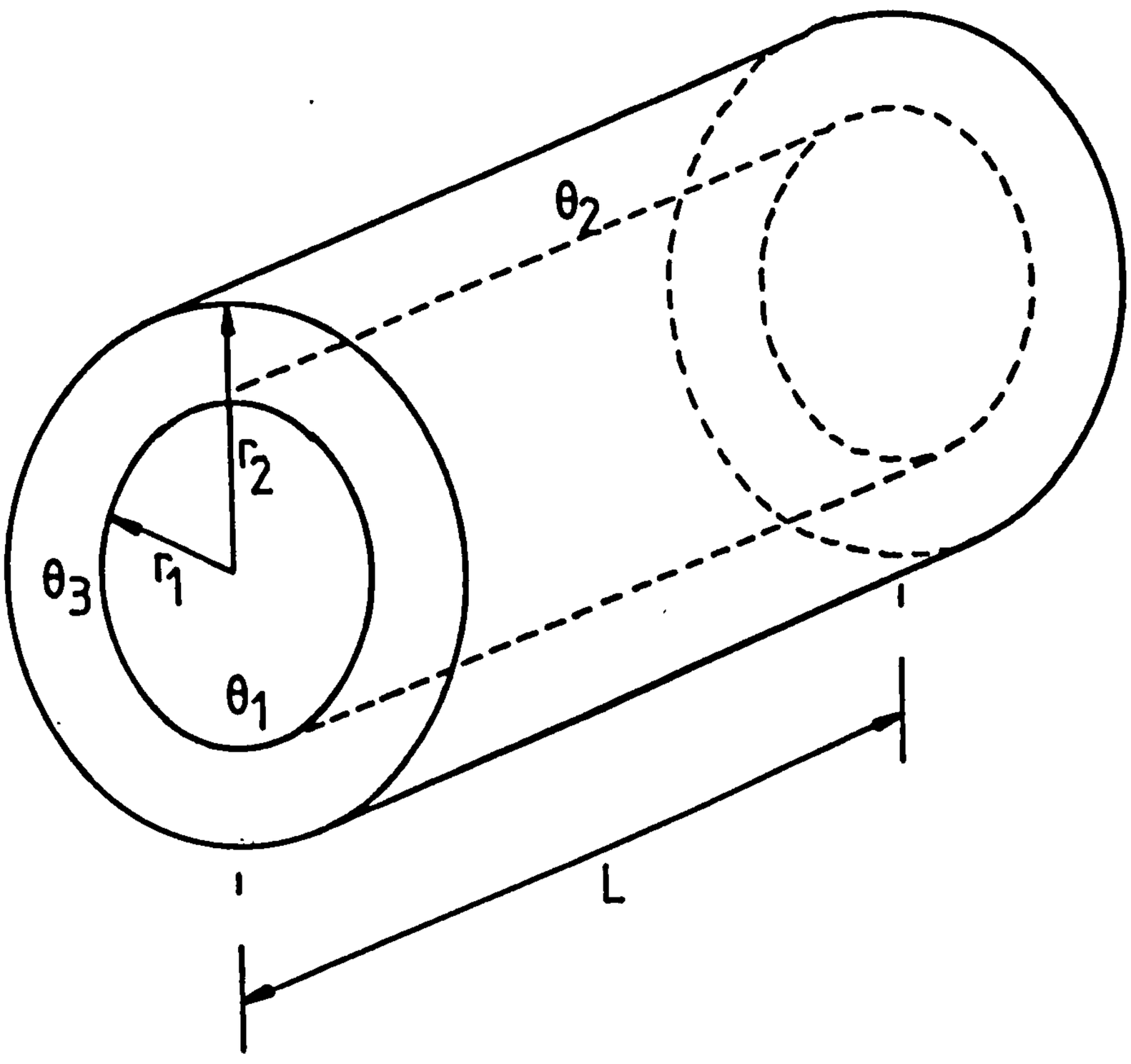

Figure 5·3 General Cylindrical Section

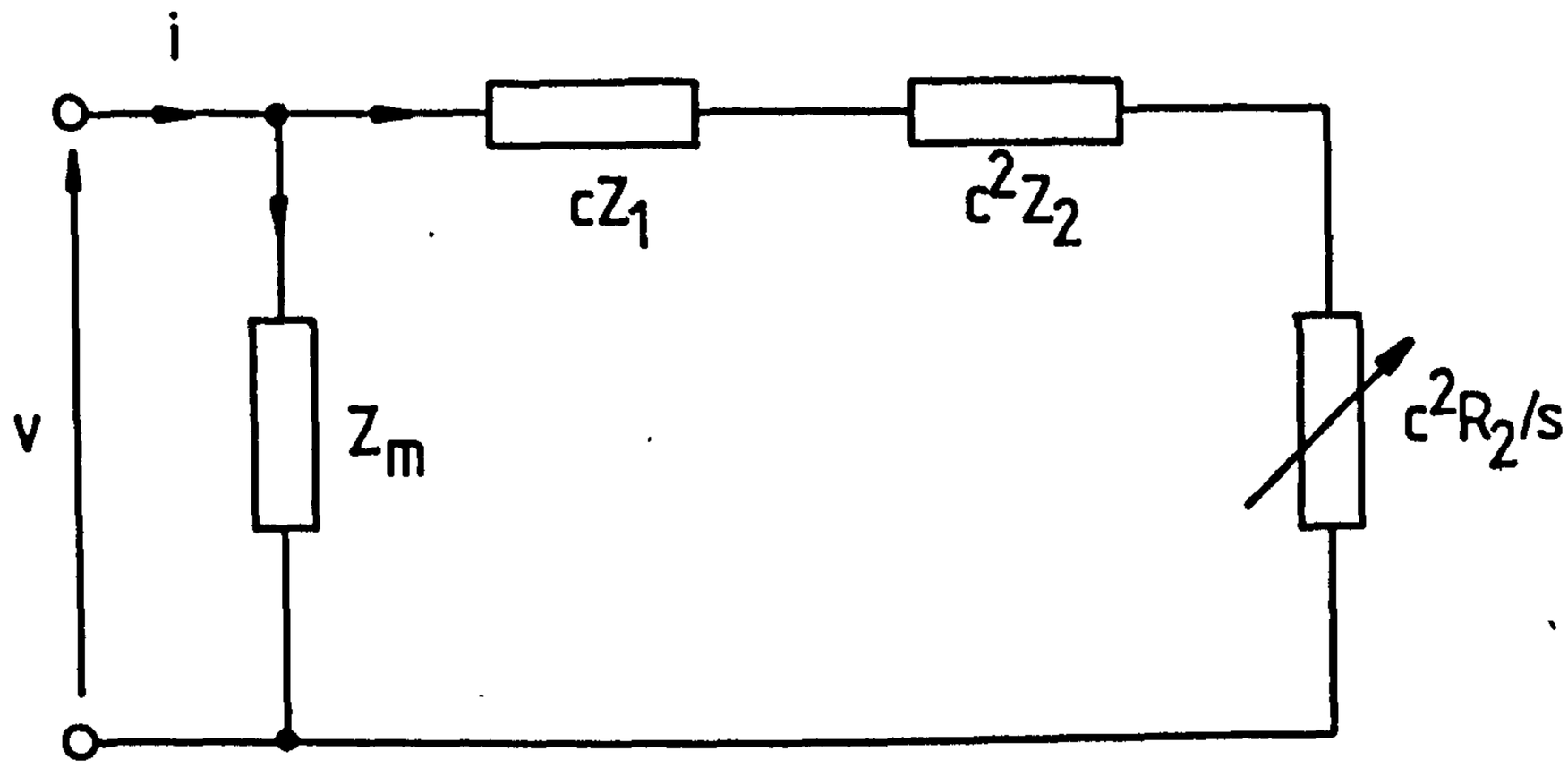

$$Z_1 = R_1 + jX_1$$
$$Z_2 = R_2 + jX_2$$
$$Z_m = R_m + jX_m$$

Figure 5·4 Induction Motor Electrical Equivalent Circuit

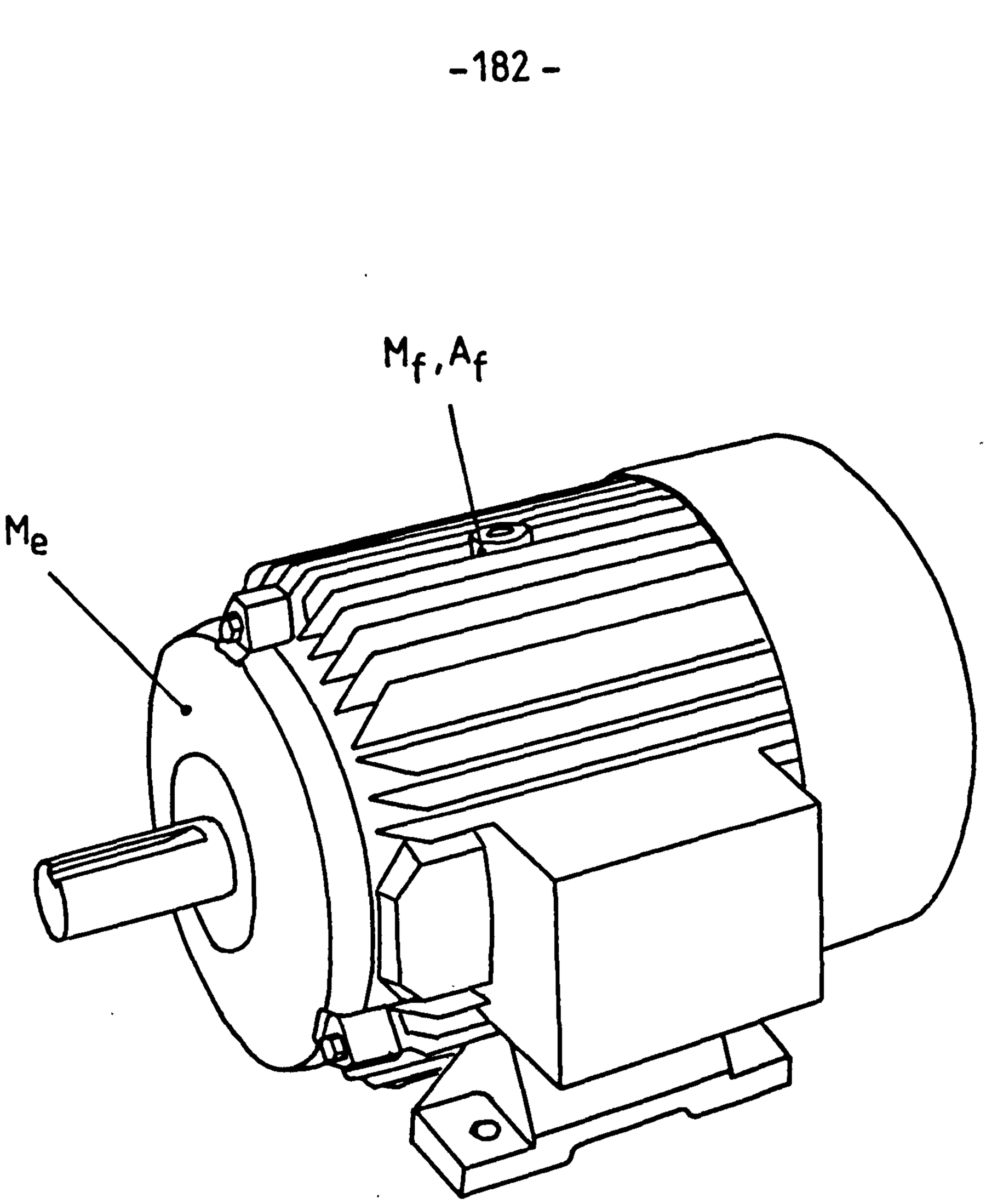

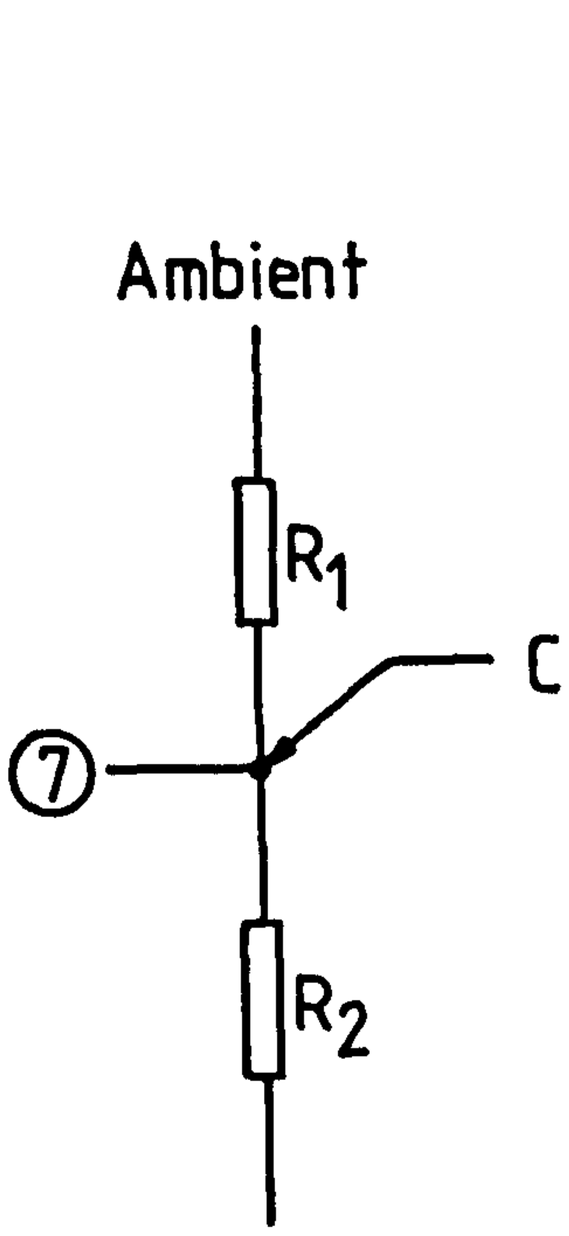

$$R_1 = \frac{2}{h_{1s}(h_{1r})A_f}$$

$$R_2 = \frac{1}{h_c \pi L r}$$

$$C = M_e c_s + \frac{1}{2} M_f c_a$$

Figure 5·5·1 Frame

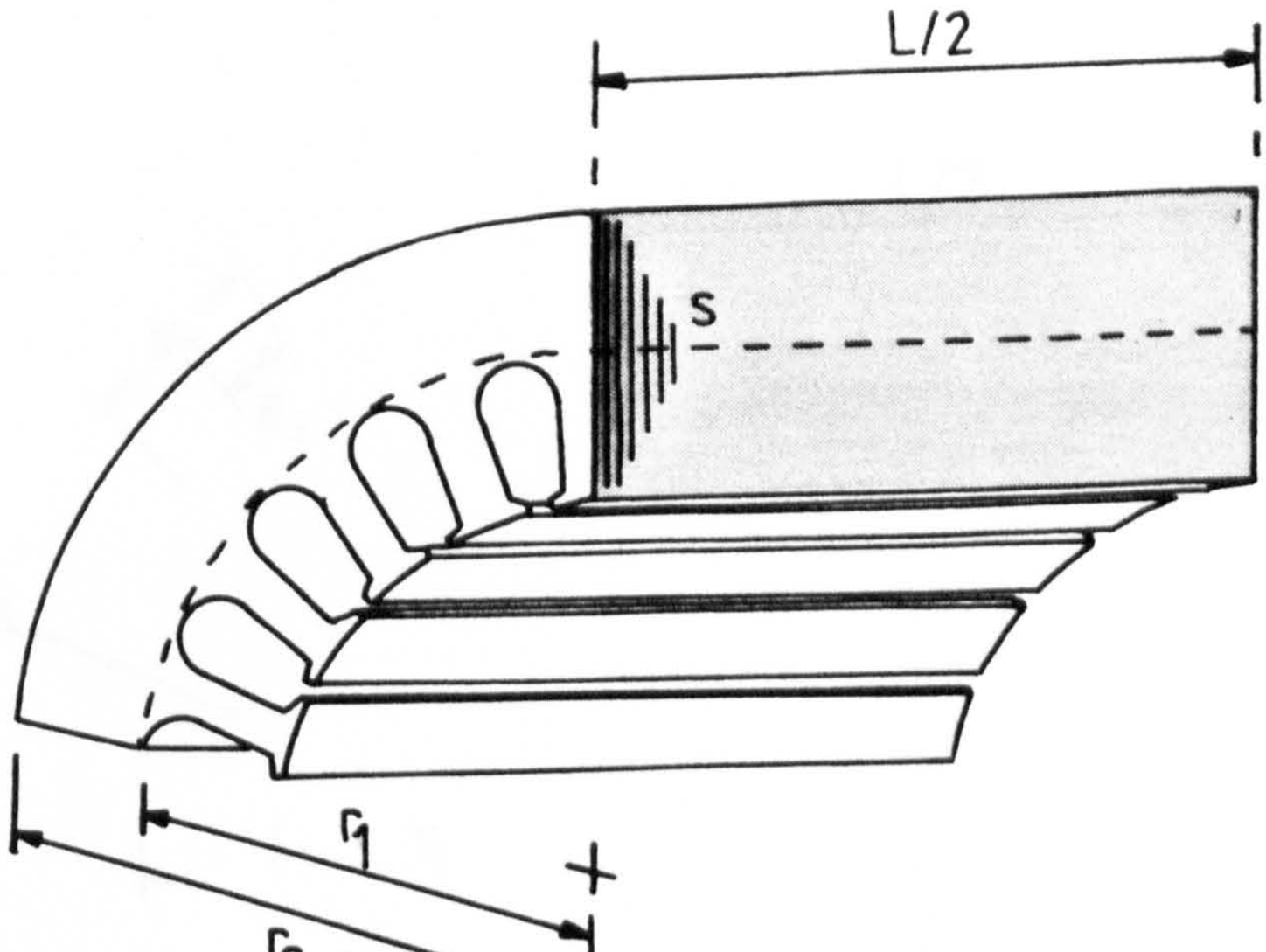

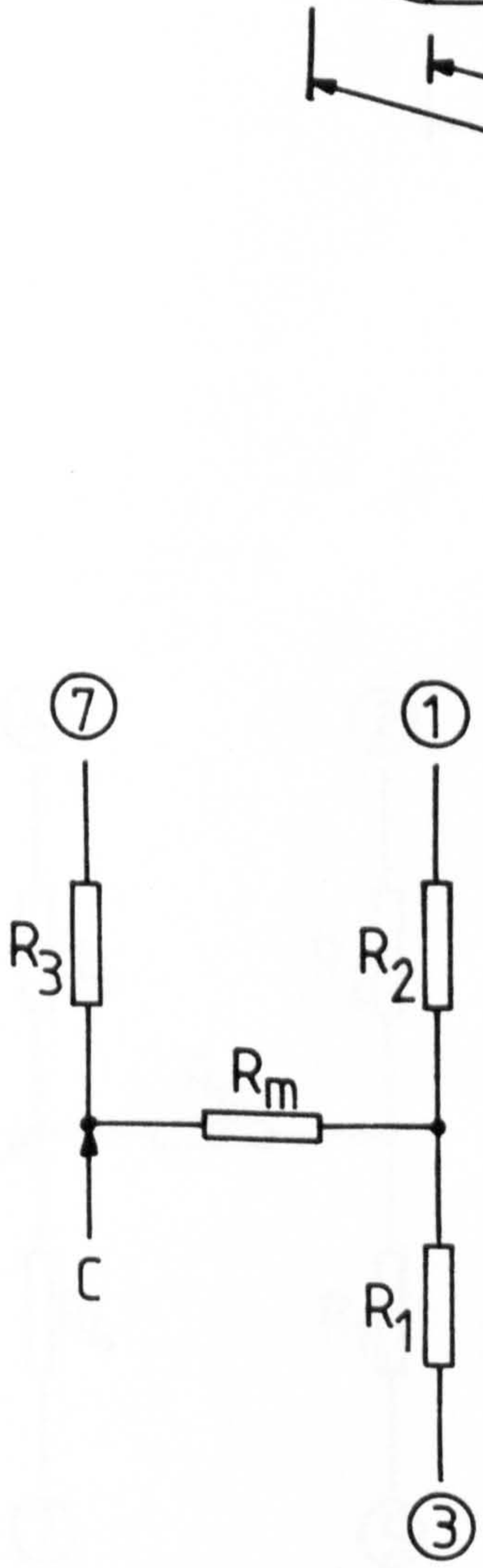

$$R_1 = \frac{1}{2\pi k_{rl} L s}\left(\frac{2r_2^2 \log_e(r_2/r_1)}{(r_2^2 - r_1^2)} - 1\right)$$

$$R_2 = \frac{1}{2\pi k_{rl} L s}\left(1 - \frac{2r_1^2 \log_e(r_2/r_1)}{(r_2^2 - r_1^2)}\right)$$

$$R_m = \frac{-1}{4\pi k_{rl} L s (r_2^2 - r_1^2)}\left(r_1^2 + r_2^2 - \frac{4r_2^2 r_1^2 \log_e(r_2/r_1)}{(r_2^2 - r_1^2)}\right)$$

$$R_3 = \frac{L}{6\pi k_{al}(r_2^2 - r_1^2)}$$

$$C = \frac{c_s \rho_s \pi L s (r_2^2 - r_1^2)}{2}$$

Figure 5·5·2 Stator Iron

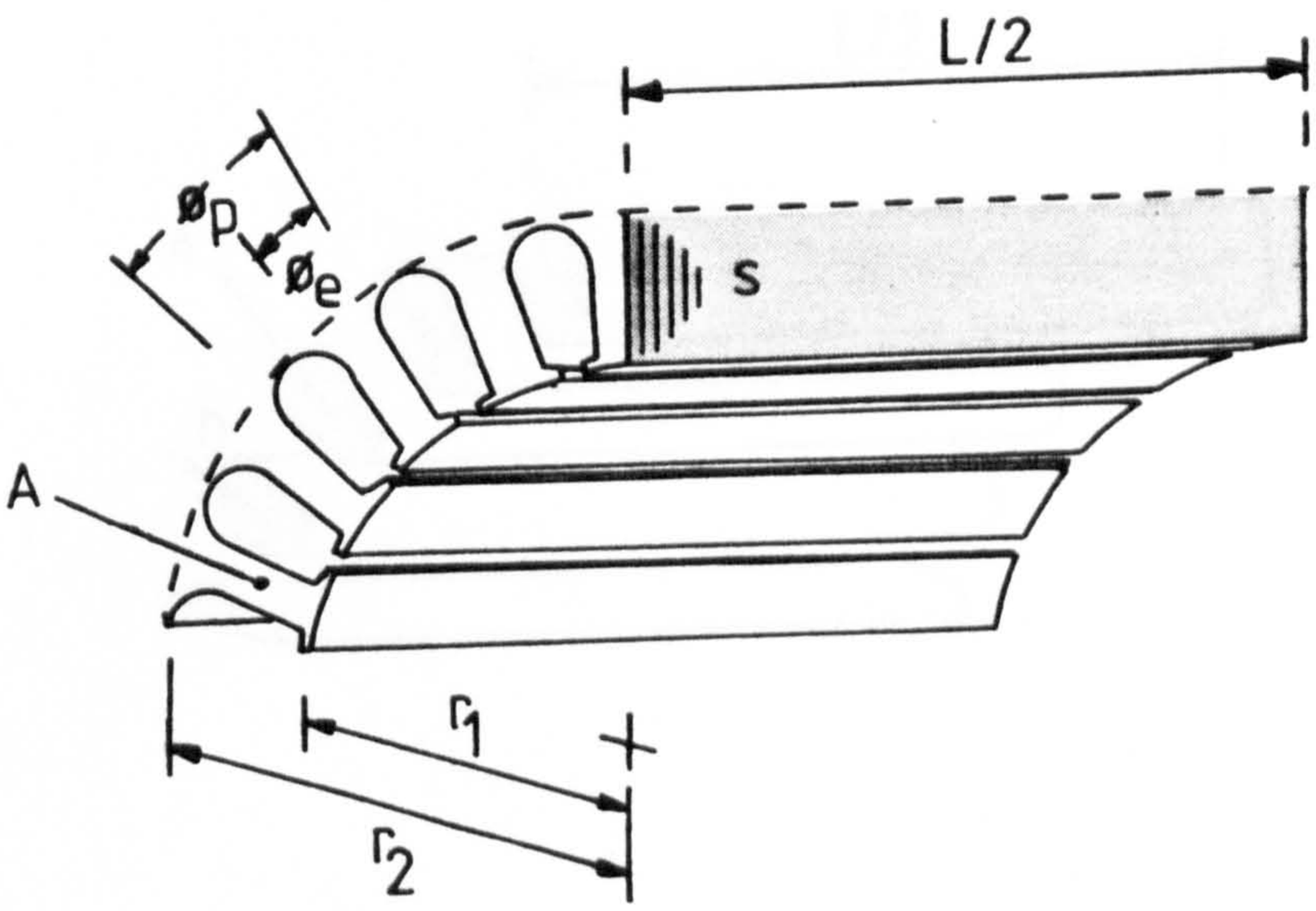

$$R_1 = \frac{\phi_p}{2\pi k_{rl} L s \phi_e}\left(\frac{2\log_e(r_2/r_1)r_2^2}{(r_2^2-r_1^2)} - 1\right)$$

$$R_2 = \frac{\phi_p}{2\pi k_{rl} L s \phi_e}\left(1 - \frac{2r_1^2\log_e(r_2/r_1)}{(r_2^2-r_1^2)}\right)$$

$$R_m = \frac{-\phi_p}{4\pi k_{rl} L s \phi_e (r_2^2-r_1^2)}\left(r_1^2+r_2^2 - \frac{4r_2^2r_1^2\log_e(r_2/r_1)}{(r_2^2-r_1^2)}\right)$$

$$R_3 = \frac{\pi\phi_e(r_2^2-r_1^2)}{k_{rl} L s \phi_p (r_2-r_1)^2 n^2}$$

$$R_4 = \frac{L\phi_p}{6\pi k_{al}\phi_e(r_2^2-r_1^2)}$$

$$C = \frac{c_s\rho_s\pi L s \phi_e(r_2^2-r_1^2)}{2\phi_p}$$

$$u = \frac{3}{4}(u_{V1}v^2 + u_{I1}i^2)$$

Figure 5·5·3 Stator Teeth

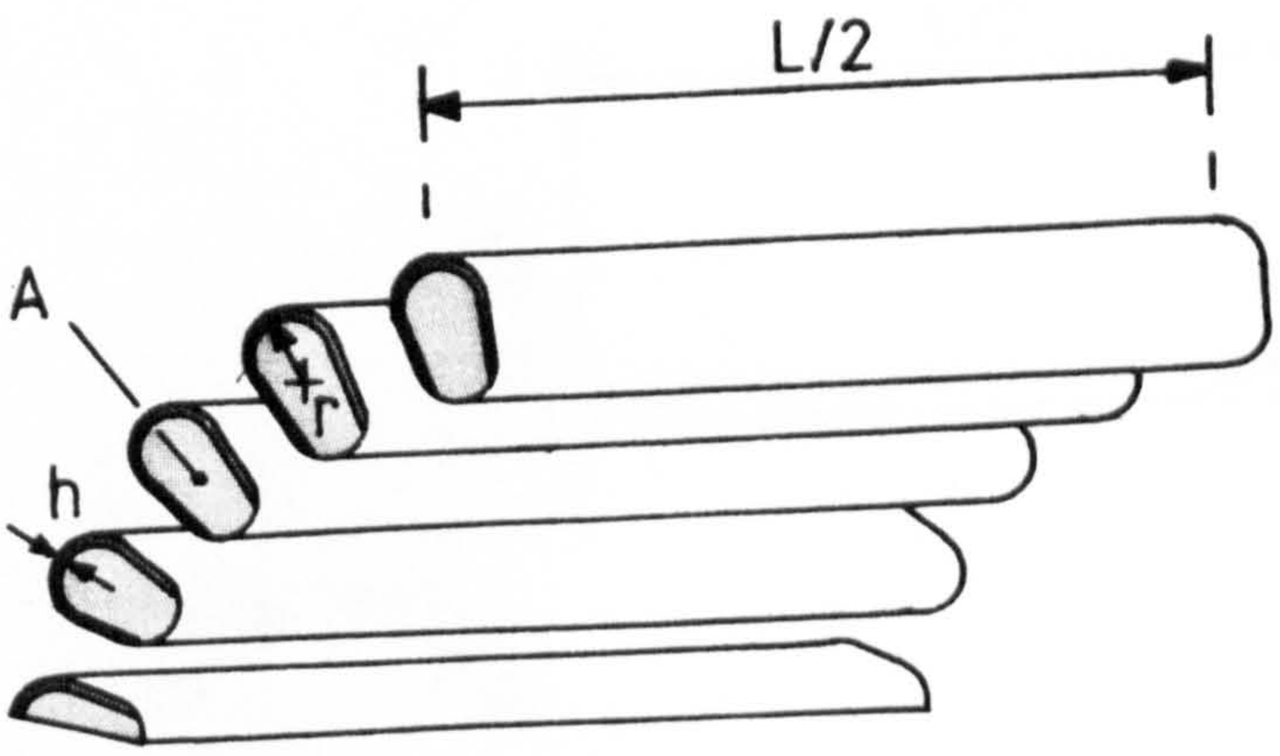

$$R_1 = \frac{4h}{\pi k_i L r n} + \frac{2}{\pi k_i L F n}$$

$$R_2 = \frac{2}{\pi k_i L F n}$$

$$R_3 = \frac{2h}{\pi k_i L r n} + \frac{1}{\pi k_i L F n}$$

$$R_4 = \frac{L}{6 k_c A n}$$

$$C = \frac{c_c \rho_c A L n}{2}$$

$$u = \frac{3}{2} \alpha u_{I2} i^2$$

Figure 5·5·4 Stator Winding

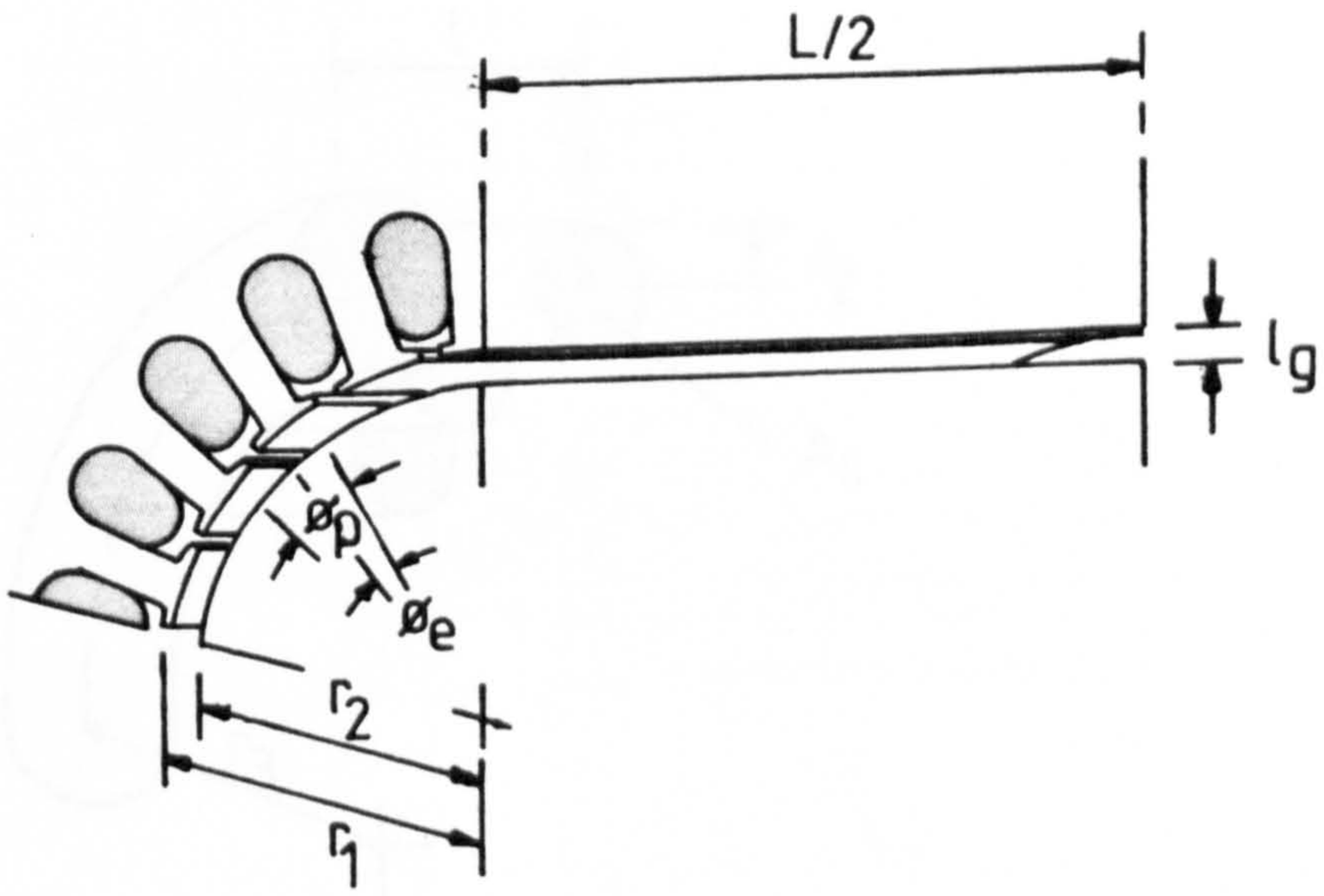

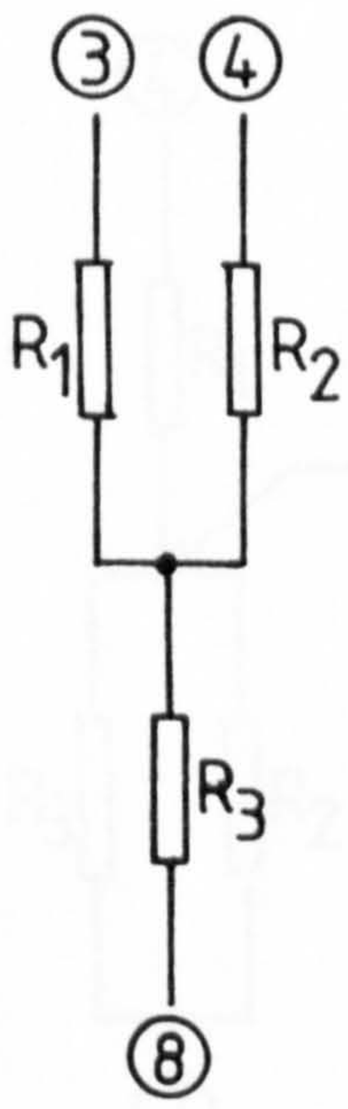

$$R_1 = \frac{\phi_p}{\phi_e \pi r_1 h_{2s}(h_{2r}) L}$$

$$R_2 = \frac{\phi_p}{(\phi_p - \phi_e) \pi r_1 h_{2s}(h_{2r}) L}$$

$$R_3 = \frac{1}{\pi r_2 L h_{2s}(h_{2r})}$$

Figure 5·5·5 Air Gap

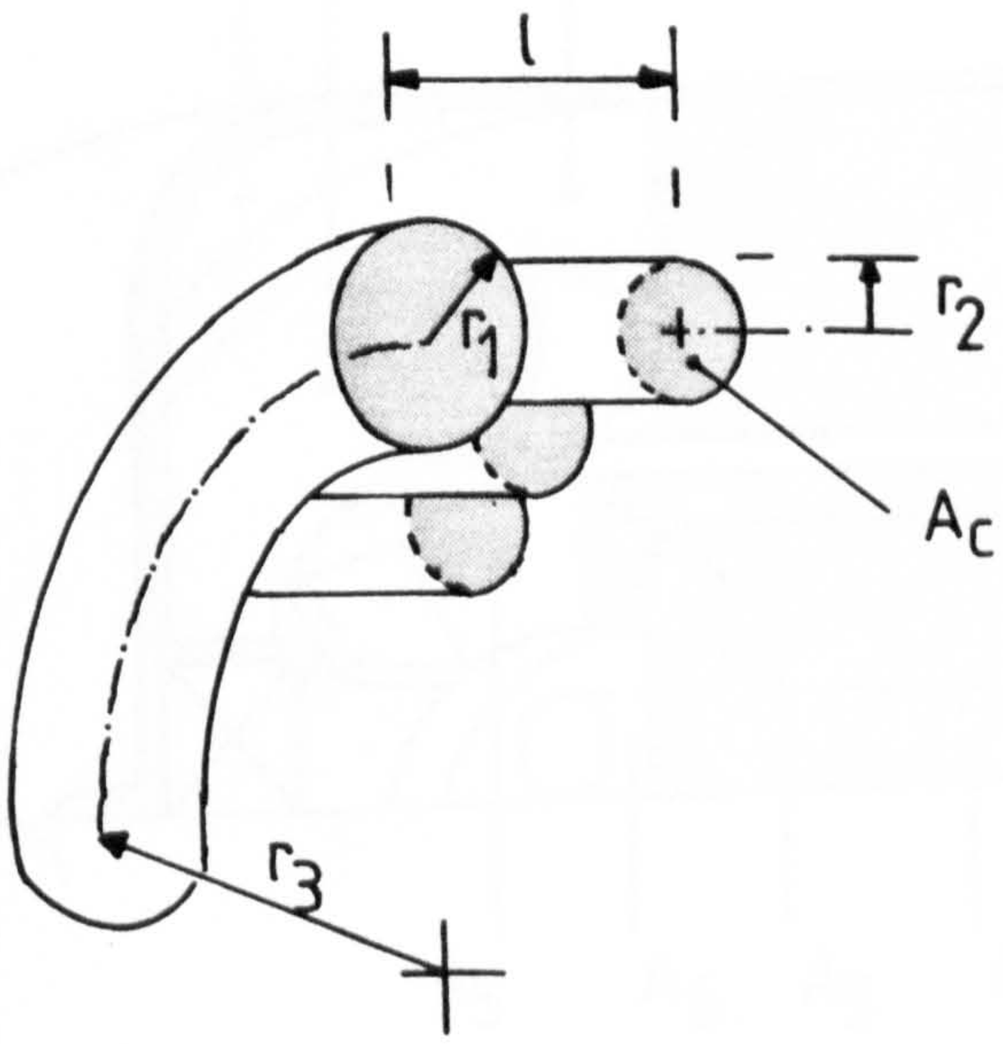

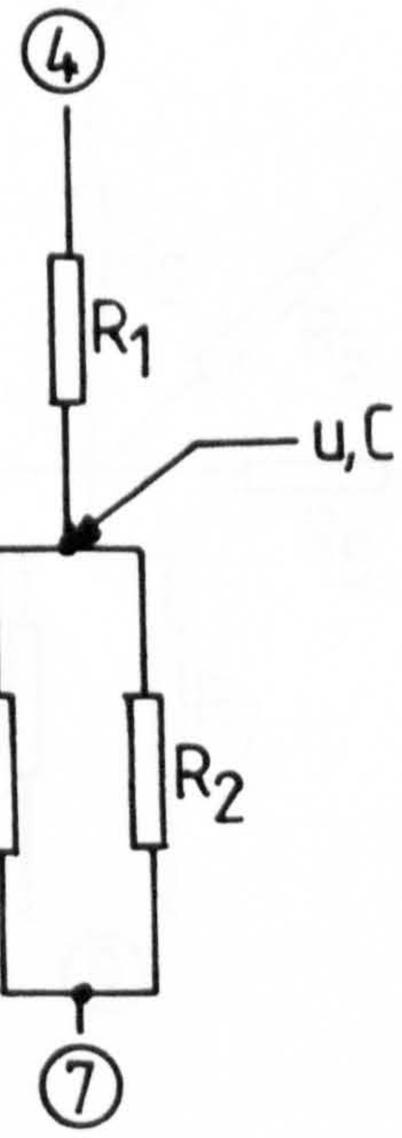

$$R_1 = \frac{lw}{nA_c k_c}$$

$$R_2 = \frac{r_1 w}{2\pi F k_i (r_1 4\pi r_3 - n r_2^2)}$$

$$R_3 = \frac{w}{2\pi F k_i l n}$$

$$C = \frac{\varrho_c c_c A_c n(1-\alpha)L}{2w\alpha}$$

$$u = \frac{3(1-\alpha)u_{I2} i^2}{2}$$

Figure 5·5·6 Endwinding

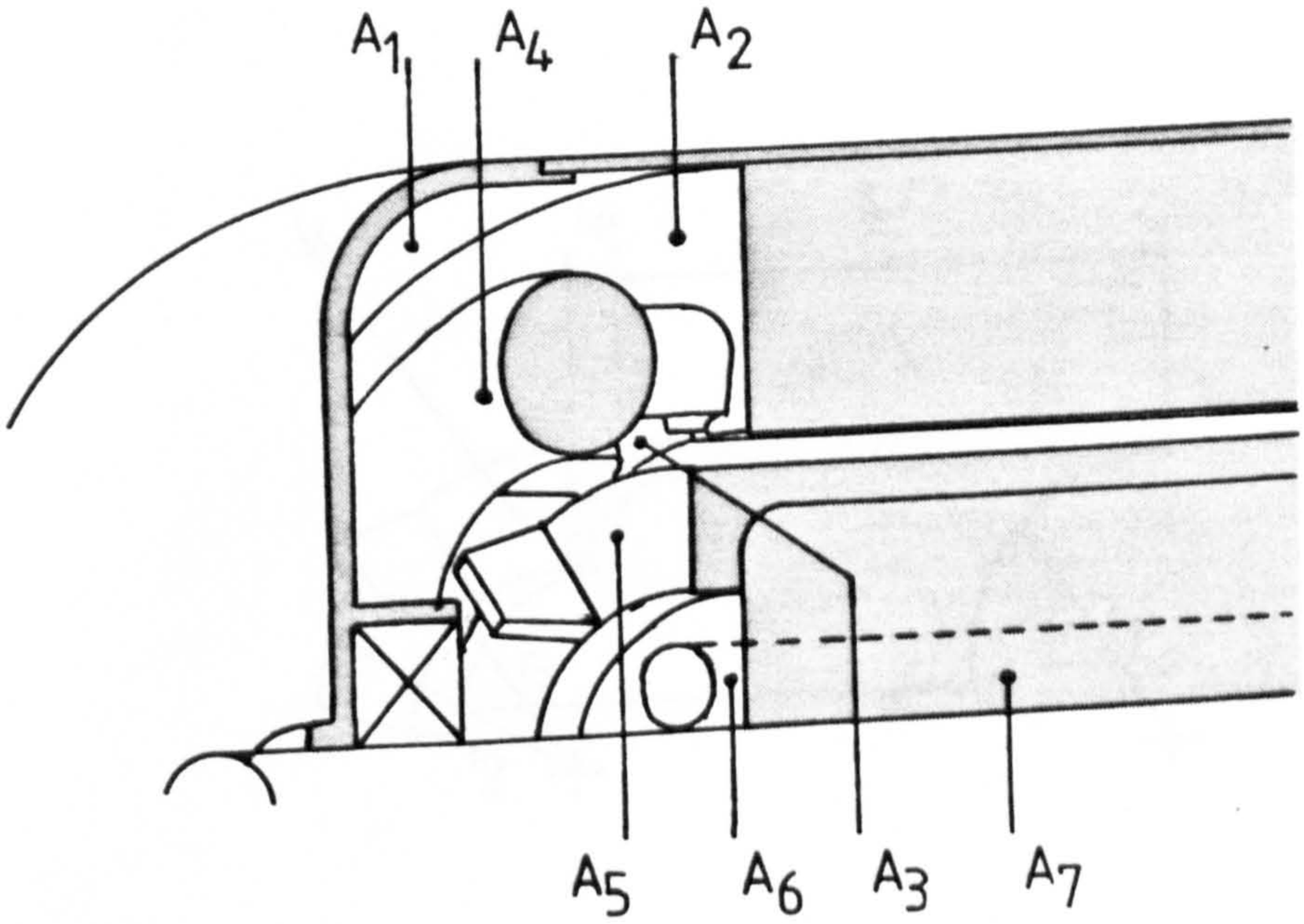

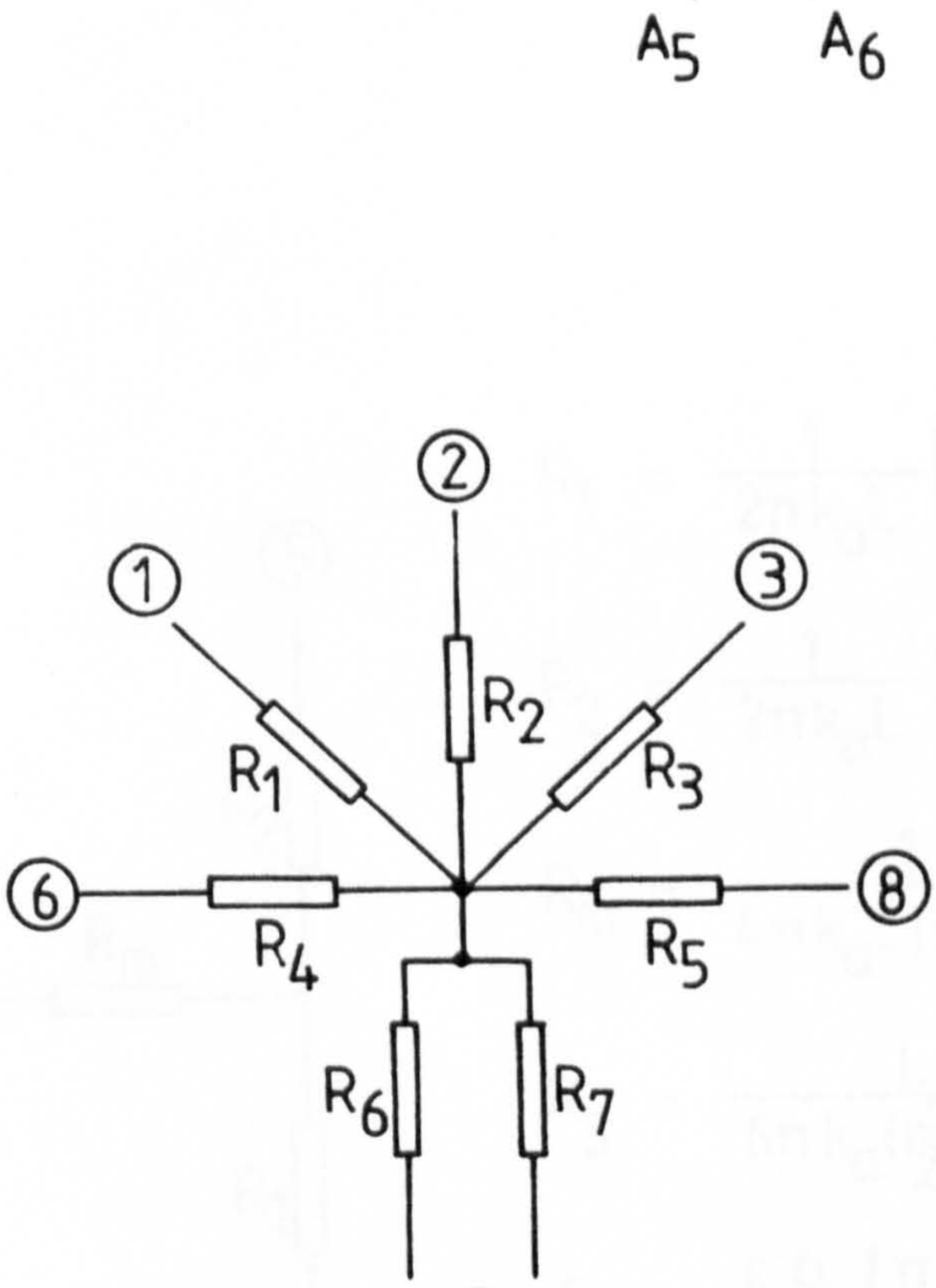

$$R_1 = \frac{1}{h_{3s}(h_{3r})A_1}$$

$$R_2 = \frac{1}{h_{3s}(h_{3r})A_2}$$

$$R_3 = \frac{1}{h_{3s}(h_{3r})A_3}$$

$$R_4 = \frac{1}{h_{3s}(h_{3r})A_4}$$

$$R_5 = \frac{1}{h_{3s}(h_{3r})A_5}$$

$$R_6 = \frac{1}{h_{3s}(h_{3r})A_6}$$

$$R_7 = \frac{1}{h_{4s}(h_{4r})A_7}$$

Figure 5·5·7 Endcap Air

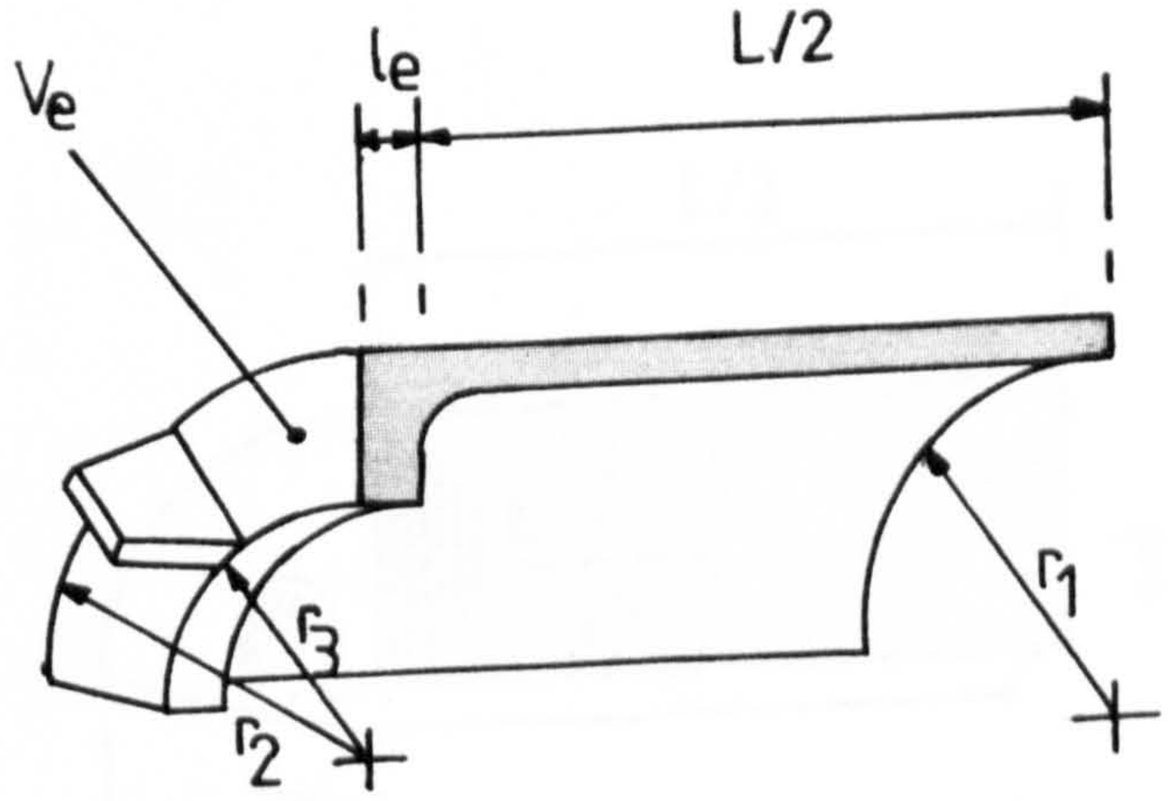

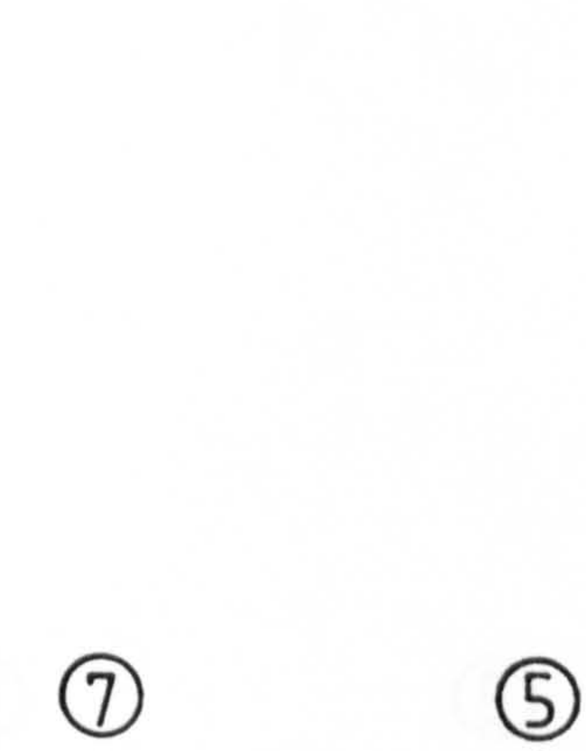

$$R_1 = \frac{1}{2\pi k_a L}\left(\frac{2r_2^2 \log_e(r_2/r_1)}{(r_2^2-r_1^2)} - 1\right)$$

$$R_2 = \frac{1}{2\pi k_a L}\left(1 - \frac{2r_1^2 \log_e(r_2/r_1)}{(r_2^2-r_1^2)}\right)$$

$$R_m = \frac{-1}{4\pi k_a L(r_2^2-r_1^2)}\left(r_1^2 + r_2^2 - \frac{4r_2^2 r_1^2 \log_e(r_2/r_1)}{(r_2^2-r_1^2)}\right)$$

$$R_3 = \frac{L}{6\pi k_a(r_2^2-r_1^2)} + \frac{l_e}{\pi k_a(r_2^2-r_3^2)}$$

$$C = c_a \rho_a\left(\frac{\pi L(r_2^2-r_1^2)}{2} + V_e\right)$$

⑨

$$u = \frac{3}{4}(u_{v1}v^2 + u_{I1}i^2) + \frac{3}{2}(u_{v3}v^2 + u_{I3}i^2)$$

Figure 5·5·8 Rotor Winding

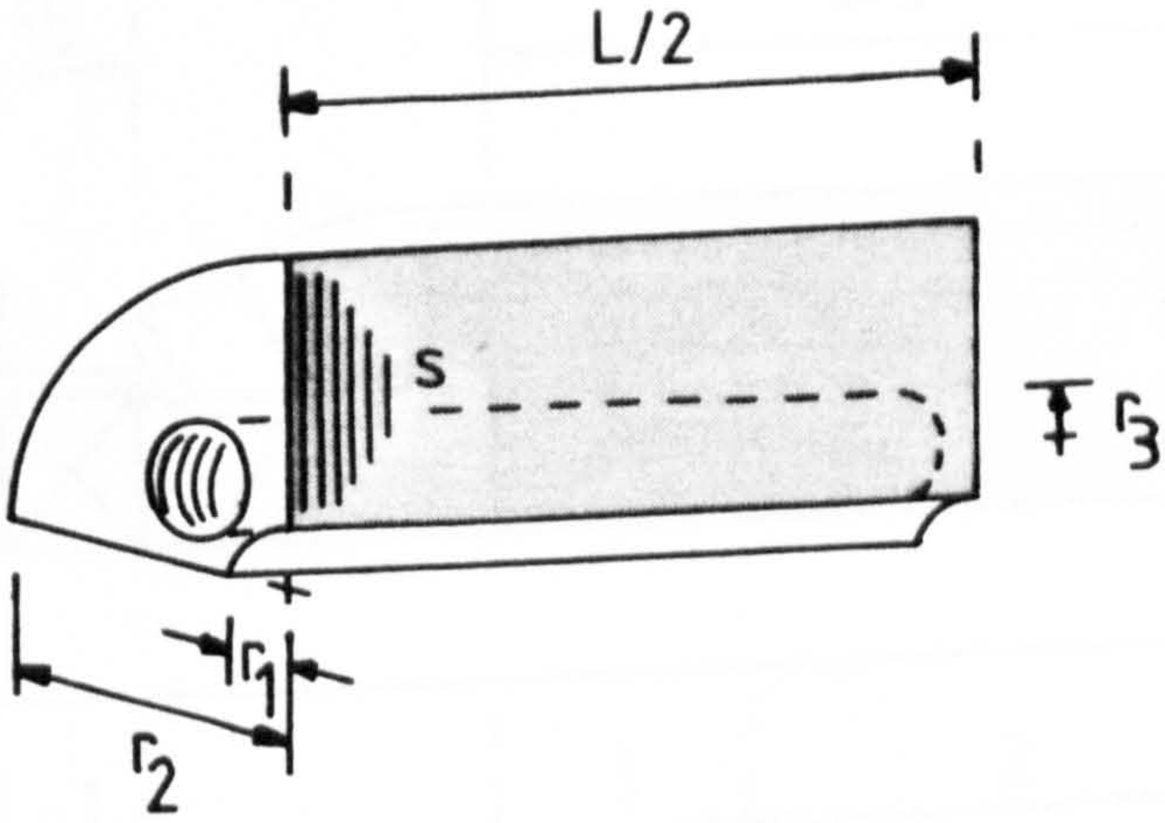

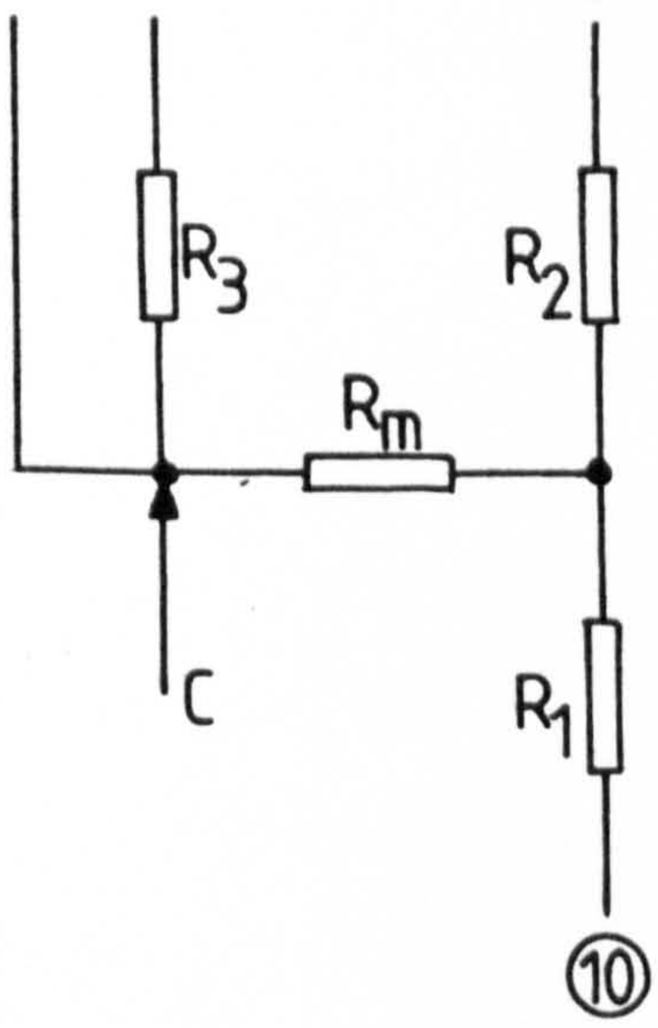

$$R_1 = \frac{(r_2^2 - r_1^2)}{2\pi k_{rl} L s (r_2^2 - r_1^2 - n r_3^2)} \left(\frac{2 \log_e (r_2/r_1) r_2^2}{(r_2^2 - r_1^2)} - 1 \right)$$

$$R_2 = \frac{(r_2^2 - r_1^2)}{2\pi k_{rl} L s (r_2^2 - r_1^2 - n r_3^2)} \left(1 - \frac{2 r_1^2 \log_e (r_2/r_1)}{(r_2^2 - r_1^2)} \right)$$

$$R_m = \frac{-1}{4\pi k_{rl} L s (r_2^2 - r_1^2 - n r_3^2)} \left(r_1^2 + r_2^2 - \frac{4 r_2^2 r_1^2 \log_e (r_2/r_1)}{(r_2^2 - r_1^2)} \right)$$

$$R_3 = \frac{L}{6\pi k_{al} (r_2^2 - r_1^2 - n r_3^2)}$$

$$C = \frac{c_s \rho_s \pi L s (r_2^2 - r_1^2 - n r_3^2)}{2}$$

Figure 5·5·9 Rotor Iron

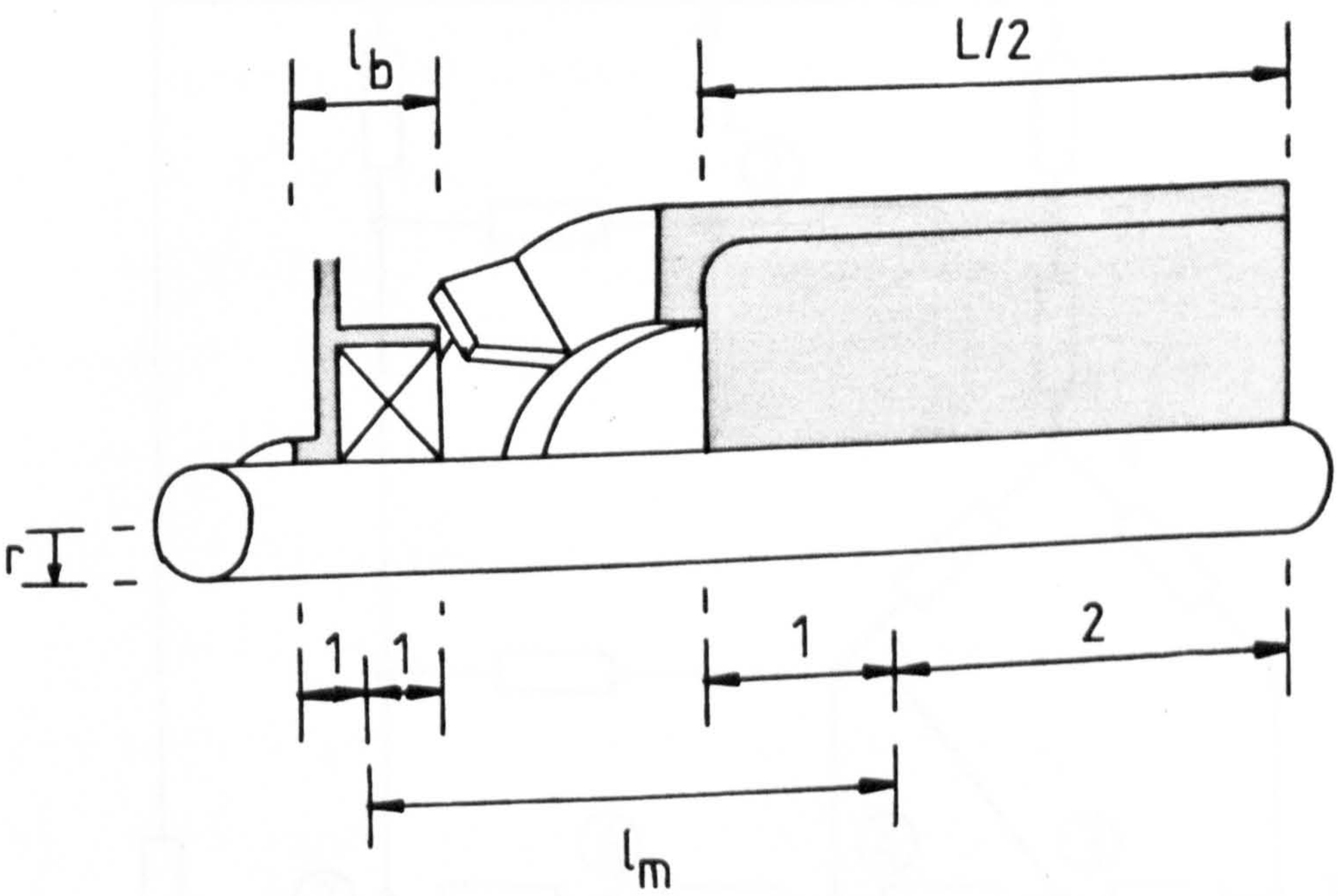

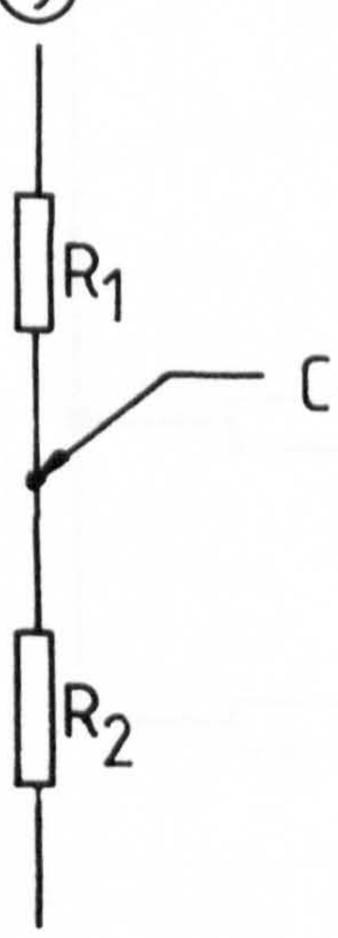

$$R_1 = \frac{1}{2\pi k_s L} + \frac{l_m}{2\pi k_s r^2}$$

$$R_2 = \frac{1}{4\pi k_s l_b} + \frac{l_m}{2\pi k_s r^2}$$

$$C = \rho_s c_s \pi r^2 (l_m + \frac{1}{2} l_b + \frac{1}{3} L)$$

Figure 5·5·10 Shaft

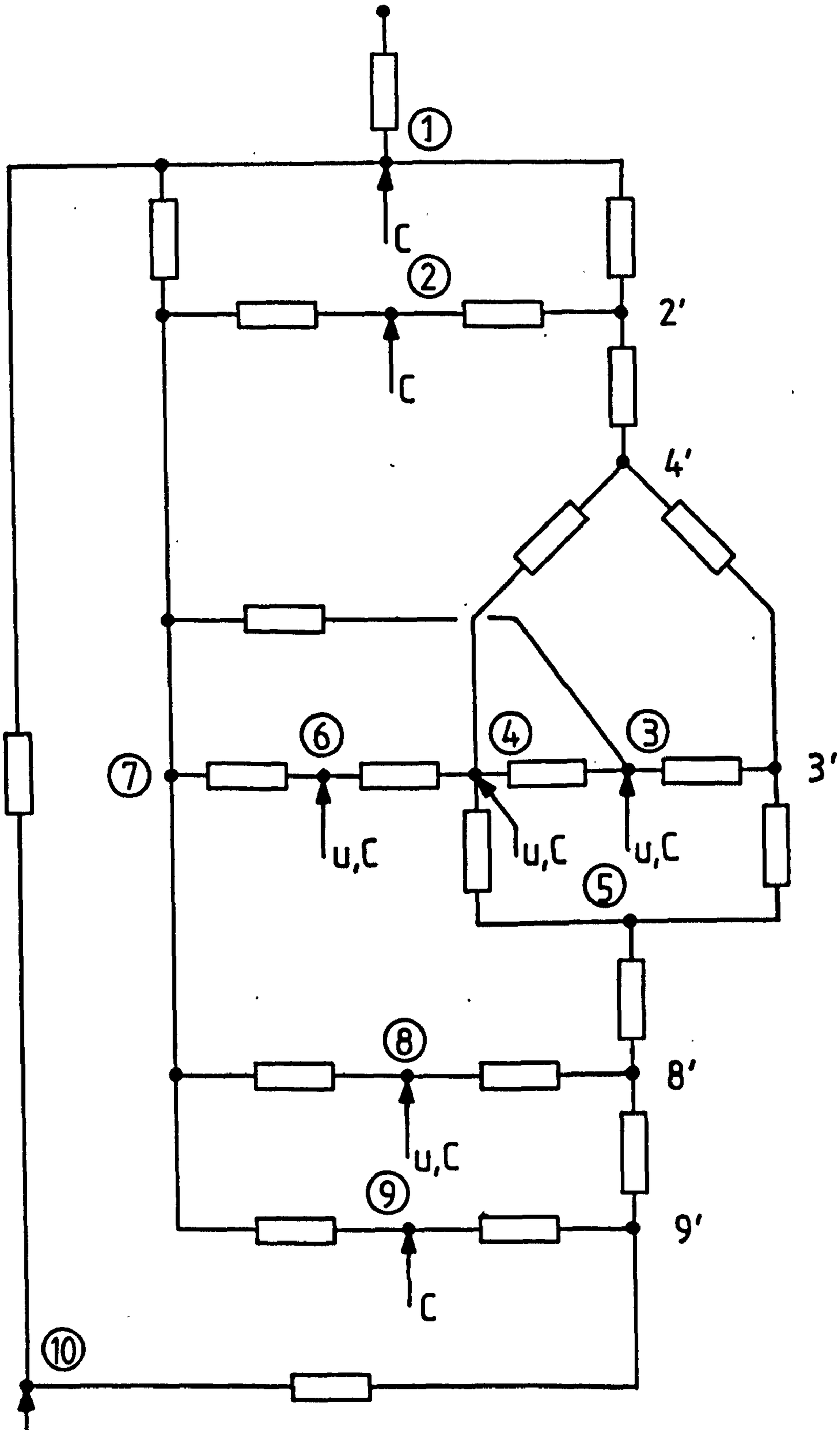

Figure 5·6 Induction Motor Thermal Equivalent Circuit

CHAPTER 6

MICROPROCESSOR THERMAL PREDICTION DEVICE AND MODEL RESULTS

6.1 INTRODUCTION

A control algorithm is presented in Chapter 3, that can be used to reduce the ageing in an electrical multi-machine system. This algorithm needs information on the machines' winding temperatures to calculate their switching sequence. The previous chapter has shown that the thermal performance of an induction motor can be described by a compact linear thermal model, that only requires a knowledge of the motor's phase voltages and currents. The combination of these factors suggests that a thermal prediction device could be designed for induction motors and provide a system controller with the necessary thermal information. The device would use a microprocessor to calculate the machines temperatures through a continual monitoring of the supply to the motor.

In addition to this specific application, a thermal prediction device can perform several other useful functions. It can be used in machine protection as a replacement for the conventional method of mounting thermometers in the machine's windings. The microprocessor can perform parallel tasks to the thermal calculations, such as supply condition monitoring and stall protection. The thermal model stored

in the device would also be available for estimating future temperatures in the motor from information on possible trends in the load. The latter facility could be used in sophisticated system controllers or a reliability analysis.

The chapter decribes a feasibility study of a thermal prediction device for a 5.5kW TEFC cage induction motor. The performance of the device is tested against measurements of the winding temperatures of the machine. A microprocessor was programmed to perform the thermal prediction and also record the measured motor temperatures. The thermal calculation software is described in detail, but only an outline of the remaining software and the system hardware is provided.

The final section of the chapter discusses the results of load tests on the motor. Here, the machine temperatures are compared with the results obtained from the thermal models of Chapter 5. The real time thermal prediction calculations, performed by the microprocessor, are also presented. These were based upon the original thermal model and are compared against the measured temperatures and a simulated performance of the model.

6.2 TEMPERATURE MEASUREMENT

The temperatures in various parts of the induction motor were measured with platinum resistance thermometers. These devices have a linear positive temperature coefficient over the range of temperatures found within a motor, i.e. 0-150^{o}C. They were choosen in preference to thermocouples

as they would not require a reference junction and because of the ease with which measurements could be obtained.

Each thermometer consisted of a small coil of platinum wire in a ceramic casing, which had a diameter of approximately 1mm and a length of 10mm. To facilitate their insertion into the machine, the devices were formed into thin probes by encasing their leads in a hard resin, Figure 6.1.

Nine thermometers were located in a vertical plane through the axis of induction motor. Three were placed in bore holes drilled into the stator of these the centre hole was accurately positioned such that a thermometer placed in the hole would rest in the centre of a stator tooth. The other two holes were drilled to a depth that would align the thermometers with the radial centre of the stator iron portion of the thermal model, Figure 6.2.

Two thermometers were strapped onto each endwinding . The first was used to measure the endwinding surface temperature and the second was set above the winding to be in contact with the circulating endcap air as shown in Figure 6.3.

Of the remaining two thermometers, one was inserted inside the endwinding furthest from the external cooling fan, whereas the other was pushed deep into a stator slot winding.

An additional pair of external thermometers were used to monitor the machine surface and the surrounding ambient temperatures. Throughout thermal cement and

and tight bonding was used to ensure that a good contact existed between the thermometers and the machine.

A four wire technique was used to obtain the temperatures. This involved the passing of a constant current, via two of the wires, through the platinum resistances and measuring the corresponding potential drop with the other pair of wires. The method ensured that the effect of the resistance of the interconnecting leads would be eliminated.

The full circuit diagram of the temperature measuring unit is given in Figure 6.4. All the thermometers were connected in series and fed from the constant current source ICI,F2, R2. Their voltages were multiplexed by digitally controlled analogue switches, IC6 and IC7, to a differential amplifier, IC3-IC5. The circuit values were choosen such that the current source reference voltage would be equal to the output of the differential amplifier across a thermometer at $0^{o}C$. The voltage reference could then be subtracted from the differential signal, IC3, to give an output V_o directly proportional to the temperature in degrees Centigrade, the actual scaling being $10mV/^{o}C$.

Other salient features of the circuit were that, for accuracy, 1% metal film resistors were used and that for maximum stability the 5.6V zener reference source, Z1, was biased with a current source, F1 and R1, at it's point of zero temperature regulation (i.e. when its

breakdown was an equal combination of avalanche and zener effects).

Through the use of the platinum resistance thermometers and the above circuit, it was possible to digitally select the temperature of a part of the machine and obtain a direct reading to within a 2% accuracy. The calibration of the measuring circuit was confirmed before each load test, by including a precision resistance box in the chain of platinum elements, and comparing the relationship between the output temperature reading and the resistor value with the manufacturers calibration curve of the thermometers.

6.3 MICROPROCESSOR HARDWARE

As mentioned in the introduction, the microprocessor program was designed to perform the two parallel operations of recording the motor temperature and power conditions, and demonstrating the thermal calculations. A certain amount of overlap existed between those two functions, both in the hardware and software design.

The hardware support for the 8085A microprocessor was that available on the Intel SDK85 development system[46],[47]. This consisted of two kilobytes of programmable memory (8755 EPROM), 256 bytes of random access memory (8155) and a keypad and a six character display with a controller chip. The 8155 integrated circuit also contained a programmable timer/counter, which acted as the

system's real time clock.

Both the 8155 and 8755 integrated circuits had built in input/output ports that were used to interface the microprocessor to an analogue to digital converter (ICL7109) and a tape punch. A schematic of the hardware is given in Figure 6.5.

The microprocessor obtained readings of the machine's temperatures and r.m.s. phase voltage, current and power through the 12 bit analogue to digital converter. For simplicity, the electrical measurements were confined to a single motor phase which implied the assumption that the machine would always be operating under balanced conditions. The scaled outputs of the calibrated voltage, current and power sensors and the temperature measurement circuit of Section 6.2 were multiplexed to the convertor through analogue switches. The microprocessor could then select a particular signal by a 5 bit digital address.

A low cost integrating analogue to digital converter was employed, which achieved the 12 bit conversion in approximately 40 milli-seconds, a time which was considered small compared with the thermal and mechanical time constants of the machine. A sample and hold circuit was not necessary, again because of the slow response of the machine and also since the integrating technique averages the data throughout the conversion cycle. The resolution of the converter was somewhat greater than required, especially when the accuracy of the analogue measurements was considered.

However, since there was little constraint on the conversion time of the device 12 bit accuracy was chosen to ensure that quantisation errors in the conversion were negligible.

An 8 bit tape punch was used to record the measurements taken by the microprocessor and the results of the temperature prediction program. This was interfaced onto the microprocessor system through an 8 bit buffered data bus and two 'handshake' control lines. The results were printed on the tape in a format compatable with the Liverpool University ICL 1906S main frame computer, where the tape could be read for subsequent analysis.

Finally, the keyboard and display allowed the user to communicate with the microprocessor, to initiate the data logging and thermal prediction software and also to display any of the recorded or calculated values.

6.4 GENERAL SOFTWARE OUTLINE

In this section the software used to record and print the data is briefly outlined. A more detailed account of the software operation is contained in Appendix A8.

A flexible data logging system was developed in the software, Figure 6.6. This was based around a 16 word, 24 bit stack. A word would contain a value read from the analogue to digital converter and an identification code. This code contained the source address of the reading and a classification in terms of whether it was a temperature, voltage, current or power signal.

Two timing cycles were employed to update the information in the stack and send it to the tape punch, these were called the auxiliary and print cycles. A mask contained in the stack word identification code determined whether that particular word would be updated in either or both of the two cycles. In the auxiliary cycle the recorded values were simply updated from the analogue to digital converter, provided that the appropriate mask was set. However, in the print cycle not only was the data updated, but the new values were scaled in accordance with their signal classification (i.e. temperature, voltage etc.), converted into a 4 digit decimal number and punched onto the tape in an ASCII code.

The timing of the two cycles was controlled from the interval counter on the 8155 integrated circuit and a hour, minute and second clock held in the microprocesor's memory. The auxiliary cycle could be programmed to repeat itself after an integer number of seconds, whereas the print cycle could only occur in integer multiples of minutes. At the start of every print cycle, the time in hours and minutes of the cycle was punched onto the tape.

The auxiliary cycle was designed to be used in conjunction with the temperature prediction and display routines. The print cycle was written solely to output data.

A set of monitor routines were provided, that could be accessed by an operator through the keyboard and

the digital display. These allowed the data indentification codes to be assigned to each stack word, the auxiliary and print cycle repetition rates to be set, and the data logging process to be started and terminated. A further command could be used to display any of the values in the stack and the current time.

A complex program structure was necessary to ensure that the microprocessor's c.p.u. time could be utilised fully. This required a five tier internal program structure and three external interrupts and is discussed fully in the Appendix A8.

The entire data logging and thermal prediction software used 1.9 kilobytes of source code in the EPROM and 196 bytes of random access memory. During the data logging process, the c.p.u spent the majority of it's time in an idle state waiting for the analogue to digital converter. In a printing cycle, the microprocessor could be tied for up to 1.5 seconds in handshaking the contents of the stack with the slow tape punch. However, because of the program interrupt structure this activity did not interferewith higher priority processes.

It was estimated that approximately sixty per cent of the c.p.u. time was available for the thermal calculations, which, in fact, were found to require only ten per cent.

6.5 THERMAL PREDICTION SOFTWARE

The matrix equations that governed the thermal operation of the induction motor were developed in Chapter 5. These were shown to reduce to the 8th order linear differential equations:

$$[C] \quad \frac{d[\theta]}{dt} = [Y][\theta] + [u] \qquad (3.6)$$

where:

$$[Y] = [Y]_s$$

$$[u] = 0$$

when the machine was stationary, and:

$$[Y] = [Y]_r$$

$$[u] = [u_I]\, i^2 + [u_v]\, v^2$$

when the motor was running.

The solution to this equation was obtained by the use of eigenvalues and eigenvectors[48]. Dividing Equation (3.6) through by the matrix [C], yields:

$$\frac{d[\theta]}{dt} = [Y'][\theta] + [C]^{-1}\,[u] \qquad (6.1)$$

where: $[Y'] = [C]^{-1}\,[Y]$

The matrix [Y'] is a square 8 row real matrix. which has eight negative eigenvalues λ, and non zero eigenvectors [X] that satisfy the equation:

$$[Y'][X] = \lambda[X] \tag{6.2}$$

The eigenvalues λ are the solution of the matrix characteristic equation:

$$\text{Det}\,([Y'] - \lambda[I]) = 0 \tag{6.3}$$

Defining an arbitary variable z, that is related to the temperature [θ] and a particular eigenvector [X] such that:

$$[\theta] = [X]\,z \tag{6.4}$$

Then Equation (6.1) can be rewritten as:

$$[X]\frac{dz}{dt} = \lambda[X]z + [C]^{-1}[u] \tag{6.5}$$

This has a solution in the time domain of:

$$z(t) = e^{\lambda t}z(0) + e^{\lambda t}\int_0^t e^{-\lambda t}\,[X]^{-1}[C]^{-1}[u(t)]\,dt \tag{6.6}$$

for the initial condition z(0). Re-substituting Equation (6.4), gives a particular solution to the original differential equation as:

$$[\theta(t)] = [X]e^{\lambda t}[X]^{-1}[\theta(0)] + [X]e^{\lambda t}\int_0^t e^{-\lambda t}[X]^{-1}[C]^{-1}[u(t)]\,dt \tag{6.7}$$

This continuous equation is approximated by a digital, step-by-step, solution by assuming constant heat generation $[u(n\Delta T)]$ over a time period ΔT. Using the notation $[\theta(n\Delta T)]$ as the matrix of nodal temperatures during the nth time interval T, Equation (6.7) becomes:

$$[\theta(n\Delta T)] = [X]e^{\lambda\Delta T}[X]^{-1}[\theta(\overline{n-1}\Delta T)]$$

$$+[X]\frac{1}{\lambda}(e^{\lambda\Delta T}-1)[X]^{-1}[C]^{-1}[u(n\Delta T)] \qquad (6.8)$$

Equation (6.8) holds for each of the eight eigenvalues and eigenvectors of the characteristic matrix [Y']. The general step-by-step solution will thus be composed of the sum of all the particular solutions and can be expressed in matrix form as:

$$[\theta(n\Delta T)] = [X'][D_1][X']^{-1}[\theta(\overline{n-1}\Delta T)]$$

$$+ [X'][D_2][X']^{-1}[C]^{-1}[u(n\Delta T)] \qquad (6.9)$$

where $[D_1]$ = diagonal matrix with elements $e^{\lambda\Delta T}$ for each λ of [Y']

$[D_2]$ = diagonal matrix with elements $\frac{1}{\lambda}(e^{\lambda\Delta T}-1)$

$[X']$ = square matrix with column vectors of the eigenvectors in corresponding row order to the eigenvalues in $[D_1]$.

The full solution of Equation (6.9) can be expanded for the two cases of the machine rotating or stationary.

These are:

$$[\theta(n\Delta T)] = [X']_s[D_1]_s[X']_s^{-1}[\theta(\overline{n-1}\Delta T)] \qquad (6.10)$$

for the motor stationary and:

$$[\theta(n\Delta T)] = [X']_r[D_1]_r[X']_r^{-1}[\theta(\overline{n-1}\Delta T)]$$

$$+ [X']_r[D_2]_r[X']_r^{-1}[C]^{-1}([u_I]i^2 + [u_V]v^2) \qquad (6.11)$$

with the motor running.

The stationary equation is an exact solution, whereas the running equation assumes that the induction motor's r.m.s. current and voltage remains constant throughout the interval ΔT.

The eigenvalues and eigenvectors were calculated on the mainframe computer from the original motor equations by a standard numerical libary routine[49].

A step interval, ΔT, of one second was choosen for the temperature prediction calculations performed by the microprocessor. This was the smallest interval that could be used, with the microprocessor performing the data logging duties as well. Also for simplicity, a constant phase voltage was assumed. However, should there be a need to monitor the phase voltage, for example with a machine operated under a variable voltage speed controller, voltage generation calculations could be performed along similar lines to those of the current generation.

The microprocessor needed only to perform matrix multiplications and additions to predict the machine

temperatures from Equations (6.10) and (6.11). At each step the calculation required the previous temperature matrix, the new phase current and the four constant matrices:

$$[A]_s = [X']_s[D_1]_s[X']_s^{-1}$$

$$[A]_r = [X']_r[D_1]_r[X']_r^{-1}$$

$$[B_1]_r = [X']_r[D_2]_r[X']_r^{-1}[C]^{-1}[u_I]$$

$$[B_2]_r = [X']_r[D_2]_r[X']_r^{-1}[C]^{-1}[u_V]v^2 \qquad (6.12)$$

These matrices were evaluated for the original thermal model of Section 5 and a 244V phase voltage and a one second step interval.

The temperatures in the above equations are referenced to the ambient. To accommodate for fluctuations in the ambient temperatures, the calculations were performed assuming a zero ambient and only adjusted to their absolute values when the temperatures needed to be displayed or printed.

Both the temperature and constant matrices of Equations (6.10) and (6.11) were stored to 16 bit accuracy. Each row calculation were performed using integer additions and multiplications with sub totals stored in a 24 bit accumulator. The current i was measured from the analogue to digital converter as a 12 bit binary number. This was converted into a 16 bit integer, representing its

square, by performing a multiplication accurate to a full 24 bits and then rounding off the lower byte.

The scaling of the calculated temperatures was made directly compatible with the measured values by adjusting the [B] matrices with appropriate factors. The representation in the microprocessor of the constant matrices of Equation (6.12) was equivalent to a set of integer matrices, scaled such that:

$$[A]_s^I = INT([A]_s \times 2^{16})$$

$$[A]_r^I = INT([A]_r \times 2^{16})$$

$$[B_1]_r^I = INT([B_1]_r \times 2.048 \times 2^{16})$$

$$[B_2]_r^I = INT([B_2]_r \times 1.25 \times 2^{16}) \qquad (6.13)$$

Here, the matrices on the left are the integer equivalents to those on the right and 'INT' is the operation that rounds up a decimal number to an integer. The negative elements of the matrix $[B_2]_r^I$ were stored as their binary two's complement. The scaled matrices are listed in Table 6.1 in hexidecimal format.

Similarly, the binary equivalents of the variable matrices were given by:

$$[\theta(n\Delta T)]^{I} = \mathrm{INT}([\theta(n\Delta T)] \times 2^{16}/204.8)$$

$$i^{2I} = \mathrm{INT}((i/20.48)^{2} \times 2^{16}) \qquad (6.14)$$

The temperature calculation was thus performed by choosing on either zero or non-zero current, one of the two integer equations:

$$[\theta(n\Delta T)]^{I} = ([A]^{I}_{s} . [\theta(\overline{n-1}\Delta T)]^{I})/2^{8} \qquad (6.15)$$

$$[\theta(n\Delta T)]^{I} = ([A]^{I}_{r} . [\theta(\overline{n-1}\Delta T)]^{I} + [B_1]^{I} . i^{2I})/2^{8} + [B_2]^{I} \qquad (6.16)$$

In the above, the operator '.' is equal to a multiplication of two 16 bit binary integers, with the result taken only from the most significant 24 bits. A division by 2^8 is equivalent to a final rounding down of the 24 bit result to 16 bits.

This calculation proceedure was simple to implement on the microprocessor. It was found through integer simulation on the mainframe computer to give no noticeable error in the temperature expressed accurate to one decimal point, compared with decimal calculations at the mainframe's full 32 bit accuracy.

A full commented listing of the thermal calculation software is given in Appendix A9. This was merged onto the data logging system on the microprocessor by reserving the top eight locations of the data stack for the measured

values of current and ambient temperature and the calculated temperatures for six of the thermal nodes, Table 6.2. These temperatures were taken from the matrix $[\theta(n\Delta T)]^{I}$, reduced to 12 bit accuracy, added to the ambient temperature and then written onto the stack. By this method, the predicted values could be then printed or displayed in an identical manner to the temperatures measured from the motor.

6.6 PERFORMANCE OF MICROPROCESSOR PREDICTION UNIT AND UPDATED THERMAL MODEL

The results in this section are presented in two parts. Initially, the temperatures that were calculated by the microprocessor prediction routines are compared against measured values for the varying load test given in Figure 6.7. The test included periods when the induction motor was running at overloads or was stationary. The second part uses the same load to simulate the performance of the thermal model described in Chapter 5 to illustrate the improvements over the original model.

The temperatures of some of the components in the thermal model that were computed in the microprocessor are shown, together with values read from the embedded thermometers, in Figures 6.8 through to 6.12. The motor frame temperature Figure 6.8 was in good agreement with the measured valves, which was expected since the frame heat transfer coefficients were taken directly from experimental tests. In both the heating and the cooling sections of the

curve, the calculated time constants appeared to be slightly smaller than the measured ones. This would be a result of a low estimation of the total machine thermal capacitance.

The predicted stator iron and teeth temperatures, Figures 6.9 and 6.10, were always lower than the measurements. This was attributed to a higher thermal resistance between the frame and stator than was originally modelled. The surface contact between the rough stator laminations and the aluminium frame was re-examined and accommodated for in the later thermal model.

The stator winding and endwinding temperatures again were calculated low as a result of the errors in the iron temperatures mentioned above. These temperatures would be expected to be higher than the measurements because the themometers could not be placed accurately in the centre of the windings.

An interesting thermal effect occurred in the motor immediately after it was switched off. The frame temperature appeared to rise several degrees before it began to fall. When the motor was running a radial temperature gradient would be established as the internal heat generation was transferred to the outside surface. However, when the heat generation was removed, this additional stored thermal energy would be transferred rapidly to the stator and frame as the entire machine attained a uniform temperature. This energy could not be immediately dissipated externally and consequently the frame temperature rose. Similarly, the frame temperature initially dropped when the machine was

restarted because of the improved cooling of the frame from the external fan and the initial heat generation had not yet diffused to the motor surface. The microprocessor thermal prediction followed these effects well.

The load test illustrated that a microprocessor could be used successfully to calculate the temperatures in an induction motor. However, certain inadaquacies became apparent in the original thermal model. A second model was developed to improve on the results by the introduction of secondary nodes, a more careful examination of the heat transfer processes when the machine was stationary and improvements in the model of the surface contact between the stator iron and the frame.

The temperatures of the second thermal model were computed on a mainframe computer by an integer simulation of the microprocessor's performance for the load of Figure 6.7. Tests on the earlier model had shown that the integer simulation was accurate to within a degree Centigrade of the real time predictions by the microprocessor. The results presented in Figures 6.13 to 6.17 would thus follow accurately the output of the prediction device if time had been available to program the second model into the microprocessor.

The stator iron and teeth temperatures were in better agreement with the thermometers when the machine was running. However, there was still an error when the motor was stationary. On cooling, the internal motor temperatures all fell quickly to follow the same cooling

curve. In the model, this curve was approximately equal to the frame temperature. The measured values appeared to follow the stator iron temperature and were initially (at time2.0 hours) 7°C higher than the frame temperature, but eventually this difference would fall to zero if the machine were to continue to cool to ambient. At the time 2.0 hours the frame temperature was measured to be approximately 35°C above the 22°C ambient and the ratio of the frame to ambient thermal resistance to the stator iron to frame resistance was calculated from the model to be equal to 4.9. If all the heat transferred out of the machine were to pass via the stator-frame interface then the stator iron would be expected to be at a temperature of 35°C divided by 4.9, i.e. 7°C above the frame, which agreed with the measured result. However, the present model suggested that the majority of the heat flow to the frame occurred via the alternative routes of the endcap air and rotor shaft to frame interfaces. To correct for this, the stationary model endcap air film coefficient should be increased and additional resistance added to the shaft-frame interface, to accommodate for the insulating properties of the lubricant in the bearings.

The winding temperatures in Figure 6.16 and 6.17 were greater than the measurements, the difference increasing rapidly with load. This was not unexpected, because the heat generation in the windings was a function of the load current squared and the temperature drop across any thermal path between say, the centre of the endwinding and the embedded thermometer,depended upon this generation.

The weighting of the endwinding model, to obtain the central winding temperatures, similarly acted as an increase in the thermal path of the internal heat generation. This is illustrated in Figure 6.18,where the endwinding temperature is plotted against the measured values for a severely changing load with up to 75 per cent overloads. The dotted curves on the figure give the results obtained from an unweighted model (weighting factor equal to unity) and show that substantial temperature differences only occurred at high loads.

The time constants of the model winding temperatures appeared to be lower than the actual machine. This was confirmed by a constant load test at 8 Amps, the results of which are shown in Figure 6.19. The steady values of temperature were heading towards good agreement with the measurements, and thus the model thermal capacitance was in error. The weight of the copper in the windings was accurately determined from the motor manufacturer, which suggested that the neglected capacitance of the insulation and bindings on the windings may have a significant contribution.

The model of Chapter 5 in the main gave a good description of the thermal performance of the induction motor, the only major error being in lower temperatures that were obtained when the machine was cooling. The lower thermal capacitance present in the winding models would not entirely compensate for the higher peak temperatures

obtained from the model as compared with embedded thermometers. Large temperature differences may well exist between the central endwinding temperature and a carefully placed thermometer. The ageing of an electrical machine is an exponential function of its winding temperature and differences between the actual peak and measured temperatures can cause a considerable multiplication in the ageing, expecially at high loads. This underlines the advantage of using an accurate thermal model for machine protection over embedded thermometers or simple RC or I^2t models derived from thermal measurements.

Table 6·1 Hexidecimal Thermal Prediction Matrices

$$[A]^{I}_{S} = \begin{bmatrix} 0000 & 000F & 0004 \\ 0054 & 0004 & 0001 \\ 017C & 0006 & 001C \\ F48E & 0374 & 006E \\ 022E & FD03 & 0018 \\ 0069 & 0025 & E047 \\ 0001 & 0008 & 046C \\ 0000 & 0001 & 0090 \end{bmatrix}_{4} \quad \begin{bmatrix} 0008 & 0002 & 0003 & 0007 & 0025 & 1E75 & F94A & 3BC4 \end{bmatrix}_{9} \quad 10 \quad \begin{bmatrix} 000C & 0000 & 0000 & 0000 & 0000 & 0024 & 0231 & C182 \end{bmatrix}$$

$$= \begin{bmatrix} FE66 & 0158 & 0004 \\ 021A & F987 & 0404 \\ 000E & 08C8 & F589 \\ 0003 & 0274 & 0512 \\ 006F & 0014 & 000E \\ 002D & 0009 & 005D \\ 000D & 0002 & 0002 \\ 0227 & 0002 & 0000 \end{bmatrix}_{1} \quad \begin{bmatrix} 0002 & 0001 \end{bmatrix}_{2} \quad 3 \quad \begin{bmatrix} 0004 & 0001 & 0000 & 0000 & 0000 & 0000 & 0000 & 000C \end{bmatrix}$$

$$[A]^{I}_{r} = \begin{bmatrix} FD96 & 0157 & 0004 \\ 0219 & F987 & 0404 \\ 000E & 08C8 & F589 \\ 0003 & 0274 & 0512 \\ 006F & 0014 & 000E \\ 002D & 0009 & 005D \\ 000D & 0002 & 0002 \\ 0226 & 0002 & 0000 \end{bmatrix}$$

$$[B_1]^{I}_{r} = \begin{bmatrix} 0000 \\ 0000 \\ 0000 \\ 0146 \\ 0143 \\ 0413 \\ 0001 \\ 0003 \end{bmatrix} \qquad [B_2]^{I}_{r} = \begin{bmatrix} 0000 \\ 000C \\ 0D24 \\ 0068 \\ FFFF \\ C9AC \\ FFED \\ FFD4 \end{bmatrix}$$

Table 6·2 Reserved Data Stack Words for Temperature Calculations

TOP

CURRENT
AMBIENT TEMPERATURE
FRAME TEMPERATURE
STATOR IRON TEMPERATURE
STATOR TEETH TEMPERATURE
STATOR WINDING TEMPERATURE
ENDWINDING TEMPERATURE
ROTOR WINDING TEMPERATURE

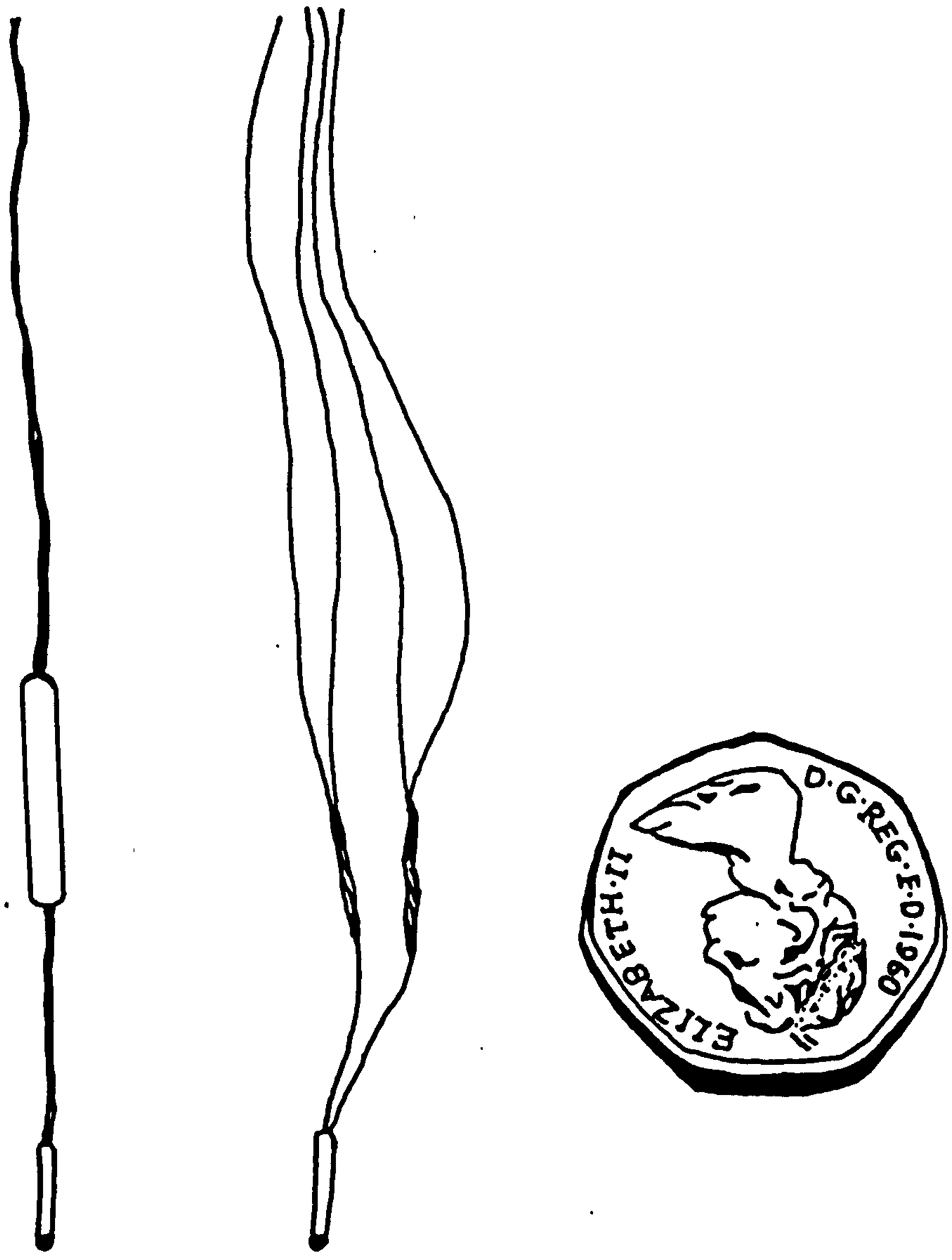

encased probe

four wire connection

Figure 6·1 Platinum Resistance Thermometers

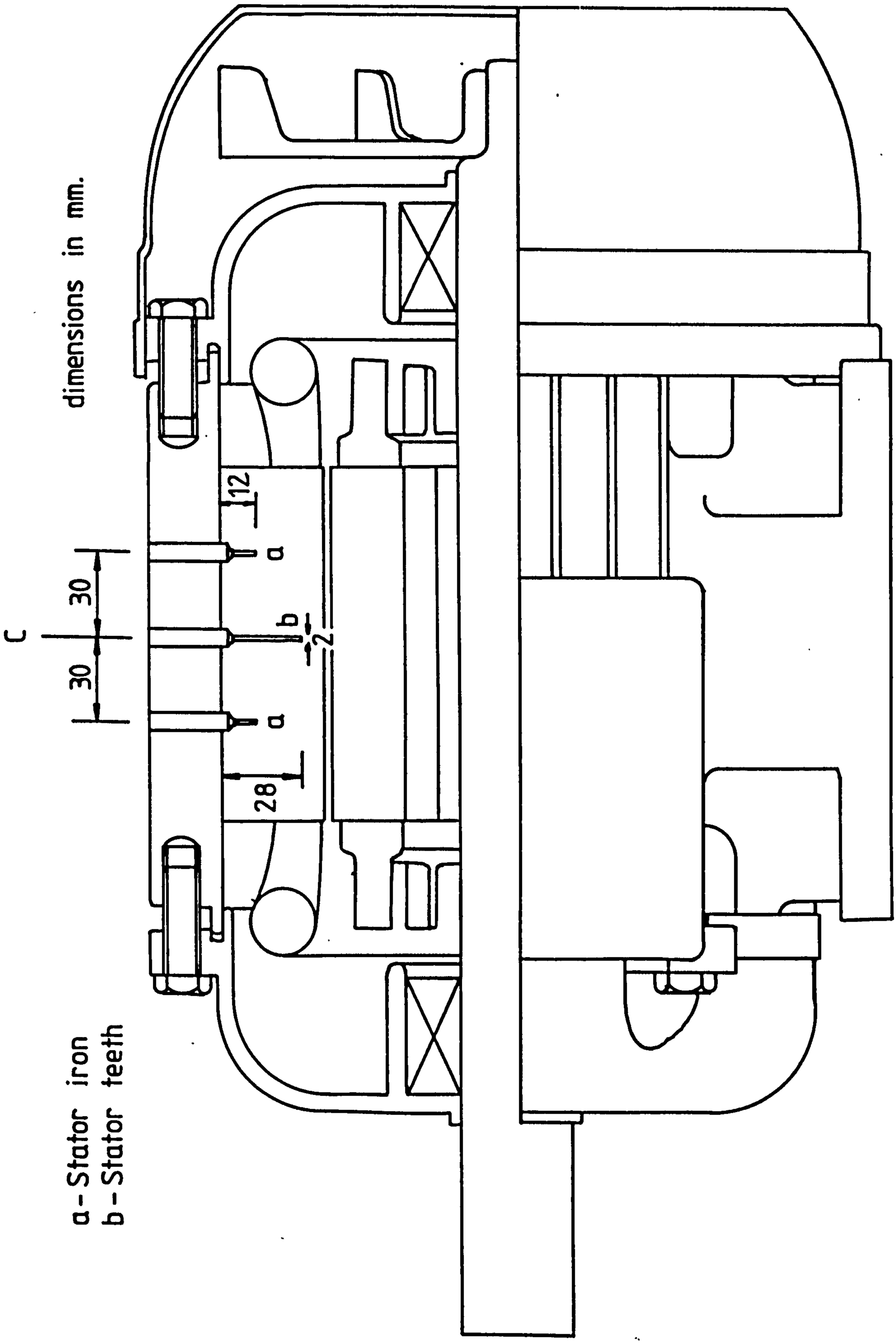

Figure 6·2 Position of Bore Holes for Stator Iron and Teeth Thermometers

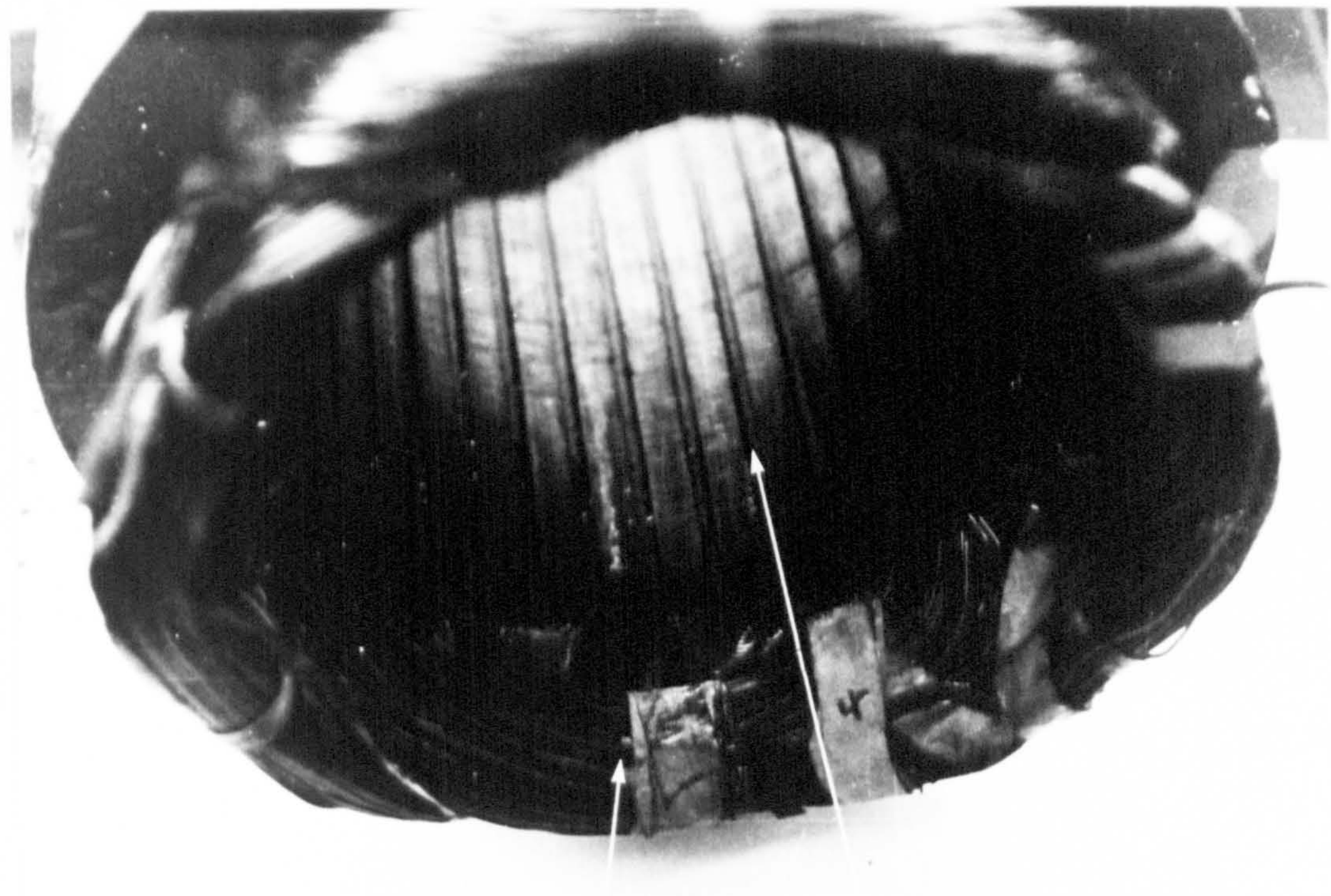

Endcap air thermometer

4 Stator winding thermometer

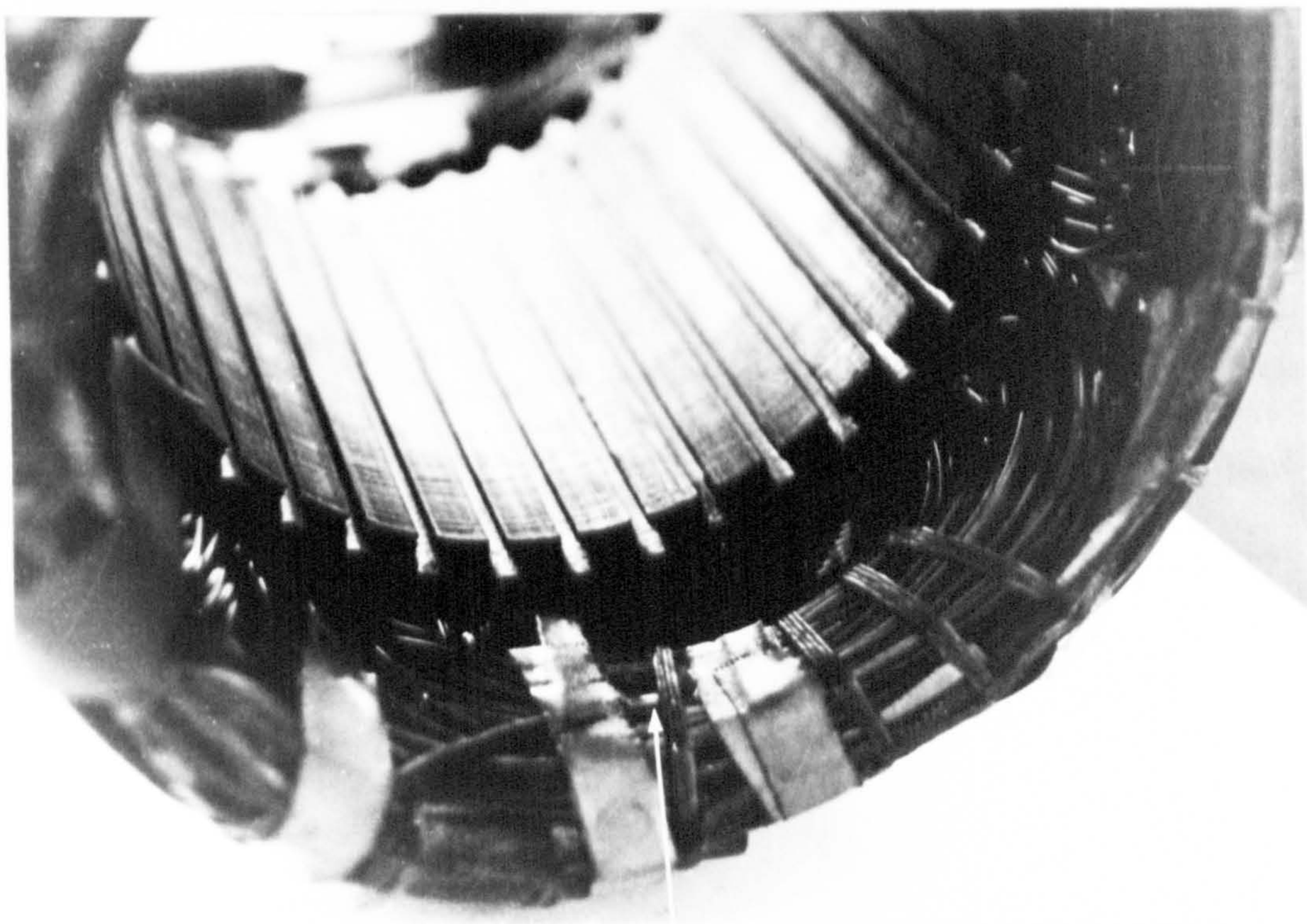

1 Endwinding surface thermometer

Figure 6·3 Location of Thermometers on Windings

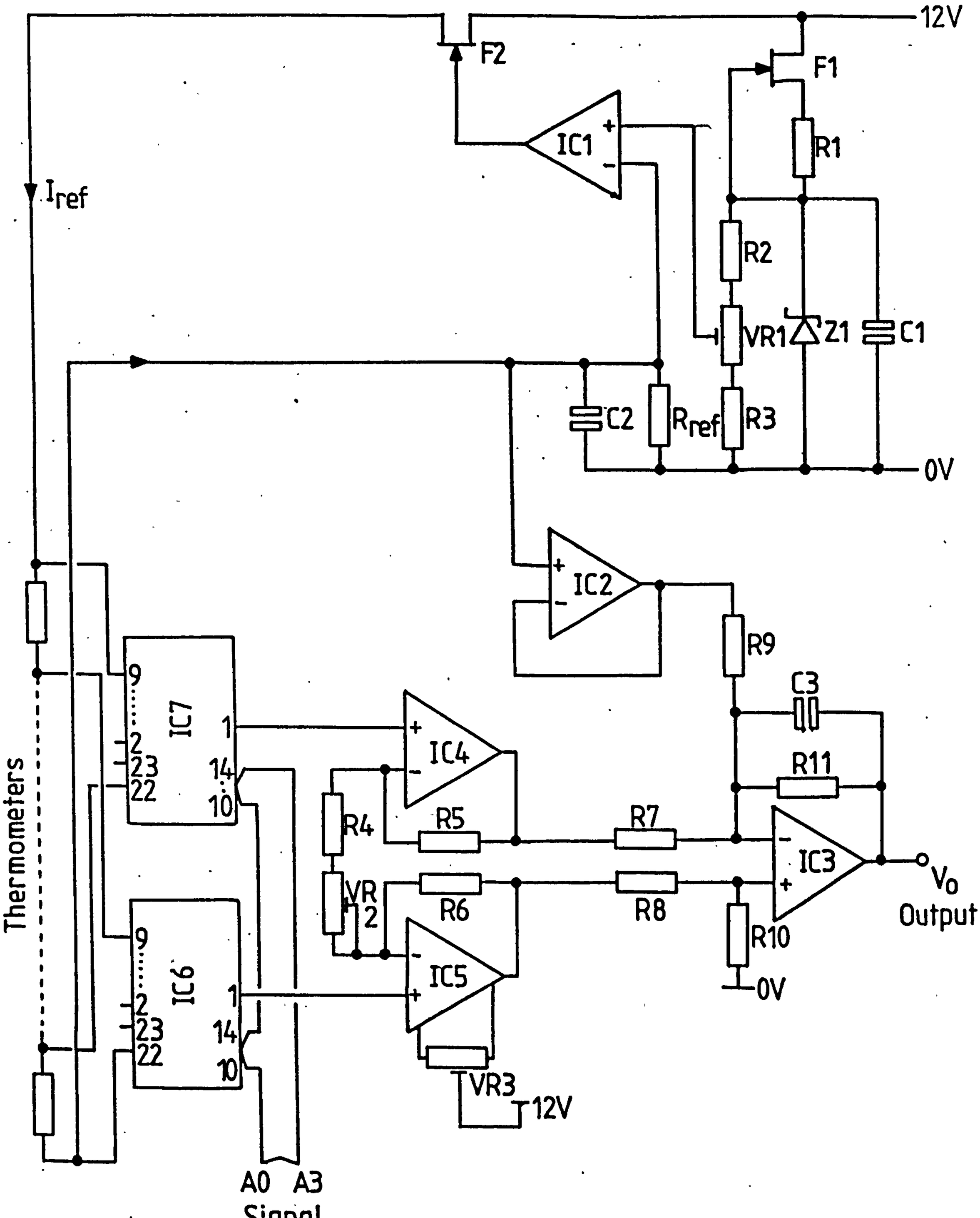

Figure 6·4 Thermometer Circuit

R1	100R	C1	10µ
R2	2K2	C2,C3	0µ1
R3	1K8		
R4	4K7	Z1	5V6
R5,R6	22K	F1,F2	2N2425
R7-R9	30K		
R10,R11	15K	IC1-IC3	741
VR1,VR2	500R	IC4,IC5	355
VR3	25K	IC6,IC7	4067

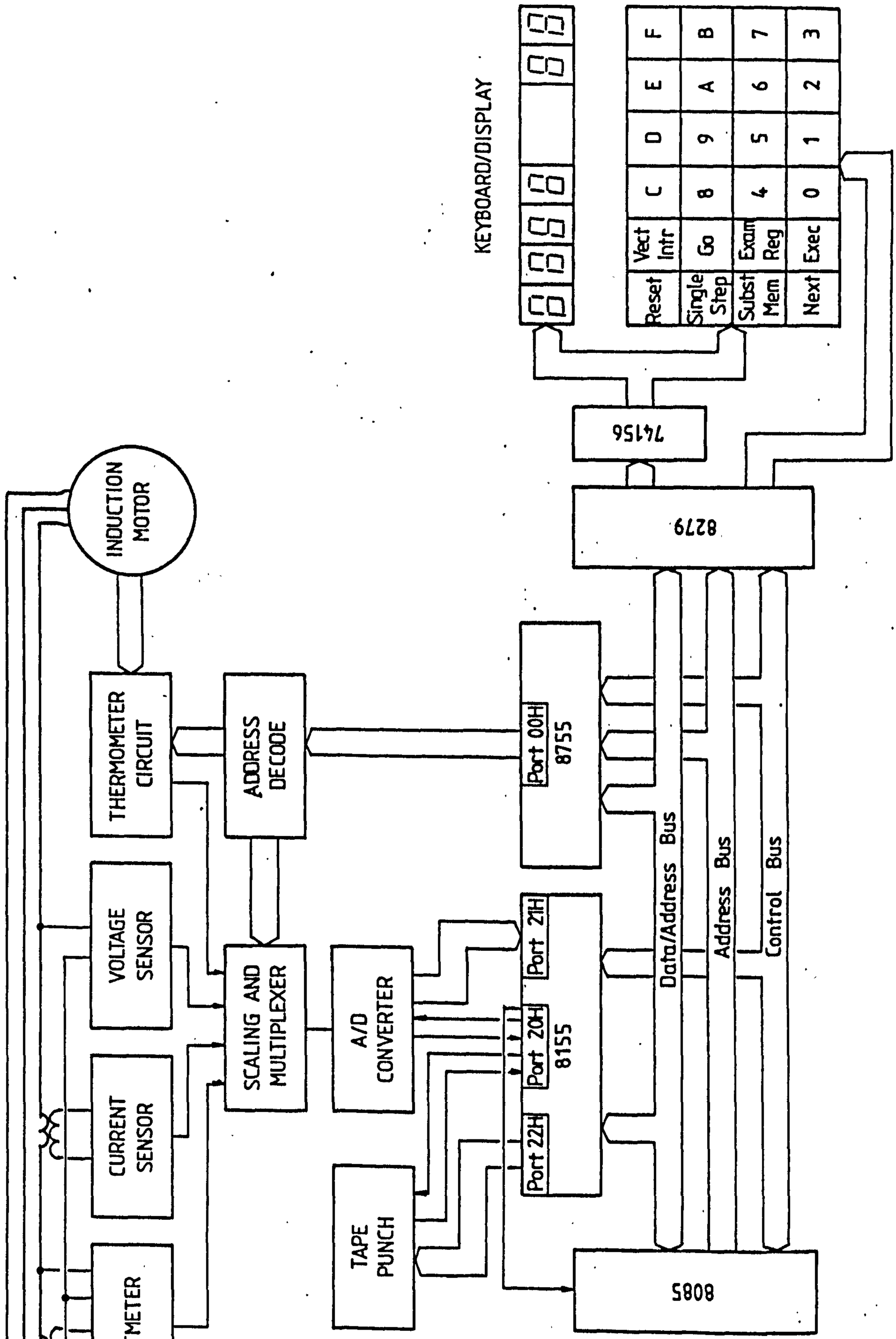

Figure 6·5 Hardware Schematic

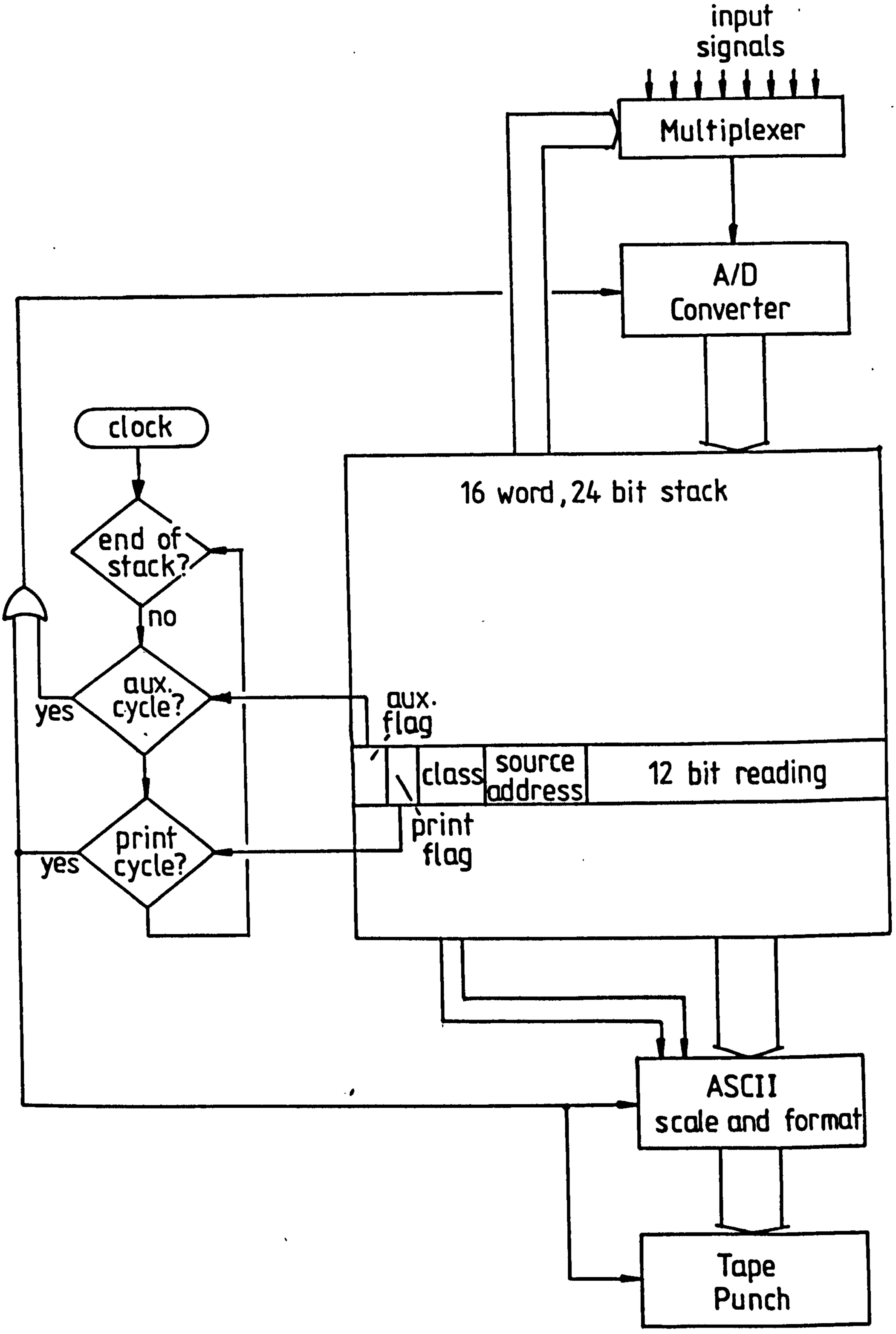

Figure 6·6 Data Logging Process

Figure 6·7 Motor Phase Current during Thermal Test

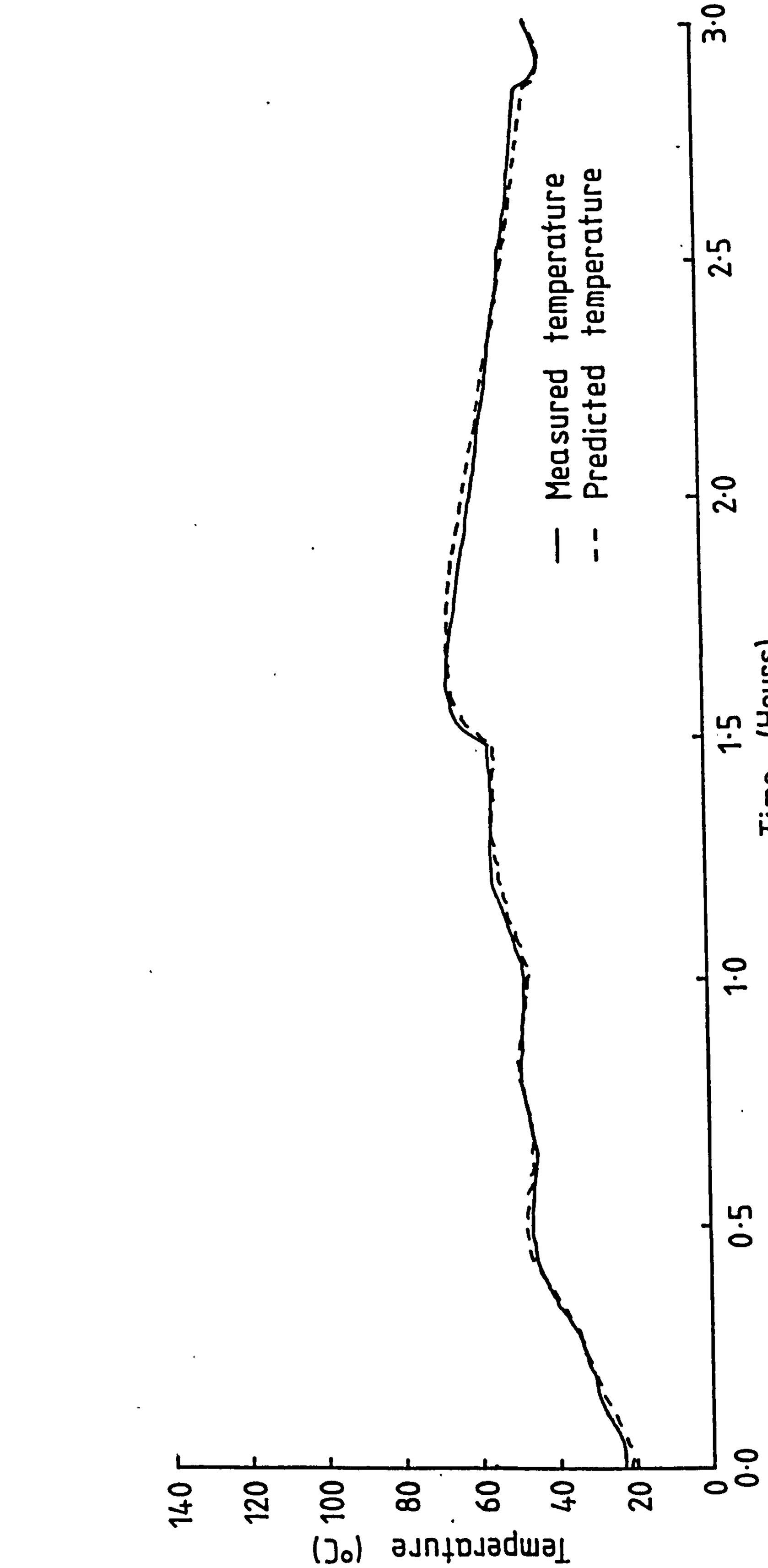

Figure 6·8 Microprocessor Predicted and Measured Frame Temperature

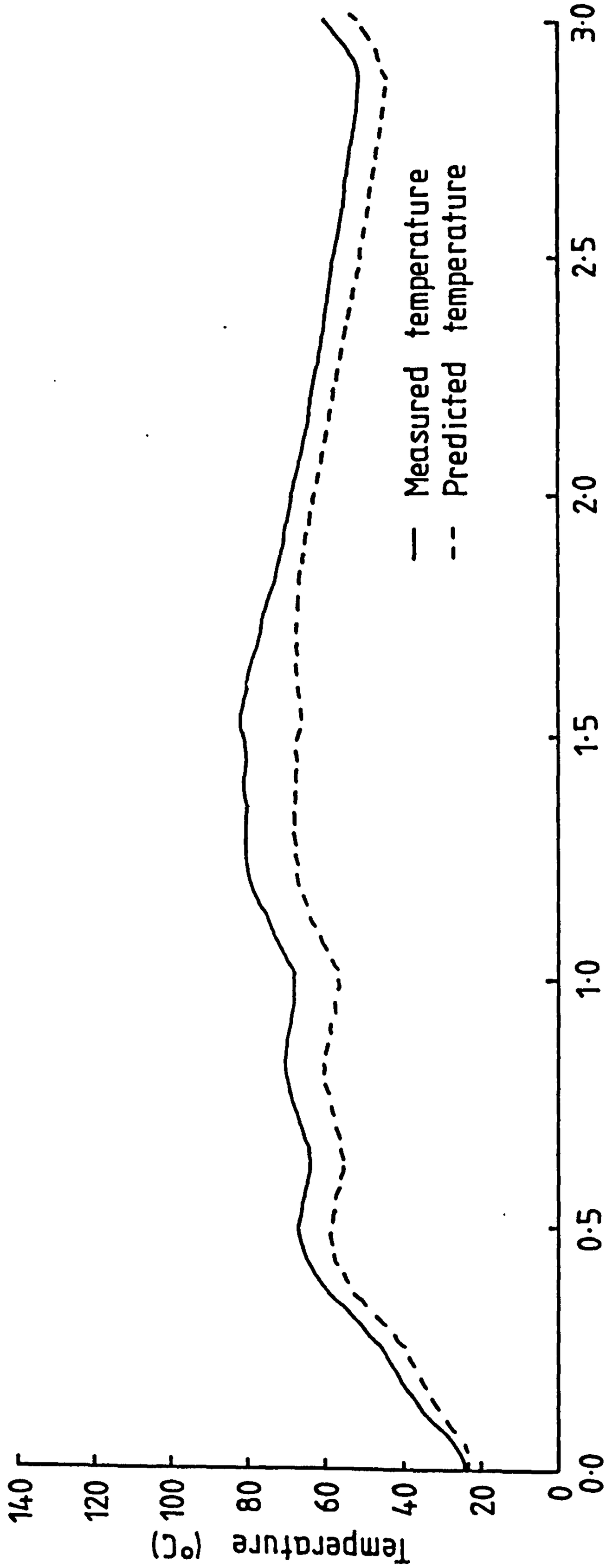

Figure 6·9 Microprocessor Predicted and Measured Stator Iron Temperature

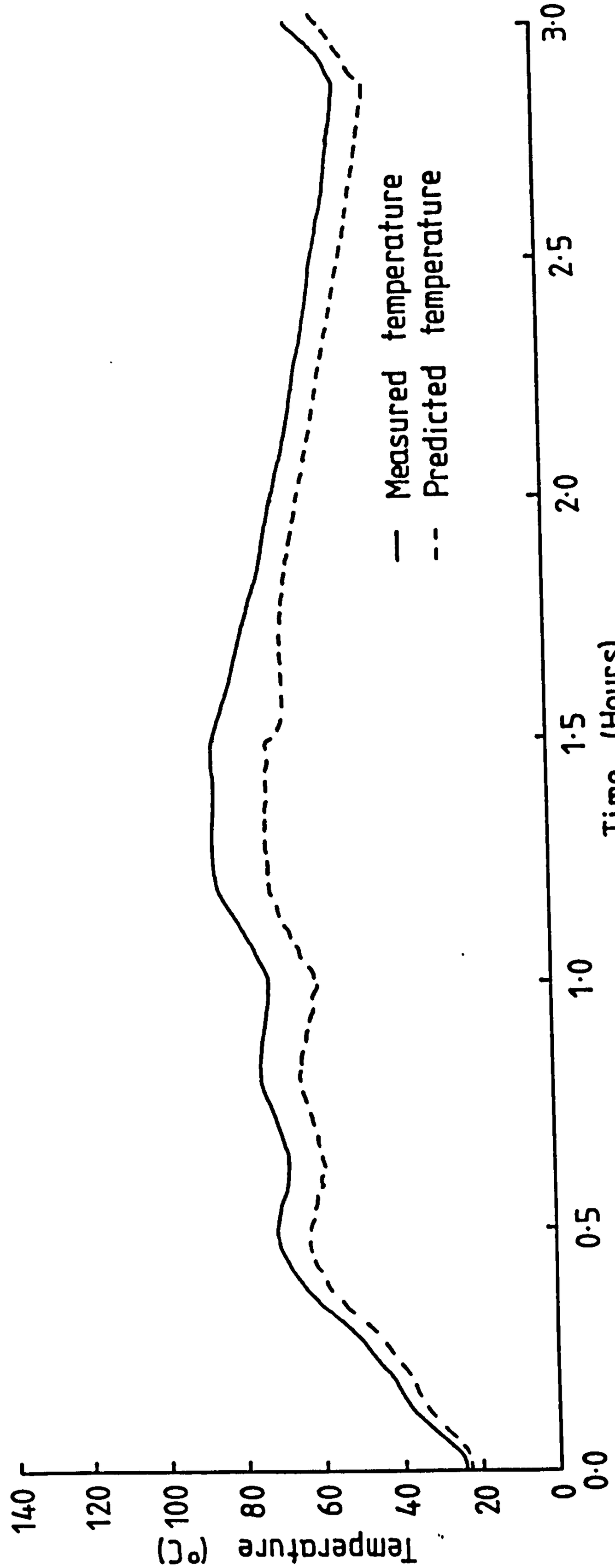

Figure 6·10 Microprocessor Predicted and Measured Stator Teeth Temperature

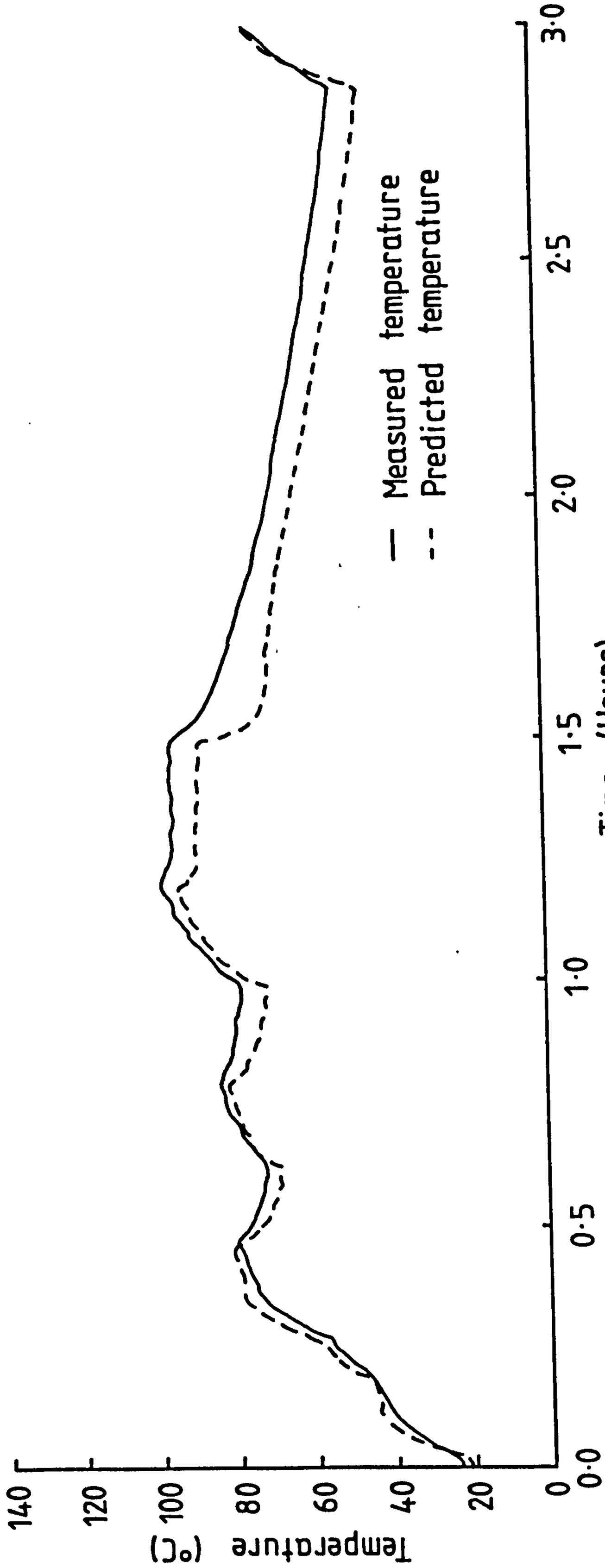

Figure 6·11 Microprocessor Predicted and Measured Stator Winding Temperature

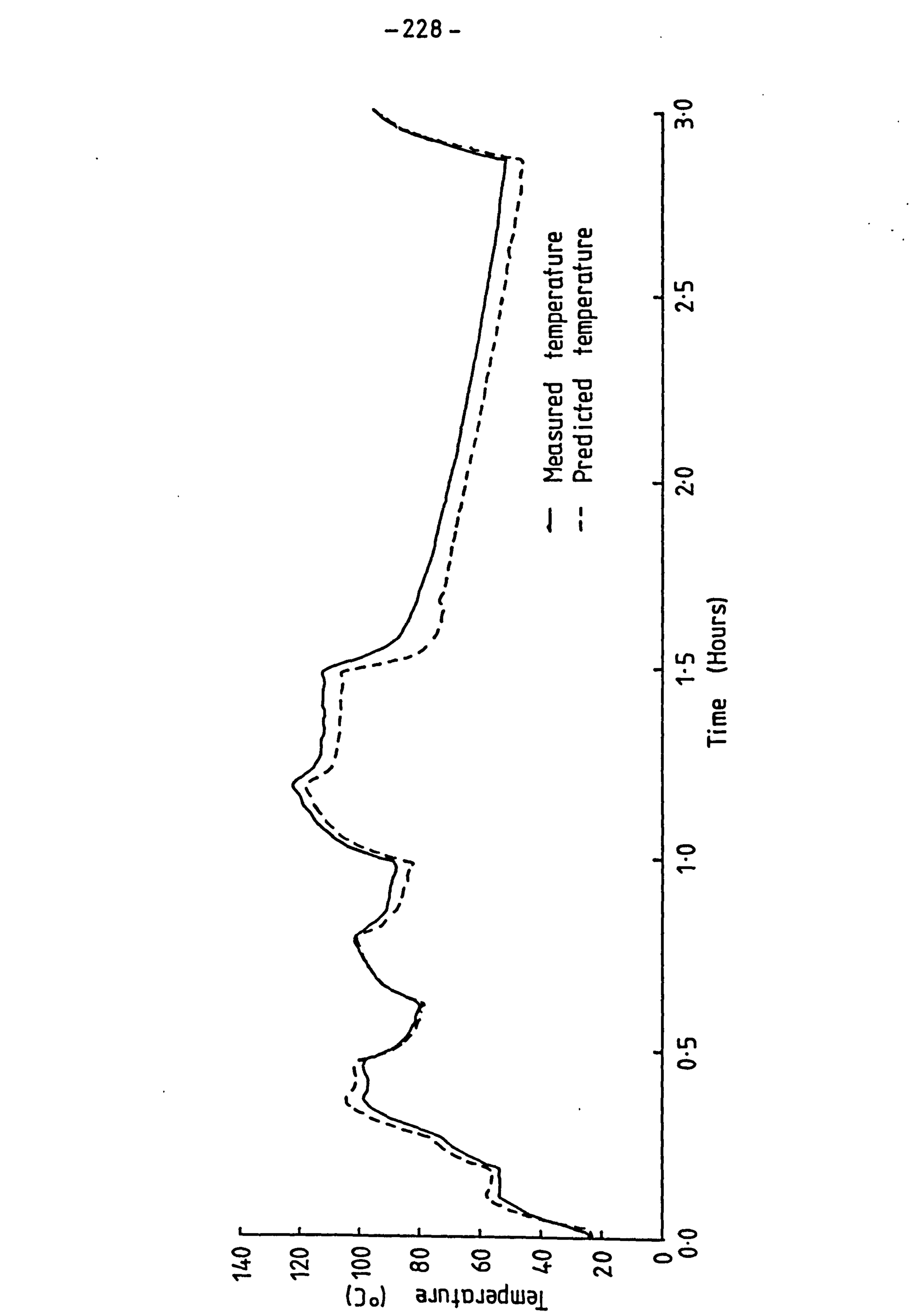

Figure 6·12 Microprocessor Predicted and Measured Endwinding Temperature

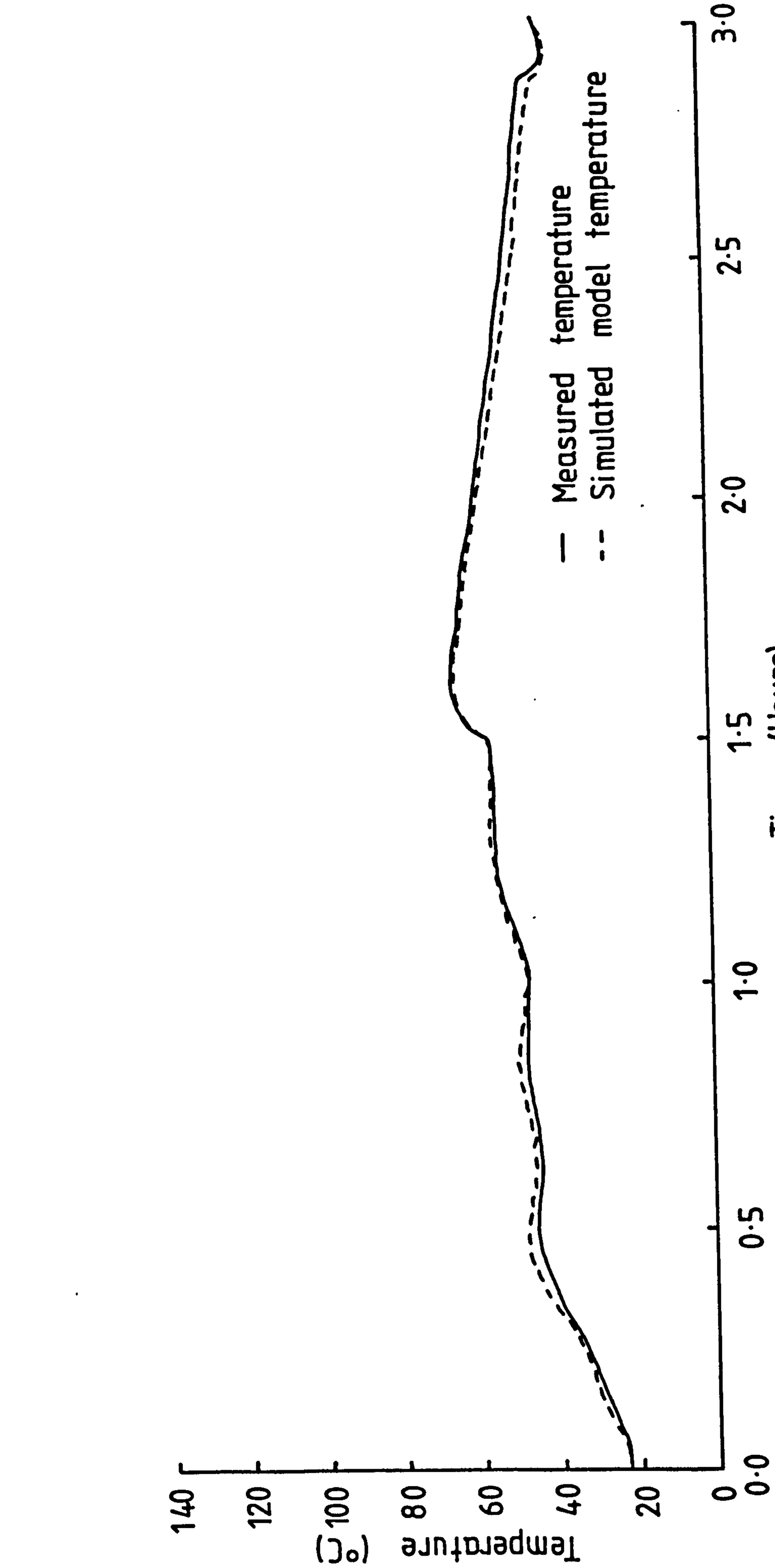

Figure 6·13 Simulated Second Model and Measured Frame Temperature

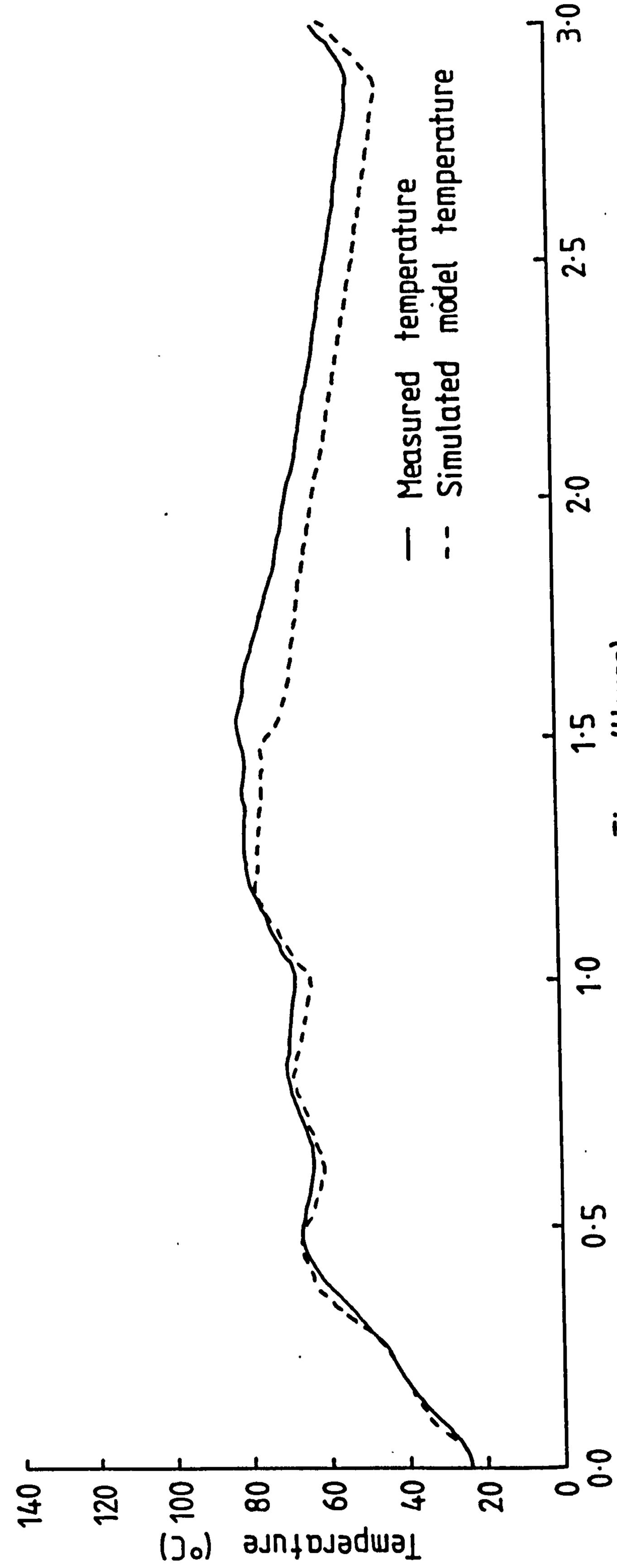

Figure 6·14 Simulated Second Model and Measured Stator Iron Temperature

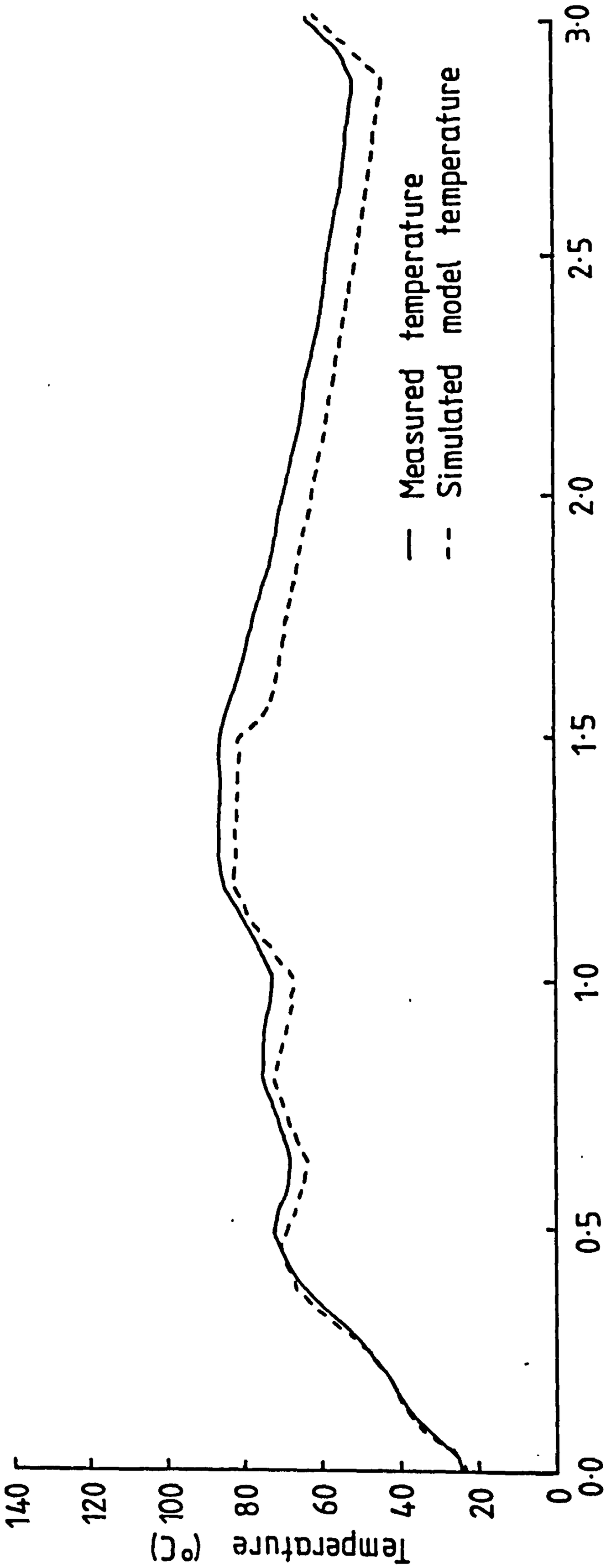

Figure 6·15 Simulated Second Model and Measured Stator Teeth Temperature

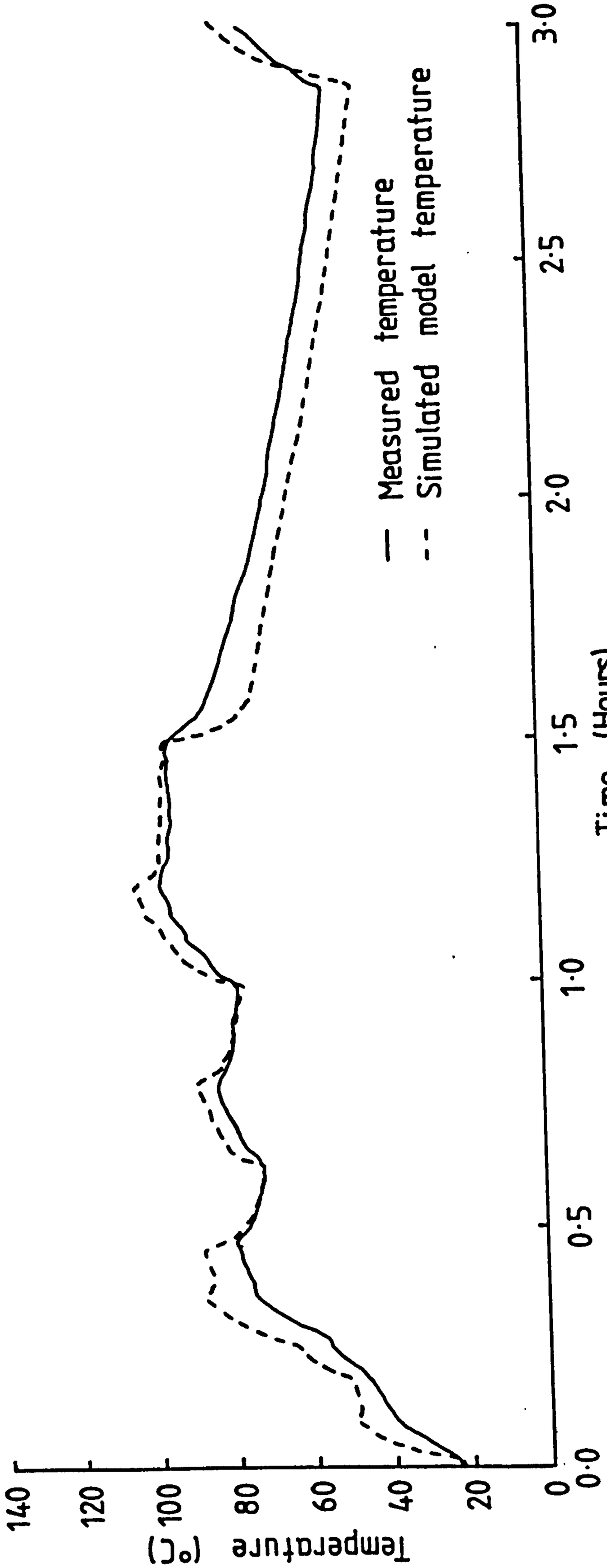

Figure 6·16 Simulated Second Model and Measured Stator Winding Temperature

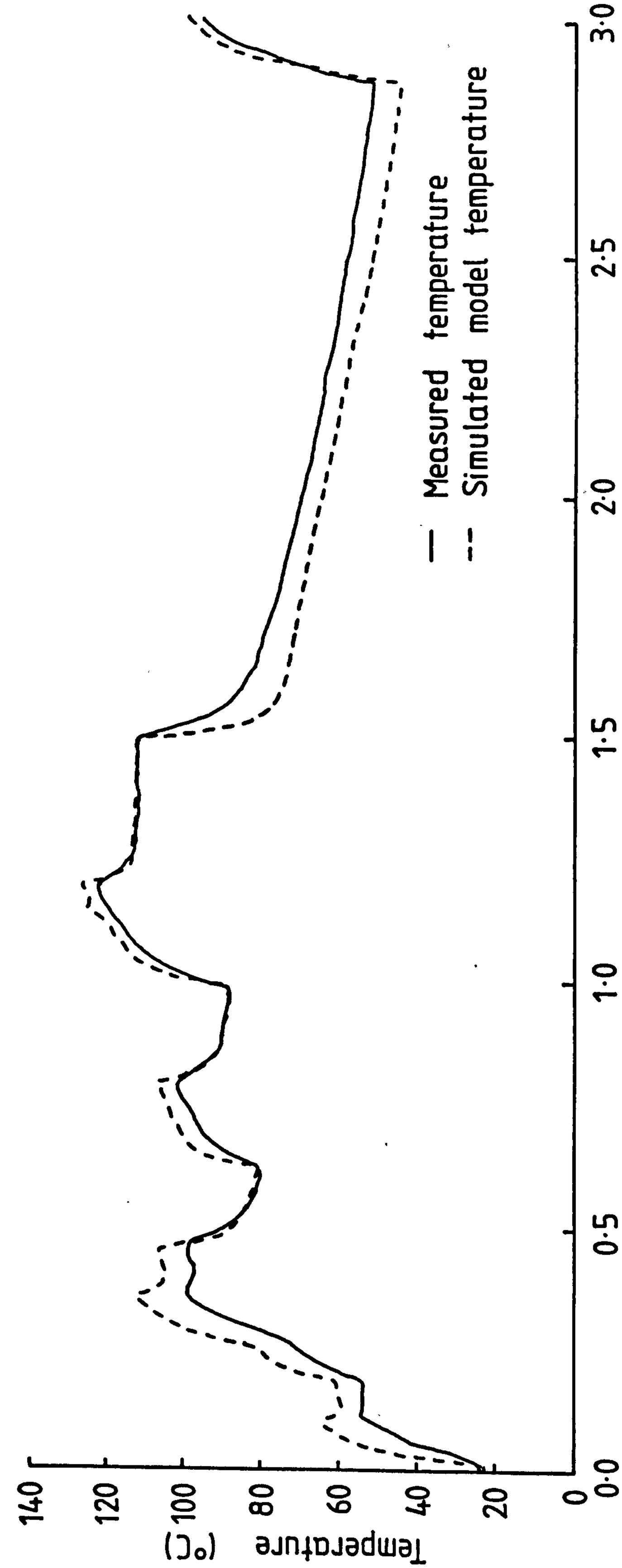

Figure 6·17 Simulated Second Model and Measured Endwinding Temperature

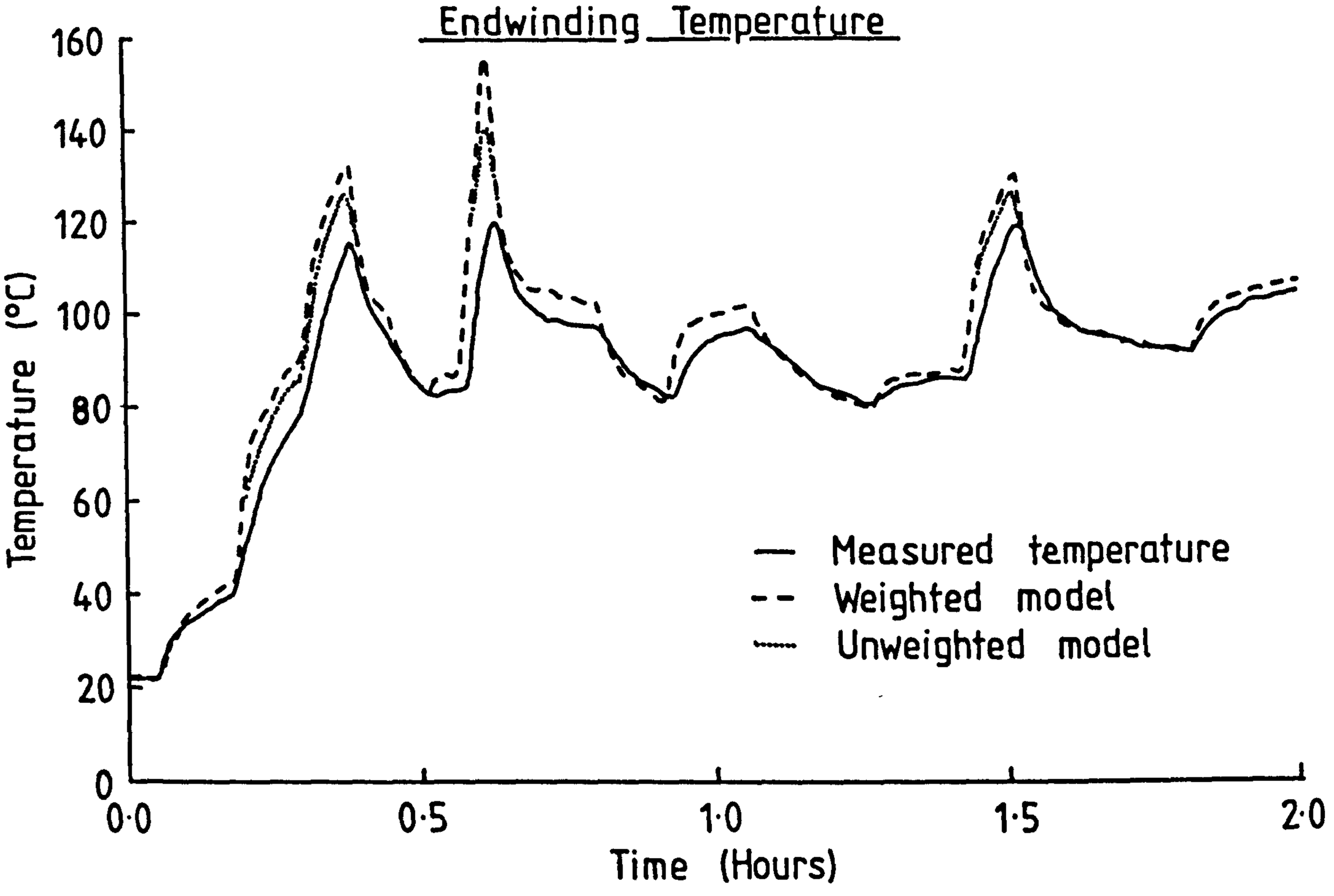

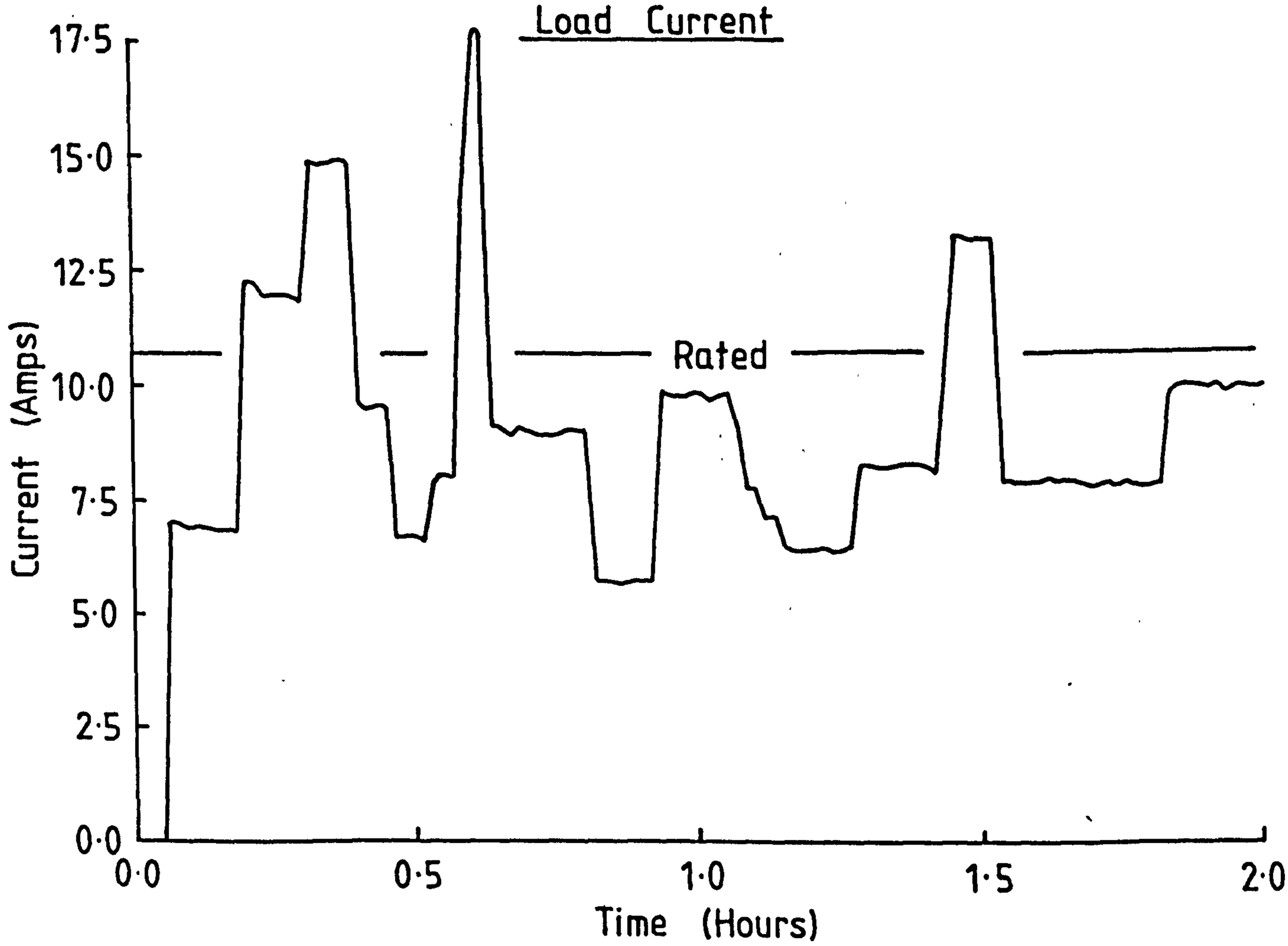

Figure 6·18 Effect of Weighting on Modelled Endwinding Temperature

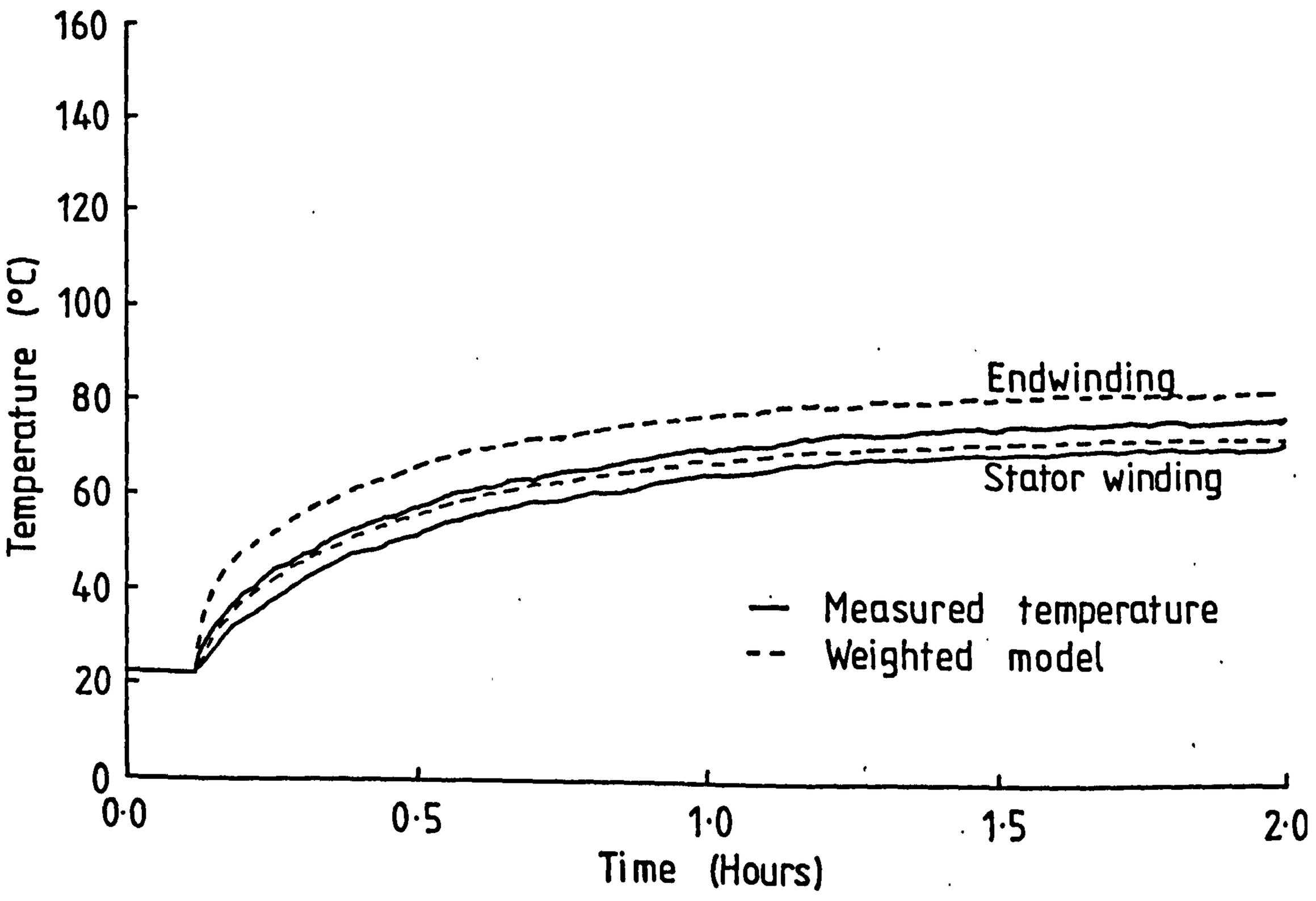

Figure 6·19 Model and Measured Winding Temperatures for an 8A Load

CHAPTER 7

SUMMARY AND CONCLUSIONS

The careful utilisation of electrical and mechanical drives can lead to reductions in their energy consumption at the penalty of a possible increase in the ageing of the machines. A stochastic method of analysis has been applied to this problem, to provide a simple but flexible theory for the evaluation of the losses and electrical ageing in both single and parallel machine drives. The load on a drive was represented by a stationary bounded probability distribution, an approach which required a minimal knowledge of the load. The energy loss in different sized similar machines were modelled with a single quadratic loss characteristic and sizing factors. The energy consumption and ageing of the machine drives could then be approximated from only the first, second and fourth moments of the load distribution. The work provided a method for obtaining the key parameters for a full costing of a drive, where the energy costs would need to be weighed against the capital and maintenance or replacement costs of the machines over the lifetime of the plant.

The stochastic analysis lent itself towards optimisation techniques, where the energy consumption of the drives could be minimised in terms of the machine ratings and their parallel switching control. Direct analytical

solutions were found for the best energy fit of the rating of a single machine to a load and the switching control of a parallel drive where all the machines were equally rated. The latter proved to be independant of the load and could be immediately applied to any existing parallel machine system without any knowledge of the load. A numerical method was applied to the more complex energy optimisation of both the machine sizes and their switching in the parallel drive.

The theoretical work could not be substantiated entirely from experimental results. However, a case study was performed on an industrial parallel drive, that consisted of four equally rated induction motor driven pumps. The study demonstrated that stochastic methods could be used successfully in the modelling of an actual plant. As a result, changes were made in the drive switching control and the energy consumption of the plant was reduced by an estimated 2.4 per cent. The remainder of the theory was tested on example systems with arbitrary choices of load distributions.

The potential of saving energy in electrical machines appeared to be greater in a correct choice of machine rating, rather than in the switching control. With pumps the converse applied, because of the nature of the pump loss characteristics and their low similarity indices. Where there is a combination of an electrical motor driving a pump, the lower efficiency pump dominates the analysis and the energy consumption is affected to a greater extent

by the switching control as opposed to the machine sizes.

The efficiencies of electrical drives that have been optimised in size or switching control were only in the order of one per cent higher than the original rated figures. However, the improvements could still amount to considerable reductions in the electricity costs over the expected lifetimes of the drives. A correctly sized system would generally suggest that smaller machines should be installed and would lower the capital cost and the energy required to manufacture the drive.

The energy reductions in electrical drives are comparable with the errors in the single loss expression, that is used to model the series of machines. Greater accuracy could be obtained in the loss for a fixed machine size by taking into account higher order terms above those of the quadratic approximation. To obtain improvements over different machine sizes, individual loss characteristics would have to be derived for each machine.

The variations in the energy consumption of pumps are somewhat greater and could be as high as 8 per cent. This maximum could only be achieved through heavy overloads on the pumps, which would result in a considerable drop in the minimum output head. However good reductions in the energy can still occur under a more practicable operation of the pumps.

The greatest potential for energy savings in electrical drives exists in cases of wide varying loads, where the selection of a machine size may require it to

operate under large overloads. To measure the effects of overloads on the ageing of a machine's winding insulation, a stochastic thermal analysis was developed for a stationary load distribution. The theory was based upon a linear thermal model of the machine and could be applied to single machines or alternatively, equally sized parallel drives which have a rotational method of load sharing. It was tested against a deterministic analysis, which included the non-linear effects of starting surges and had seperate thermal models for the machine rotating or stationary. The theory gave a higher estimates of the machine ageings; to within a 20 per cent error of the deterministic results.

The ageing of electrical machines were shown to be influenced by the variance of the load as well as the mean. Ageing control algorithms in equally sized parallel drives would all tend to produce similar mean temperatures in the machines, but the measure of their effectiveness is the extent to which they constrain the temperature variance. By characterising the ageing algorithms in terms of the time dependant position of a machine in the load switching sequence, an ideal ageing control was identified as one that would, independantly of the load, ensure that a machine would have an equal probability of being in every position at all times. A possible implement-ation of this was suggested, where the machines' switching positions would be determined from their winding temperatures. Although not ideal, this control produced the required possitional probability and resulted in an ageing much lower than a conventional rotational control. A combination

of this form of ageing control and a loss optimisation could in fact reduce both the ageing and the energy consumption of a typical parallel machine system.

The stochastic thermal analysis provided a direct method of estimating the ageing of an electrical machine from the basic statistics of its loading. From known steady state temperatures in the machine windings, the ageing could be simply formulated on a pocket calculator from tables of the assumed load distribution, to a reasonable degree of accuracy. The alternative deterministic methods would require excessive computation, since the ageing would need to be calculated for every change in the load-time curve. However, the validity of the stationary load model assumed in the theory would need to be confirmed for the particular case studied.

A linear thermal model of electrical machines was required for the stochastic ageing analysis. Although a number of similar models have been reported in the literature, a direct example of a dynamic model was not found. To test the accuracy of a linear thermal analysis, a model was developed for a 5.5kW TEFC cage induction motor and consisted of only an eight element matrix equation. The agreement between its performance and measured temperatures was good, both dynamically and in the steady state. In fact, it was felt that the model gave a better estimation of the peak winding temperatures than the thermometers, because of the difficulty of mounting the latter in the windings.

The parameters of the thermal model were derived from formulae, which contained the motor dimensions and constant values of conductivities and film coefficients obtained from the literature and basic experimental tests. The model could be expanded for a range of induction motors with similar geometries, by appropriate changes in the dimensions in the thermal impedance equations. Hence, a thermal similarity rule could be developed over a manufacturers range of machine sizes, akin to that of the losses. The convective and surface heat transfer impedances, which are dominant in these models, reduce by a dimension squared. The power loss in an induction motor increases with the cube of the dimensions. Thus, the machines would tend to run hotter as their ratings increase. This effect is generally compensated for in the design of the machine by an increase in the fan powers and additional cooling paths. Because of this, a thermal similarity rule may become complex and requires extra research.

The success of the thermal model led to the development of a microprocessor based thermal prediction device. This was seen to have two seperate applications, one as part of a controller that would implement the ageing algorithms in a parallel machine systems and the other as a stand alone motor protection device. The 8 bit microprocessor easily performed the thermal calculation to good accuracy and still had 90% of its processing time free for other duties.

Motor protection devices have been available commercially for sometime. Two recently introduced devices use analogue models of the motor's winding temperatures for a protection that allows a fuller utilisation of the machine. One of these devices [13] uses a single RC thermal model. The other [14] is more complex and has two seperate capacitances and generations to model the core and the windings. It also uses different thermal impedances for a stationary and running machine. The accuracy of these simple models is questionable, although the second device does attempt to provide a more realistic solution.

A microprocessor based device, similar to the one proposed in the thesis, can provide a better accuracy for no greater manufacturing cost. The microprocessor can also perform the additional facilities included in commercial devices, such as earth leakage and phase loss protection. The intelligence of the microprocessor could be exploited by adding a higher degree of protection, where the controller uses the thermal model to estimate future temperatures in the machine from an assumption of the loading continuing in a set manner. This would give prior knowledge of motor overloads or likely failures.

The thermal models could be constructed from basic dimensional information of the motors and tested against the thermal measurements performed by a manufacturer during the original design of the machines. It would be feasible for a motor manufacturer to produce remote protection devices for its entire product range based on a

standard microprocessor module and individual sets of model parameters contained in seperate 'plug in' memory units for each machine. Accurate thermal models would also be a useful design tool for the production of any future machines and fit well into the philosophy of CAD now popular in the mechanical design of machines.

The stochastic analysis applied in this thesis has been effective in computing the energy usage and ageing of the machine drives considered. The work could be extended to more complex energy saving schemes that utilise variable speed controllers. An immediate application could be in the assessment of the popular variable voltage or 'power factor' controllers now available for induction motors. Other areas of future work would be a comprehensive study of ageing over a wide range of machine sizes and a full costing of the energy savings suggested in the thesis. Finally, the work on the microprocessor protection device should be extended to a prototype that may be exploited commercially.

REFERENCES

1. Hunt, R.E., Seabury, F., Valence, P.F., 'Energy efficiency and electric Motors - A technical, economic and policy analysis of efficiency standards in commercial and industrial electric motors and equipment', No.PB-259129, National Technical information Service, U.S. Dept. of Commerce, Springfield.

2. Taylor, L.J., 'Energy conservation using a.c. Motors', 40th Annual Westinghouse Machine Tool Forum, 8 June 1976, Pittsburgh.

3. Avinger, H., Kracke, G., Neuhaus, W., 'Improving the efficiency of electrical machines - Possibilities and Limits', Siemens Power Engineering II, 1980, No.9, pp.283-290.

4. 'Energy trends, a statistical bulletin', Department of Energy, October 1982.

5. Luborsky, F.E., Becker, J.J., Frishmann, P.G., Johnson, L.A., 'Potential of amorphous alloys for applications in magnetic devices', Journal of Applied Physics, 49, 1978, pp.1769-1774.

6. 'Energy saving electric motors', Technical Leaflet F.ME 896 E.

7. Knights, D.E., 'Ample scope for cutting electric motor running costs', Electrical Contractor, April 1977, pp.18-20.

8. Knights, D.E., 'Efficient use of electricity in motor drives', Electronics and Power, 23, 1977, pp.921-924.

9. Ben-Dov, E., Harley, R.G., 'Optimal selection of of electrical power equipment', University of Natal, Durban, Research Report EMPS-19, January 1979.

10. Holmes,L., 'Energy-saving motor controllers - background and update', Electronics and Power, March 1982, pp.232-235.

11. Melsa, J.L., Sage, A.P., 'An introduction to probability and stochastic processes', Wiley, 1973.

12. Szogyen, J.R.M., 'The cooling of electric motors', Proc. IEE, EPA, Vol. 2, No.2, April 1979, pp.59-67.

13. 'Motor master protection relay for 3 phase a.c. induction motors', GEC Measurements, Publication 17-012.

14. 'Electronic motor protection unit CET3', Sprecher & Schuh, Publication 22-53.

15. Mellor, P.H., Turner, D.R., 'Efficiency optimisation of multi-machine systems', Proc. 16th Univ.Power Eng.Conf., Sheffield, 1981.

16. Pearson, K., 'Tables of the incomplete beta-function', Cambridge University Press, 1934.

17. Gill, P.E., Murray, W., 'Quasi-Newton methods for linearly constrained optimisation', NPL, Report NAC 32, 1973.

18. Simoni, L., 'A general approach to the endurance of electrical insulation under temperature and voltage', IEEE Trans. on Elect.Ins., EI-16, No.4, August 1981, pp.277-289.

19. Dakin, T.W., 'Electrical insulation deterioration', Electrotechnology, December 1960, pp.123-130.

20. Dakin, T.W., 'Electrical insulation deterioration treated as a chemical rate phenomenon', AIEE Trans., No.67, 1948, pp.113-122.

21. Perez, I.J., Kassakian, J.G., 'A stationary thermal model for smooth air-gap rotating electric machines', Electric Machines and Electromechanics, Vol.3, No.3-4, 1979, pp.285-303.

22. Preston, S.B., Thomas, M.A., Pennington, G.A., 'Non-steady state thermal performance of electrical machines', Proc. IME, Vol.184, Pt.3E, 1969-70,pp.9-14.

23. Myers, G.E., 'Analytical methods in conduction heat transfer', McGraw-Hill, 1971.

24. Papoulis, A., 'Probability, random variables and stochastic processes', McGraw-Hill, 1965.

25. Whitman, L.C., 'Simplified methods of the calculation of insulation life characteristics', IEE Trans., PAS, October 1961, pp.685-687.

26. Micheal, K., 'The thermal behaviour of insulation in electrical machines', Brown Boveri Review, Vol.49, No.11-12, 1962, pp.630-639.

27. Neave, H., 'A random number package', Computer Applications in the Natural and Social Sciences, No.14, Univ. of Nottingham, 1972.

28. Lazarkiewicz, S., Trokolanski, A.T., 'Impeller Pumps', Pergamon, 1965.

29. Mellor, P.H., Turner, D.R., 'Improving multi-pump system efficiency', Report to Boss Brewing Ltd., University of Liverpool, 1980.

30. Mellor, P.H., Turner, D.R., 'A stochastic approach to the ageing of electrical machines', Proc.17th Univ. Power Eng.Conf., Manchester, 1982.

31. Roberts, T.J., 'The solution of the heat flow equations in large electrical machines', Proc. IME, Vol.184. Pt.3E, 1969, pp.70-83.

32. Wilson, E.L., Nickell, R.E., 'Application of the finite element method to heat conduction analysis', Nuclear Engineering Design, 1966.

33. Screenivasan, V.K., Sengupta, D.P., 'Thermal design of a totally enclosed fan cooled induction motors', IEEE PES Winter Meeting, Paper A 77 097-9, 1977.

34. Kotnik, R.L., 'An equivalent thermal circuit for non-ventilated induction motors', Trans. AIEE, Vol.73, Pt. 3A, 1954, pp.1604-1609.

35. Soderberg, C.R., 'Steady flow of heat in large turbine generators', Trans. AIEE, Vol. 50, June 1931, pp.787-802.

36. Imre, L., Jagasits, Z., Barcza, J., 'Computer simulation of the transient warming of rotary electric machines', Proc.2nd Int.Conf. on Numerical Methods in Thermal Problems, Venice, July 1981, pp.685-696.

37. 'Heat transfer and fluid flow data book', General Electric, 1969.

38. Taylor, G.I., 'Distribution of velocity and temperature between concentric cylinders'. Proc.Royal Society, Vol. 159, A, 1935, pp.546-578.

39. Gazley, C., 'Heat transfer characteristics of rotational and axial flow between concentric cylinders', Trans. ASME, January 1958, pp.79-89.

40. Luke, G.E., 'The cooling of electric machines', Trans. AIEE, Vol.45, 1923, pp.1278-1288.

41. Roberts, T.J., 'Determination of the thermal constants of the heat flow equations of electrical machines', Proc. IME, Pt. 3E, 1969, pp.84-92.

42. Mori, Y., Nakayami, W., 'Forced convective heat transfer in a straight pipe rotating around a parallel axis', Int. J.Heat Transfer, Vol.10, pp.1179-1194.

43. Say, M.G., 'Alternating Current Machines', Pitman, 1976.

44. Brunot, A.W., Buckland, F.F. 'Thermal contact resistance of laminated and machined joints', Trans. ASME, April 1950, pp.253-257.

45. Kreyszig, E., 'Advanced engineering mathematics', Wiley, 1972.

46. 'MCS-85 user's manual', Intel Corporation, 1978.

47. 'SDX-85 user's manual', Intel Corporation, 1976.

48. De Russo, P.M., Roy, R.J., Clare, C.M., 'State variables for engineers', Wiley, 1965.

49. Wilkinson, J.H., Reinsch, C., 'Handbook for automatic computation', Linear Algebra, Springer-Verlag, 1971, Vol.2, pp.212-240.

50. Naot, Y., 'A unified theory of electrical machines based upon a physical model', IEEE PES Winter Power meeting, January 1977.

51. Kittredge, C.P., 'Estimating the efficiency of prototype pumps from model tests', Jnl. of Engineering for Power, Trans. ASME, April 1968, pp.129-139.

52. Moody, L.F., 'Hydraulic machinery', Handbook of Applied Hydraulics, Davis, C.V., ed., 1st ed., pp.607-680.

53. Lennox, S.C., Chadwick, M., 'Mathematics for engineers and applied scientists', Heinemann, 1974, Chap.5.

54. Alger, P.L., 'Induction machines', Gordon and Breach, 2nd Edition, 1970.

55. 'ICL7109, 12 bit binary A/D converter for micro-processor interfaces', Intersil, Application Note,1979.

APPENDIX A1

INDUCTION MOTOR LOSS FUNCTION

The electrical performance of an induction motor, which is running under normal conditions, can be successfully modelled by an equivalent circuit. One particularly accurate form[43] of the equivalent circuit is given in Figure 5.4. The variable resistance in the right of the Figure is associated with the total mechanical output of the machine.

In the notation of the equivalent circuit, the total loss L in the machine can be written in the form:

$$L = a + 3(i_2/c)^2 \, cR_{s/c} \qquad (A1.1)$$

where i_2/c = magnitude of current i_2/c

and $cR_{s/c}$ = resistive component of impedance $cZ_{s/c}$

The constant 'a' term in the above equation is composed of iron losses, tooth stray losses, a proportion of the stator copper loss and any mechanical windage and friction losses. Its value will be a function of the excitation of the machine.

At low slip, the reactive component of the current i_2/c will be small and the output power W of the machine can be expressed in terms of the magnitudes of the referred rotor current and phase voltage, within less than 1% error over the full working range, as:

$$W = 3(vi_2/c - (i_2/c)^2 \, cR_{s/c}) \qquad (A1.2)$$

The above equation can be rearranged to give i_2/c in terms of W, such that:

$$i_2/c = \frac{v}{2cR_{s/c}}\left(1-\left(1-\frac{4cR_{s/c}W}{3v^2}\right)^{\frac{1}{2}}\right) \qquad (A1.3)$$

The motor loss is found from a combination of Equations (A1.1) and (A1.3) as:

$$L = a + \frac{3}{4}\frac{v^2}{cR_{s/c}}\left(1-\left(1-\frac{4cR_{s/c}W}{3v^2}\right)^{\frac{1}{2}}\right)^2 \qquad (A1.4)$$

Evaluating the square on the R.H.S. yields:

$$L = a + \frac{3v^2}{4cR_{s/c}}\left(2-\frac{4cR_{s/c}}{3v^2}W - 2\left(1-\frac{4cR_{s/c}}{3v^2}W\right)^{\frac{1}{2}}\right) \qquad (A1.5)$$

The square root term can be expanded through the use of the binomial series, since the dimensionless factor:

$$\frac{4\,cR_{s/c}W}{3v^2} < 1 \qquad (A1.6)$$

to give:

$$L = a + \frac{3v^2}{4cR_{s/c}}\left(2-\frac{4cR_{s/c}W}{3v^2} - \right. \qquad (A1.7)$$

$$\left. 2\left(1-\tfrac{1}{2}\left(\frac{4cR_{s/c}W}{3v^2}\right) - \frac{1}{8}\left(\frac{4cR_{s/c}W}{3v^2}\right)^2 - \frac{1}{16}\left(\frac{4cR_{s/c}W}{3v^2}\right)^3 + \ldots\right)\right)$$

which is further simplified to:

$$L = a + \left(\frac{cR_{s/c}}{3v^2}\right)W^2 + 2\left(\frac{cR_{s/c}}{3v^2}\right)^2 W^3 + \ldots \qquad (A1.8)$$

The accurate loss function of Equation (2.12) for an induction motor can thus be written as:

$$\gamma(W) = \frac{a}{W} + \left(\frac{cR_{s/c}}{3v^2}\right)W + 2\left(\frac{cR_{s/c}}{3v^2}\right)^2 W^2 + \ldots \qquad (A1.9)$$

A quadratic approximation of the loss function, in which the terms in W^2 and above have been neglected, will be off the form;

$$\gamma(W) = \frac{a}{W} + \frac{W}{c} \qquad (2.14)$$

where $$c = \frac{3v^2}{(cR_{s/c})} \qquad (A1.10)$$

The c on the L.H.S of Equation (A1.10) refers to the notation in the loss function rather than the Say[43] equivalent circuit.

The efficiency of a 11kW TEFC cage induction motor,calculated from a quadratic loss model,is compared against a manufacturers characteristic in Figure A1.1. A good fit occurs over the majority of the working range of the motor, with a maximum efficiency error of 2% in the lower powers.

The calculation of losses from the equivalent circuit parameters and the quadratic approximation in Equation (A1.9) is unlikely to introduce errors in excess of 10% at large output powers and provides a simple method of estimating the losses in existing induction motors.

Alternatively the loss function parameter can be found directly from a fit to an efficiency curve obtained from a full set of load tests on the machine. This yields excellent agreement in the higher powers, as is illustrated in Figure A1.1.

The losses of a series of induction motors, that have been designed to a common criteria and are geometrically similar, can be developed from a single mathematical model[9,50]. This can be expressed in terms of a sizing factor α and a similarity index β in the form of Equation (2.13) below:

$$\gamma(\alpha,W) = \alpha^{-\beta}\gamma(W/\alpha) \qquad (2.13)$$

Consider a set of induction motors that are designed with the same specific magnetic and electrical loadings and have dimensions D, both length and radius, that are increased proportionately with rating. The following set of relationships can be listed,

Core Area		varies with	D^2
Working Flux	Φ	"	D^2
Current Sheet Diameter		"	D
Current Sheet Depth		"	D
Current Loading	I	"	D^2
Output Power	W	"	$D^4 = \alpha$
Current Sheet Resistance	R	"	1/D
Copper Loss	I^2R	"	D^3
Core Volume		"	D^3
Core Loss		"	D^3

Total Losses	$W\gamma(\alpha,W)$	"	D^3
Loss Function	$\gamma(\alpha,W)$	"	$1/D = \alpha^{-\frac{1}{4}}$

The machine sizing α is proportional to the dimension to the fourth power and the losses are proportional to the dimension cubed. Hence, the loss function is inversely proportional to the dimension. The similarity index β of Equation (2.13) is thus equal to:

$$\beta = 0.25 \qquad \text{(A1.11)}$$

In this simple analysis stray load and mechanical losses have not been considered. However, the sizing relationship will generally hold for machines with equal numbers of poles and similar mechanical design.

The loss function and similarity index for a set of transformers can be derived in an identical manner. A three phase transformer can be considered, in this instance, to be a member of the induction motor family.

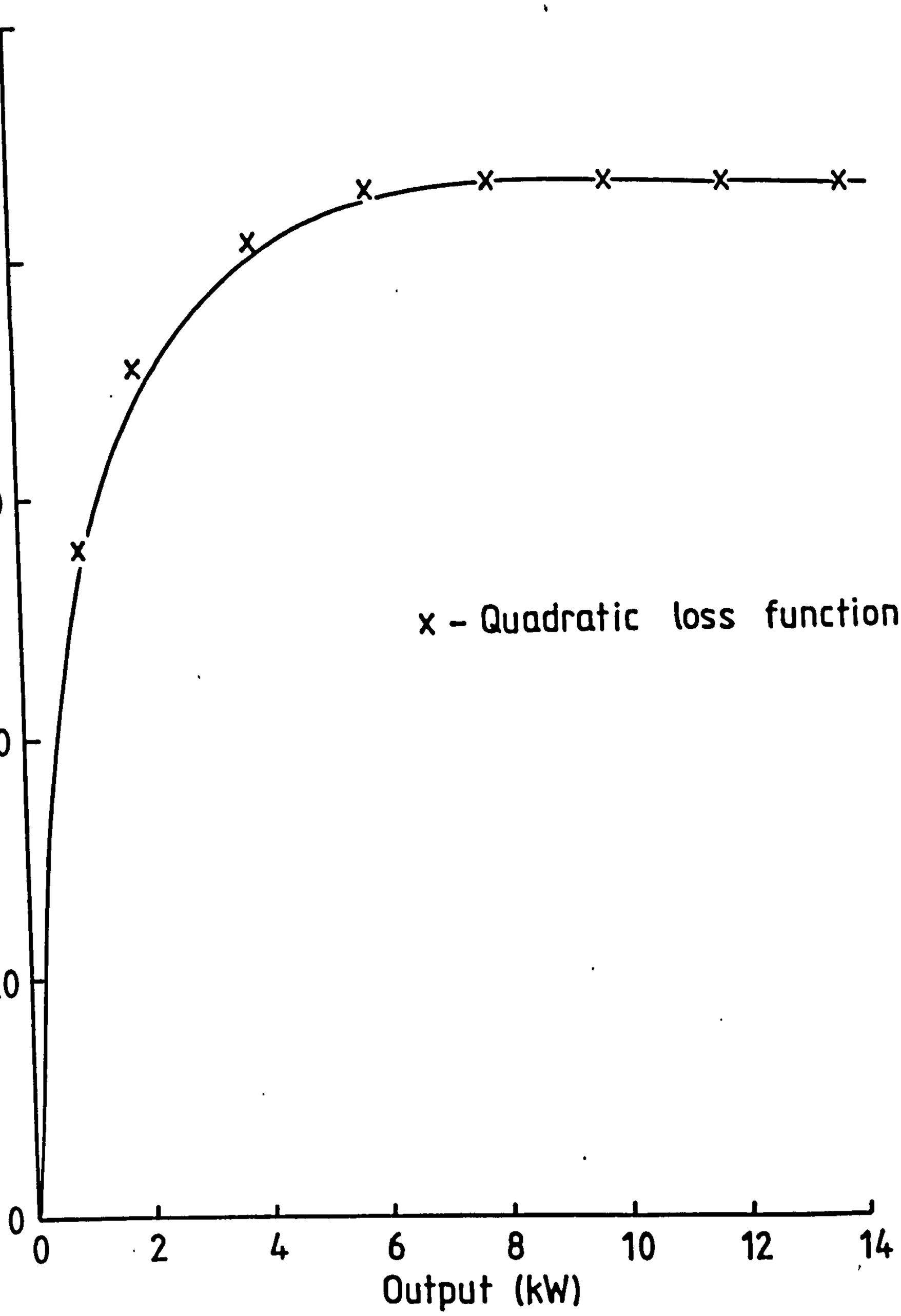

Figure A1·1 Efficiency Characteristic for 11kW 1500rpm Cage Motor.

APPENDIX A2

CENTRIFUGAL PUMP LOSSES WITH SIMILAR DESIGN AND HEAD CHARACTERISTICS

The appendix briefly develops a sizing rule for the losses in geometrically similar pumps, operating under dynamically similar conditions. For detailed information the reader is referred to the references by Kittredge[51] and Moody[52].

The affinity laws for similar centrifugal pumps are given by:

$$Q/\omega D^3 = \text{const} \qquad \text{(A2.1)}$$

$$\omega D/\sqrt{H} = \text{const} \qquad \text{(A2.2)}$$

where Q = rated output flow

H = rated output head

D = diameter of the pump impeller

ω = shaft speed of the impeller.

When a variety of different sized pumps are operated in parallel, the machines will need to have indentical head characteristics in order that they may share the load in proportion to their flow ratings. This would require the pumps to be operated at different shaft speeds and planetary gear boxes may have to be employed if they are to be driven from a fixed speed induction motors. The

gearbox efficiencies are assumed to be high in comparison with those of the pumps.

The affinity laws will now reduce to:

$$Q/D^2 = \text{const} \qquad \text{(A2.3)}$$

A sizing factor α can be used to rate the machine in terms of its output flow. From Equation (A2.3) this is seen to be proportional to the square of the impeller diameter D.

The losses in a centrifugal pump are divided into friction, leakage and hydraulic losses. In a set of high quality pumps the friction and leakage losses can be taken to be small compared with the hydraulic loss. Moody[52] has suggested that the dimensionless hydraulic losses for a set of pumps can be given by the similarity rule:

$$\gamma(\alpha,Q) \text{ varies with } (1/D)^{0.2} \qquad \text{(A2.4)}$$

Other authors have proposed slightly different sizing indices, which are summarised in the first paper[51]. However, for the purpose of this thesis, Equation (A2.4) was taken as giving a reasonably accurate assessment of the performance of the pumps.

A combination of Equations (A2.3) and (A2.4) will yield the standard loss equation in the form:

$$\gamma(\alpha,Q) = \alpha^{-\beta}\gamma(Q/\alpha) \qquad (2.13)$$

where $\beta = 0.1$

APPENDIX A3

THE DETERMINATION OF THE GRADIENT AND HESSIAN MATRICES OF THE SYSTEM LOSSES FOR A QUADRATIC LOSS FUNCTION

The total multimachine system losses are given by:

$$L = T \sum_{i=1}^{n} \int_{W_{\ell i-1}}^{W_{\ell i}} p_T(W) \sum_{j=1}^{i} \gamma(\alpha_j, k_{ji}W)\, k_{ji}W dW \qquad (2.25)$$

where k_{ji} is the load sharing factor

$$k_{ji} = \alpha j / \sum_{m=1}^{i} \alpha_m \qquad (2.26)$$

When a quadratic loss function of Equations (2.13) and (2.14) is assumed, the loss function $\gamma(\alpha,w)$ is given by:

$$\gamma(\alpha,w) = \alpha^{-\beta}\left(\frac{a\alpha}{W} + b + \frac{W}{\alpha c}\right) \qquad (A3.1)$$

The system power loss, where the load interval T is dropped for clarity, can be written as:

$$L = \sum_{i=1}^{n} \int_{W_{\ell i-1}}^{W_{\ell i}} p_T(W) \sum_{j=1}^{i} \alpha_j^{1-\beta} \left(a + \frac{bW}{\sum_{m=1}^{i} \alpha_m} + \frac{W^2}{c\left(\sum_{m=1}^{1} \alpha_m\right)^2}\right) dW \qquad (A3.2)$$

The n elements of the gradient matrix [g] are obtained from:

$$[g] = \frac{\partial L}{\partial [\alpha]} \tag{2.43}$$

and the rth element can be shown to be equal to:

$$\frac{\partial L}{\partial \alpha_r} = \sum_{i=1}^{n} \int_{W_{\ell i-1}}^{W_{\ell i}} \alpha_r^{-\beta} \{H_i(W) - I_i(W)\} p_T(W) dW \tag{A3.3}$$

where:

$$H_i(W) = (1-\beta) \left(a + \frac{bW}{\sum_{m=1}^{i} \alpha_m} + \frac{W^2}{c\left(\sum_{m=1}^{i} \alpha_m\right)^2} \right) \tag{A3.4}$$

and:

$$I_i(W) = \frac{\sum_{j=1}^{i} \alpha_j^{1-\beta}}{\left(\sum_{m=1}^{i} \alpha_m\right)^2} \left(bW + \frac{2W^2}{c \sum_{m=1}^{i} \alpha_m} \right) \tag{A3.5}$$

The determination of the elements of the nxn Hessian matrix [G] is somewhat more complex and is based upon the equation:

$$[G] = \frac{\partial^2 L}{\partial [\alpha]^2} + \frac{d[W_\ell]}{d[\alpha]} \frac{\partial^2 L}{\partial [W_\ell] \partial [\alpha]} \tag{2.42}$$

$$+ \frac{\partial^2 L}{\partial [W_\ell] \partial [\alpha]}^T \frac{d[W_\ell]}{d[\alpha]} + \frac{d[W_\ell] \partial^2 L}{d[\alpha] \partial [W_\ell]^2} \frac{d[W_\ell]}{d[\alpha]}$$

The matrix $d[W_\ell]/d[\alpha]$ is obtained from the optimum switching limit condition $\partial L/\partial [W_\ell] = 0$ as of Equation (2.30). Equation (2.30) is expressed in terms of a quadratic loss function as:

$$\left(\sum_{j=1}^{r} \alpha_j\right)^{1-\beta} \left(a + \frac{bW_{\ell r}}{\sum_{m=1}^{r} \alpha_m} + \frac{W_{\ell r}^2}{c\left(\sum_{m=1}^{r} \alpha_m\right)^2}\right) \qquad \text{(A3.6)}$$

$$= \left(\sum_{j=1}^{r+1} \alpha_j\right)^{1-\beta} \left(a + \frac{bW_{\ell r}}{\sum_{m=1}^{r+1} \alpha_m} + \frac{W_{\ell r}}{c\left(\sum_{m=1}^{r+1} \alpha_m\right)^2}\right)$$

The elements $dW_{\ell r}/d\alpha_s$ for s = 1 to n and r = 1 to n are obtained from (A3.6), and are written in the notation of (A3.4) and (A3.5) as:

$$\frac{dW_{\ell r}}{d\alpha_s} = \frac{\{\alpha_s^{-\beta}(H_{r+1}(W_{\ell r}) - H_r(W_{\ell r})) - I_{r+1}(W_{\ell r}) + I_r(W_{\ell r})\}W_{\ell r}}{\left(\sum_{m=1}^{r} \alpha_m\right) I_r(W_{\ell r}) - \left(\sum_{m=1}^{r+1} \alpha_m\right) I_{r+1}(W_{\ell r})} \qquad s \leqslant r$$

$$\frac{dW_{\ell r}}{d\alpha_s} = \frac{\{\alpha_s^{-\beta} H_{r+1}(W_{\ell r}) - I_{r+1}(W_{\ell r})\}W_{\ell r}}{-\left(\sum_{m=1}^{r+1} \alpha_m\right) I_{r+1}(W_{\ell r})} \qquad s = r+1$$

$$\frac{dW_{\ell r}}{d\alpha_s} = 0 \qquad s > r+1$$

(A3.7)

The matrix $\partial^2 L/\partial[W_\ell]\partial[\alpha]$ is formed out of the direct differentiation of Equation (A3.3). In the previous notation, with a transposition of the suffixes from r to t for clarity, the elements of the matrix are given for t=1 to n by:

$$\frac{\partial^2 L}{\partial W_{\ell r}\,\partial \alpha_t} = \{\alpha_t^{-\beta} H_r(W_{\ell r}) - I_r(W_{\ell r}) - \alpha_t^{-\beta} H_{r+1}(W_{\ell r}) + I_{r+1}(W_{\ell r})\} p_T(W_{\ell r}) \quad t \leqslant r$$

$$\frac{\partial^2 L}{\partial W_{\ell r}\,\partial \alpha_t} = -\{\alpha_t^{-\beta} H_{r+1}(W_{\ell r}) + I_{r+1}(W_{\ell r})\} p_T(W_{\ell r}) \quad t = r+1$$

$$\frac{\partial^2 L}{\partial W_{\ell r}\,\partial \alpha_t} = 0 \quad t > r+1 \qquad \text{(A3.8)}$$

The second and third components of the Hessian matrix of Equation (2.42) can now be constructed by summing over all r the product of Equations (A3.7) and (A3.8). Hence the elements s, t of:

$$\frac{d[W_\ell]\,\partial^2 L_{s,t}}{d[\alpha]\,\partial[W_\ell]\,\partial[\alpha]} = \sum_{r=1}^{n} \frac{dW_{\ell r}}{d\alpha_s} \frac{\partial^2 L}{\partial W_{\ell r}\,\partial \alpha_t} \qquad \text{(A3.9)}$$

and similarly with the transpose matrix.

The first component of the Hessian matrix $\partial^2 L/\partial[\alpha]^2$ is derived from Equation (A3.3), where its s,t elements are given by:

$$\frac{\partial^2 L}{\partial \alpha_s \partial \alpha_t} = \sum_{i=s}^{n} \int_{W_{\ell i-1}}^{W_{\ell i}} \{K_i(W) - (\alpha_s^{-\beta} + \alpha_t^{-\beta}) J_i(W)\} p_T(W)\, dW \qquad s<t$$

$$\frac{\partial^2 L}{\partial \alpha_s^2} = \sum_{i=s}^{n} \int_{W_{\ell i-1}}^{W_{\ell i}} \{K_i(W) - \beta\alpha_s^{-(\beta+1)} H_i(W) - 2\alpha_r^{-\beta} J_i(W)\} p_T(W)\, dW \qquad s=t$$

$$\frac{\partial^2 L}{\partial \alpha_s \partial \alpha_t} = \frac{\partial^2 L}{\partial \alpha_t \partial \alpha_s} \qquad s>t \qquad \text{(A3.10)}$$

where:

$$J_i(W) = \frac{(1-\beta)}{\left(\sum_{m=1}^{i} \alpha_m\right)^2} \left(bW + \frac{2W^2}{c \sum_{m=1}^{i} \alpha_m} \right) \qquad \text{(A3.11)}$$

and:

$$K_i(W) = \frac{2 \sum_{j=1}^{i} \alpha_j^{(1-\beta)}}{\left(\sum_{m=1}^{i} \alpha_m\right)^3} \left(bW + \frac{3W^2}{c \sum_{m=1}^{i} \alpha_m} \right) \qquad \text{(A3.12)}$$

The final component of the Hessian matrix is constructed from Equation (A3.7) and the matrix $\partial^2 L / \partial W_\ell^2$. Because of the independance of the switching limits the off diagonal terms of this matrix are zero, leaving only the diagonal elements, which can be shown to be equal to:

$$\frac{\partial^2 L}{\partial W_{\ell r}^2} = \{I_r(W_{\ell r}) - I_{r+1}(W_{\ell r})\} \frac{p_T(W_{\ell r})}{W_{\ell r}} \qquad \text{(A3.13)}$$

APPENDIX A4

APPROXIMATION FOR AGEING MEAN FROM TEMPERATURE MEAN AND VARIANCE

The mathematics of this appendix use the following series expansions.

(i) The Taylor series[53] expansion of

$(1+x)^{-m}$, for m a positive integer and $|x|<1$,

where :

$$(1+x)^{-m} = 1-mx + \frac{(m+1)mx^2}{2} + \ldots + \frac{(m+n-1)!}{n!(m-1)!}(-1)^n x^n + \ldots \qquad (A4.1)$$

(ii) An approximation for the expectation of x^n, where x is a random variable with a known continuous distribution. Denoting the mean of x, as μ_x, variance V_x and nth central moment as V_x^n , where:

$$\mu_x = \varepsilon x \qquad (A4.2)$$

$$V_x = \varepsilon(x-\mu_x)^2$$

$$V_x^n = \varepsilon(x-\mu_x)^n$$

then by expansion it can be shown that:

$$V_x = \varepsilon x^2 - \mu_x^2 \qquad (A4.3)$$

$$V_x^3 = \varepsilon x^3 - 3\mu_x Vx - \mu_x^3$$

$$V_x^4 = \varepsilon x^4 - 4\mu_x Vx^3 - 6\mu_x^2 V_x - \mu_x^4$$

$$V_x^n = \varepsilon x^n - n\mu_x V_x^{n-1} - \ldots - \frac{n!}{2(n-2)!}\mu_x^{n-2} V_x - \mu_x^n$$

Re-arranging the above and assuming the variance of x is small such that the terms V_x^n for $n>3$ are negligible, the following approximation can be applied.

$$\varepsilon x^n \simeq \mu_x^n + \frac{n!}{2(n-2)!}\mu_x^{n-2} V_x \qquad n \geq 2 \qquad \text{(A4.4)}$$

Now, let a random variable y be related to x such that:

$$y = \frac{1}{1+x} \quad , \qquad |x| < 1 \qquad \text{(A4.5)}$$

Then the mean of y, μ_y is given by:

$$\mu_y = \varepsilon\frac{1}{1+x} \qquad \text{(A4.6)}$$

Applying Equation (A4.1) and then the Approximation (A4.4), yields:

$$\mu_y = \varepsilon \sum_{n=o}^{\infty} (-1)^n x^n \qquad \text{(A4.7)}$$

$$\simeq 1 - \mu x + \sum_{n=2}^{\infty} (-1)^n (\mu_x^n + \frac{n!}{2(n-2)!}\mu_x^{n-2} V_x) \qquad \text{(A4.8)}$$

$$= \sum_{n=o}^{\infty} (-1)^n \mu_x^n + \frac{V_x}{2} \sum_{n=o}^{\infty} (-1)^n \frac{(n+2)!}{n!} \mu_x^n \qquad \text{(A4.9)}$$

Using the converse of Equation (A4.1), the above reduces to:

$$\mu_y \simeq \frac{1}{1+\mu_x} + \frac{V_x}{(1+\mu_x)^3} \qquad \text{(A4.10)}$$

A similar approximation can be found for the expectation of y squared, such that:

$$\varepsilon y^2 = \varepsilon \frac{1}{(1+x)^2} \qquad \text{(A4.11)}$$

$$\simeq \frac{1}{(1+\mu_x)^2} + \frac{3V_x}{(1+\mu_x)^4} \qquad \text{(A4.12)}$$

The variance V_y, of y can now be obtained from Equations (A4.10) and (A4.11), since:

$$V_y = \varepsilon y^2 - \mu_y^2 \qquad \text{(A4.13)}$$

$$\simeq \frac{V_x}{(1+\mu_x)^4} - \frac{V_x^2}{(1+\mu_x)^6} \qquad \text{(A4.14)}$$

The latter term in Equation (A4.14) will be small and can be neglected.

Finally let a third random variable z be such that:

$$z = e^y \qquad \text{(A4.15)}$$

Then the mean μ_z of z is given by:

$$\mu_z = \varepsilon e^y \qquad \text{(A4.16)}$$

$$= \varepsilon e^{\mu_y} e^{(y-\mu_y)} \qquad \text{(A4.17)}$$

Taking a series expansion of the R.H.S.,

yields:

$$\mu_z = e^{\mu_y} \varepsilon\{(1+(y-\mu_y) + \frac{(y-\mu_y)^2}{2} + ...\} \qquad (A4.18)$$

and neglecting 3rd order deviations of y and greater,

then:

$$\mu_z \simeq e^{\mu_y} (1+ \frac{Vy}{2}) \qquad (A4.19)$$

These equations can now be applied to the expression of the mean ageing in Equation (3.4) to a nodal absolute temperature θ_i with mean and variance of $\mu_{\theta T}^{i}$ and $V_{\theta T}^{ii}$. Where:

$$\mu_R = \varepsilon_{P_{\theta T}(\theta)} \{ \exp(B(1/\theta_{ref} - 1/\theta_i) \} \qquad (3.4)$$

$$= \varepsilon_{P_{\theta T}(\theta)} \{ \exp(B/\theta_{ref}).\exp(-B/\theta_i) \} \qquad (A4.20)$$

The latter term of Equation (A4.20) and the substitutions of:

$$x = \frac{\theta_i - 273}{273} \qquad (A4.21)$$

$$y = \frac{B}{\theta_i} = \frac{B}{273} \cdot \frac{1}{1+x} \qquad (A4.22)$$

can be applied to Equations (A4.10), (A4.14) and (A4.19). Then the ageing mean will approximate to:

$$\mu_R = \left(1+ \frac{V^{ii}_{\theta T} B^2}{2(\mu^i_{\theta T})^4}\right) \exp\ B\left(\frac{1}{\theta_{ref}} - \frac{1}{\mu^i_{\theta T}} - \frac{V^{ii}_{\theta T}}{(\mu^i_{\theta T})^3}\right) \qquad \text{(A4.23)}$$

The above expression is shown in Chapter 3 to be accurate to around 15% in estimating the machine ageing compared with results obtained from a deterministic analysis.

APPENDIX A5

A VERSITILE DATA LOGGER

The data recording device described in this Appendix was developed to act as a stand alone peripheral to micro-computer systems that use the IEEE 488 communication bus, such as the Commodore 'PET'.

The device was based upon an Intel 8085 micro-processor and had a certain amount of inbuilt flexibility and memory capacity so that it was simple to use and required a minimum amount of access from the controlling micro-computer. This Appendix provides a technical specification of the device, a complete set of circuit diagrams in Figure A5.1 and a source code listing in Table A5.1.

Applications of the device include the data logging task described in Chapter 4 of this thesis and an automatic weather station in a University Geography Department.

P1 DATA RECORDER

1. DESCRIPTION OF DEVICE

The data recorder combines an eight channel data logger with an IEEE 488 bus interface. The eight channels consist of seven analogue voltage inputs and an event counter. The analogue inputs are sampled approximately every 4 seconds and averaged over periods of 15 minutes. The averaged values are stored in an internal memory, which has a capacity of holding 24 hours of data. The event counter registers the total number of events that occur within the 15 minute periods.

The instantaneous analogue recordings and the running sum of the event counter, together with the averaged inputs for the previous 24 hours, can by accessed by using IEEE 488 bus commands. With each set of data values transmitted via the IEEE 488 bus, a time is provided in hours, days and minutes, which is either the time of the instantaneous recording or the time up to which the previous 15 minutes of data had been averaged. The data recordings are read by the micro-computer as decimal values scaled from 0.00 to 1.00, provided to two decimal places. The time is given as two figure integers.

When the data recorder is powered on, or when the reset switch is toggled off then on, the internal clock is set to a time of day 1, hour 0 and minute 0. After each successive quarter of an hour the averaged input is stored and the event counter reset. After 24 hours the day counter is incremented and the new inputs are written over

the values which were stored 24 hours previously.

The device sets a service request signal on the IEEE 488 data bus either every 12 or 24 hours. The service request is reset immediately the device is accessed from the IEEE bus.

2. INPUT CHANNEL SPECIFICATIONS

Channels	1-7	-	Voltage input, single ended with common negative
			Range 0-3 Volts
			Linearity ±1%
			Offset <15mV
			Impedance 500kΩ
Channel 8			Event counter
			Count occurs when a switch across the event terminals is closed. Maximum on state impedance - 100Ω.

3.1 IEEE 488 Bus Specifications

The device has a primary address of '8'. This address can be reset by altering the least significant 4 bits of the microproccessor program source code at memory locations 0110H and 0128H. For example to set a primary address of '10' the source code at address 0110H should be changed from 48H to 4AH and the code at address 0128H from 28H to 2AH.

The secondary address (SA) commands are:

SA = 0 Input present value of data.

1-24 Input average data at start of hour SA-1 and set incremental pointer to that hour.

25 Input average data for the 15 minutes after the incremental pointer and advance pointer.

26 Set service request to a 12 hour period.

27 Set service request to a 24 hour period.

The data recorder will respond to the following specialised IEEE 488 bus commands

DCL - General device clear

SDC - Selective device clear

SPE - Serial Poll Enable

SPD - Serial Poll Disable.

3.2 Input Format

The Commodore PET Basic IEEE bus commands should be off the form:

```
OPEN  LF,8,SA
INPUT # LF,A,B,C,D,E,F,G,H,I,J,K
```

where LF = channel logical file number

SA = secondary address

A = integer time in days

B = integer time in hours

C = integer time in minutes

D = event count scaled such that a count of 250 = 1.00

E-K = voltage inputs for channels 1 to 7 such that an input of 3 Volts = 1.00.

An exception to this rule is when using the secondary addresses SA of 26 to 27, when the format is:

INPUT # LF,A

A = 0 if a 24 hour service request is set.

1 if a 12 hour service request is set.

3.3 Examples

(1) The commands:

```
10  OPEN 5,8,0
20  INPUT#5,A,B,C,D,E,F,G,H,I,J,K
```

will input the most recent recorded data at the time the command is issued.

(2) Similarly the commands:

```
10  OPEN 5,8,17
20  OPEN 6,8,25
30  INPUT#5,A,B,.....
40  PRINT A,B,.....
50  FOR N = 1 to 7
60  INPUT#6,A,B,.....
70  PRINT A,B,.....
80  NEXT N
```

will input the stored average data for hour 16, 0 minutes to hour 17 and 45 minutes and print the results on the screen.

Finally the commands:

```
10  OPEN 5,8,26
20  INPUT#5,A
```

will set the service request to a 12 hour period.

Table A5·1 Data Logger Source Code

```
0000  F331EA0B3E4FD30421230822830B3EFF
0010  21000806057723O5C21500C33F002F02
0020  73015B02C35F00
002C  C30203
0034  C34101
003C  C36700061EAF772305C24200JE013206
004C  083E4F3207083E183020E650C25500FB
005C  C32F02E5210A0834E1FBC9F5C5D5E5DB
006C  04E680CA90003E0490D27E00E1D1C1F1
007C  FBC9211E0031EA0B5148060009 4A5E23
008C  56EBFBE90606FB2107087EF642E64ED3
009C  04DB04E640C29D007EE64CD30477DB00
00AC  2F210808E67FFE60
00B4  D2FA00577EE6FE777AFE40D20801FE20
00C4  D22701FE14CADE00FE04CAE300FE18CA
00D4  EC00FE19CAF300C330017747C330017E
00E4  E602CA3001C3DE007EF60477C330017E
00F4  E6FB77C33001E61F4F7EE601CA300106
0104  02C33001FE5F0600CA3001FE48C23001
0114  06047EE604C230017EF603770E000602
0124  C33001FE28C230017E
012D  F602773A0708F641D304DB04E640CA37
013D  01C39300F53E4FD30432070820F60EE6
014D  0F30E601CA6101F1E5210C0039366123
015D  3601E1C9FB31EA0BF320FBE620C26501
016D  3E1830C32F0279FE1AD2E401FE00CA07
017D  02FE19CA8B013D0707E6FC3209083A09
018D  08212308160O5F06091905C296010F0F
019D  E63F577BE60347
01A4  CAAE01AFC60F05C2A8015F3A06084F3A
01B4  050892DAC401C2CC013A040893D2CC01
01C4  0D793CC2CC010E63CD63023A09083CFE
01D4  60DAD901AF320908 3E0DCDD902C38B01
01E4  C2F7013A0808F6083208083E30CDD902
01F4  C315023A0808E6F7320808 3E31CDD902
0204  C3150221040 85E2356234E210A08CD63
0214  023A0708E647320708
021D  3E0DCDD9023A0708F60CD304320708C3
022D  2F022103 08AFB6C22F0223B6C22F023A
023D  0808E608C24E0223B6CA4E02FE0CC22F
024D  023A0708E6FBD30432070 8C32F023EC0
025D  CDD902C32F02F5C5D5790600CDA7023E
026D  2CCDD9027ACDA7023E2CCDD9027BCDA7
027D  020E093E2CCDD9027E2316FFDE1914D2
028D  8902C61907075F7A
0295  0601CDA702057BCDA7020DC28002D1C1
02A5  F1C9C5D5160A1E0092DAB5021CC3AD02
02B5  824F7BCDD602CDD902CDCE0279CDD602
02C5  CDD902CDCE02D1C1C905C03E2ECDD902
02D5  C9F630C9C5D3003A0708F6C3D30447DB
02E5  04E602CAE40278F610D30447DB04E601
02F5  CAF10278E6EFD30432070 8C1C9F53E0D
0305  30C5D5E5FB21000834
030E  7ED614C2AC03772A0308232203082104
031E  087ED63CC23803772334 7ED618C23803
032E  7723347ED664C23803772101083 47ED6
033E  0FC2AC0377110B0821130 8AF32850BD3
034E  08C3C1033A850B3C32850BF608D30879
035E  12137E81772 3D26803342 33A850BE607
036E  C24D03210208 34C2AC032A830BEB2113
037E  083A0A081213AF
0385  320A0806087E36002 3E6807ECA95033C
0395  12360023130 5C28A03217DF419D2A803
03A5  112308EB22830BF320FBE610C2AC03F3
03B5  20E602F60830E1D1C1F1FBC9060807 8D3
03C5  0C4F780FFE80CADD0347DB04E62079C2
03D5  D9038080 90C3C403DB04E620CA52030D
03E5  C35203
```

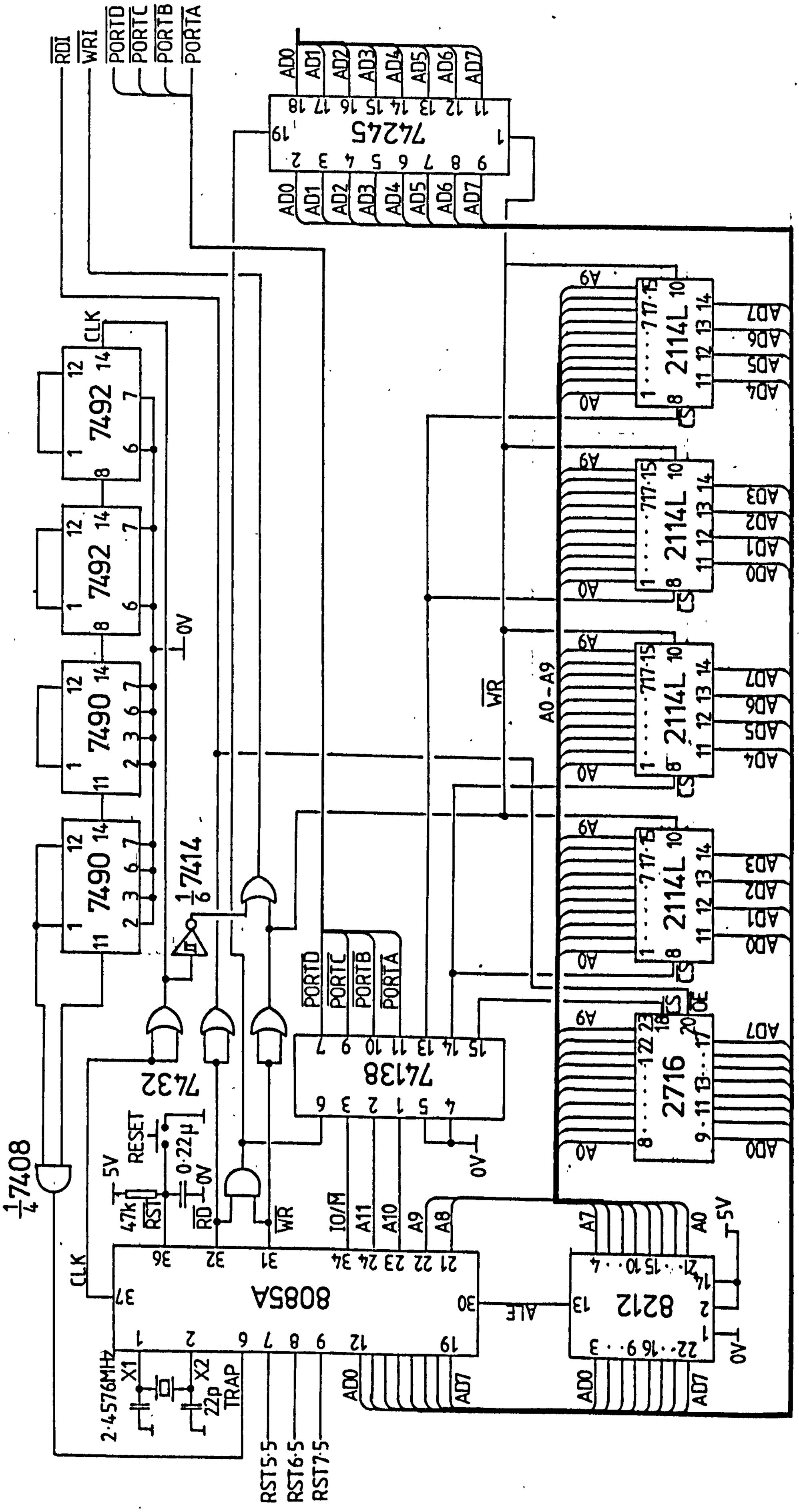

Figure A5·1a Microprocessor Circuit

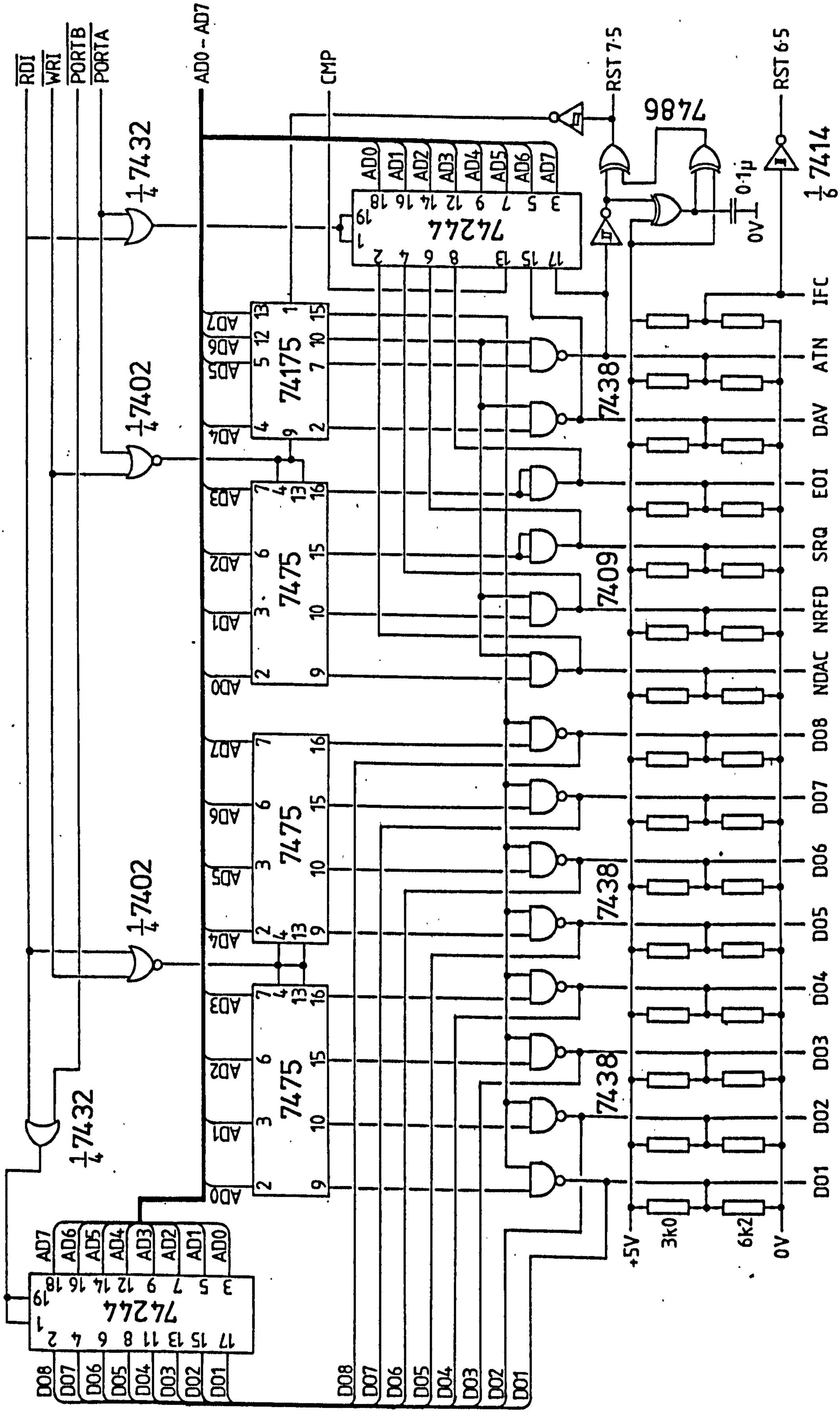

Figure A5·1b IEEE 488 Bus Interface

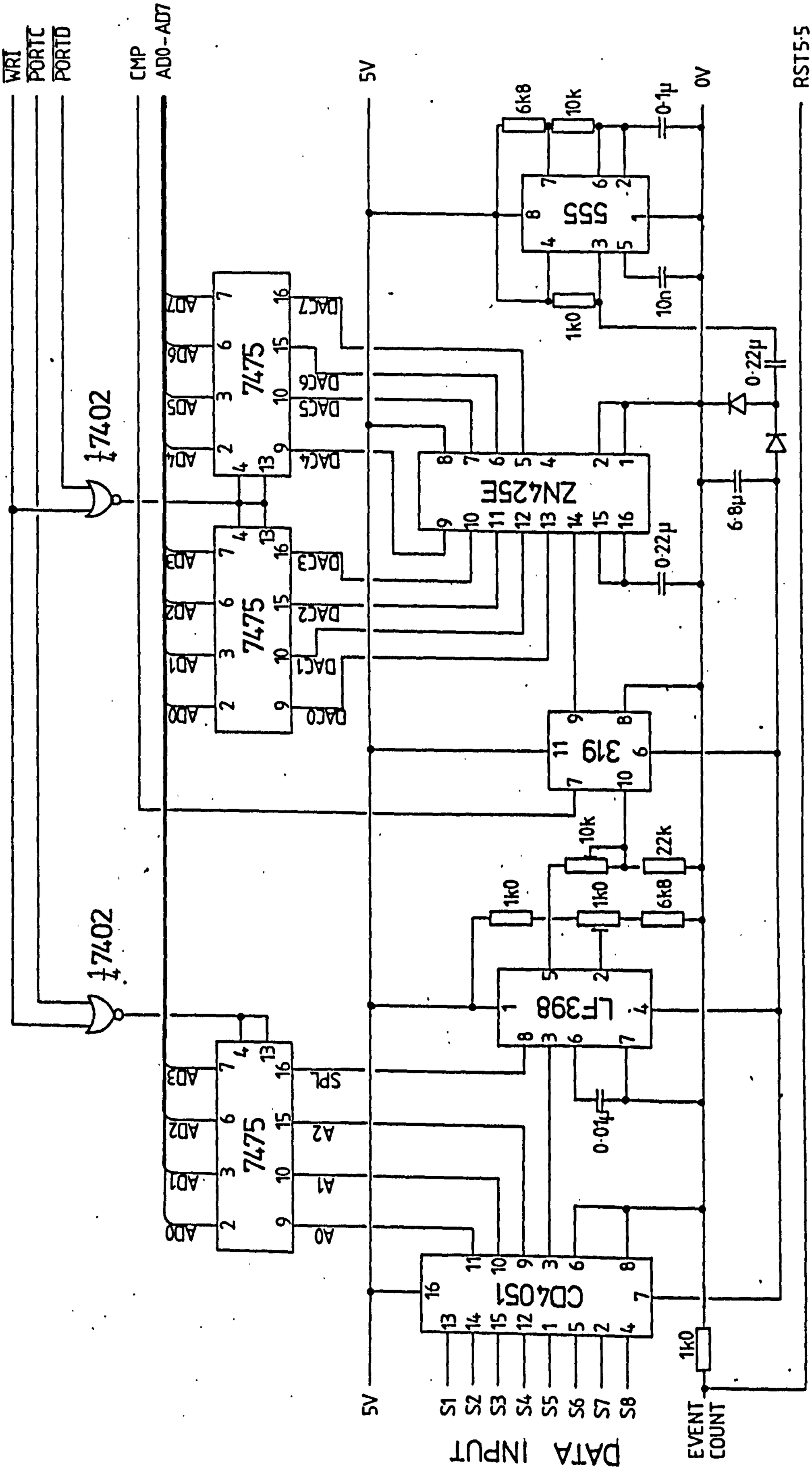

Figure A5·1c Analogue Circuit

APPENDIX A6

ONE DIMENSIONAL, RADIAL HEAT FLOW IN A CYLINDER

Figure A6.1 shows a uniform cylinder of constant thermal conductivity k_r in the radial direction, that has an internal heat generation g''' per unit volume. The heat flow in the radial direction can be modelled by the T network[21] of constant thermal resistances given in Figure A6.2, where θ_1 and θ_2 are surface temperatures, θ_m is the mean radial temperature and u is the total heat generation in the cylinder. The heat generation u is simply given by:

$$u = \pi(r_2^2 - r_1^2)Lg''' \qquad (A6.1)$$

The values of the thermal resistance R_1 to R_3 can be determined by solving the heat equation for the two specific cases of zero internal heat generation and zero surface temperature, and then applying superposition.

(i) Zero Internal Heat Generation

With no internal heat generation, the temperatures in the cylinder are described in radial co-ordinates by the heat equation:

$$\frac{d^2\theta}{dr^2} + \frac{1}{r}\frac{d\theta}{dr} = 0 \qquad (A6.2)$$

with the boundary conditions:

$$\theta = \theta_1 \quad \text{at} \quad r = r_1 \tag{A6.3}$$

$$\theta = \theta_2 \quad \text{at} \quad r = r_2$$

The general solution to the differential Equation (A6.2) is in the form:

$$\theta = A\log_e r + B \tag{A6.4}$$

The constants A, B can be found from the boundary conditions, and in particular A is given by:

$$A = \frac{(\theta_2-\theta_1)}{\log_e(r_2/r_1)} \tag{A6.5}$$

As there is no heat generation, the central node of the equivalent T network must be at the mean temperature of the cylinder, which is calculated from:

$$\theta_m = \frac{2}{(r_2^2-r_1^2)} \int_{r_1,\theta_1}^{r_2,\theta_2} \theta\, r\, dr$$

$$= \frac{2}{(r_2^2-r_1^2)} \left\{\left[\theta\, \frac{r^2}{2}\right]_{r_1,\theta_1}^{r_2,\theta_2} - \int_{r_1,\theta_1}^{r_2,\theta_2} \frac{d\theta}{dr}\, \frac{r^2}{2}\, dr\right\}$$

$$= \frac{r_2^2\theta_2-r_1^2\theta_1}{(r_2^2-r_1^2)} - \frac{A}{2} \tag{A6.6}$$

The total heat flow q_1, flowing into the thermal branch R_1 is equal to:

$$q_1 = - 2\pi r_1 k_r L \left.\frac{d\theta}{dr}\right|_{r=r_1}$$

$$= - 2\pi k_r LA \qquad \text{(A6.7)}$$

The value of the thermal resistance R_1 can now be obtained by dividing the temperature difference across R_1 by the heat flow through it. Hence:

$$R_1 = \frac{\theta_1 - \theta_m}{q_1}$$

$$= \frac{1}{2\pi k_r LA} \left(\theta_1 - \frac{r_2^2\theta_2 - r_1^2\theta_1}{r_2^2 - r_1^2} + \frac{A}{2}\right) \qquad \text{(A6.8)}$$

After substituting for A from Equation (A6.5), the above can be simplified to:

$$R_1 = \frac{1}{4\pi k_r L}\left(\frac{2r_2^2 \log_e(r_2/r_1)}{(r_2^2 - r_1^2)}\right. \qquad \text{(A6.9)}$$

In a similar manner the thermal resistance R_2 is obtained from the expression:

$$R_2 = \frac{1}{4\pi k_r L}\left(1 - \frac{2r_1^2 \log_e(r_2/r_1)}{(r_2^2 - r_1^2)}\right) \qquad \text{(A6.10)}$$

(ii) Zero Surface Temperatures.

For surface temperatures of θ_1 and θ_2, the equivalent thermal circuit of the cylinder reduces to Figure A6.2. The heat equation that includes generation is given by:

$$\frac{d^2\Theta}{dr^2} + \frac{1}{r}\frac{d\theta}{dr} + \frac{g'''}{k_r} = 0 \qquad (A6.11)$$

and the boundary conditions are:

$$\theta = 0 \quad \text{at} \quad r = r_1 \qquad (A6.12)$$

$$\theta = 0 \quad \text{at} \quad r = r_2$$

This equation has a general solution of:

$$\theta = A \log_e r - \frac{g'''}{4k_r} r^2 + B \qquad (A6.13)$$

where;

$$A = \frac{g'''(r_2^2 - r_1^2)}{4k_r \log_e(r_2/r_1)} \qquad (A6.14)$$

The cylinder mean temperature can be evaluated, in the manner of Equation (A6.6), as:

$$\theta_m = -\frac{A}{2} + \frac{g'''(r_2^2 + r_1^2)}{8k_r} \qquad (A6.15)$$

The thermal resistance R_3 is determined from this mean temperature, the total heat generation and the parallel combination of the resistances R_1 and R_2 (Figure A6.2).

Denoting the latter as $R_1//R_2$, then:

$$R_3 = \frac{\theta_m}{u} - R_1//R_2 \qquad \text{(A6.16)}$$

The parallel resistance is taken from Equations (A6.9) and (A6.10), since:

$$R_1//R_2 = \frac{1}{4\pi k_r L}\left(\frac{2\log_e(r_2/r_1)}{(r_2^2-r_1^2)^2}\, r_1^2 r_2^2 + \frac{(R_1^2 + r_2^2)}{(r_2^2-r_1^2)2\log_e(r_2/r_1)}\right) \qquad \text{(A6.17)}$$

The substitution of the above expression and Equations (A6.1), (A6.14) and (A6.15) into Equation (A6.16) yields the following formulae for R_3:

$$R_3 = -\frac{1}{8\pi k_r L(r_2^2-r_1^2)}\left(r_1^2+r_2^2 - \frac{4r_2^2 r_1^2 \log_e(r_2/r_1)}{(r_2^2-r_1^2)}\right) \qquad \text{(A6.18)}$$

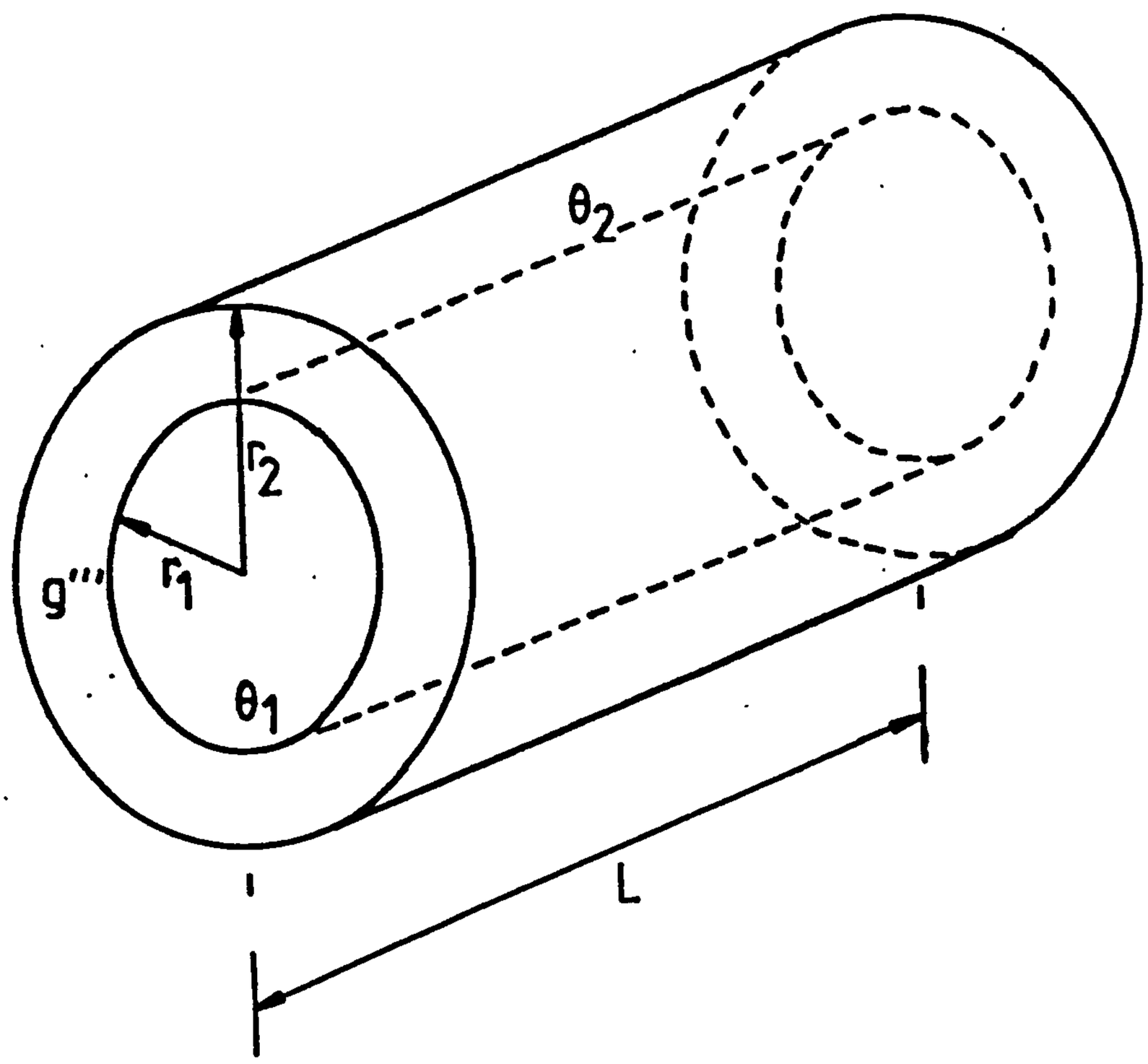

Figure A6·1 General Cylindrical Section

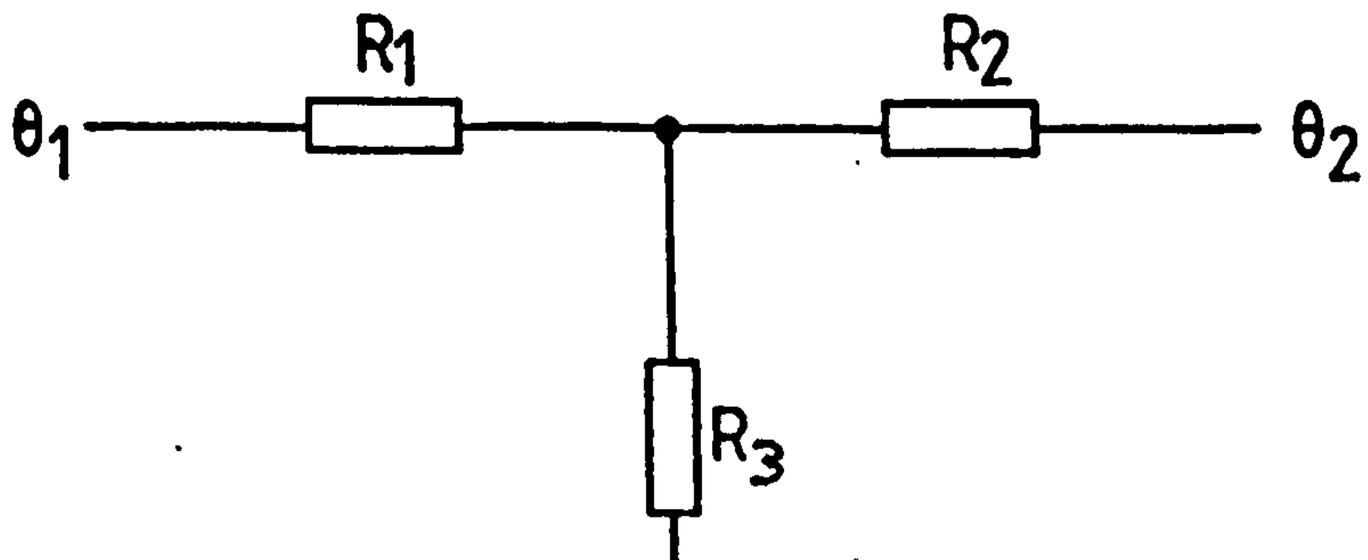

Figure A6·2 Cylinder Radial Equivalent Thermal Circuit

APPENDIX A7

DETERMINATION OF INDUCTION MOTOR LOSSES FROM ITS ELECTRICAL EQUIVALENT CIRCUIT

The standard equivalent circuit of a single phase of a balanced induction motor is given in Figure A7.1. This can be reduced to a simpler, but no less accurate, form of Figures 5.4 and A7.2 [43], where:

$$Z_{s/c} = R_{s/c} + jX_{s/c} \qquad \text{(A7.1)}$$

$$R_{s/c} = R_1 + cR_2$$

$$X_{s/c} = X_1 + cX_2$$

$$Z_m = R_m + jX_m$$

$$c = 1 + (R_1 + jX_1)/Z_m$$

In Figure A7.2, the variable resistance is associated with the total mechanical power output of the machine. The constant 'c' is a complex number slightly greater than unity, with a small reactive component, and can be assumed to be purely numeric. In addition, cZ_m can be taken to be purely reactive, since the zero slip iron and stator copper losses will generally only represent a small proportion of the magnetisation current. This

assumption is only made to ease the analysis and does not suggest that the iron losses are neglected but are added at a later stage.

From Figure A7.2 and the phasor diagram of Figure A7.3, the following equation is obtained:

$$(i_2/c)^2 = i^2 + i_{mo}^2 - 2ii_{mo}\sin\phi \qquad (A7.2)$$

Here i_2, i, i_{mo} are the magnitudes of the respective currents and ϕ is the supply current phase angle. The reactive power loss Q in the machine is given by:

$$Q = i_{mo}^2 cX_m + (i_2^2/c)^2\, cX_{s/c} \qquad (A7.3)$$

Substituting for i_{mo} and i_2 in the above yields:

$$Q = \frac{v^2 cX_m}{(cZ_m)^2} + \left(\frac{i^2 + v^2}{(cZ_m)^2} - \frac{2vi}{cZ_m}\sin\phi\right) cX_{s/c} \qquad (A7.4)$$

However, the reactive power Q is also given by:

$$Q = vi\,\sin\phi \qquad (A7.5)$$

and hence Equation (A7.4) reduces to:

$$Q = \frac{cX_{s/c}\, Z_m}{(Z_m + 2X_{s/c})}\, i^2 + \frac{v^2}{cZ_m}\,\frac{(X_m + X_{s/c})}{(Z_m + 2X_{s/c})} \qquad (A7.6)$$

A similar expression can be obtained for the power losses W_L in the machine, as:

$$W_L = \frac{c\ R_{s/c}\ Z_m}{(Z_m + 2X_{s/c})}\ i^2 + \frac{v^2}{cZ_m}\ \frac{(R_m + R_{s/c})}{(Z_m + 2X_{s/c})}$$

$$+ \frac{2v^2}{cZ_m^2}\ \frac{(X_{s/c}R_m - X_m R_{s/c})}{(Z_m + 2X_{s/c})} \qquad \text{(A7.7)}$$

This equation can be further simplified by taking the magnitude of X_m to be approximately equal to Z_m. An additional term W_w is added to the power loss to account for any windage and friction loss in the machine.

The total power loss per phase is then written as:

$$W_L = W_w + \frac{cR_{s/c}\ Z_m}{(Z_m + 2X_{s/c})}\ i^2 + \frac{v^2 R_m}{cZ_m^2} \qquad \text{(A7.8)}$$

$$- \frac{v^2}{cZ_m}\ \frac{R_{s/c}}{(Z_m + 2X_{s/c})}$$

The electrical losses in Equation (A7.8) are seen to be proportional to the square of the motor's phase current and voltage. They can be subdivided into iron losses and stator and rotor copper losses to give the constants of Equation (5.20).

The ageing analysis of Chapter 3 relates the losses in a machine's thermal model to its output power by the function F(W) in Equation (3.8). This appendix has derived equations for an induction motor's losses in

terms of its terminal conditions. To obtain the ageing analysis function, these terminal conditions need to be expressed as a function of the output power W. This is achieved by comparing Equation (A7.8) with Equation (A1.8) from Appendix A1, which are both equal to the total loss in the machine.

The constant 'a' term in Equation (A1.8) must be equal to the no load losses in Equation (A 7.8), and an approximate relationship between W, i and v can be written as:

$$\frac{1}{3}\left(\frac{cR_{s/c}}{3v^2}\right)W^2 = \frac{cR_{s/c}\,Z_m}{(Z_m + 2X_{s/c})}\,i^2 - \frac{v^2\,R_{s/c}}{cZ_m(Z_m + 2X_{s/c})} \qquad (A7.9)$$

If the machine is operated with a constant supply voltage, the above can be rearranged to give i^2 in terms of W^2:

$$i^2 = \frac{(Z_m + 2X_{s/c})W^2}{9v^2\,Z_m} + \frac{v^2}{(cZ_m)^2} \qquad (3.67)$$

Equation (3.67) can be substitued into Equation (5.20) to give formulae for the losses in the thermal model components in terms of the load W, i.e. the function F(W) .

The induction motor equivalent circuit parameters can be obtained from conventional light load and locked rotor tests. Alternatively, they can be found from a load test by connecting the machine to a constant voltage supply and loading it with some form of dynamometer.

A series of tests will need to be performed over the entire expected working range of the motor, which should include up to 25% overloads, since these are of interest in ageing analysis. A set of readings should be taken for the motor phase current i, real and reactive power W_{in}, Q and the shaft load W_s. If Equations (A7.6) and (A7.8) are written in the form:

$$Q = w\, i^2 + x \qquad \text{(A7.10)}$$

$$W_{in} = W_s = y i^2 + z \qquad \text{(A7.11)}$$

then the constants w, x, y and z are directly available from the test results. The z term may include external mechanical losses such as windage and friction in the dynamometer.

At zero slip, the magnetising loss in the induction motor is given by:

$$Q = \frac{v^2}{(cZ_m)^2}\, cX_m \simeq \frac{v^2}{cZ_m} \qquad \text{(A7.12)}$$

and occurs when:

$$i = \frac{v}{cZ_m} = \frac{Q}{v} \qquad \text{(A7.13)}$$

Equation (A7.13) may be solved either analytically or graphically with Equation (A7.10) to yield a value for

cZm. The quantities $cX_{s/c}$ and $cR_{s/c}$ can then be found from the test results, as:

$$cX_{s/c} = \frac{w \quad cZ_m}{cZ_m - 2w} \qquad (A7.14)$$

$$cR_{s/c} = \frac{y \quad cZ_m}{cZ_m - 2y} \qquad (A7.15)$$

These impedances can now be split into the component parts of Equation (A7.1). The stator resistance R_1 can be directly measured from a d.c. test. If the leakage reactances X_1 and X_2 are assumed to be in the same ratio as the stator and rotor resistances, the following apply:

$$X_1 = R_1 \frac{cX_{s/c}}{cR_{s/c}} \qquad (A7.16)$$

$$c = \frac{1}{(1 - X_1/cZ_m)}$$

$$R_2 = (R_{s/c} - R_1)/c$$

$$X_2 = (X_{s/c} - X_1)/c$$

The core loss resistance R_m can only be obtained accurately if the windage and friction component of 'z' is measured seperately.

Load tests were performed on a 4 pole, 5.5kW, cage induction motor by coupling it to a d.c. generator.

The absorbed power W_s was calculated from the sum of the generator output power, copper loss and brush loss. The input real and reactive powers were recorded on seperate meters for accuracy. The stator resistance was calculated from a d.c. test whilst the machine was still hot. Finally, the total windage and friction was measured by running the d.c. machine as a motor at the induction machine's synchronous speed. The load test results and the associated equivalent circuit parameters are presented in Table A7.1.

A comparison between these values and the results of light load and locked rotor tests is provided in Table A7.2. The locked rotor results are given for a cold machine, a hot machine and a hot machine with a correction to take account of the magnetisation impedance. In the table, both the magnetisation impedance and the final corrected locked resistance $R_{s/c}$ are in reasonable agreement with the load test, however there is a large discrepency in the leakage values.

Ultimately, the load test parameters must give the best description of the motor operation, because they are calculated from fitting the equivalent circuit directly to the measured machine performance over its normal working range. This will be conditional to there being no loss of accuracy in the parameter evaluation from the measurements on the machine. The constant w and y in Equations (A7.10) and (A7.11) were obtained from changes of around 20% in the full scale deflection of the power meters, over the entire

range of test results. Although precision ± 1% f.s.d. meters were used, errors in the load test $R_{s/c}$ and $X_{s/c}$ values were estimated to be as high as ± 7%. In comparison the errors in the measurements taken from the locked rotor test were small.

The load test parameters were verified by plotting a circle diagram (Figure A7.4) and a input current slip characteristic (Figure A7.5). In the latter the slip was measured relative to a stroboscope syncronised to the supply frequency. The circle diagram gave a good fit to the motor currents and the value of the rotor resistance R_2 obtained from the slip curve agreed well with the load test value.

It was concluded that the load test was performed to reasonable accuracy and its results could be applied to the induction motor thermal model. The discrepancy in the $X_{s/c}$ values can only be attributed to the conditions of low excitation and high rotor frequencies during the locked rotor test. The final $R_{s/c}$ values in Table A7.2 were in good agreement, but the table demonstrates the errors involved in performing locked rotor tests with the machine cold or without correcting for the magnetisation branch impedance. The accurate estimation of induction motor performances directly from locked rotor and light load tests has been considered by a great number of authors, for example Alger devotes an entire chapter in his book [54] to deriving correction factors to explain the machines operation at full load or stall.

Table A7·1 Load Test Results for 5·5kW 1500rpm TEFC Cage Motor

w	2·34	
x	1·081	kVA
y	2·78	
z	0·189	kW
W_w	0·165	kW
cX_m	52·6	Ω
cR_m	3·9	Ω
$cX_{s/c}$	2·57	Ω
$cR_{s/c}$	3·05	Ω
R_1	1·68	Ω
c	1·03	

Table A7·2 Locked Rotor and Light Load Test Results for 5·5kW Motor

	Test	Cold	Hot	Corrected
Locked Rotor:	$X_{s/c}$	3·37 Ω	3·42 Ω	3·52 Ω
	$R_{s/c}$	2·18 Ω	2·65 Ω	3·01 Ω

Light Load: X_m 53·6 Ω

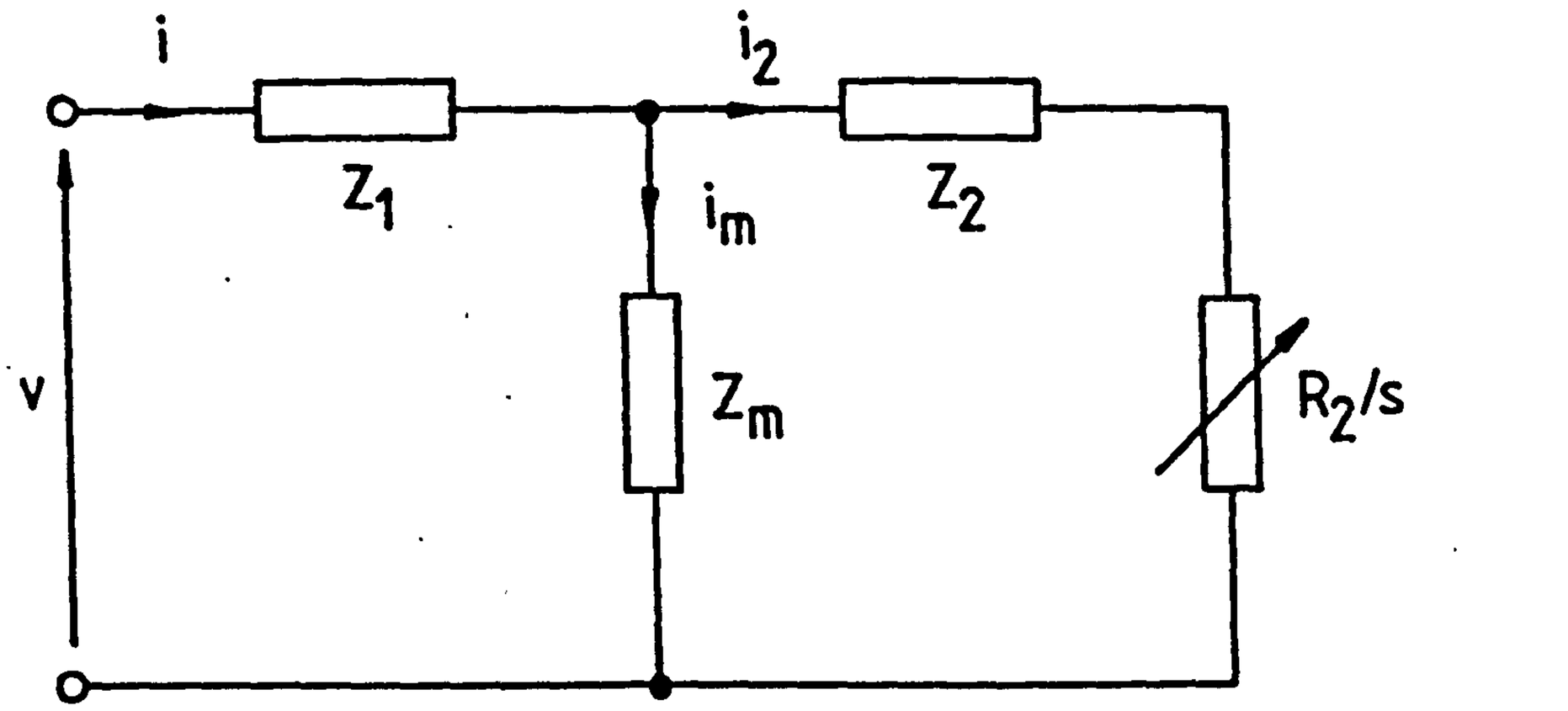

$$Z_1 = R_1 + jX_1$$
$$Z_2 = R_2 + jX_2$$
$$Z_m = R_m + jX_m$$

Figure A7·1 Standard Induction Motor Equivalent Circuit

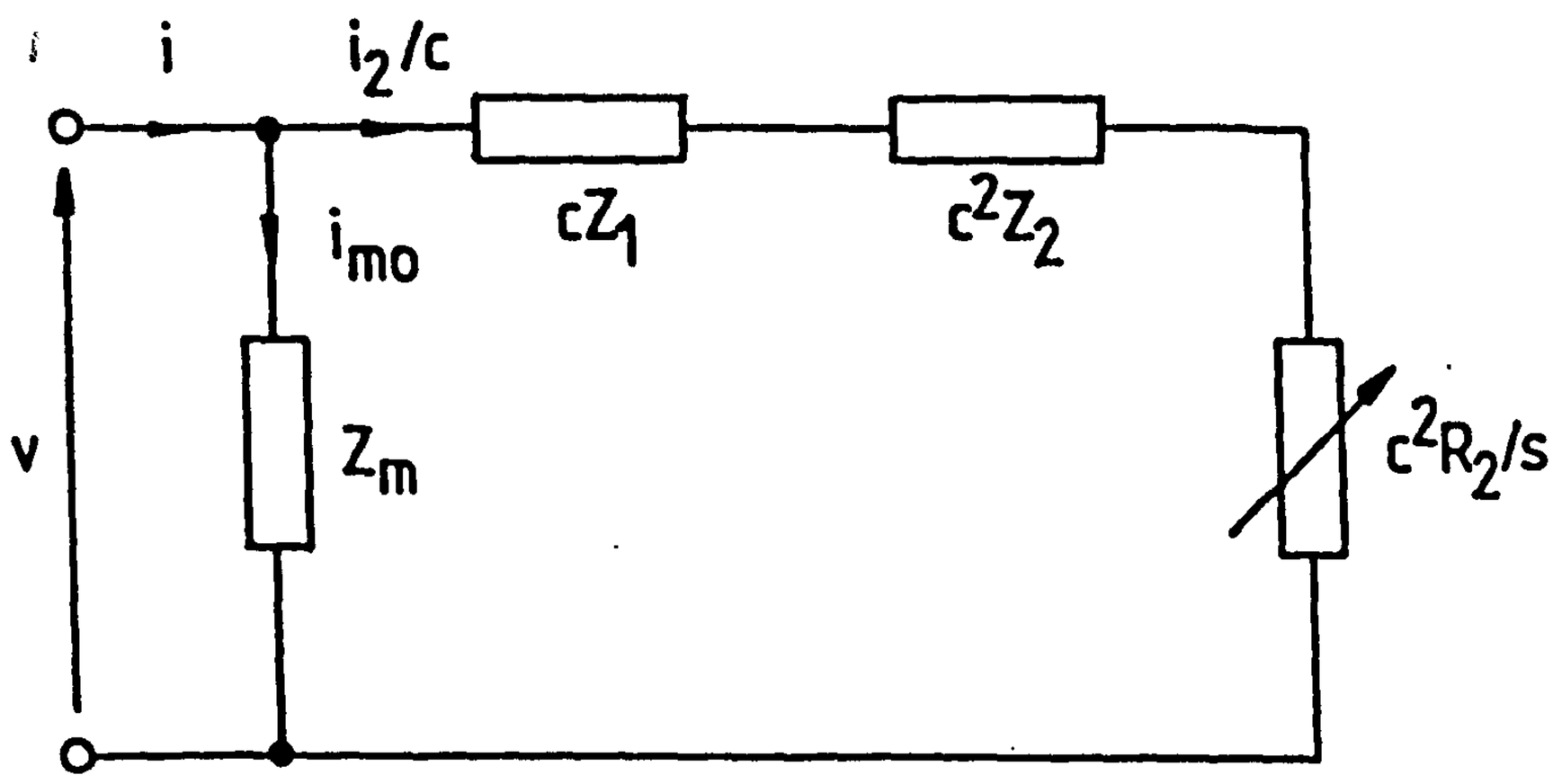

Figure A7·2 Alternative Induction Motor Equivalent Circuit

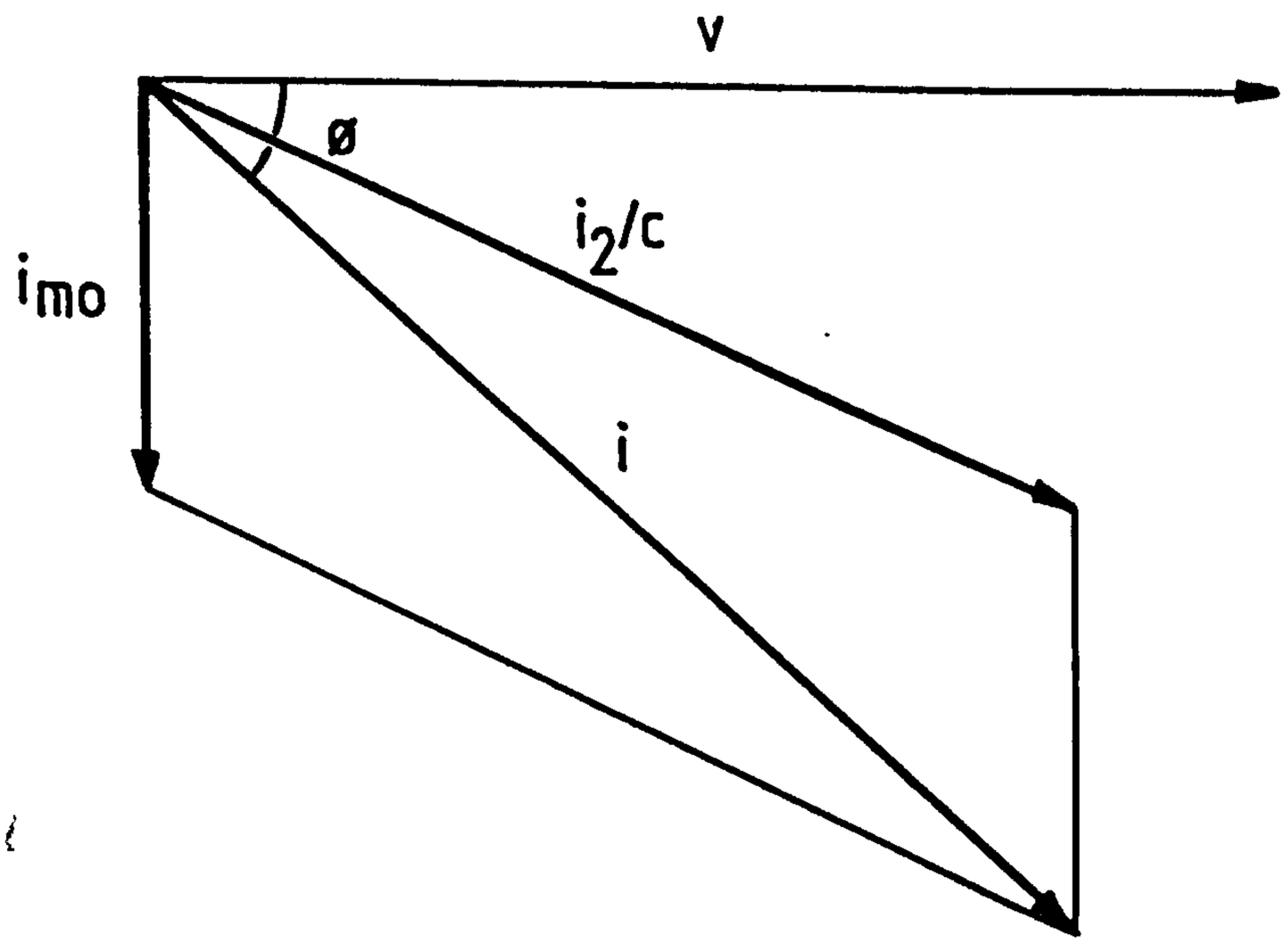

Figure A7-3 Equivalent Circuit Phasor Diagram

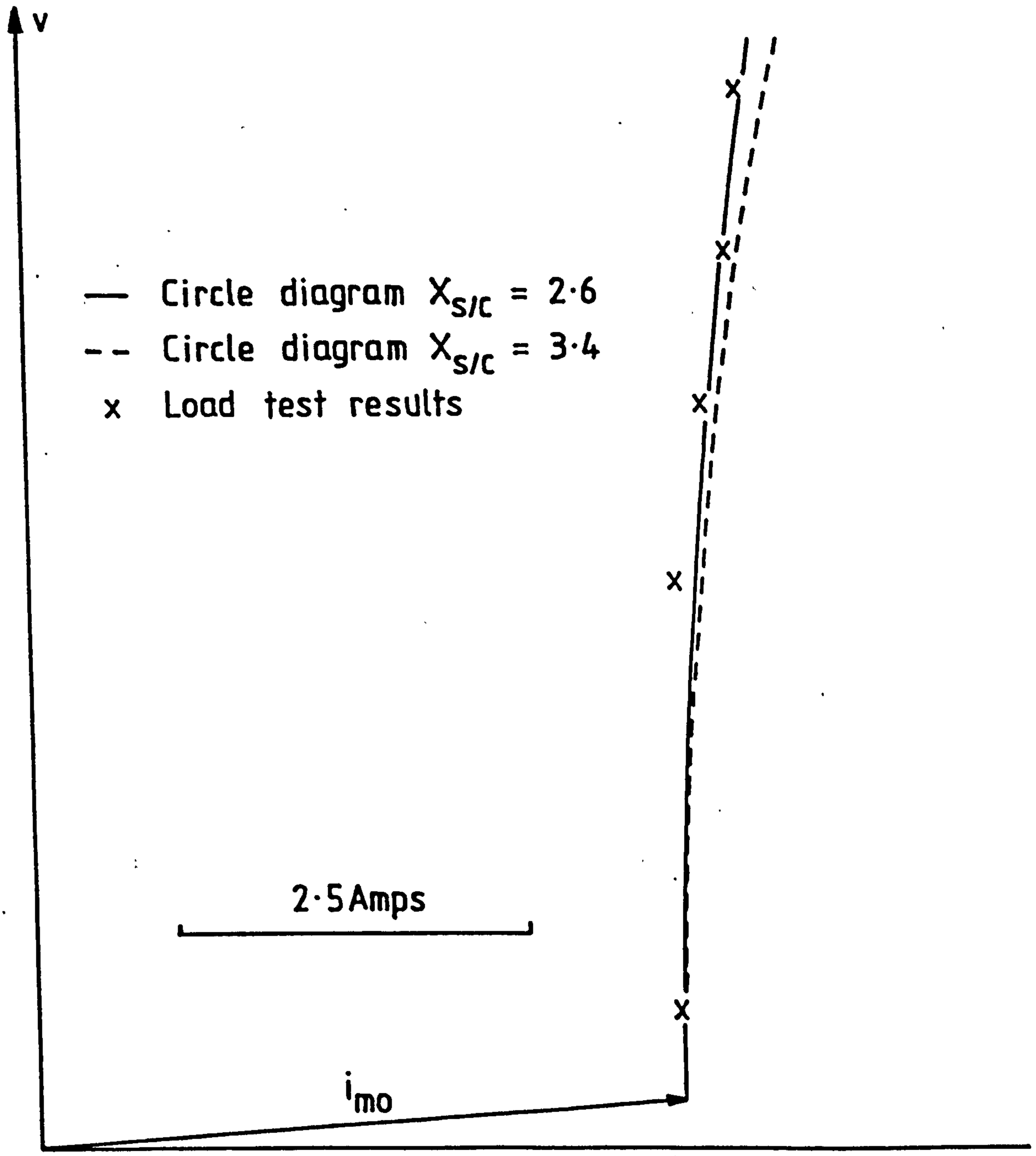

Figure A7·4 Circle Diagram for 5·5kW 1500rpm TEFC Cage Motor.

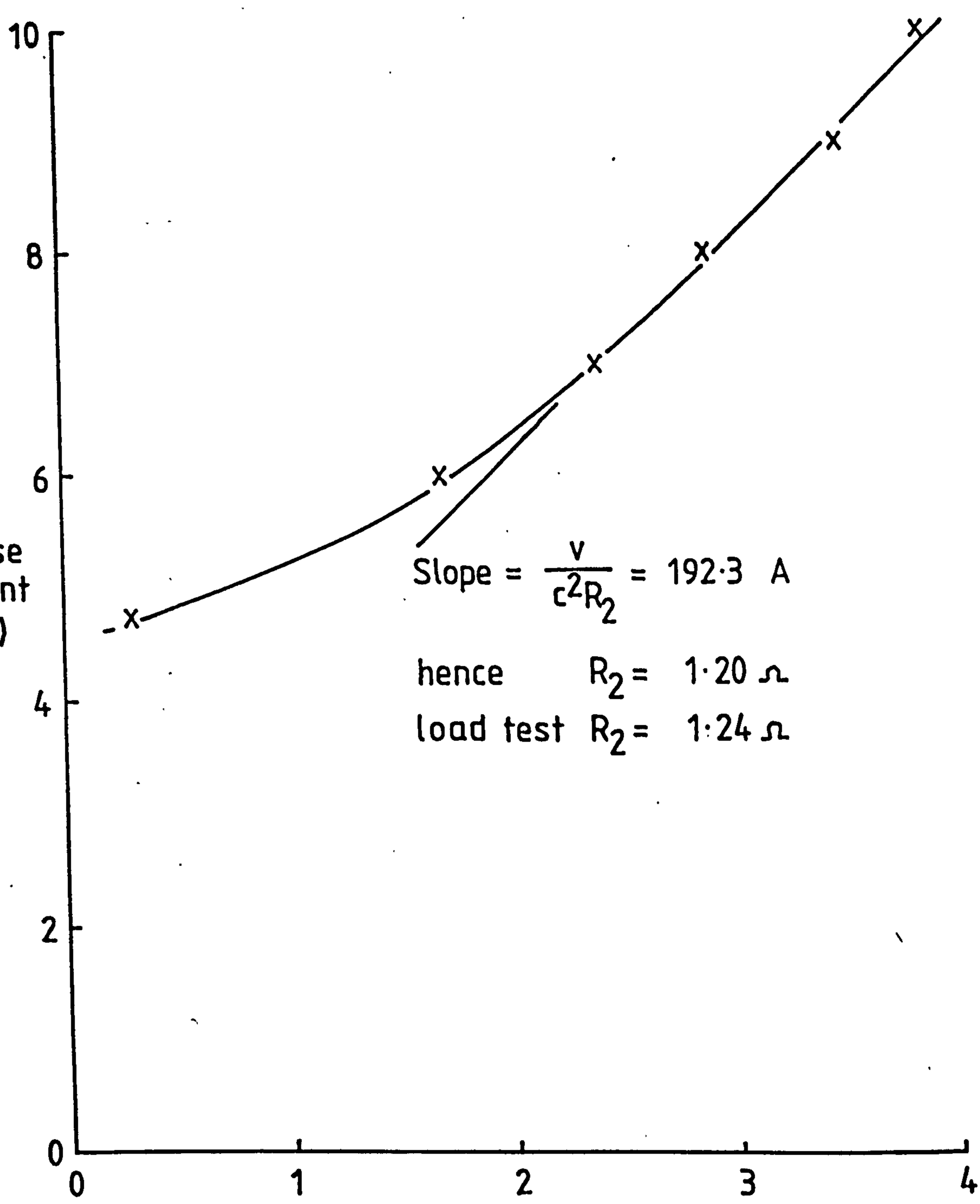

Figure A7·5 Current – Slip Locus for 5·5kW 1500rpm TEFC Cage Motor.

APPENDIX A8

LISTING OF THE CALCULATION SOFTWARE USED IN THE MICROPROCESSOR THERMAL PREDICTOR

```
1112 {*****************************************************************
1113 {
1114 { FUNCTION: CALC - CALCULATION ROUTINE
1115 {
1116 { CALLS: MULT24,ADD24,MULT16
1117 { DESCRIPTION: THE ROUTINE FETCHES THE RECENTLY MEASURED VALUES
1118 {               OF CURRENT AND AMBIENT TEMPERATURE AND STORES
1119 {               THEM TOGETHER WITH THE LAST SET OF CALCULATED
1120 {               TEMPERATURES AS A MATRIX IN ROM. IT THEN PERFORMS
1121 {               THE CALCULATION T = AG WHERE THE MATRIX A IS THE
1122 {               COMBINED EIGEN AND GENERATION MATRIX FOR THE SET
1123 {               SAMPLE INTERVAL. DIFFERENT MATRICES ARE USED DEPENDING
1124 {               ON WHETHER THE MACHINE IS RUNNING OR STATIONARY. THE
1125 {               CALCULATED RESULTS ARE THEN STORED IN THE DISPLAY
1126 {               REGISTERS.
1127 { NOTES:       THE FIRST 2 DISPLAY REGISTER POSITIONS ARE RESERVED FOR
```

```
 LOC  OBJ          LINE        SOURCE STATEMENT

                   1128 ;              I AND TAMB,THE NEXT 6 ARE THEN USED TO STORE THE
                   1129 ;              CALCULATED TEMPERATURES.
                   1130 ;              ILIMT = TEST FOR MOTOR RUNNING
                   1131 ;              RMSCN = INTIAL MATRIX G,CONTAINING THE PREVOUS T AND I**2 GENERATION
                   1132 ;              TRAM  = FINAL MATRIX T
                   1133 ;              TRADD = TEMPORARY REGISTER
                   1134 ;              SMATX = STATIONARY MATRIX A
                   1135 ;              RMATX = RUNNING MATRIX A
                   1136 ;              DACC  = 24 BIT ACCUMULATOR ADDRESS
 0011              1137 ILIMT    EQU     11H
                   1138 ;
 04B4 210920       1139 CALC:    LXI     H,DSTOR+4 ;LOAD ADDRESS OF THE CURRENT INTO
 04B7 110920       1140          LXI     D,DSTOR+4 ;H,L AND D,E
 04BA 7E           1141          MOV     A,M       ;REMOVE ANY SIGN OR OVERFLOW BITS
 04BB E60F         1142          ANI     0FH
 04BD 77           1143          MOV     M,A
 04BE CD6A05       1144          CALL    MULT24    ;SQUARE CURRENT
 04C1 21C420       1145          LXI     H,DACC
 04C4 7E           1146          MOV     A,M       ;RESTORE LOW BYTE AND ZERO ACCUMULATOR
 04C5 32B120       1147          STA     RMSCN+17
 04C8 AF           1148          XRA     A
 04C9 77           1149          MOV     M,A
 04CA 23           1150          INX     H
 04CB 7E           1151          MOV     A,M       ;RESTORE HIGH BYTE AND ZERO ACCUMULATOR
 04CC 32B020       1152          STA     RMSCN+16
 04CF AF           1153          XRA     A
 04D0 77           1154          MOV     M,A
 04D1 3AB020       1155          LDA     RMSCN+16 ;FETCH HIGH BYTE OF I SQUARED
 04D4 DE11         1156          SBI     ILIMT    ;TEST FOR MACHINE RUNNING I)ILIMIT
 04D6 113B06       1157          LXI     D,SMATX  ;LOAD ADDRESS OF RUNNING MATRIX
 04D9 DADF04       1158          JC      CALA
 04DC 11DB06       1159          LXI     D,RMATX  ;LOAD ADDRESS OF STATIONARY MATRIX
 04DF 21B220       1160 CALA:    LXI     H,TRAM   ;LOAD START ADDRESS OF TEMPORARY
 04E2 22C220       1161          SHLD    TRADD    ;RAM AND SAVE
 04E5 0608         1162          MVI     B,8      ;B CONTAINS ROW COUNT
 04E7 21A020       1163 CALB:    LXI     H,RMSCN  ;LOAD RAM TABLE
 04EA 0E09         1164          MVI     C,9      ;C CONTAINS COLUMN COUNT
 04EC CD6A05       1165 CALD:    CALL    MULT24
 04EF 0D           1166          DCR     C        ;PERFORM 9 ROW MULTIPLICATIONS,
 04F0 C2EC04       1167          JNZ     CALD     ;THE 8 TEMPERATURE AND ONE I**2
 04F3 C5           1168          PUSH    B        ;SAVE COUNT
 04F4 1A           1169          LDAX    D
 04F5 47           1170          MOV     B,A      ;ADD GENERATION CONSTANT TERM TO ACCUMULATOR
 04F6 3E80         1171          MVI     A,80H
 04F8 A0           1172          ANA     B        ;REDUCE HIGH BYTE IF CONSTANT
 04F9 CA0305       1173          JZ      CALH     ;IS NEGATIVE
 04FC 3AC620       1174          LDA     DACC+2
 04FF 3D           1175          DCR     A
 0500 32C620       1176          STA     DACC+2
```

```
LOC  OBJ          LINE        SOURCE STATEMENT

0503 13           1177 CALH:  INX     D
0504 1A           1178        LDAX    D       ;ADD IN CONSTANT
0505 4F           1179        MOV     C,A
0506 13           1180        INX     D
0507 CDBD05       1181        CALL    ADD24
050A C1           1182        POP     B       ;RETRIEVE ROW COUNT
050B 2AC220       1183        LHLD    TRADD
050E 3AC620       1184        LDA     DACC+2  ;LOAD RESULT ADDRESS
0511 77           1185        MOV     M,A     ;AND STORE ROW TEMPERATURE
0512 23           1186        INX     H
0513 3AC520       1187        LDA     DACC+1
0516 77           1188        MOV     M,A
0517 23           1189        INX     H
0518 22C220       1190        SHLD    TRADD
051B 21C420       1191        LXI     H,DACC
051E 0E03         1192        MVI     C,3
0520 AF           1193        XRA     A
0521 77           1194 CALE:  MOV     M,A     ;ZERO ACCUMULATOR
0522 0D           1195        DCR     C
0523 23           1196        INX     H
0524 C22105       1197        JNZ     CALE
0527 05           1198        DCR     B       ;DECREMENT ROW COUNT
0528 C2E704       1199        JNZ     CALB    ;LOOP TO CALCULATE NEXT VALUE
052B 11B220       1200        LXI     D,TRAM
052E 21A020       1201        LXI     H,RMSCN
0531 0610         1202        MVI     B,16
0533 1A           1203 CALF:  LDAX    D
0534 77           1204        MOV     M,A     ;RELOAD NEW RESULTS
0535 23           1205        INX     H       ;FROM TEMPORARY REGISTER
0536 13           1206        INX     D       ;TRAM TO RMSCN
0537 05           1207        DCR     B
0538 C23305       1208        JNZ     CALF
053B 212020       1209        LXI     H,DSTOR+27
053E 11AB20       1210        LXI     D,RMSCN+11
0541 2B           1211 CALG:  DCX     H       ;LOAD NEW TEMPERATURES TO 12 BIT ACCURACY
0542 1A           1212        LDAX    D       ;INTO DISPLAY REGISTERS,AND OFFSET WITH AMBIENT
0543 4F           1213        MOV     C,A     ;MOVE CALCULATED VALUES INTO
0544 1B           1214        DCX     D       ;B,C
0545 1A           1215        LDAX    D
0546 47           1216        MOV     B,A
0547 1B           1217        DCX     D
0548 E5           1218        PUSH    H       ;SAVE DISPLAY ADDRESS
0549 2E04         1219        MVI     L,04
054B AF           1220 CALX:  XRA     A       ;CLEAR CARRY
054C 78           1221        MOV     A,B
054D 1F           1222        RAR
054E 47           1223        MOV     B,A     ;DIVIDE CALCULATED VALUE
054F 79           1224        MOV     A,C     ;BY 16
0550 1F           1225        RAR
```

```
 LOC  OBJ          LINE        SOURCE STATEMENT

 0551 4F           1226         MOV     C,A
 0552 2D           1227         DCR     L
 0553 C24B05       1228         JNZ     CALX
 0556 E1           1229         POP     H        ;RETRIEVE DISPLAY ADDRESS
 0557 3A0D20       1230         LDA     DSTOR+8
 055A 81           1231         ADD     C        ;ADD IN AMBIENT TEMPERATURE
 055B 77           1232         MOV     M,A      ;AND STORE
 055C 2B           1233         DCX     H
 055D 3A0C20       1234         LDA     DSTOR+7
 0560 88           1235         ADC     B
 0561 77           1236         MOV     M,A
 0562 2B           1237         DCX     H        ;MOVE TO NEXT DISPLAY ADDRESS
 0563 7D           1238         MOV     A,L      ;TEST IF ALL VALUES HAVE BEEN TRANSFERED
 0564 FE0E         1239         CPI     LOW DSTOR+9
 0566 C24105       1240         JNZ     CALG
 0569 C9           1241         RET
                   1242 ;
                   1243 ;*****************************************************************************
                   1244 ;
                   1245 ; SUBROUTINE MULT24
                   1246 ; CALLS: MULT16,ADD24
                   1247 ; DESCRIPTION: THE ROUTINE MULTIPLIES THE TWO 16 BIT NUMBERS
                   1248 ;              CONTAINED AT ADDRESSES H,L AND D,E AND ADDS
                   1249 ;              THE MOST SIGNIFICANT 24 BITS INTO AN ACCUMULATOR
                   1250 ;              AT DACC.IT INCREMENTS THE INPUT ADDRESSES.
                   1251 ;
 056A C5           1252 MULT24: PUSH    B
 056B 1A           1253         LDAX    D
 056C 46           1254         MOV     B,M
 056D CD9A05       1255         CALL    MULT16   ;PRODUCT OF MOST SIGNIFICANT BYTES
 0570 E5           1256         PUSH    H
 0571 2AC520       1257         LHLD    DACC+1
 0574 09           1258         DAD     B        ;ADD INTO TOP OF 24 BIT ACCUMULATOR
 0575 22C520       1259         SHLD    DACC+1
 0578 E1           1260         POP     H
 0579 23           1261         INX     H
 057A 46           1262         MOV     B,M
 057B CD9A05       1263         CALL    MULT16   ;PRODUCT OF MSB OF D,E WITH LSB OF H,L
 057E CDBD05       1264         CALL    ADD24    ;ADD TO ACCUMULATOR
 0581 13           1265         INX     D
 0582 2B           1266         DCX     H
 0583 1A           1267         LDAX    D
 0584 46           1268         MOV     B,M
 0585 CD9A05       1269         CALL    MULT16   ;PRODUCT OF LSB OF D,L WITH MSB OF H,L
 0588 CDBD05       1270         CALL    ADD24    ;ADD TO ACCUMULATOR
 058B 23           1271         INX     H
 058C 46           1272         MOV     B,M
 058D CD9A05       1273         CALL    MULT16   ;PRODUCT OF LEAST SIGNIFICANT BYTES
 0590 48           1274         MOV     C,B
```

```
 LOC  OBJ          LINE        SOURCE STATEMENT

 0591 0600         1275          MVI     B,0     ;TRANSFER MSB OF THIS PRODUCT TO C
 0593 CDBD05       1276          CALL    ADD24   ;ADD ONLY SHIFTED MSB TO ACCUMULATOR

 0596 23           1277          INX     H
 0597 13           1278          INX     D
 0598 C1           1279          POP     B
 0599 C9           1280          RET
                   1281 ;
                   1282 ;*****************************************************************************
                   1283 ;
                   1284 ; SUBROUTINE MULT16
                   1285 ; CALLS: ADD24
                   1286 ; DESCRIPTION: THE TWO 8 BIT NUMBERS IN THE ACCUMULATOR AND REGISTER B
                   1287 ;              ARE MULTIPLIED TOGETHER AND THE ANSWER IS GIVEN IN B,C
                   1288 ;
                   1289 ;
 059A D5           1290 MULT16: PUSH    D
 059B E5           1291         PUSH    H
 059C 210000       1292         LXI     H,00    ;ZERO H,L
 059F 48           1293         MOV     C,B
 05A0 0600         1294         MVI     B,0     ;ZERO B
 05A2 1E08         1295         MVI     E,8     ;LOAD A COUNY OF 8
 05A4 0F           1296 M16A:   RRC
 05A5 57           1297         MOV     D,A     ;ROTATE ACCUMULATOR AND SAVE IN D
 05A6 D2AA05       1298         JNC     M16B
 05A9 09           1299         DAD     B       ;ADD IN B,C TO H,L IF CARRY IS SET
 05AA 1D           1300 M16B:   DCR     E       ;REDUCE COUNT
 05AB CAB805       1301         JZ      M16C    ;EXIT IF ZERO
 05AE 79           1302         MOV     A,C
 05AF 17           1303         RAL
 05B0 4F           1304         MOV     C,A
 05B1 78           1305         MOV     A,B     ;ROTATE B,C LEFT
 05B2 17           1306         RAL
 05B3 47           1307         MOV     B,A
 05B4 7A           1308         MOV     A,D
 05B5 C3A405       1309         JMP     M16A    ;RETURN TO START
 05B8 44           1310 M16C:   MOV     B,H
 05B9 4D           1311         MOV     C,L     ;SAVE ANSWER IN B,C
 05BA E1           1312         POP     H
 05BB D1           1313         POP     D
 05BC C9           1314         RET
                   1315 ;
                   1316 ;*****************************************************************************
                   1317 ;
                   1318 ; SUBROUTINE ADD24
                   1319 ; CALLS: NOTHING
                   1320 ; DESCRIPTION: THE 16 BIT NUMBER CONTAINED IN B,C IS ADDED INTO
                   1321 ;              A 24 BIT ACCCUMULATOR LOCATED AT DACC
                   1322 ;
                   1323 ;
```

```
LOC  OBJ          LINE        SOURCE STATEMENT

05BD E5           1324 ADD24: PUSH    H
05BE 2AC420       1325        LHLD    DACC     ;LOAD LOWER BYTES OF ACCUMULATOR
05C1 09           1326        DAD     B        ;ADD IN B,C
05C2 22C420       1327        SHLD    DACC
05C5 D2CC05       1328        JNC     A24A
05C8 21C620       1329        LXI     H,DACC+2
05CB 34           1330        INR     M        ;INCREASE HIGH BYTE IF CARRY
05CC E1           1331 A24A:  POP     H
05CD C9           1332        RET
                  1333 ;
```

APPENDIX A9

DESCRIPTION OF SOFTWARE USED TO MEASURE TEMPERATURES IN THE INDUCTION MOTOR

The appendix describes the following details of the thermal data logging software, that was based around the SDK85 development system[47].

1) External connections to the development system
2) Signal scaling
3) Monitor Command Routines
4) Tape punch Format
5) Program Structure

A9.1 EXTERNAL CONNECTIONS TO THE DEVELOPMENT SYSTEM

The external connections to the ports on the 8755 and 8155 integrated circuits in the SDK85 development system are given in Table A9.1. Both the tape punch and the ICL7109 A/D converter[55] were handshaked to the 8155 ports by using the method described in the application notes[46] for this integrated circuit. A link is required between the RST 6.5 interrupt on the 8085 micro-processor and an 8155 port, apart from this the development system remains unchanged.

A9.2 SIGNAL SCALING

The inputs to the A/D convertor were scaled to give a full scale 12 bit output from the convertor at

temperatures, current, voltage and powers of 204.8°C, 20.48 Amps, 409.6 Volts, 4.096kW respectively.

A9.3 MONITOR COMMANDS

Five Monitor Commands were available and these are listed together with their function in Table A9.2. The monitor commands are entered by pressing the appropriate key on the SDK 85 development system and are executed by successive application of the 'NEXT' key. During the execution of a command a code word will be shown on the left hand side of the display and the present set value on the right. This value may be altered by using the hexadecimal keypad. If an incorrect sequence of key operations is made a error message will be displayed and the command will be terminated.

A9.4 TAPE PUNCH FORMAT

The standard ASCII binary tape format was used with an even parity bit. The data is punched as an ASCII sequential file named :EE35.DFILE. Each record consists of a series of five digit numbers separated by a single space. The first number on each record is always the time of the print cycle in the format Minutes.Seconds and; remaining entries are in the order of the data stack in the scaling set by the stack word code.

The tape is headed by the command IN :EE35, DFILE,T**** and terminated by ****.

A9.5 PROGRAM STRUCTURE

A five tier program structure was set up in order that the microprocessor time could be utilised fully. This is illustrated in Figure A9.1.

The program execution enters the higher levels only through external interrupts to the processor. Once in a level it can only exit if all the operations in the level have been completed, and then the execution continues in the immediate lower level unless it is interrupted at a higher level.

The highest level of interrupt is initiated from the real time counter in the 8155 integrated circuit. This is used to increase the program timer and also sense the start of an input cycle; when the first data word is selected from the stack and the analogue address of the signal source outputted. The processor then waits for approximately 1ms for the data to stabilise and initiates the A/D conversion. The program now moves to the lower level and a return to the input routine only occurs when a RST 6.5 interrupts informs the processor that the conversion has been completed. This cycle is repeated until all the required data has been read. At the end of each auxiliary cycle, the third program level carries out the thermal calculations taken from the new data and updates the visual display.

The fourth program level consists of the software required to output data to the printer. This section is only accessed at the end of a print cycle; where the required data is fetched from the stack, scaled, converted to five ASCII characters (including the decimal point) and

fed a byte at a time to the tape punch. Because of the interrupt structure several auxiliary input cycles can be performed whilst the slow printing is being completed.

The lowest program level contains the monitor routines. These are accessed from the keyboard, via an interrupt generated from its controller integrated circuit, only when all the other program duties are completed. If the monitor is not required the program execution will idle until an external interrupt restarts the process.

Table A9·1 External Connections to SDK-85 Development System

Data Source Address:- Port 00H

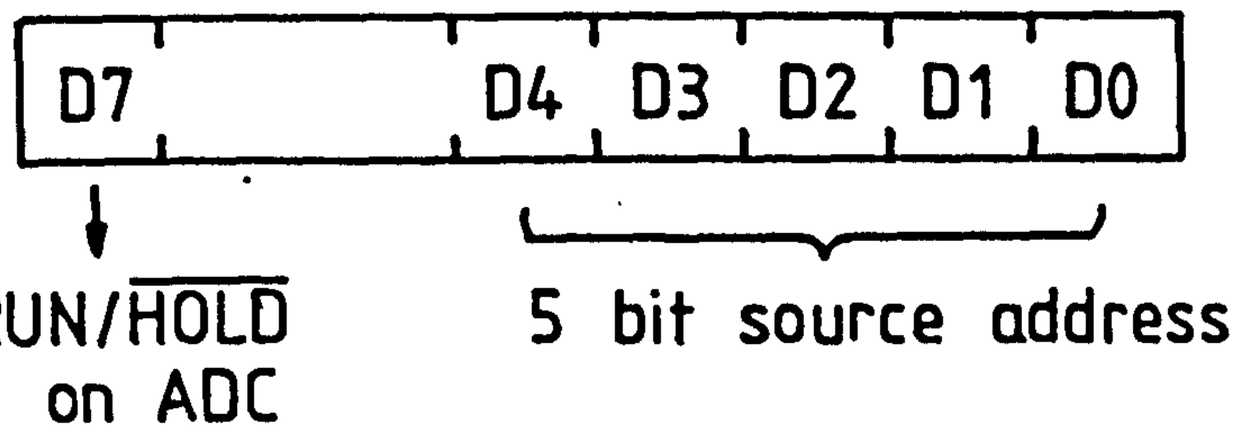

ADC (ICL7109) Input:- Port 21H

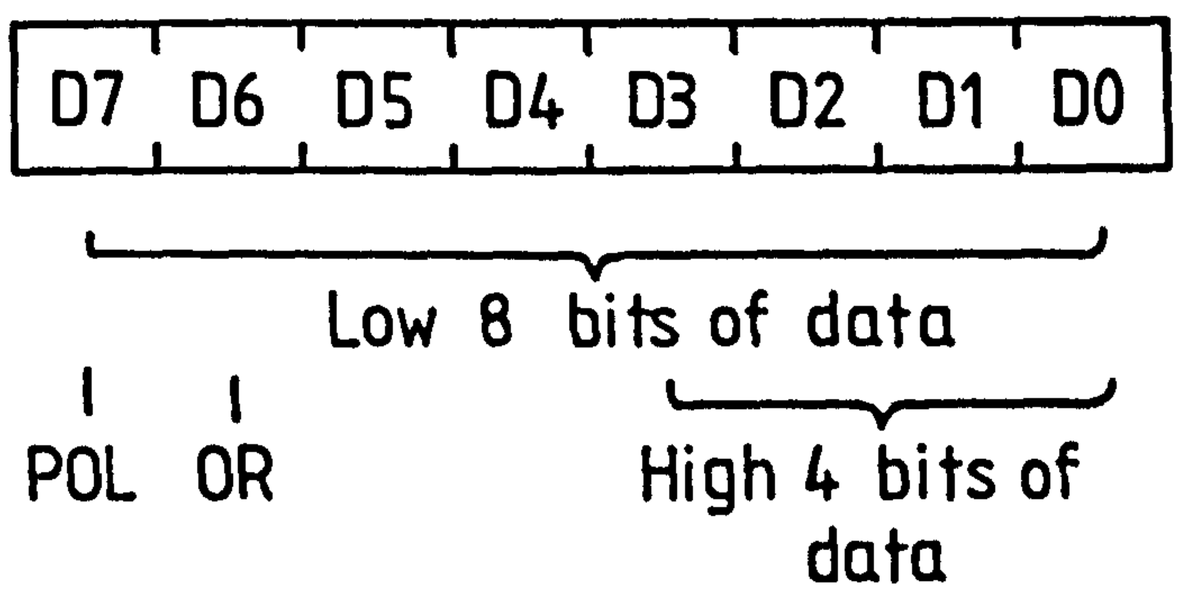

Tape Punch Output:- Port 22H

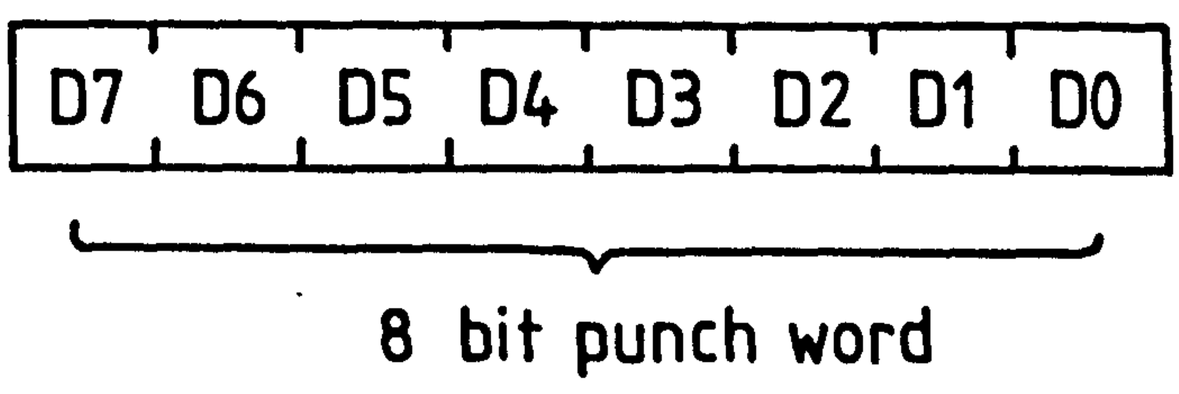

Control:- Port 20H

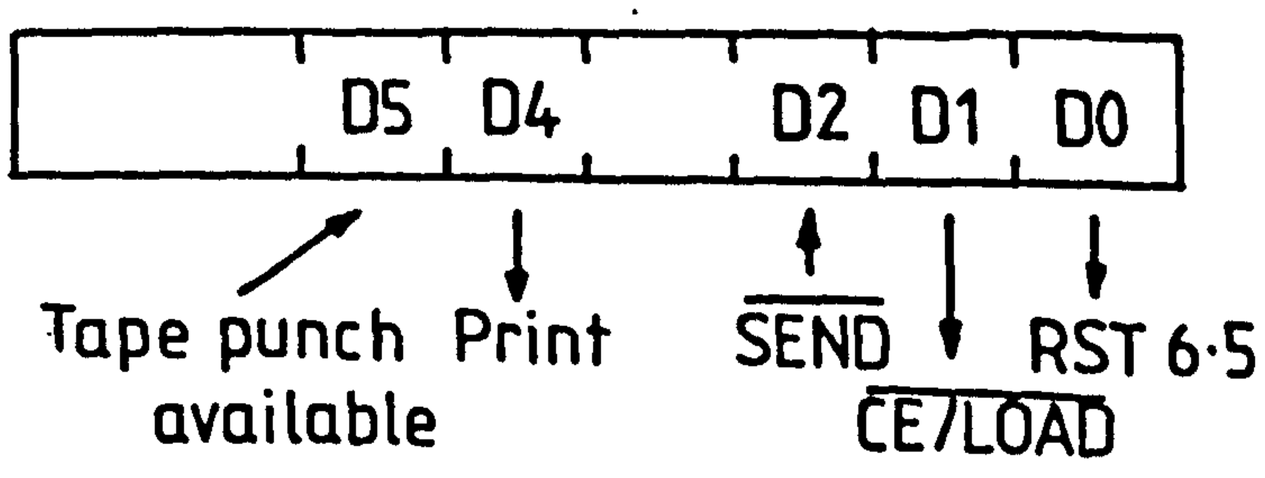

Table A9·2 Monitor Commands

Command	Key	Display	Function
Data Code	EXAM REG	CD00 XX	Sets the hex. identification code and data address for the first word of the data stack.
	NEXT	CD01 XX	As above for the second word.
	⋮		
	NEXT	CD15 XX	Similar for all sixteen words of the data stack.
Time Interval	SINGLE STEP	AU XX	Sets the auxiliary cycle time in decimal seconds.
	NEXT	Pr XX	Sets the print cycle time in decimal minutes. An input of zero will set the print time equal to the auxiliary cycle time.
Display	EXEC	DSP XX	The data which has the decimal source address that is set with, this command will be displayed on exit from the monitor. An input greater than 16 will display the time.
Go	GO	GO	Prints the header on the punched tape and initialises the data logging software.
	NEXT		Starts the execution of the data logging and thermal calculations.
Stop	GO	SP	Stops the data logging after the completion of the next print cycle and prints the tape terminator.
Error	Any Key	Err	An invalid key has been pressed. Return to monitor.

All commands except 'Stop' are executed with the 'Next' key.

XX Data field will display the current value set by the command and can be changed by hexidecimal or decimal input from the keypad.

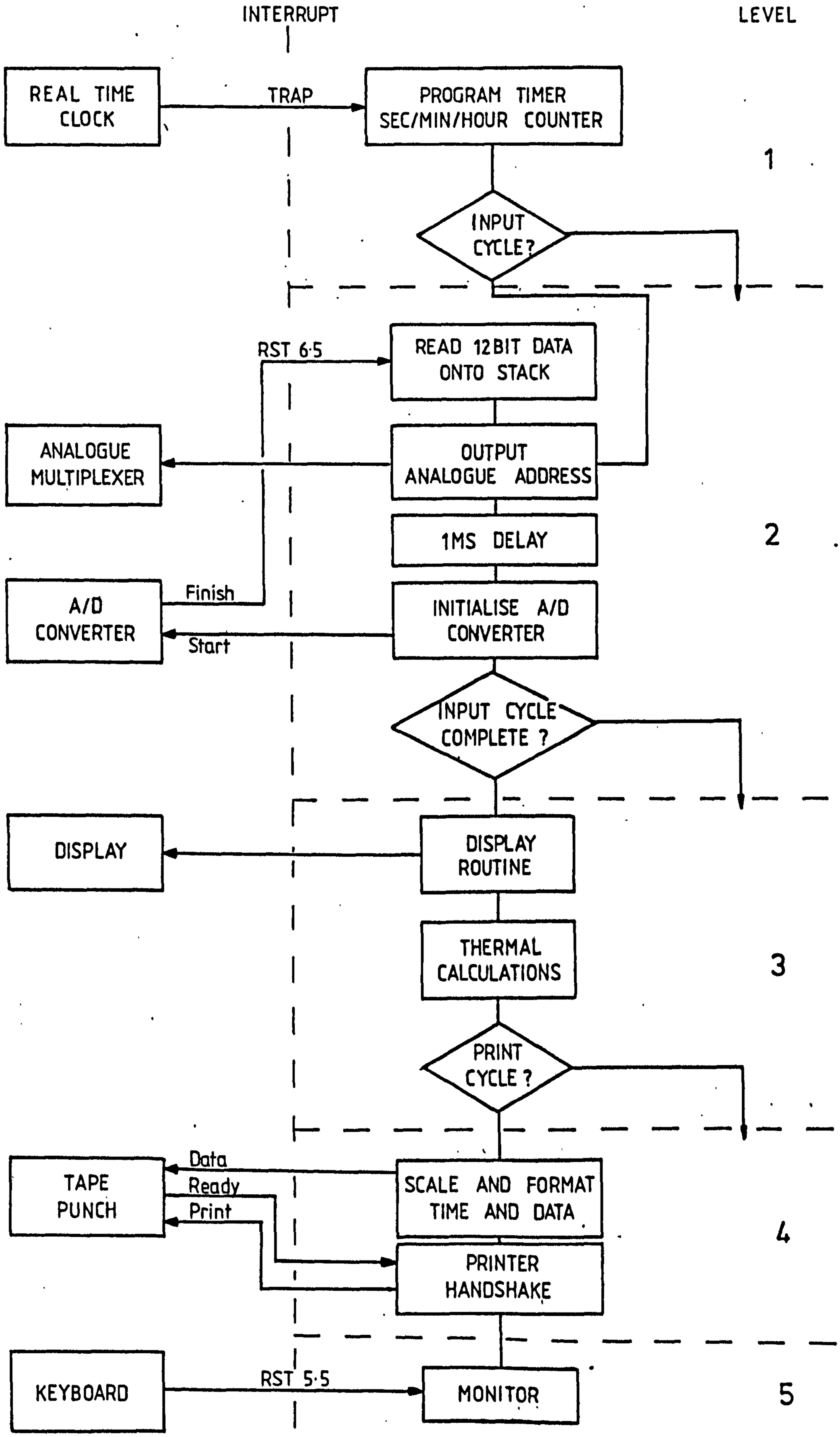

Figure A9·1 Software Hierarchy

APPENDIX A10

PUBLICATIONS

IMPROVING MULTI-PUMP SYSTEM EFFICIENCY

A report to Bass Brewing Ltd.

from

P.H. Mellor and D. R. Turner

The University of Liverpool

1. Introduction

In an earlier paper[1] it has been shown that significant energy savings can be achieved in a multi-machine system by a careful selection of the control parameters. This report applies the principles in that paper to a particular multi-machine system and investigates their effects upon the overall system performance.

The system investigated is the pumping station that provides the cold glycol which is used in the refrigeration processes of the plant. The station consists of four pump-motor sets that are operated in parallel, details of which are given in Fig. 1. The control of the station is such that the pump-motor sets are switched on or off to meet changes in the demand of the plant coolant flow. The actual values of flow at which this switching occurs effects the overall energy consumption of the pumping station, for a given plant flow demand. This report investigates the effects of changes in those flow switching limits for a typical weakly plant flow demand.

A summary of the equations used in the theoretical model of the system is included in the final section of the report. The mathematics of these equations are based upon the theory presented in the original paper[1].

2. Experimental Results

Over a period of one week the glycol flow and the power input to the motor-pump sets were monitored using a microprocessor based data logging device coupled to a PET microcomputer (Fig. 2). The results obtained over the week are summarised in table 1. It can be seen that there is discrepancy between the actual values of flow at which the machines are switched and the preset values on the controller. Data was only available for three of the motor-pump sets as the flow demand was not sufficiently large for it to be necessary to use the fourth set.

Figure 3 shows a comparison of the power input flow relationship obtained from the measurements with those of a theoretical model, equations (1) and (2), based on manufacturers data. The difference between the measured and the manufacturers data is attributed to an increase in the constant power losses of the machine sets; that is the rotational friction losses of the driving shaft and the pump impellers. This suggests that cleaning the pumps could lead to a possible improvement of 3 kw in the power consumed by each of the pump-motor sets. In order to compensate for this additional loss the constant or 'a' term in the loss function of the machine (equation 1) is increased to give a modified fit to the data (Fig. 3).

The glycol flow distribution for the week measured is shown as a histogram in Figure 4, which is compared with the assumed 'Beta' distribution function used for the theoretical evaluation of the system losses and power consumption. Figures 5 and 6 give a comparison of the measured motor-pump power input distributions with those evaluated from the theoretical load distribution function through the use of equation (8) and the modified loss function. It can be seen that there exists a good agreement between these theoretical distributions and the observed data.

Using the theoretical descriptions of the system the optimum flow switching limits can be found, and the effects of them upon the system evaluated. Table 2 summarises the system performance over the week measured for the switching limits used at present, the optimum limits and for switching limits of 10% and 15% above those used at present. A substantial reduction in the system power consumption is achieved by applying the optimum limits, but these limits would require an excessive overloading of the pump motor sets. However a 10% or 15% increase in the switching limits towards the optimum would still achieve savings in energy, estimated at 4.7% and 6.1% of total energy or 7.9% and

10.0% of present losses respectively.

3. Theoretical Equations

It is not proposed to cover the theoretical development of the equations used in this report. For the notation used in the following equation reference should be made to the additional paper[1]. However, since at any time the system demand on the pumping station is a specific flow of coolant, in the following equations the systems are modelled in terms of the glycol flow, Q, rather than the absolute power P. The actual power outputted by the pumping station for a specific flow Q depends upon the system head which is a function of the loading on the individual pumps running at that time. The power losses and the output power in each of the individual pump-motor sets are modelled as quadratic functions of the flow Q by a loss function $\gamma(Q)$ and a head function $H(Q)$ such that

$$\text{Power loss} = Q\ \gamma(Q) \qquad -(1)$$

$$\text{Power output} = Q\ H(Q) \qquad -(2)$$

Where $\gamma(Q)$ and $H(Q)$ are of the form

$$\gamma(Q) = \frac{a}{Q} + b + \frac{Q}{c} \qquad -(3)$$

$$H(Q) = \frac{d}{Q} + e + \frac{Q}{F} \qquad -(4)$$

For constants a to f Table 3 gives the values of these constants from data supplied from the manufacturers of the pumps and motors.

The optimisation theory[1] shows that the optimum switching limits Q_{lr}, for the r = 1 to 4 pump motor sets can be determined from the solution of the equation

$$\gamma(Q_{lr}) = \gamma\left(\frac{r}{r+1}\ Q_{lr}\right) \qquad (5)$$

In order to evaluate the effects of the switching limits on a specific

weekly system flow demand, it is necessary to represent the flow in terms of a frequency distribution $f(Q)$. This distribution is modelled as a Beta[2] function with the same mean and variance of the system load. The power losses and total output power can thus be evaluated from the loss and head functions by means of the following equations

$$\text{Total losses} = \sum_{r=1}^{n} r^2 \int_{\frac{r-1}{r} Q\,l_{r-1}}^{Q\,l_r} Q\,\gamma(Q)\,f(r\,Q)\,dQ \qquad (6)$$

$$\text{Output power} = \sum_{r=1}^{n} r^2 \int_{\frac{r-1}{r} Q\,l_{r-1}}^{Q\,l_r} Q\,H(Q)\,f(rQ)\,dQ \qquad (7)$$

In addition the input power distribution $g_r(P)$ for each of the r motor-pump sets can be obtained in terms of their output power P from the load distribution $f(Q)$ from the equation below.

$$g_r(P) = \sum_{i=r}^{n} \cdot 1\; f(iQ) \Big/ \frac{dP}{dQ} \qquad -(8)$$

Where $P = Q(\gamma(Q) + H(Q))$

4. References

1. Mellor, P.H., Turner, D.R. "Efficiency optimisation of multi-machine systems", UPEC. Sheffield 1981.

2. Pearson, E.S., Johnson, N.L. "Tables of the Incomplete Beta Function", Cambridge Univ. Press, Cambridge, England, 1958.

Table 1 Load Data of Experimental Week

Mean Glycol Flow		m^3/hr	330
Energy Consumption Of Each Pump Motor Set	1	MW hr	5·3
	2	MW hr	3·5
	3	MW hr	2·3
	4	MW hr	0·0
Total Energy Input		MW hr	11·1
Measured Switching Limits	Q_{l_1}	m^3/hr	245
	Q_{l_2}	m^3/hr	407

Table 2

Variation In System Performance With Switching Limits

Case			①	②	③	④
Switching Limits	Q_{l_1}	m^3/hr	245	255	267	381
	Q_{l_2}	m^3/hr	407	510	534	661
	Q_{l_3}	m^3/hr	696	766	800	1000
	Q_{l_4}	m^3/hr	1000	1000	1000	—
Total Loss		MW-hr	4.7	4.3	4.2	3.9
Total Input		MW-hr	11.1	10.6	10.4	9.4
Efficiency		%	57.6	59.0	59.3	58.5
Minimum System Head		mWg	38	37	35	20
Percentage Of Time That Pumps Are Running	1	%	100	100	100	100
	2	%	62	60	57	37
	3	%	33	19	16	6
	4	%	0	0	0	0
Percentage Of Time That Motors Are Overloaded	1	%	0	0	0.9	36.0
	2	%	0	0	0.5	11.2
	3	%	0	0	0	0
	4	%	0	0	0	0

Case ① Present day rated

② 10 % Overload

③ 15% Overload

④ Optimum

Table 3 Loss And Head Function Parameters

Loss Function $\Upsilon(Q)$

a	23·3
b	-0·138
c	2750

Units of Q - m^3/hr

$Q\Upsilon(Q)$ - kW

Modified 'a' parameter - 26·5

Head Function H(Q)

d	-6·50
e	0·218
f	-2820

Units of Q - m^3/hr

QH(Q) - kW

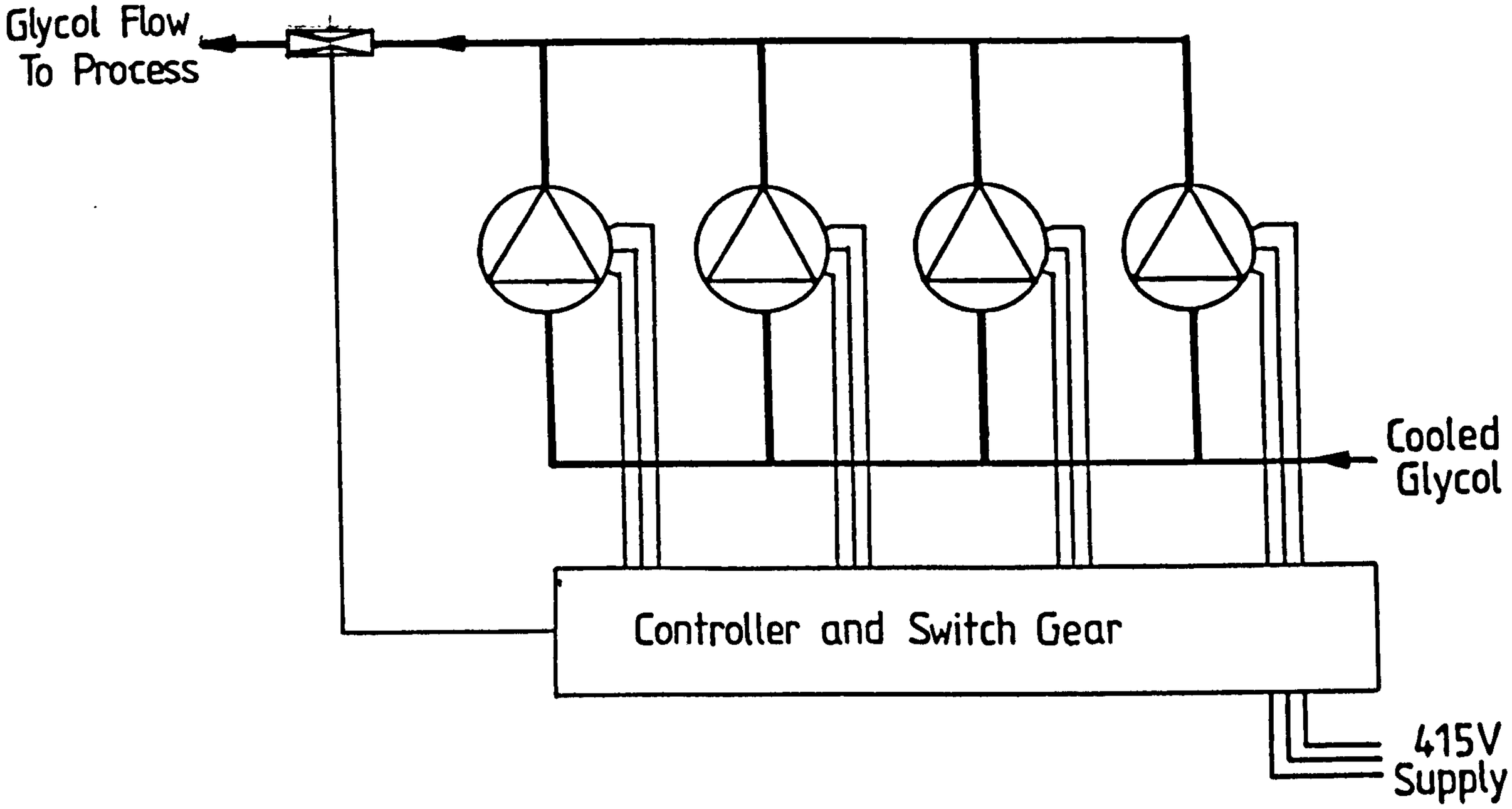

Fig. 1

Key

- Motor Pump Set
- Pipe Line
- 3 ϕ 415V Supply
- Current Transformer
- Dahl Tube

Fig. 2

GRAPH OF PUMP-MOTOR

INPUT POWER AGAINST FLOW

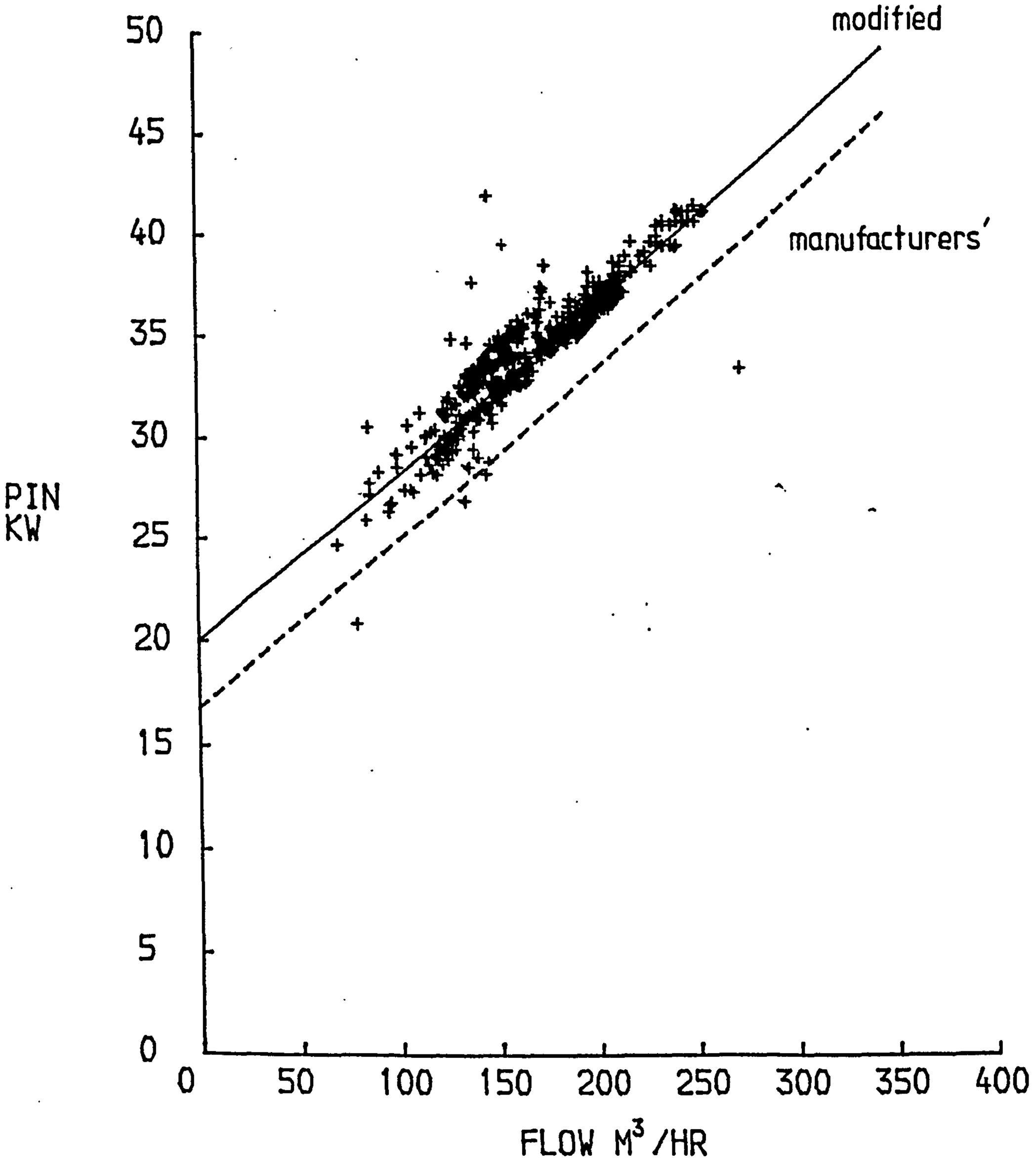

Fig 3

SYSTEM LOAD DISTRIBUTION

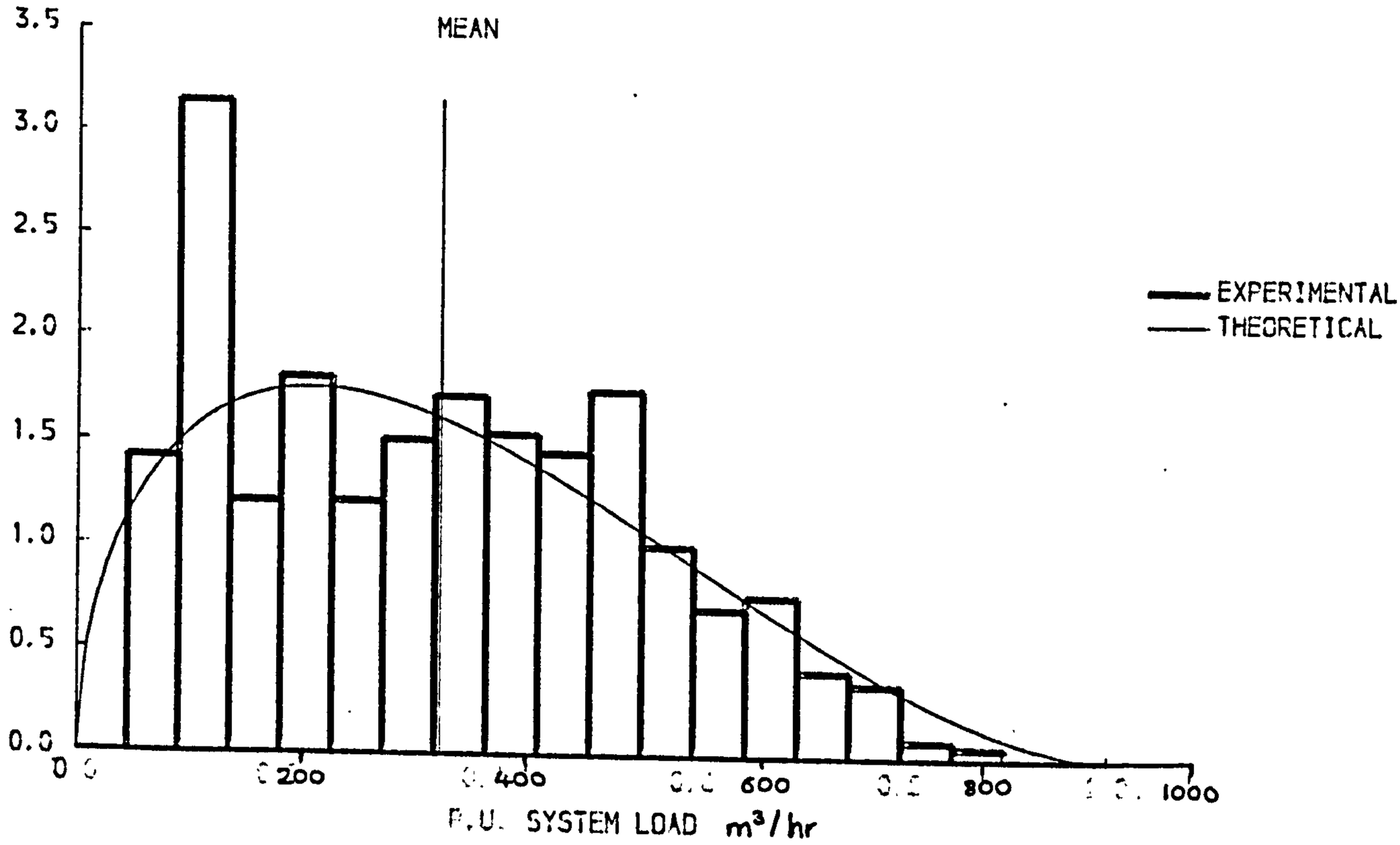

Fig 4

MACHINE NUMBER 1

INPUT LOAD DISTRIBUTION

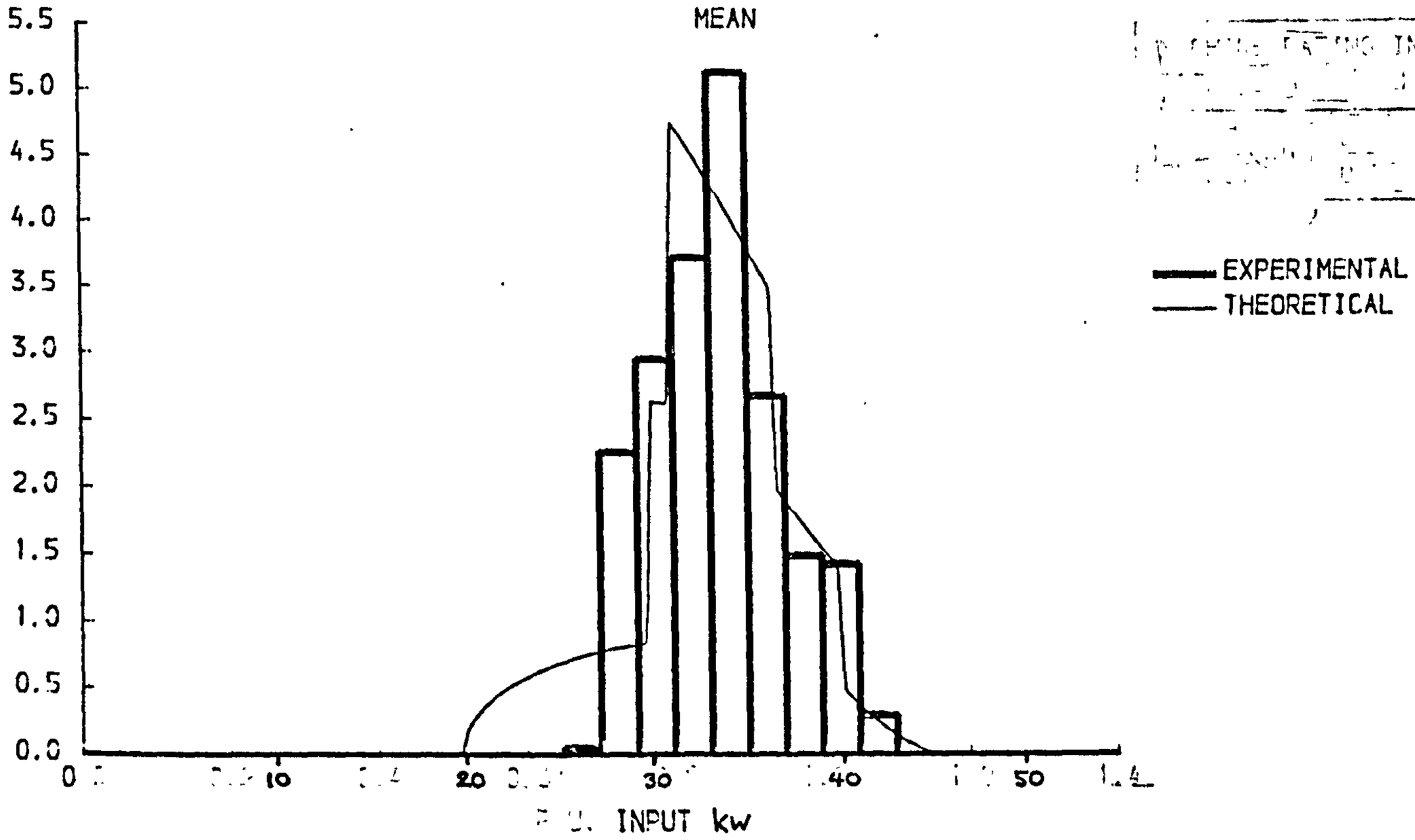

MACHINE NUMEER 2

INPUT LOAD DISTRIBUTION

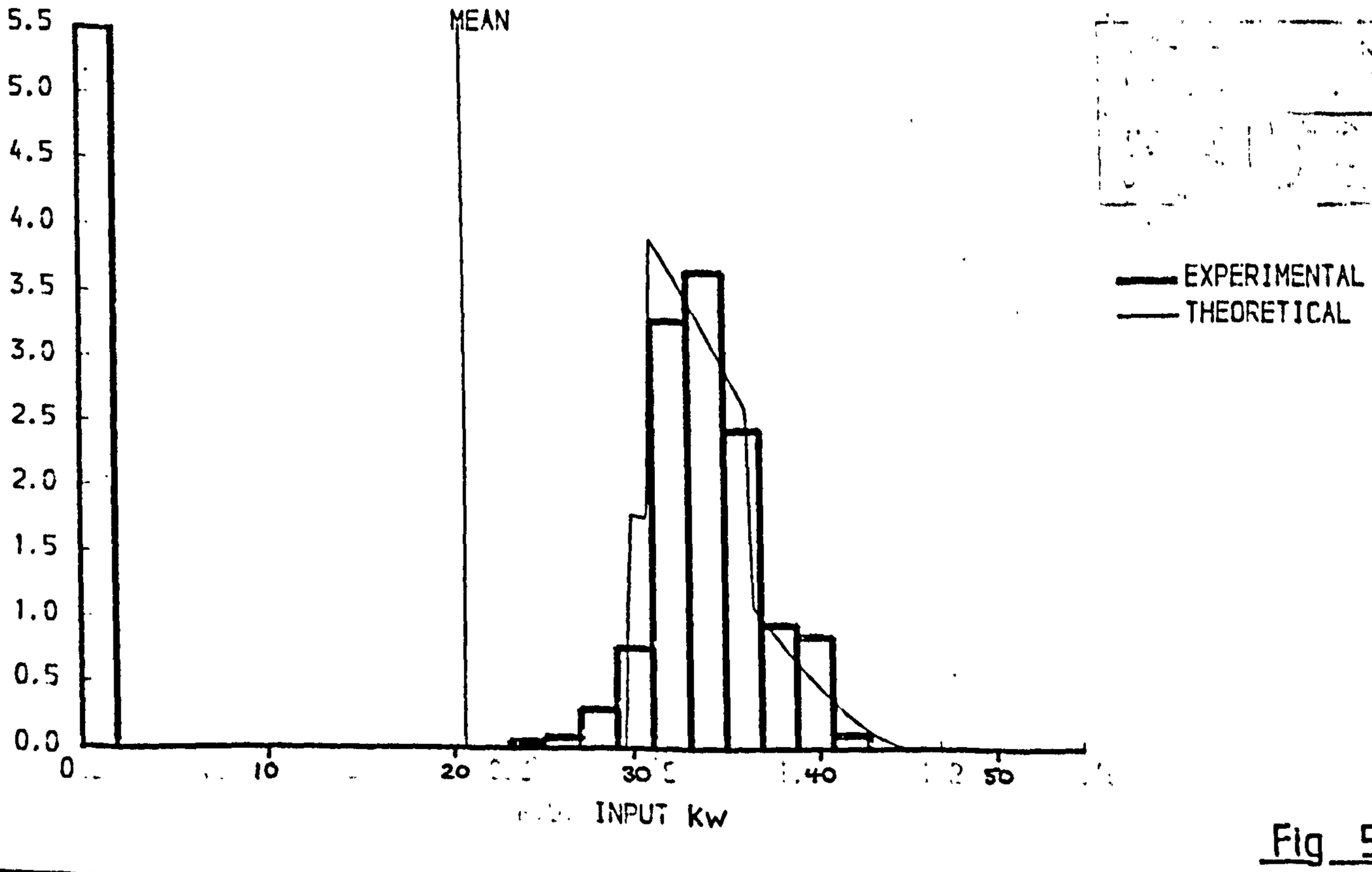

Fig 5

MACHINE NUMBER 3

INPUT LOAD DISTRIBUTION

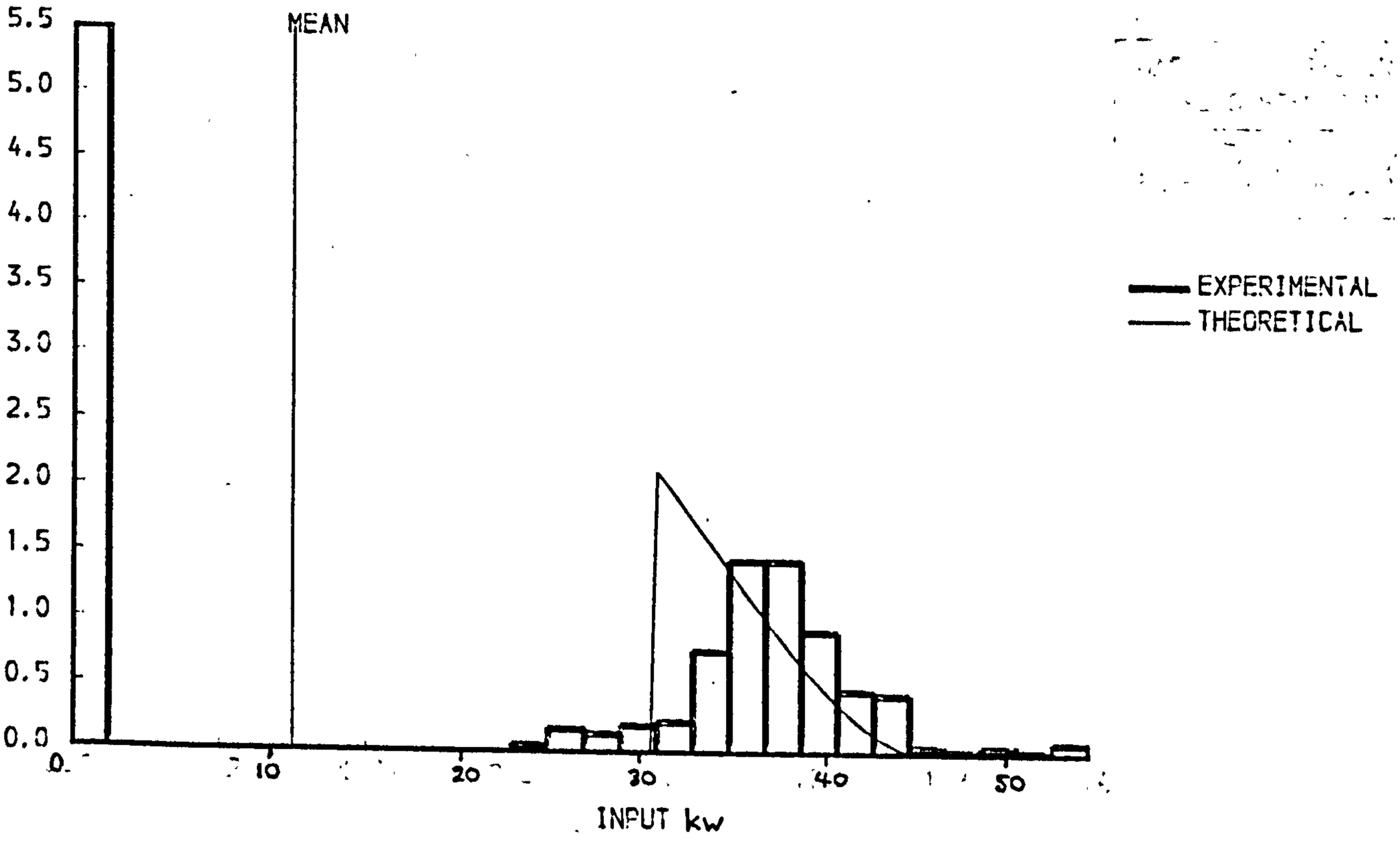

MACHINE NUMBER 4

INPUT LOAD DISTRIBUTION

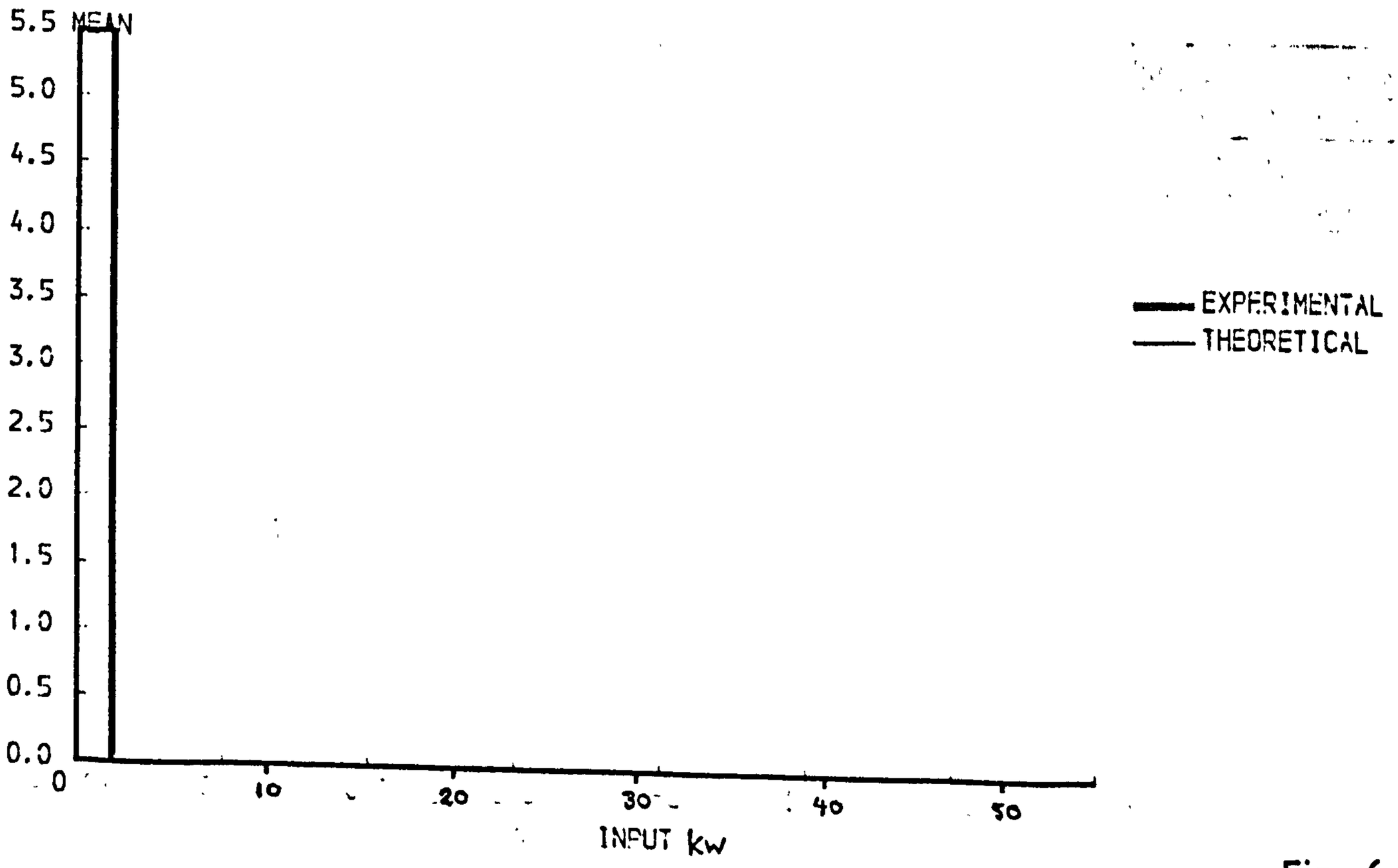

Fig 6

Efficiency optimisation of multi-machine systems

P.H. Mellor and D.R. Turner

The University of Liverpool

Introduction

In many industrial situations large loads are supplied by a number of prime movers operating in parallel. At light load one prime mover supplies the system requirements and when this increases to a predetermined power limit an additional machine is switched on and the load shared between them, and so on as the load increases further.

This paper proposes a method of determining the power switching limits which will give optimum overall system efficiency. The system on which the work was based involved a number of 3 phase induction motors driving pumps to provide a large refrigeration load, but the work is applicable to many types of prime mover.

System Definition

A multi-machine system, where n identical machines are used to provide the load, is considered. Each individual machine has a rated output power of P_α. As the system load reaches prescribed limits machines are either switched on or off, thus if there are r machines running, an additional machine is switched on when the system load reaches rP_{Lr}, that is when the load on each of the r machines reaches, P_{Lr}, the switching limit for this interval.

For a maximum system load of P_{smax} the number of machines, n, must lie between the limits

$$\frac{P_{smax}}{P_{Ln}} \leq n < \frac{P_{smax}}{P_{L(n-1)}} + 1 \qquad (1)$$

The upper limit represents the case when n - 1 machines are sufficient to provide the full system load.

Load Distribution

System loads are often represented by their variation with time over a fundamental period, as shown in Fig. 1. This type of presentation can be transformed into a load frequency distribution f (P), in which the probability of a load occuring is plotted against system load. This transformation is achieved by

$$f(P) = \frac{\Delta t}{\Delta P} \qquad (2)$$

where the area under the load frequency distribution is equal to the time Δt for which the load is in the range

$$P - \tfrac{1}{2}\Delta P, \quad P + \tfrac{1}{2}\Delta P \quad \text{(Fig. 2)}$$

Machine Losses

The losses in a given machine at a load P are defined using a loss function $f_\alpha(P)$, such that

$$\text{Machine losses} = \gamma_\alpha(P)\, P \qquad (3)$$

The subscript α is introduced to allow for variations in the loss function with changes in the machine rating P_α. The loss function is related to the machine's efficiency by the expression

$$\text{Efficiency } \eta_\alpha = \frac{1}{1 + \gamma_\alpha(P)}$$

For a 3 phase induction motor $\gamma_\alpha(P)$ is of the form

$$\frac{P}{a} + \frac{b}{P} \qquad (4)$$

where a and b are constants dependant upon the machine. Subsequent analysis shows that the optimum switching limits are independant of the form of this loss function.

System Losses

In order to derive an expression for the total system loss, the losses when only r machines, L_r, are considered

$$L_r = r \int^{\Delta t_r} \gamma_\alpha(P)\, P\, dt$$

where Δt_r is the time interval during which r machines are operating.

$$\text{Or} \qquad L_r = r \int^{\Delta P_r} \gamma_\alpha(P)\, Pfr(P)\, dP$$

where P_r is the power interval during which r machines run
P is the individual machine loading and
$f_r(P)$ is the load frequency distribution of one of the r machines.

During this interval with r machines running

$$P = P_s/r \text{ , where } P_s = \text{system load}$$

$$\text{and} \qquad f_r(P) = rf(rP)$$

and the system power limits of this interval are $(r-1)\, P_{l(r-1)}$ at the lower end and rP_{lr} at the upper end.

$$\text{Thus} \quad \frac{r-1}{r} P_{l(r-1)} > P \geq P_{lr}$$

$$\text{and hence} \quad L_r = r \int_{\frac{r-1}{r} P_{l(r-1)}}^{P_{lr}} \gamma_\alpha(P) rf(rP)\, P\, dP \text{ ,}$$

The total loss, L_T, is determined by summing the interval losses, L_r, over the system load range

$$L_T = \sum_{\frac{r-1}{r} P_{1(r-1)}}^{} r^2 \int^{P_{1r}} \gamma_\alpha(P)\, P\, f(rP)\, dP \qquad (5)$$

Optimisation of machine switching limits

The optimum switching limits (P_{1r}'s) are those which minimise the total system loss L_T. These canbe achieved by setting the partial derivatives $\partial L_T / \partial P_{1r}$ to zero. Thus for the r th switching limit

$$\frac{\partial L_T}{\partial P1_r} = \frac{\partial}{\partial P_{1r}} \sum_{\frac{r-1}{r} P_{1(r-1)}}^{} r^2 \int^{P_{1r}} \gamma_\alpha(P)\, P\, f(rP)\, dP = 0$$

When performing the differentiation all terms in the summation not containing P_{1r} can be ignored.

$$\frac{\partial L_r}{\partial P_{1r}} = \frac{\partial}{\partial P_{1r}} \left[r^2 \int_{\frac{r-1}{r} P_{1(r-1)}}^{P_{1r}} \gamma_\alpha(P)\, P\, f(rP)\, dP + (r+1)^2 \int_{\frac{r}{r+1} P_{1r}}^{P_{1(r-1)}} \gamma_\alpha(P)\, P f(r+1)P)\, dP \right]$$

The first term in the expression is equal to

$$\frac{\partial}{\partial P_{1r}} \int_0^{P_{1r}} r^2 \gamma_\alpha(P)\, Pf(rP)\, dP - \frac{\partial}{\partial P_{1r}} \int_0^{\frac{r-1}{r} P_{1(r-1)}} r^2 \gamma_\alpha(P)\, Pf(rP)\, dP$$

As $P_{1(r-1)}$ is independant of P_{1r}, the latter part of this expression is zero, giving the result

$$\frac{\partial}{\partial P_{1r}} \int_{\frac{r-1}{r} P_{1r-1}}^{P_{1r}} r^2 \gamma_\alpha(P)\, Pf(rP)\, dP = r^2 \gamma_\alpha(P_{1r})\, P_{1r}\, f(rP_{1r})$$

Similarly

$$\frac{\partial}{\partial P_{1r}} \int_{\frac{r}{r+1}P_{1r}}^{P_{1(r+1)}} (r+1)^2 \gamma_\alpha(P)\, P f(\,(r+1)P)\, dP = \frac{\partial}{\partial P_{1r}} \int_{P_{1r}}^{\frac{r+1}{r}P_{1(r+1)}} r^2 \gamma_\alpha \frac{rP}{r+1}\, P f\,(rP)\, dP$$

$$= -r^2 \gamma_\alpha \frac{rP_{1r}}{r+1} \quad P_{1r} \; f(rP_{1r})$$

Thus

$$\frac{\partial L_T}{\partial P_{1r}} = r^2 P_{1r} f\,(rP_{1r}) \left[\gamma_\alpha\,(P_{1r}) - \gamma_\alpha \left(\frac{rP_{1r}}{rH} \right) \right]$$

Setting $\partial L_T / \partial P_{1r}$ to zero gives the solution

$$\gamma_\alpha(P_{1r}) = \gamma_\alpha \left(\frac{rP_{1r}}{r+1} \right) \qquad (6)$$

The value of P_{1r} which satisfies (6) is the optimum switching limit for the r th machine interval. Fig. 3 shows a typical loss function and illustrates the solutions for the switching limits. As the number of machines running, r, increases, the switching limits will tend towards the power at which an individual machine will operate at minimum losses.

For a 3 phase induction motor with the loss function of equation (4), the solution for the rth switching limit can be shown to be

$$P_{1r} = \sqrt{\frac{(r+1)\ ab}{r}} \qquad (7)$$

The analysis shows clearly that for a given set of machines, the optimum switching limits are independant of the system load. An extension of the work would be to optimise the system losses for variations in the machine rating P_α, so that the optimum size, number and switching limits of prime movers could be found.

Conclusions

In certain industrial situations it is possible to achieve significant energy, and thus financial savings simply by changing the existing switching limits. A study of a local manufacturers plant in which four induction

motors drive centrifugal pumps (table 1 and fig. 3) to circulate refrigerant around a process, suggest that a careful selection of switching limits can reduce the power losses of the plant by 8.3%, that is achieve an energy saving of 2%.

Another important aspect of this type of system is the energy penalty paid if the switching limits are less than the individual machine rating. This is illustrated in fig. 4 which shows the daily losses of the system mentioned above against the maximum switching limit expressed in per unit to the machine/pump rating. It is seen that the curve rises sharply for switching limits below 1.0 p.u. representing an increase in cost.

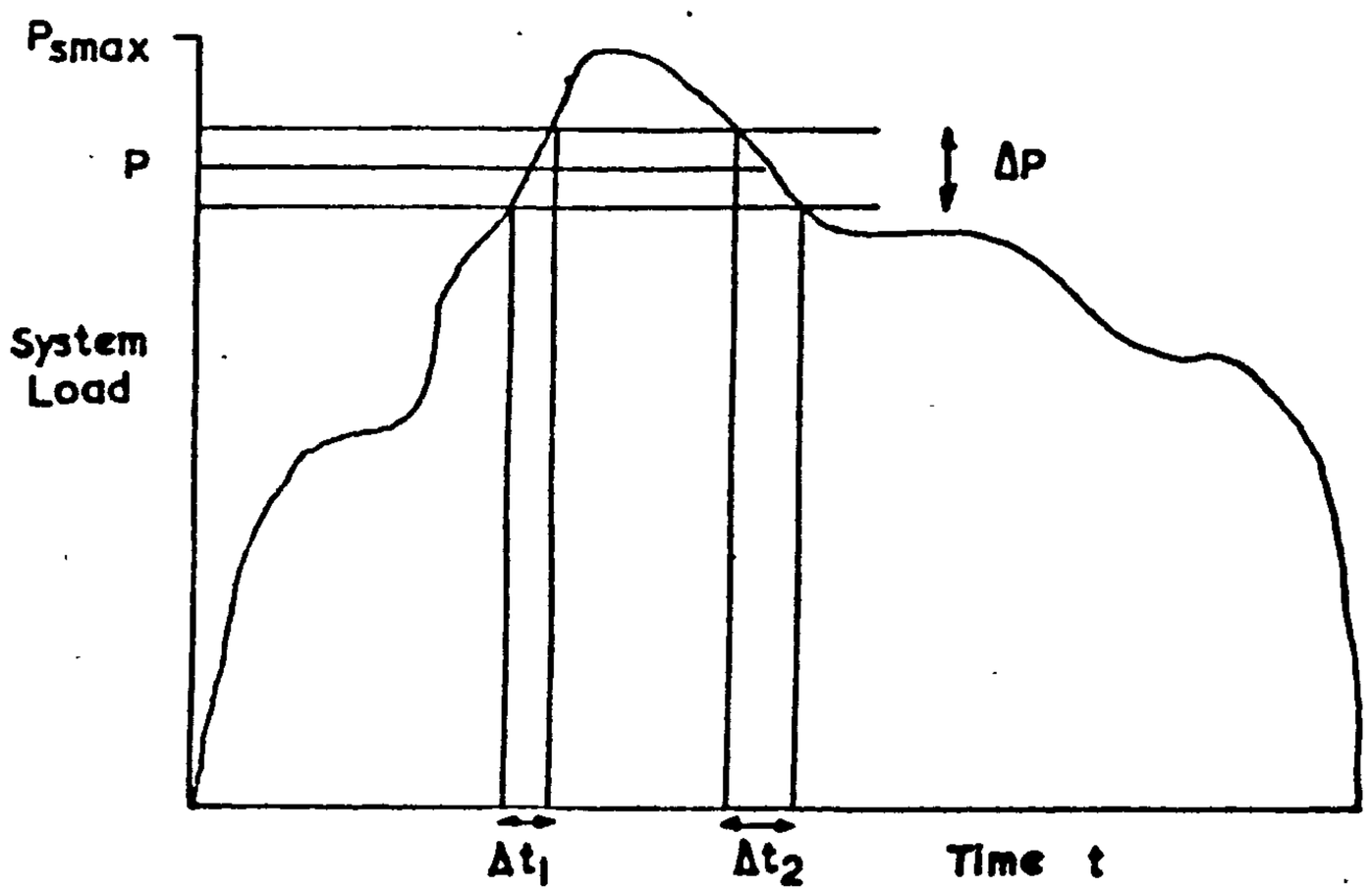

Figure 1

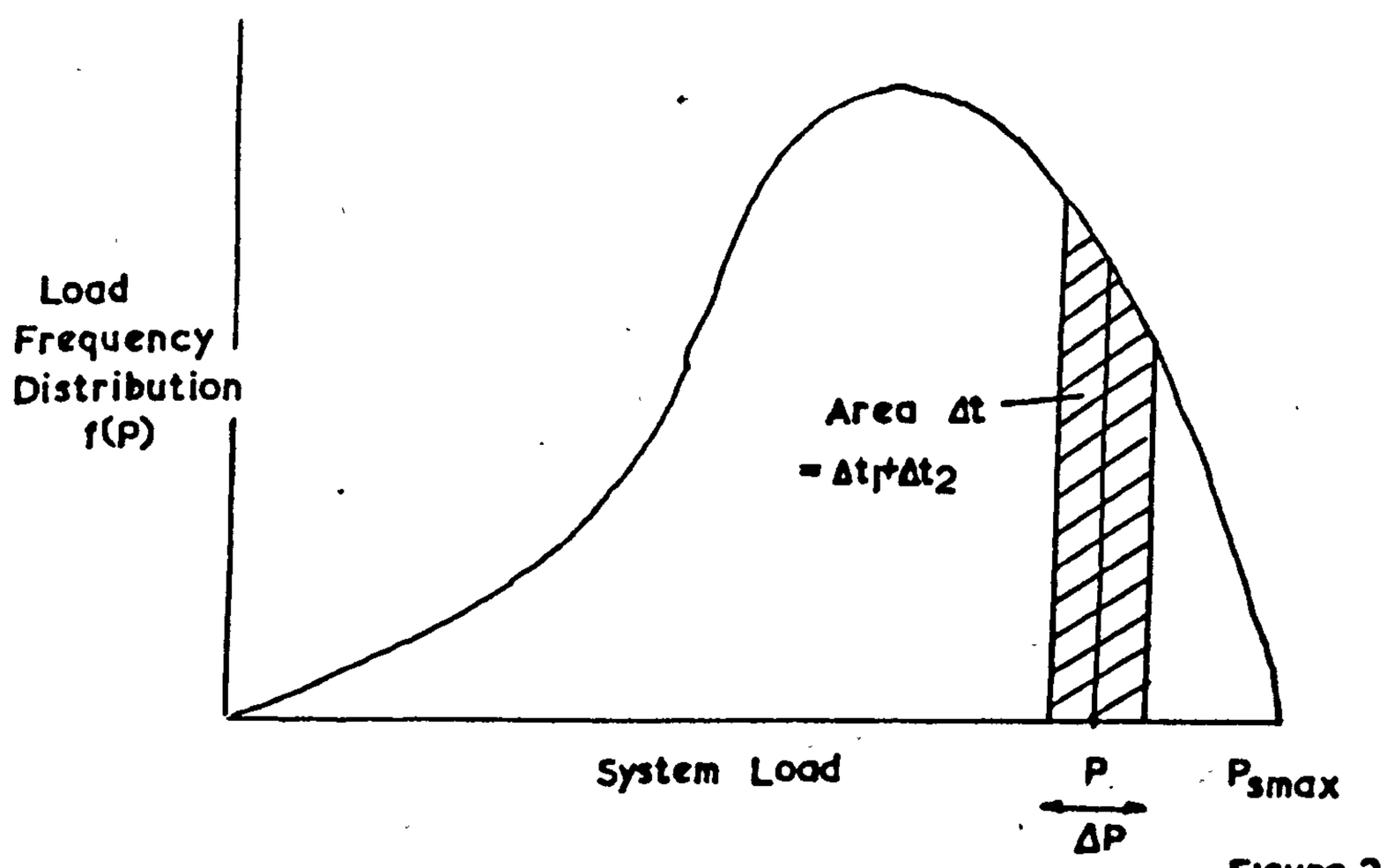

Figure 2

Optimum Switching Limits p.u.

r	Pl_r
1	1·41
2	1·22
3	1·15
4	1·12

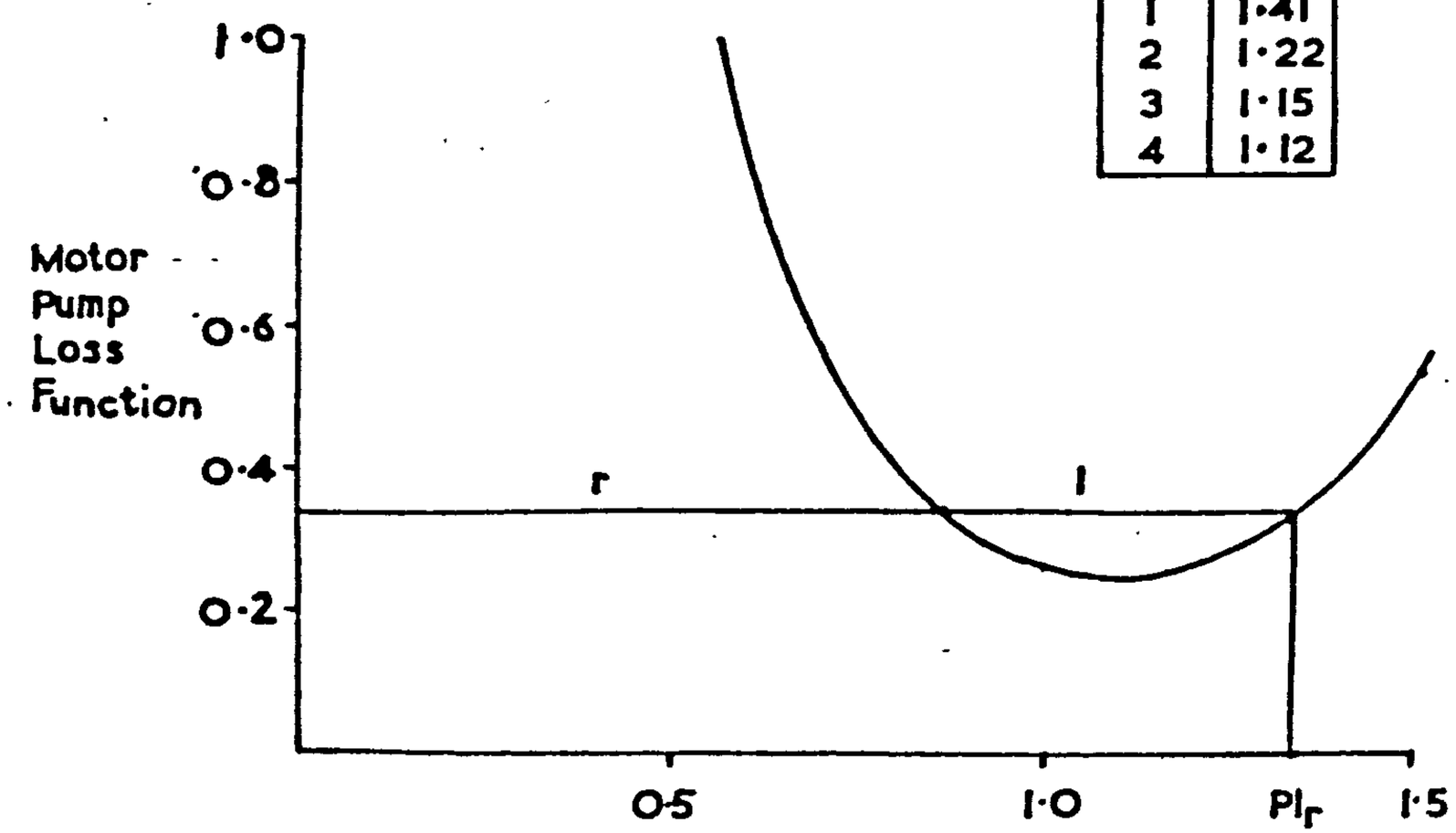

Figure 3

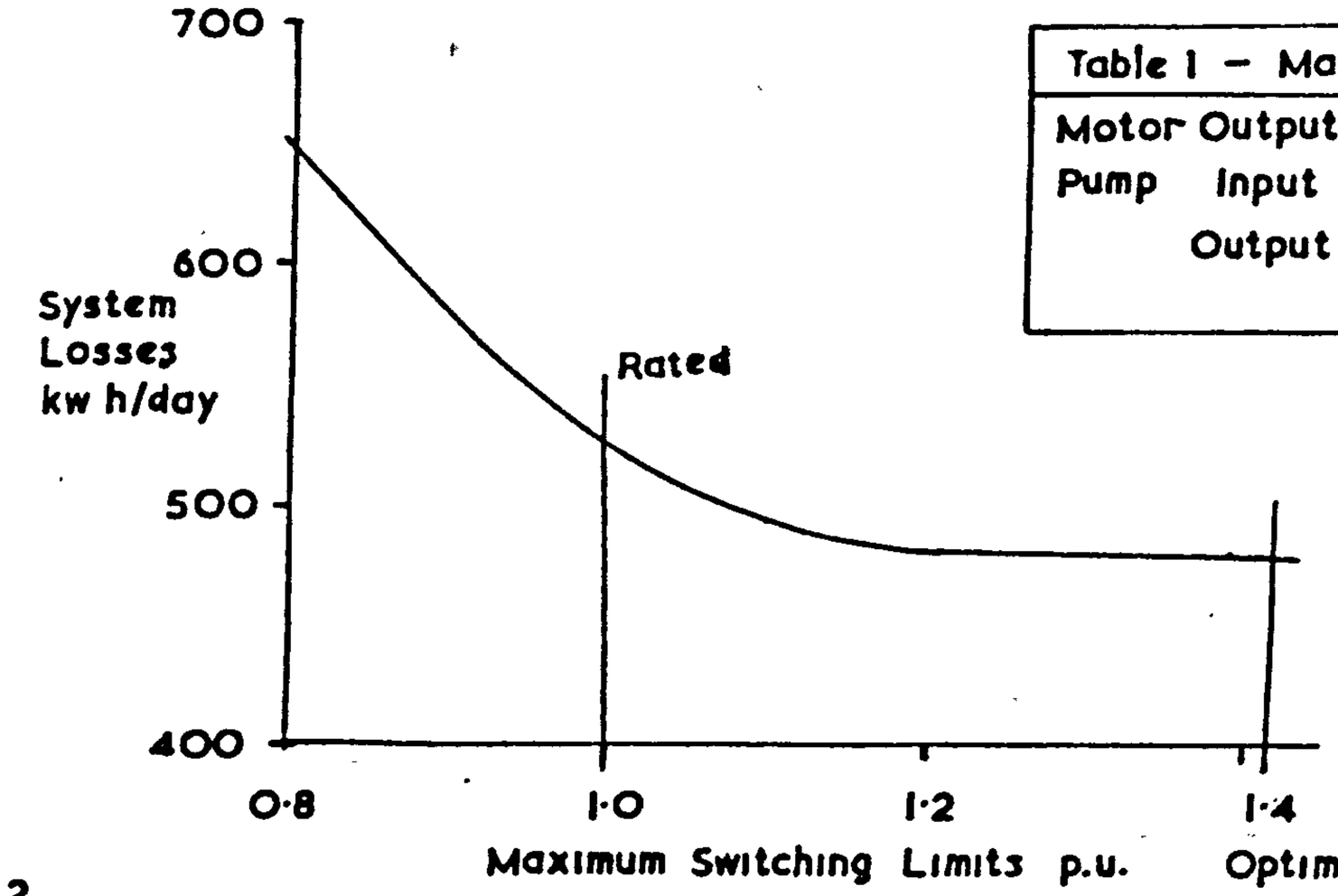

Figure 4

Table 1 – Machine Ratings	
Motor Output	37·3 kw
Pump Input	31·8 kw
Output	232 m^3/h
	39·2 mWG

A Stochastic Approach to the Aging of Electrical Machines

P.H. Mellor & D.R. Turner

The University of Liverpool

Introduction

In a recent paper the authors discussed a method of improving the efficiency of multi-machine systems by careful choice of the control parameters (1). An inherent feature of this work was that the machines were required to supply loads in excess of their continous ratings for short periods of time. Such overloading is only permissible if the machine temperature is below the design upper limit and remains so, however it is bound to have an effect on the aging of the machine insulation and the paper suggests a method whereby this effect can be quantified to enable a economic judgement to be made of the value of improved efficiency. The paper describes briefly the thermal model used, indicates the relationship between aging and insulation temperature and uses a stochastic approach to describe the load demand. The effect on the aging of a multi-machine subjected to different control strategies is discussed.

Thermal Model

A number of authors have described thermal models for electrical machines (2)-(5) and the approach adopted here is that of a lumped parameter network, shown in fig. 1. It is seen that only a few nodes are used, thus discrete parts of the machine such as the frame or end winding are each represented by a single node having generation g_i and thermal capacitance c_i. The model assumes that heat transfer between the nodes is linear, implying that radiation effects are ignored as negligible. The thermal sources are equal to the machines losses, which are modelled by a quadratic loss junction (1), $\gamma(\omega) = a/\omega + b + \frac{\omega}{c}$, such that the losses are given by $\omega.\gamma(\omega)$ where ω is the output power. The choice of node numbers when using such models is dependent upon the conflicting requirements of detailed temperature distribution, accuracy and speed of computation. In this instance a detailed knowledge of the temperature distribution is not needed, but it is important to have a low computation time, and thus only a few nodes are used. Experience of small and medium sized induction motors shows that the majority of electrical insulation failures occur in the end windings, and measurements on a 5.5 kW cage induction motor showed that the end winding temperature to be higher than that of the slot portion of the coil. Thus this temperature, derived from the thermal model is used as the "input" to the aging equation.

The parameters for the model are derived by calculation from the dimensions of the machine, using straightforward thermal equations (3) and the model was found to give good results.

Aging Equation

The accepted equation for the thermal life of insulation is due to Dekin (6) and is:

$$L_T = \exp(b/\theta - a) \qquad (1)$$

L_T expected life of insulation at temperature θ

θ insulation temperature ^oK

a, b insulation constants

The aging of an insulation can be expressed as the expected life at temperature θ compared to the expected life at temperature θ_{ref}.

i.e. $$R = \frac{L_T}{L_{ref}}, \qquad L_{ref} = \exp(b/\theta_{ref} - a)$$

If the temperature θ is a function of time, then the aging of the insulation is given by

$$R = \frac{1}{T} \int_0^T \exp(b/\theta_{ref} - b/\theta)\, dt \qquad (2)$$

Description of Multi-machine System

The multi-machine system considered was that of the earlier paper (1) where n machines are operated in parallel to provide a system load. With changes in the load, machines are either switched on or off to meet the demand, where the actual power levels at which switching occurs are referred to as the system switching limits. The loadings on any one of the machines can be determined from the system load characteristic, the values of the switching limits and the position of that machine in the switching sequence defined such that the i^{th} machine is that which switches on when (i - 1) machines are at their limit. Previous work has shown that the overall system energy consumption can be controlled by changing the values of the switching limits. Aging control can be effected on a particular machine by changing its position in the switching sequence, for example a typical aging control would be to rotate the machines, say every week, so that their aging would be shared equally. Such a rotational control is compared with other examples of aging control at the end of the paper.

Stochastic Aging Analysis

The work in this paper is concerned with developing a method by which the system aging can be assessed from a stochastic system load, where at any time an exact value of load is not known but where the load can take any value with known probability. The equations can be formulated by either a deterministic approach or a more abstract stochastic method. Since the resultant equations are solved by similar computational methods, the more flexible deterministic approach is used here. A digital computer is used to generate a large number of load characteristics or samples, that fit the statistics of the system load. For every sample it is then a simple matter to determine the aging in each machine from its thermal model for a given control strategy, and then by collecting together all the samples the overall aging distribution found.

For a linear thermal model of the type used to describe each machine a discrete differential equation can be written down, in which it is assumed that the load on the machines is constant over small time intervals, and is of the form

$$[\theta(k+1, z)]_r = [A].[\theta(k, z)]_r + [G].[u(k, z)]_{r=1,n} \qquad (3)$$

where $[\theta(k, z)]_r$ = column matrix of the nodal temperatures in machine r, at time step k during load sample z

$[A]$ = Thermal matrix of machine

$[G]$ = Generation matrix of machine

$[u(k, z)]$ = Column matrix of the heat generation in each node of the thermal model.

The nodal heat generation will depend upon the system load for that event and time step and position of the machine in the control sequence. The machine's position can be defined in terms of a control matrix $[\Lambda(k,z)]_r$, which is a column matrix of order n whose elements are either zero or unity such that if the machine is in position i, say, then only the ith element of the control matrix will be unity. By representing the system load as a column matrix $[W(k,z)]$, with elements equal to the proportion of the load that is provided by each position in ths switching sequence, then the load taken by machine r, $W_r(k,z)$ is given by

$$W_r(k,z) = [\Lambda(k,z)]^T_r \cdot [W(k,z)]$$

In the above the positional load matrix $[W(k,z)]$ is obtained from the total system load $W_s(k,z)$ and the switching limits.

The heat generated in the machine can then be expressed as some function of the machine loading, denoted by

$$[u(k,z)]_r = [F(W_r(k,z)]$$

To produce values of system load $W_s(k,z)$ random number generating routines have to be provided that will produce values to the load that will fit the load statistics for every time interval k and load event z. However, if the system load is modelled to act as a random variable with a white stationary distribution then only a single random number routine $\mathcal{R}$ is required such that

$$W_s(k,z) = \mathcal{R}(kz)$$

In this manner a series of values of temperatures $[\theta(k,z)]_r$ for all r of the n machines can be found from a known initial condition. Likewise a series of aging values $R(k,z)$ over each time step are calculated from the values of hot spot temperature and the aging equation (2).

From such information any statistical parameter of the system can be calculated, however the two that are of particular interest are overall aging mean and the variation with time of the machine positional probability. The latter is used to assess the performance of a particular aging control algorithm. These two parameters are obtained from the equations

$$R_{mean} = \sum_{k=1}^{kmax} \sum_{z=1}^{zmax} \frac{R(k,z)}{kmax\ zmax}$$

$$[P_\Lambda(k)]_r = \sum_{z=1}^{zmax} \frac{\Lambda(k,z)\quad r}{zmax}$$

respectively.

The effect of starting can be accomodated in the aging analysis by the inclusion of an additional nodal heat generation $[Ustart]_r$ in the thermal equations at the time steps, k, in which starting occurs. This generation is equal to the additional copper loss caused by the large surge currents that occur when a machine is started on load. Thus equation (6) can be adjusted to include $[Ustart]_r$ such that

$$[u(k,z)]_r = [F(W_r(k,z))] + [Ustart]_r$$

for a start in time step k, and this implies that the machine loading $W_r(k-1,z)$ in the previous time step, k-1, must be zero.

Results

A set of results have been obtained for an imaginary multi-machine system which consists of four 5.5 kW TEFC cage induction motors operating in parallel mechanically. The load duty on the system is in the form of a stationary, white stochastic load with a mean of 15.5 kW, a standard deviation of 2.5 kW and a load cycle of 24 hours. The latter is purely arbitrary and in this instance is kept small to minimise computational time. The system load distribution was modelled by a Beta function (7), with upper and lower limits of 0 and 22 kW respectively.

The thermal model described earlier was checked by measurements as a 5.5 kW TEFC cage induction motor subjected to a varying load. Figure 2 shows the endwinding temperature, both predicted and measured, and the agreement is seen to be good.

Table 1 gives the values of the total machine agings and energy consumption for three different aging control strategies and two sets of power switching limits. The three control strategies are:-

(a) rotational - every 6 hours.

(b) ideal - defined as that which gives an equal probability of a machine being in any position at anytime, where the machines position is independant of its load or temperature. The ideal control strategy can be considered as the extreme of a rotational control where the interval of rotation approaches zero and starting effects in the machine are neglected. However starting effects cannot be ignored, so such a control may not be physically realisable but still should be analysed or it gives a basis of minimum aging to which other control strategies can approximate.

(c) temperature - in which when a switching limit is reached the coolest machine is switched on (increasing load) or the hottest machine is switched off (decreasing load). This control attempts to meet the first criteria of the ideal control, which is to give an equal probability of a machine being in any position at anytime, by continually ordering the machines in terms of their temperature without demanding any more starts on a machine than the number required by the system load.

Each of these strategies is such that the mean expected agings of the four machines are identical giving the three agings for each set of switching limits in Table 1.

It is seen that as expected the ideal strategy gives the lowest aging whilst the temperature strategy comes second. It is also seen that the saving in energy is proportionally greater than the loss of life involved when using the optimum switching limits and the temperature control strategy. Indeed for many conventional systems which are at present operating under the rotational control strategy (1) with switching limits set at the machines ratings, a change to optimum switching limits and temperature control strategy would increase both the system efficiency and the life of the machines.

Acknowledgements

The authors wish to thank Mr A. Gibson of Bass Brewing Ltd. for his encouragement in this work and the University of Liverpool for providing laboratory and computer facilities.

References

(1) Mellor, P H and Turner D R "Efficiency optimisation of multi-machine systems" Proc. 16th Univ. Power Eng. Conf., Sheffield, April 1981

(2) Sreenivasan, V K and Sengupta D P "Thermal design of totally enclosed fan cooled induction motors IEEE, PES Winter meeting, Paper A77 097-9, 1977.

(3) Perez I J and Kassakian J G "A stationary thermal model for smooth air gap rotating electric motors" Electric Machines and Electro mechanics Vol 3 No 3-4, 1979 pp 285-303

(4) Szogyen, J R M "Coding of electric motors" IEE, EPA Vol 2 No 2 April 1979

(5) Imre, L., Jagasits, Z and Barcza, J "Computer simulation of the transient warming of rotary electric machines" Proc 2nd Int. Conf. on Numerical methods in thermal problems, Venice, July 1981

(6) Dekin, T W "Electrical insulation deterioration treated as a chemical rate phenomenon" AIEE Trans. No. 69 1948 pp 113-122

(7) Pearson, K "Tables of the incomplete β functions "Camb. Univ. Press 1934.

Table 1 Ageing factor and total loss for a four machine system

		Control Stratagies			Total loss (kWhr)
		(1)	(2)	(3)	
Switching limits	Rated	0.0224	0.0174	0.0205	80.0
	Optimum	0.0232	0.0180	0.0209	77.9

Ageing base: 120° C
10,000 hrs

Control Stratagies (1) rotational
(2) ideal
(3) temperature

Switching limits Rated: 1.0 pu on each machine
Optimum: 1.21 pu between machine positions 1 + 2
1.05 pu " " " 2 + 3
0.99 pu " " " 3 + 4

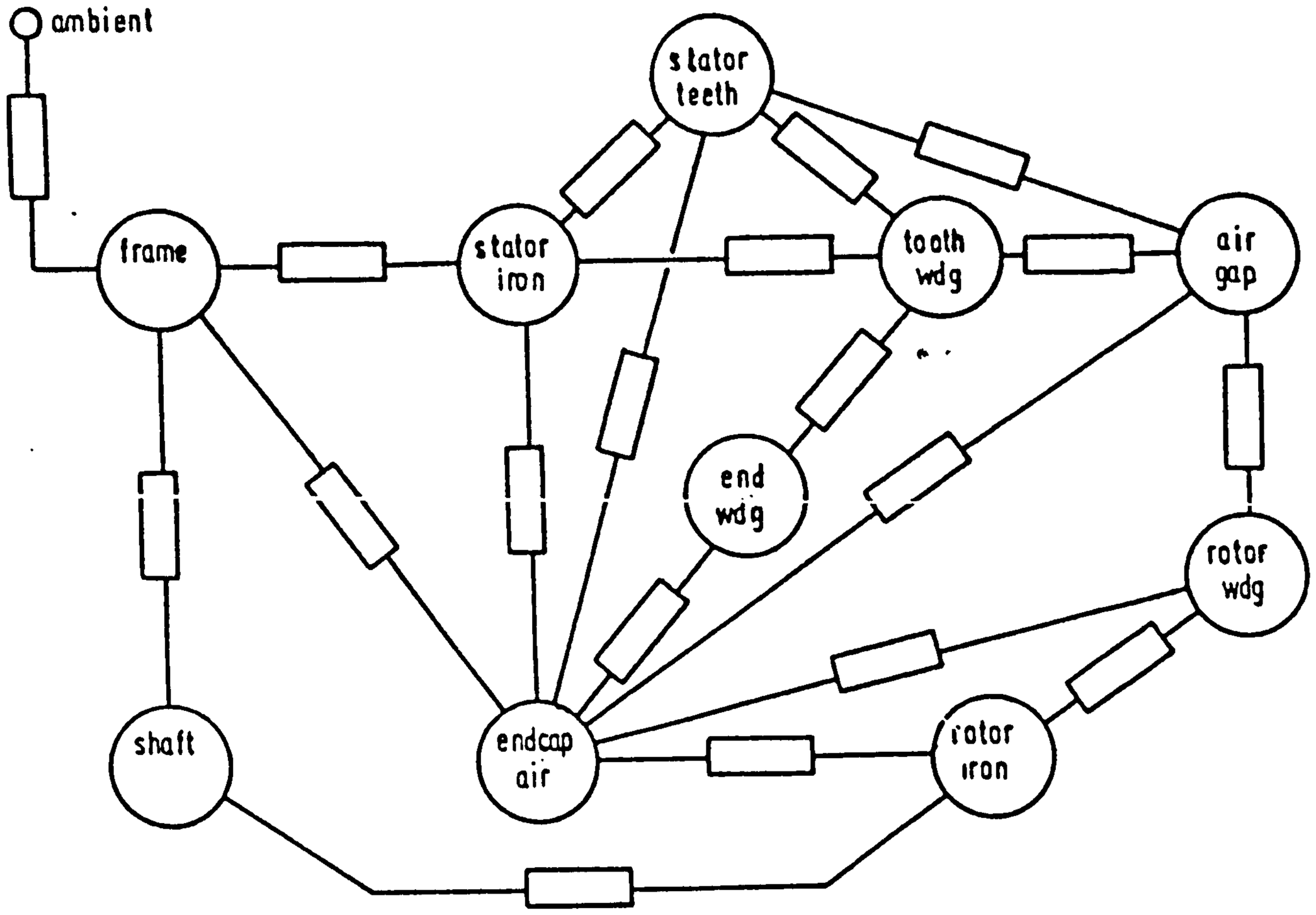

Figure 1 Thermal model network

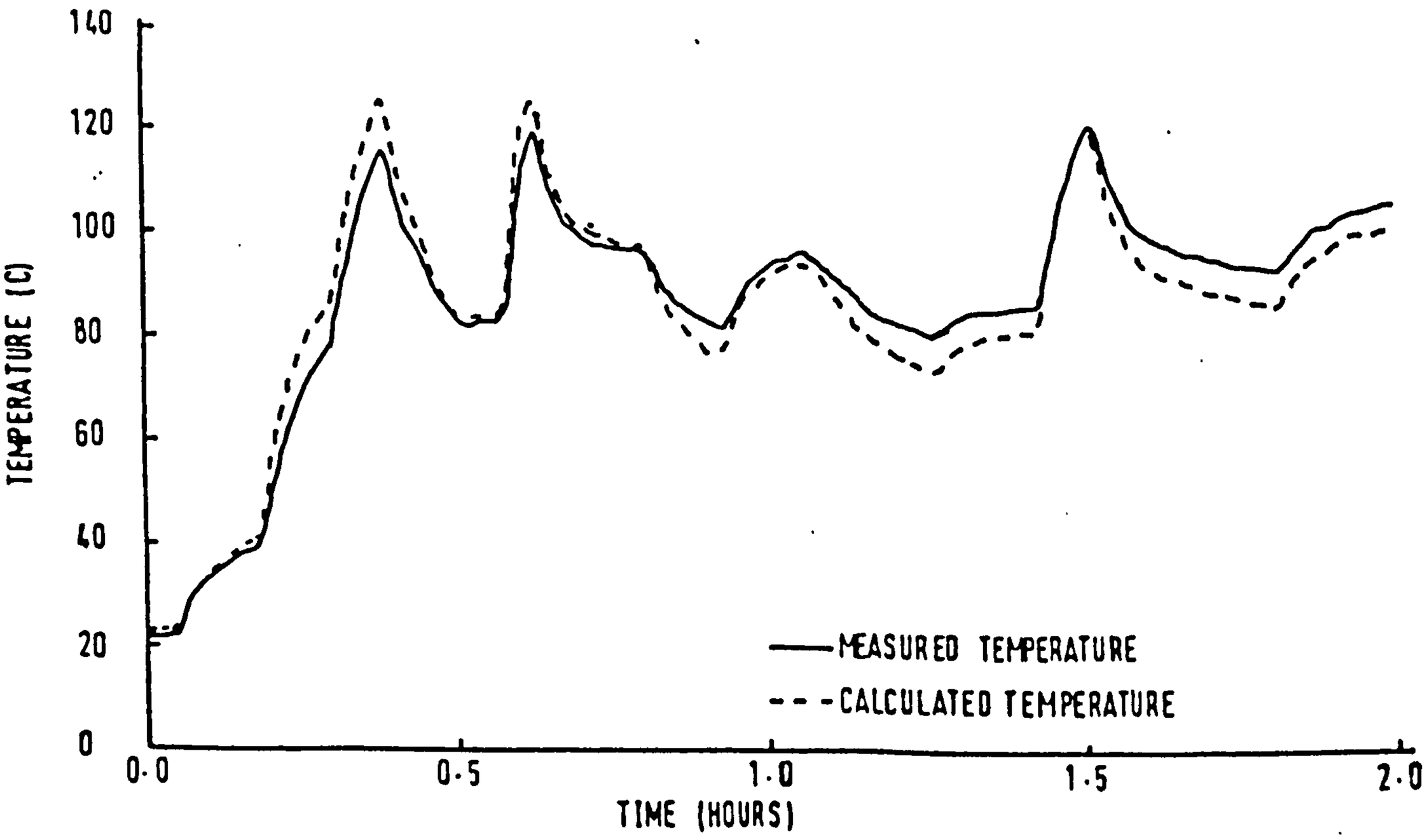

Figure 2 Variation of endwinding temperature for changing load